Larry L. Barton · Dennis A. Bazylinski
Huifang Xu *Editors*

Nanomicrobiology

Physiological and Environmental Characteristics

Springer

Nanomicrobiology

Larry L. Barton • Dennis A. Bazylinski
Huifang Xu
Editors

Nanomicrobiology

Physiological and Environmental Characteristics

Springer

Editors
Larry L. Barton
Department of Biology
University of New Mexico
Albuquerque
New Mexico
USA

Dennis A. Bazylinski
School of Life Sciences
University of Nevada at Las Vegas
Las Vegas
Nevada
USA

Huifang Xu
Department of Geoscience
University of Wisconsin-Madison
Madison
Wisconsin
USA

ISBN 978-1-4939-1666-5 ISBN 978-1-4939-1667-2 (eBook)
DOI 10.1007/978-1-4939-1667-2
Springer New York Heidelberg Dordrecht London

Library of Congress Control Number: 2014947975

Printed on acid-free paper

Springer is part of Springer Science+Business Media (www.springer.com)

Preface

For many years, bacteria or prokaryotes, unlike eukaryotes, have been thought of as microorganisms without organelles, as "bags of enzymes" and as an enveloped collection of randomly placed macromolecules. With the advent and use of the electron microscope in the 1950s, followed by decades of tremendous development of new technologies for analyzing prokaryotic cells down to the nanometer level, we now know that these nucleus-free cells are far from being disorganized. They are, in fact, extremely complex with regard to structure and (micro)compartmentalization. In addition, without getting into the semantics of what constitutes a "true" organelle, it is clear that prokaryotes often compartmentalize using some sort of coating or barrier essentially constituting an organelle. Examples of these are numerous, some of which, including carboxysomes and magnetosomes, are discussed in detail in this volume.

Given the changes in way we look at prokaryotes based on the previous paragraph, it seems only natural that we would now examine how prokaryotes use nanosystems to microcompartmentalize and exploit what we learn in a new, burgeoning scientific field we refer to as nanotechnology. This volume we believe is among the first to be devoted entirely to nanomicrobiology and the nanosystems of bacteria.

The emphasis of this volume is on those processes or nanostructures that have machine-like function and geomicrobial activities that occur at a specific site within or on the cell, again demonstrating the importance of microcompartmentalization by prokaryotes. The authors of the chapters in this book are leaders in these specific fields, thus ensuring they provide state-of-the-art reviews of their specific topics. We hope to convey that the rapidly evolving field of nanosystem technology embraces many areas for the development of futuristic scientific, commercial and medical endeavors. In addition, the biological and physical features of these bacterial structures should stimulate scientists and others interested in nanotechnology research to adapt some of these principles to their research efforts.

Larry L. Barton
Dennis A. Bazylinski
Huifang Xu

Contents

Contributors

Larry L. Barton Department of Biology, University of New Mexico, Albuquerque, NM, USA

Dennis A. Bazylinski School of Life Sciences, University of Nevada at Las Vegas, Las Vegas, NV, USA

Gordon C. Cannon Department of Chemistry and Biochemistry, The University of Southern Mississippi, Hattiesburg, MS, USA

Sabine Heinhorst Department of Chemistry and Biochemistry, The University of Southern Mississippi, Hattiesburg, MS, USA

Stefan Howorka Department of Chemistry, Institute of Structural and Molecular Biology, University College London, London, UK

Brenda L. Kirkland Department of Geosciences, Mississippi State University, Mississippi State, MS, USA

Christopher T. Lefèvre CEA/CNRS/Aix-Marseille Université, Biologie Végétale et Microbiologie Environnementales, Laboratoire de Bioénergétique Cellulaire, Saint Paul lez Durance, France

Brian H. Lower School of Environment and Natural Resources, The Ohio State University, Columbus, OH, USA

Chaithanya Madhurantakam Departments of Structural and Molecular Microbiology, Structural Biology Research Center, Vrije Universiteit Brussel, Brussels, Belgium

Department of Structural Biology Brussels, Vrije Universiteit Brussel, Brussels, Belgium

Robert J. C. McLean Department of Biology, Texas State University, San Marcos, TX, USA

Tâm Mignot Laboratoire de Chimie Bactérienne, CNRS UMR 7283, Aix-Marseille Université, Institut de Microbiologie de la Méditerranée, Marseille, France

Han Remaut Departments of Structural and Molecular Microbiology, Structural Biology Research Center, Vrije Universiteit Brussel, Brussels, Belgium

Department of Structural Biology Brussels, Vrije Universiteit Brussel, Brussels, Belgium

Jessup M. Shively Department of Genetics and Biochemistry, Clemson University, Clemson, SC, USA

Francisco A. Tomei-Torres Division of Toxicology and Human Health Sciences, Agency for Toxic Substances and Disease Registry, Atlanta, GA, USA

Morgane Wartel Laboratoire de Chimie Bactérienne, CNRS UMR 7283, Aix-Marseille Université, Institut de Microbiologie de la Méditerranée, Marseille, France

Huifang Xu Department of Geoscience, University of Wisconsin, Madison, WI, USA

Thomas Zocco Materials Science Division, Los Alamos National Laboratory, Los Alamos, NM, USA

Chapter 1
Nanostructures and Nanobacteria

Robert J. C. McLean and Brenda L. Kirkland

1.1 Introduction

Humans have long been fascinated by worlds and objects, not visible to the unaided eye. In the seventeenth century, two notable discoveries of the microscopic world were reported by the English philosopher, Hooke (1665), including the first identification of the cell, now recognized as the basic unit of life; and the realization that fossilized wood and mollusks likely originated from once-living organisms. A Dutch tradesman, Antony van Leeuwenhoek, who may have been inspired by Hooke's work, made his own microscopes and used these instruments to observe "animalcules" (van Leeuwenhoek 1712), which are now recognized as bacteria and protozoa. A number of refinements in light optics and lens coatings were achieved in the nineteenth and twentieth century to enhance the resolving power of light microscopes (Doetsch 1981). The effective resolution of light microscopy is now approximately 300 nm unless deconvolution or other image enhancing techniques are used (Gustafsson et al. 1999). With the discovery of the electron microscope (Knoll and Ruska 1932), and more recently scanning tunneling microscopy (Binnig and Rohrer 1984) along with field emission technology (Coene et al. 1992), we are now able to observe objects approaching molecular and atomic levels of resolution. In this context, a new unseen world involving nanometer scale structures (nanostructures), has recently emerged with potential major implications in both biology and geology (Folk 1993; McKay et al. 1996).

In 1993, Robert Folk described small spherical objects (50–200 nm) in size during scanning electron microscopy (SEM) of travertine and other carbonate minerals,

R. J. C. McLean (✉)
Department of Biology, Texas State University, 601 University Drive,
San Marcos, TX 78666, USA
e-mail: McLean@txstate.edu

B. L. Kirkland
Department of Geosciences, Mississippi State University, PO Box 5448,
Mississippi State, MS 39762-5448, USA

L. L. Barton et al. (eds.), *Nanomicrobiology,* DOI 10.1007/978-1-4939-1667-2_1

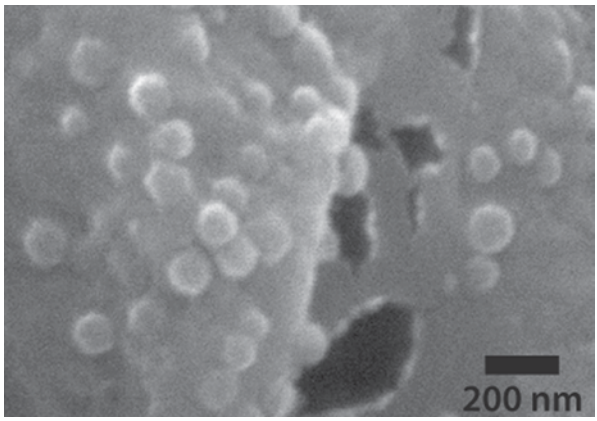

Fig. 1.1 Spherical structures interpreted as nanobacteria (nannobacteria) based on consistent spherical shape, distribution in a cluster, and association with mucilage, perhaps part of a biofilm, from a sample collected in hot springs near Viterbo, Italy. (SEM photomicrograph by F.L. Lynch)

as well as clays, silica, and some sulfide minerals (Folk 1993). These nanometer scale objects were readily observed after mild acid etching of minerals during SEM preparation. Their morphology resembled bacteria but they were much smaller than known bacteria (typically 300 nm–2 μm in size; Beveridge 1981). Based on their resemblance to bacteria, dissimilarity to crystals, and distribution in clusters; these objects were called nannobacteria. Other authors have referred to these structures as nanobacteria (reviewed in Cisar et al. 2000). Similar nano-sized objects have been described in other aqueous environments including clays (Folk and Lynch 1997), plant fossils (Dunn et al. 1997), mineral enrichment (Sillitoe et al. 1996), sediments (Folk and Lynch 2001), kidney stones (Kajander and Çifçioglu 1998; Kajander et al. 2003), vaccines (Çifçioglu et al. 1997), human arteries (Miller et al. 2004), and blood serum (Martel et al. 2010). An example of nanobacteria is shown in Figure 1.1. Arguably, one of the most dramatic descriptions of nanobacteria in the literature was their identification as evidence of possible extraterrestrial life on the Martian meteorite ALH84001 (McKay et al. 1996). As was the case in the original observations of small life (eukaryotic cells and bacteria) in the seventeenth and early eighteenth century, there was tremendous interest in understanding the nature of life at an even smaller (nanometer) scale. Several hypotheses have been developed to explain nanobacteria. These hypotheses are outlined in the following sections of this chapter and in other chapters in this volume.

1.2 Microscopy Investigations

The first descriptions of nanobacteria arose from SEM observations. An early concern dealt with the possibility of artifacts due to specimen processing and examination. Typical specimen examinations by electron microscopy occur in high vacuum (<100 mPa; Beveridge et al. 2007), under which conditions, liquid water cannot exist. Because biological specimens and many geological specimens are hydrated,

care must be taken to preserve structural integrity and minimize dehydration artifacts. Chemical fixation involving glutaraldehyde and osmium tetroxide, and dehydration protocols with a variety of organic solvents are typically used during conventional biological specimen preparations to preserve fragile structures (reviewed in Beveridge et al. 2007; Hayat 1981). One example of a commonly encountered highly hydrated biological structure is the extracellular matrix (slime) associated with surface-adherent microbial communities (biofilms; McLean et al. 2012). This material contains a variety of polysaccharides, proteins, DNA, membrane components, and a variety of ions. Depending upon the location, estimates of water composition in biofilm matrices may exceed 90% (Hunter and Beveridge 2005). For SEM, specimens are often sputter-coated with a thin film of a conductive material (typically gold or palladium), to provide electron contrast and reduce electrical charge accumulation on the specimen. Heightened contrast in biological and some geological specimens can be obtained using a variety of heavy metal stains (many of which contain Os, Pb, U, or Ru).

Several studies were conducted to see whether specimen processing contributed to the formation of nanostructures as seen by scanning electron microscopy. The early SEM observations of Italian travertine were coupled with energy dispersive X-ray (EDX) analysis (Folk 1993). In this manner, the nano-sized objects were shown to be Ca-rich and their morphology was notably distinct from inorganically precipitated minerals. While mild acid etching (1% v/v HCl for one minute) was employed to reveal nanostructures (Folk 1993), more rigorous acid treatment caused their dissolution. Mild acid etching was also shown to create spherical nanometer scale structures (Kirkland et al. 1999). Subsequent work showed that sputter coating with graphite, or limited exposure to gold sputter coating, would preserve nano-sized biological and geological structures and limit spherical artifacts due to the coating process (Folk and Lynch 1997). Further investigations on potential dehydration artifacts of bacteria within sandstone were carried out by systematically examining a variety of specimen preparation protocols for conventional SEM as well as environmental scanning electron microscopy (ESEM; Fratesi et al. 2004). This investigation revealed that some traditional dehydration practices create artifacts at the nanometer scale. Unlike conventional SEM, which requires high vacuum, the specimen chamber in ESEM is maintained under reduced air pressure thus allowing the examination of hydrated specimens. Of note from the Fratesi et al. (2004) study, ESEM observation also revealed the occurrence of nano-sized objects (nanobacteria) within biofilms in sandstone in addition to bacteria of normal morphology. Several years earlier, another research group (Uwins et al. 1998) also described nanobacteria from ESEM investigations. Membrane vesicles, nano-sized structures arising from bacterial surfaces (addressed below) have been documented within biofilm matrices (Schooling and Beveridge 2006), which might provide one explanation for this phenomenon.

Two notable studies show the potential for nano-sized artifacts during preparation for electron microscopy. Bacteria are found throughout all natural environments and are particularly common in sediments and within porous rock (Balkwill and Ghiorse 1985; Friedmann and Weed 1987). Bacterial cell surface material,

notably the extracellular matrix and sloughed cell wall material, is often anionic and can therefore bind metal ions such as Ca^{2+} (McLean et al. 1990; Ferris et al. 1987). In this context, Kirkland et al. (1999) noted within a Ca-rich environment that the presence of organic material such as polysaccharides or cytoplasmic material and bacterial cell wall fragments from phage-lysed bacteria, resulted in nano-sized objects resembling nanobacteria. In a medical context, Martel et al. (2010) showed that some proteins in human serum could also form nano-sized objects in the presence of elevated Ca^{2+}. From these findings, it is prudent to exhibit caution during the interpretation of nano-sized objects.

1.3 Examination of Nanobacteria as Independent Life Forms

The most intriguing hypothesis of nano-sized objects is that they may represent a previously unrecognized life form and possible evidence of life beyond Earth (Folk 1993; McKay et al. 1996; Kajander and Çifçioglu 1998; Uwins et al. 1998; Gillet et al. 2000). These observations and their implications have resulted in a number of investigations and conjectures.

Details of these investigations are addressed in other chapters within this volume as well as in the literature (Cisar et al. 2000; Martel et al. 2010). We shall summarize some of these findings in this section.

One defining criterion of a life-form is the capability to reproduce. Notwithstanding infectious proteins (i.e., prions; Gajdusek 1977; Prusiner 1998), the basis of heredity in eukaryotic and prokaryotic organisms is nucleic acids, notably DNA. Viruses, which require a eukaryotic or prokaryotic host to reproduce, use either DNA or RNA. Given the tremendous impact of the McKay et al. (1996) description of nanobacteria as providing potential evidence of extraterrestrial life, a workshop was organized by the US National Academy of Sciences to determine the lower size limits of life (National Academy of Sciences 1999). Based on life processes that were currently known at the time of writing, an organism capable of independent growth and reproduction, would require 250–400 proteins along with essential ribosomes, nucleic acids, proteins, and membranes. This biological package would fit into a sphere of 250 ± 50 nm. Certainly, the presence of nucleic acids is a key issue.

Uwins et al. (1998) investigated nanobacteria (referred to as "nanobes") in sandstone using the DNA-staining fluorescent molecules, 4′,6-diamidino-2-phenylindole (DAPI), acridine orange, and Feulgen. All three stains exhibited a positive response for DNA. The presence of other conventional microorganisms, as a potential source of DNA contamination, was ruled out by these investigators on the basis of SEM and ESEM examination. Transmission electron microscopy (TEM) revealed electron translucent regions at the periphery of the nanobacteria, which were interpreted as membranes. Although the specimens were processed in osmium tetroxide, these peripheral structures lack the characteristic electron-dense osmium staining that is prevalent and characteristic of membranes in other organisms (Beveridge 1999).

Other workers attribute the electron-translucent regions to a complex of organic molecules (polysaccharides or proteins) and ions such as Ca^{2+} (Kirkland et al. 1999; Martel et al. 2010). A much more rigorous approach for DNA detection was conducted by Kajander and Çifçioglu (1998), who employed PCR and sequencing, in their investigation. These investigators were able to culture nanobacteria and, by employing PCR and sequencing, were able to get a partial sequence. Of great interest, both of these studies (Uwins et al. 1998; Kajander and Çifçioglu 1998) demonstrated the ability of nanobacteria to grow in culture. In the Kajander and Çifçioglu study, nanobacteria cultures incorporated 35S-methionine and 3H-uridine, and growth was inhibited upon gamma irradiation. These authors proposed nanobacteria to be associated with kidney stones and other medically important calcification phenomena (Çifçioglu et al. 1997; Kajander and Çifçioglu 1998).

Attempts by other investigators to replicate these findings led to different conclusions. Two groups were able to culture nanobacteria and report growth inhibition by gamma radiation (Cisar et al. 2000; Martel et al. 2010). However, the partial sequence of Candidatus "*Nanobacterium sanguineum*" (Kajander and Çifçioglu 1998) matches that of *Phyllobacterium myrsinacearum* (Cisar et al. 2000), a common PCR contaminant. Nanobacteria culture growth was not inhibited by a number of antibiotics or by the presence of sodium azide (which inhibits cellular respiration; Cisar et al. 2000). Gamma radiation was shown by both Cisar et al. (2000) and Martel et al. (2010) to inhibit nanobacteria growth; however, this treatment is also capable of disrupting proteins and other macromolecules (Martel et al. 2010). One conceivable explanation by both groups is that some nano-sized objects identified as nanobacteria result from aggregations of macromolecules with Ca (Cisar et al. 2000; Martel et al. 2010). Our own work showing nano-sized objects resulting from Ca interactions with polysaccharides also supports this idea (Kirkland et al. 1999).

1.4 Nanostructures from Conventional Microorganisms

Nanobacteria have been reported in a wide variety of aqueous geological environments as well as medical environments (Folk 1993; Çifçioglu et al. 1997; Uwins et al. 1998). Conventional microorganisms (bacteria, archaea, protista, and fungi) can also exist in these environments (Ghiorse and Wilson 1988), and so it is prudent to consider whether nanostructures are derived from conventional microorganisms. Individual cells of prokaryotic organisms, including bacteria and archaea, have three common cell morphologies: (1) spherical forms referred to as cocci (coccus-sing), (2) barrel-shaped forms referred to as bacilli (bacillus-sing) or rod-shaped, and (3) a helical form referred to as spirilla (spirillum-sing; Doetsch 1981). In addition, some bacteria such as *Gallionella* sp. (Hallbeck and Pedersen 1995; Graham et al. 1991) and archaea such as *Methanospirillum hungatei* (Southam et al. 1993) have an extracellular structure in which individual cells are encased within a protein sheath. *Caulobacter crescentus* and other appendaged organisms are common in some environments (Staley and Fuerst 1989). The normal size range for prokaryotic

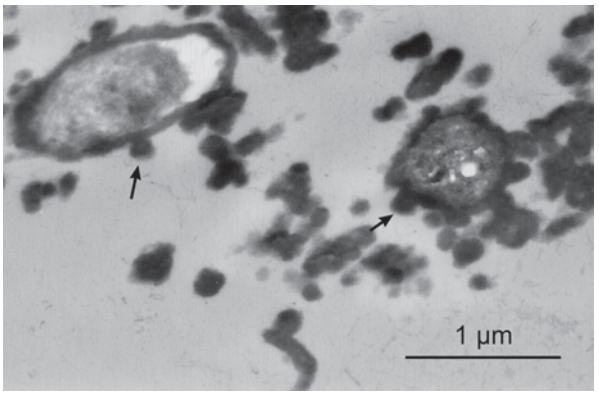

Fig. 1.2 Transmission electron micrograph of the gram-negative bacterium, *Proteus mirabilis,* grown in artificial urine (McLean et al. 1985) showing electron-dense extrusions arising from the bacterial cell surface (*arrows*). Such nanoscale extrusions consisting of bacterial extracellular polymers and possibly membrane vesicles complexed with metal ions such as Ca^{2+} may be interpreted as nanobacteria (Kirkland et al. 1999)

cells is 0.3–2 μm, although some organisms greatly exceed this size (Angert et al. 1993). We now address some issues involving known prokaryotic organisms that may give rise to nano-sized objects.

Bacteria and archaea excrete a number of extracellular polymeric substances (EPS) consisting of polysaccharides, proteins, and extracellular DNA as a function of biofilm formation (Ma et al. 2009) and these molecules have been shown to produce nano-sized aggregations in the presence of some ions such as Ca^{2+} (Kirkland et al. 1999; Figure 1.2). Other cell surface structures such as peptidoglycan and proteins are subject to sloughing due to cell wall turnover (Korgaonkar et al. 2012) and even cell death. Peptidoglycan and many other bacterial and archaeal cell surface polymers are anionic and readily nucleate mineral formation (McLean and Beveridge 1990; Ferris et al. 1986). One notable nano-sized structure (10–50 nm diameter) produced by many gram-negative bacteria are outer membrane vesicles (Mashburn and Whiteley 2005; Schooling and Beveridge 2006; Deatherage et al. 2009). Although these vesicles sometimes contain DNA (Mashburn-Warren and Whiteley 2006), they are not independent living entities, but rather are bacterial fragments. Membrane vesicles from gram-negative bacteria contain lipopolysaccharide (LPS) and are therefore capable of binding metal ions due to anionic moieties such as phosphate groups (Ferris and Beveridge 1986). In *Pseudomonas aeruginosa,* some of the genes associated with membrane vesicle formation, notably *pqsA* and *pqsH* involved with the *Pseudomonas* quinolone pathway (Mashburn-Warren et al. 2008), as well as *algU* and *mucD* associated with envelope stress (MacDonald and Kuehn 2013) have been identified. Similarly several genes, associated with envelope stress in *E. coli* (McBroom and Kuehn 2007) and lipopolysaccharide binding to peptidoglycan, are involved with vesicle formation in another gram-negative organism, *Salmonella enterica* (Deatherage et al. 2009). A number of gram-negative bacteria including *P. aeruginosa, Escherichia coli,* and *S. enterica* are genetically tractable and so detailed studies are plausible on the association of membrane vesicles and other cell surface characteristics with calcite precipitation and nanostructure formation.

A final issue deals with the size of prokaryotic bacteria under different growth and environmental conditions. Gram-positive bacteria, notably the genera *Bacillus* and *Clostridium* form resistant endospores under adverse environmental conditions. These bacterial spores represent a dormant survival mode of growth for these organisms. Spores are typically smaller (~300 nm diameter) than the growing (vegetative) forms of these organisms (often 1–2 μm in length and 300–400 nm diameter; Dick et al. 2008). Spores contain an organic chelating molecule, dipicolinic acid (Beveridge 1989) that readily binds Ca^{2+}. Gram-negative bacteria do not form endospores. A number of gram-negative bacteria will undergo a process of reductive division, during which they reproduce extensively as an R-strategy and form ultramicrobacteria (Morita 1982; Duda et al. 2012). Although the organisms they derive from may be rod-shaped, ultramicrobacteria are spherical and approximately 250 nm in diameter (Duda et al. 2012). Under appropriate nutritional conditions, ultramicrobacteria germinate into the size and morphology of their parent organism (Morita 1990). Recently, Giovanonni and co-workers cultured a marine ultramicrobacterium, *Pelagibacter ubique* (Carini et al. 2013), an extremely oligotrophic bacterium with a cell volume of ca. 0.1 μm^3 found in the pelagic ocean. This extremely small organism has very complex nutritional requirements, but retains its small morphology. Overall, ultramicrobacteria approximate the upper size range of nanobacteria (ca. 200 nm diameter).

1.5 Conclusions

As stated at the beginning of this chapter, the observations of nanobacteria raised some intriguing scientific questions on the size limits of life, and possible extraterrestrial implications (McKay et al. 1996). These fundamental questions were certainly analogous to those questions raised by the observations of Hooke (Hooke 1665) and van Leeuwenhoek (van Leeuwenhoek 1712) over 300 years ago. Although ultramicrobacteria can be cultured, these organisms (ca. 200–250 nm diameter; Morita 1988; Carini et al. 2013) are at the upper range of the size of nanobacteria (size range 50–200 nm) from other environments (Folk 1993; McKay et al. 1996; Kajander and Çifçioglu 1998; Uwins et al. 1998). While the evidence supporting nanobacteria as independent life-forms has been called into question (Cisar et al. 2000; Martel et al. 2010; Martel et al. 2012), there are intriguing concepts and potential issues that can be addressed. Firstly, the contribution of bacterial nanostructures to mineralization can be investigated. Genes are known for bacterial processes such as membrane vesicles or EPS formation. As well key genes needed for sporulation or growth transformation into an ultramicrobacteria are known in many organisms. These genes can be manipulated and roles and potential applications of nano-sized bacterial structures to mineral deposition can be performed.

One final observation that is particularly intriguing is that nanobacteria appear to be able to reproduce. This was first reported by Uwins (1998), and Kajander and Çifçioglu (1998); and confirmed by Cisar et al. (2000) and Martel et al. (2012).

Although the latter two research groups raised major questions about the DNA analysis and viability of the nanostructures, the self-assembly of the nano-sized objects provides a possible venue into exploring the chemical evolution and self-assembly phenomena that are considered to have occurred in the prebiotic Earth (Trevors and Psenner 2001).

Acknowledgments We deeply appreciate the friendship and boundless scientific enthusiasm of Robert L Folk, who stimulated many thought-provoking discussions, and exciting work. We also acknowledge the tremendous contribution of the late F. Leo Lynch to this field and to this chapter. Some of the authors' work described in this chapter was made possible by funding by the Texas Higher Education Coordinating Board (BLK, RJCM) and the National Science Foundation (EAR-9803031; BLK).

References

Angert ER, Clements KD, Pace NR (1993) The largest bacterium. Nature (Lond) 362:239–241

Balkwill DL, Ghiorse WC (1985) Characterization of subsurface bacteria associated with two shallow aquifers in Oklahoma. Appl Environ Microbiol 50:580–588

Beveridge TJ (1981) Ultrastructure, chemistry, and function of the bacterial wall. Int Rev Cytol 72:229–317

Beveridge TJ (1989) The structure of bacteria. In: Poindexter JS, Leadbetter ER (eds) Bacteria in nature, vol 3. Plenum Publishing Corporation, New York, pp 1–65

Beveridge TJ (1999) Structures of gram-negative cell walls and their derived membrane vesicles. J Bacteriol 181:4725–4733

Beveridge TJ, Moyles D, Harris B (2007) Electron microscopy. In: Reddy CA, Beveridge TJ, Breznak JA, Marzluf GF, Schmidt TM, Snyder LA (eds) Methods for general and molecular microbiology, 3rd edn. ASM Press, Washington, pp 54–81

Binnig G, Rohrer H (1984) Scanning tunneling microscopy. Physica 127B:37–45

Carini P, Steindler L, Beszteri S, Giovannoni SJ (2013) Nutrient requirements for growth of the extreme oligotroph 'Candidatus Pelagibacter ubique' HTCC1062 on a defined medium. ISME J 7:592–602

Çifçioglu N, Kuronen I, Akerman K, Hiltunen E, Laukkanen J, Kajander EO (1997) A new potential threat in antigen and antibody products: nanobacteria. In: Brown F, Burton D, Doherty P, Mekalanos JJ, Norrby E (eds) Vaccines 97. Cold Spring Harbor Laboratory Press, Cold Spring Harbor, pp 99–103

Cisar JO, Xu DQ, Thompson J, Swaim W, Hu L, Kopecko DJ (2000) An alternative interpretation of nanobacteria-induced biomineralization. Proc Natl Acad Sci U S A 97:11511–11515

Coene W, Janssen G, Op de Beeck M, Van Dyck D (1992) Phase retrieval through focus variation for ultra-resolution in field-emission transmission electron microscopy. Phys Rev Lett 69:3743–3746

Deatherage BL, Lara JC, Bergsbaken T, Rassoulian Barret SL, Lara S, Cookson BT (2009) Biogenesis of bacterial membrane vesicles. Mol Microbiol 72:1395–1407

Dick GJ, Torpey JW, Beveridge TJ, Tebo BM (2008) Direct identification of a bacterial manganese(II) oxidase, the multicopper oxidase MnxG, from spores of several different marine Bacillus species. Appl Environ Microbiol 74:1527–1534

Doetsch RN (1981) Determinative methods of light microscopy. In: Gerhardt P, Murray RGE, Costilow RN, Nester EW, Wood WA, Krieg NR, Phillips GB (eds) Manual of methods for general bacteriology. American Society for Microbiology, Washington, pp 21–33

Duda VI, Suzina NE, Polivtseva VN, Boronin AM (2012) Ultramicrobacteria: formation of the concept and contribution of ultramicrobacteria to biology. Microbiology 81:379–390

Dunn KA, McLean RJC, Upchurch GR Jr, Folk RL (1997) Enhancement of leaf fossilization potential by bacterial biofilms. Geology 25:1119–1122
Ferris FG, Beveridge TJ (1986) Site specificity of metallic ion binding in Escherichia coli K-12 lipopolysaccharide. Can J Microbiol 32:52–55
Ferris FG, Beveridge TJ, Fyfe WS (1986) Iron-silica crystallite nucleation by bacteria in a geothermal sediment. Nature (Lond) 320:609–611
Ferris FG, Fyfe WS, Beveridge TJ (1987) Bacteria as nucleation sites for authigenic minerals in a metal-contaminated lake sediment. Chem Geol 63:225–232
Folk RL (1993) SEM imaging of bacteria and nannobacteria in carbonate sediments and rocks. J Sed Petrol 63:990–999
Folk RL, Lynch FL (1997) The possible role of nannobacteria (dwarf bacteria) in clay-mineral diagenesis and the importance of careful sample preparation in high-magnification SEM study. J Sed Res 67:583–589
Folk RL, Lynch FL (2001) Organic matter, putative nannobacteria and the formation of ooids and hardgrounds. Sedimentology 48:215–229
Fratesi SE, Lynch FL, Kirkland BL, Brown LR (2004) Effects of SEM preparation techniques on the appearance of bacteria and biofilms in the carter sandstone. J Sed Res 74:858–867
Friedmann EI, Weed R (1987) Microbial trace fossil formation, biogenous, and abiotic weathering in the Antarctic cold desert. Science 236:703–705
Gajdusek DC (1977) Unconventional virus and the origin and disappearance of kuru. Science 197:943–960
Ghiorse WC, Wilson JT (1988) Microbial ecology of the terrestrial subsurface. Adv Appl Microbiol 33:107–172
Gillet P, Barrat JA, Heulin T, Achouak W, Lesourd M, Guyot F, Benzerara K (2000) Bacteria in the Tatahouine meteorite: nanometric-scale life in rocks. Earth Planet Sci Lett 175:161–167
Graham LL, Harris R, Villiger W, Beveridge TJ (1991) Freeze-substitution of gram-negative eubacteria: general cell morphology and envelope profiles. J Bacteriol 173:1623–1633
Gustafsson MGL, Agard DA, Sedat JW (1999) I5M: 3D widefield light microscopy with better than 100 nm axial resolution. J Microsc 195:10–16
Hallbeck L, Pedersen K (1995) Benefits associated with the stalk of Gallionella ferruginea, evaluated by comparison of a stalk-forming and a non-stalk-forming strain and biofilm studies in situ. Microb Ecol 30:257–268
Hayat MA (1981) Fixation for electron microscopy. Academic, New York
Hooke R (1665) Micrographia: or, some physiological descriptions of minute bodies made by magnifying glasses. J. Martyn and J. Allestry, London
Hunter RC, Beveridge TJ (2005) High-resolution visualization of Pseudomonas aeruginosa PAO1 biofilms by freeze-substitution transmission electron microscopy. J Bacteriol 187:7619–7630
Kajander EO, Çifçioglu N (1998) Nanobacteria: an alternative mechanism for pathogenic intra- and extracellular calcification and stone formation. Proc Natl Acad Sci U S A 95:8274–8279
Kajander EO, Çifçioglu N, Aho K, Garcia-Cuerpo E (2003) Characteristics of nanobacteria and their possible role in stone formation. Urol Res 31:47–54
Kirkland BL, Lynch FL, Rahnis MA, Folk RL, Molineux IJ, McLean RJC (1999) Alternative origins for nannobacteria-like objects in calcite. Geology 27:347–350
Knoll M, Ruska E (1932) The electron microscope. Z Phys 78:318–339
Korgaonkar A, Trivedi U, Rumbaugh K, Whiteley M (2012) Community surveillance enhances Pseudomonas aeruginosa virulence during polymicrobial infection. Proc Natl Acad Sci U S A 110:1059–1064
Ma L, Conover M, Lu H, Parsek MR, Bayles K, Wozniak DJ (2009) Assembly and development of the Pseudomonas aeruginosa biofilm matrix. PLoS Pathog 5:e1000354
MacDonald IA, Kuehn MJ (2013) Stress-induced outer membrane vesicle production by Pseudomonas aeruginosa. J Bacteriol 195:2971–2981
Martel J, Wu CY, Young JD (2010) Critical evaluation of gamma-irradiated serum used as feeder in the culture and demonstration of putative nanobacteria and calcifying nanoparticles. PLOS One 5:e10343

Martel J, Young D, Peng HH, Wu CY, Young JD (2012) Biomimetic properties of minerals and the search for life in the Martian meteorite ALH84001. Annu Rev Earth Planet Sci 40:167–193
Mashburn LM, Whiteley M (2005) Membrane vesicles traffic signals and facilitate group activities in a prokaryote. Nature 437:422–425
Mashburn-Warren LM, Whiteley M (2006) Special delivery: vesicle trafficking in prokaryotes. Mol Microbiol 61:839–846
Mashburn-Warren LM, Howe J, Garidel P, Richter W, Steiniger F, Roessle M, Brandenburg K, Whiteley M (2008) Interaction of quorum signals with outer membrane lipids: insights into prokaryotic membrane vesicle formation. Mol Microbiol 69:491–502
McBroom AJ, Kuehn MJ (2007) Release of outer membrane vesicles by Gram-negative bacteria is a novel envelope stress response. Mol Microbiol 63:545–558
McKay DS, Gibson EK Jr, Thomas-Keptra KL, Vali H, Romanek CS, Clemett SJ, Chillier XDF, Maechling CR, Zare RN (1996) Search for past life on Mars: possible relic biogenic activity in martian meteorite ALH84001. Science 273:924–930
McLean RJC, Beveridge TJ (1990) Metal binding capacity of bacterial surfaces and their ability to form mineralized aggregates. In: Ehrlich HL, Brierley CL (eds) Microbial mineral recovery. McGraw-Hill, New York, pp 185–222
McLean RJC, Nickel JC, Noakes VC, Costerton JW (1985) An in vitro study of infectious kidney stone genesis. Infect Immun 49:805–811
McLean RJC, Beauchemin D, Clapham L, Beveridge TJ (1990) Metal binding characteristics of the gamma-glutamyl capsule polymer of Bacillus licheniformis ATCC 9945. Appl Environ Microbiol 56:3671–3677
McLean RJC, Lam JS, Graham LL (2012) Training the biofilm generation—a tribute to JW Costerton. J Bacteriol 194:6706–6711
Miller VM, Rodgers G, Charlesworth JA, Kirkland BL, Severson SR, Rasmussen TE, Yagubyan M, Rodgers JC, Cockerill FR, Folk RL, Rzewuska-Lech E, Kumar V, Farell-Baril G, Lieske JC (2004) Evidence of nanobacteria-like structures in calcified human arteries and cardiac valves. Heart Circ Physiol 10:H1115–H1124
Morita RY (1982) Starvation-survival of heterotrophs in the marine environment. Adv Microb Ecol 6:171–198
Morita RY (1988) Bioavailability of energy and its relationship to growth and starvation survival in nature. Can J Microbiol 34:436–441
Morita RY (1990) The starvation-survival state of microorganisms in nature and its relationship to the bioavailable energy. Experientia 46:813–817
National Academy of Sciences (1999) Size limits of very small microorganisms: proceedings of a workshop. National Academic Press, Washington DC
Prusiner SB (1998) Prions. Proc Natl Acad Sci U S A 95:13363–13383
Schooling SR, Beveridge TJ (2006) Membrane vesicles: an overlooked component of the matrices of biofilms. J Bacteriol 188:5945–5957
Sillitoe RH, Folk RL, Saric N (1996) Bacteria as mediators of copper sulfide enrichment during weathering. Science 272:1153–1155
Southam G, Firtel M, Blackford BL, Jericho MH, Xu W, Mulhern PJ, Beveridge TJ (1993) Transmission electron microscopy, scanning tunneling microscopy, and atomic force microscopy of the cell envelope layers of the archaeobacterium Methanospirillum hungatei GP1. J Bacteriol 175:1946–1955
Staley JT, Fuerst JA (1989) Budding and/or appendaged bacteria. In: Staley JT, Bryant MP, Pfennig N, Holt JG (eds) Bergey's manual of systematic bacteriology, vol 3. Williams and Wilkins, Baltimore, pp 1890–1993
Trevors JT, Psenner R (2001) From self-assembly of life to present-day bacteria: a possible role for nanocells. FEMS Microbiol Rev 25:573–582
Uwins PJR, Webb RI, Taylor AP (1998) Novel nano-organisms from Australian sandstones. Am Miner 83:1541–1550
van Leeuwenhoek A (1712) A letter from Mr. Anthony Van Leeuwenhoek, F. R. S. containing some further microscopical observations on the animalcula found upon duckweed. Phil Trans 28:160–164

Chapter 2
S-layer Structure in Bacteria and Archaea

Chaithanya Madhurantakam, Stefan Howorka and Han Remaut

2.1 Introduction

The majority of bacteria and archaea develop multicomponent cell envelopes with layered supramolecular architectures surrounding the cytoplasmic membrane. Of the finest examples of such supramolecular cell wall components are surface or S-layers. These regular paracrystalline pericellular structures were first observed in the bacterium *Spirillum serpens* and in the archaeum *Halobacterium salinarum* (Houwink 1956, 1953). Following the confirmation that S-layers were of proteinaceous nature, the first S-layer protein (SLP) gene to be sequenced was that of *Brevibacillus brevis* 47 in 1986 (Tsuboi et al. 1986). It is now well established that S-layers are composed of monolayers of glycoproteins/proteins with an Mr range of 40–200 kDa, many of which have been thoroughly characterized by genetic and morphogenetic studies as well as by structural, biophysical and biochemical means (Altman et al. 1990; Fagan and Fairweather 2014; Kuen et al. 1994; Messner et al. 1986a, b; Sleytr et al. 1986, 1993). Generally, different SLPs give rise to defined monomolecular lattices, although bimolecular S-layers are known for *Clostridium difficile* (Takeoka et al. 1991) and *Bacillus anthracis* (Etienne-Toumelin et al. 1995). The two-dimensional (2D) arrays are formed through non-covalent self-assembly of the SLP subunits, though exceptionally covalent cross links between the protein subunits are found, as in *Methanosprillum hungatei* (Beveridge et al. 1985;

H. Remaut (✉) · C. Madhurantakam
Departments of Structural and Molecular Microbiology, Structural Biology Research Center, Vrije Universiteit Brussel, Pleinlaan 2, Brussels 1050, Belgium
e-mail: han.remaut@vib-vub.be

Department of Structural Biology Brussels, Vrije Universiteit Brussel, Pleinlaan 2, Brussels 1050, Belgium

S. Howorka
Department of Chemistry, Institute of Structural and Molecular Biology, University College London, London WC1H 0AJ, UK

L. L. Barton et al. (eds.), *Nanomicrobiology,* DOI 10.1007/978-1-4939-1667-2_2

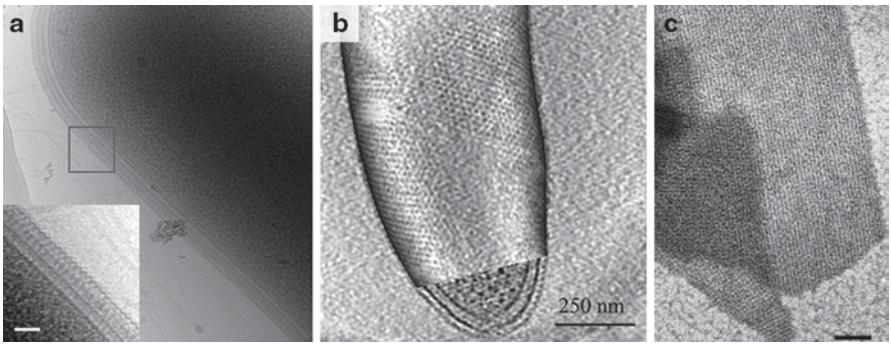

Fig. 2.1 **a** Cryo electron tomogram of the intact cell-bound S-layer (*wt*-SbpA) of *Lysinibacillus sphaericus* (formerly, *Bacillus sphaericus*), a Gram-positive soil bacterium that forms a 2D crystalline envelope with p4 symmetry (cell constant: ~13 nm). *Inset* shows the close-up view of the cell wall and the enveloping SbpA S-layer. Scale bar: 50 nm (image courtesy of Luis R. Comolli). **b** Electron tomogram of *Caulobacter crescentus* cell, overlaid with the 3D reconstruction of the RsaA S-layer, which can be seen to form hexagonal repeating units (six RsaA monomers) interconnected at their junctions by p3 symmetry. The cutaway region at the cell pole shows the S-layer as the outermost component of the cell envelope. Scale bar: 250 nm (image courtesy of Luis R. Comolli). **c** Negative stain EM micrograph of an *in vitro* self-assembly product of the *Geobacillus stearothermophilus* PV72/p2 SLP SbsB (mutant S347-HA). (Reproduced from Kinns et al. 2010). Scale bar: 100 nm

Messner et al. 2008; Sleytr and Beveridge 1999; Stewart et al. 1985). Bacterial S-layer lattices have p1, p2 (oblique), p4 (square) or p3 or p6 (hexagonal) symmetries, while archaeal S-layers are predominantly hexagonal in symmetry (Albers and Meyer 2011; Sleytr et al. 1993). Topologically, S-layers completely encapsulate the SLP-producing cell (Figure 2.1). Their mode of anchoring to the cell envelope can be broadly classified in accordance with the archaeal, Gram-positive or Gram-negative cell architecture (Pum et al. 2013). In archaea, SLPs are directly associated with the cytoplasmic membrane through a single-span transmembrane segment. The lattices form the dominant component of the cell wall and function primarily as a protective barrier, though in *Methanosarcina mazei* the SLPs were also shown to be involved in cell–cell association (Mayerhofer et al. 1992). In Gram-positive bacteria, the S-layers lie atop the peptidoglycan layer and are anchored to the peptidoglycan or the associated nonclassical secondary cell wall polymers (SCWPs; Mesnage et al. 2000; Schaffer and Messner 2005; Zhao et al. 2006). In Gram-negatives, the S-layers are associated with the lipopolysaccharides (LPS) in the outer membrane (OM; Ford et al. 2007). SLPs reach the cell surface using the general secretory pathway (SEC translocon), except in Gram-negative bacteria, where the diderm cell walls require more elaborate translocative routes such as type I and II secretion pathways (Noonan and Trust 1995; Thompson et al. 1998).

2.2 SLP Composition and Post-Translational Modifications

SLPs are distributed over a wide range of phylogenetic branches (Messner and Sleytr 1992; Sleytr et al. 1999) and generally show little (<20 % identity) to no sequence similarity, even within a single species or closely related taxons. The recent advances in SLP structural biology (Baranova et al. 2012; Ethordic et al. 2012; Fagan et al. 2009; Jing et al. 2002; Kern et al. 2011; Pavkov et al. 2003, 2008; Stetefeld et al. 2000; see below) reveal a diverse domain composition. This indicates that different SLPs do not generally have a common origin, even though relatively higher similarity is observed among S-layers of Gram-positive bacteria (Engelhardt and Peters 1998). Nevertheless, SLPs show similar overall amino acid compositions that are low in methionine and negligible cysteine. For the majority of SLPs, an enrichment in aspartic and glutamic acid results in isoelectric points (pIs) that lie in the weakly acidic range (Messner et al. 1997; Sara and Sleytr 2000), with the exception of *Methanothermus fervidus* (pI: 8.4; Brockl et al. 1991) and lactobacilli (pI: 9–11; Boot et al. 1995). An exception to the low overall sequence similarity is the ~55-amino-acid S-layer homology (SLH) motif, frequently found in tandem repeats near the N-terminus of many bacterial SLPs and surface-anchored enzymes (Mesnage et al. 2000; Schaffer and Messner 2005; Zhao et al. 2006). The X-ray structure of the three tandem SLH motifs in the *B. anthracis* surface array protein (Sap) shows that these form helix-loop-helix structures that together organize into a single three-prong spindle domain (Kern et al. 2011). The SLH domains are cell-wall-anchoring domains that bind the peptidoglycan, either directly as in *Paenibacillus alvei* CCM 2051 (Janesch et al. 2013a, b) or through the associated pyruvylated carbohydrate moieties in the nonclassical SCWPs (Mesnage et al. 2000; Schaffer and Messner 2005; Zhao et al. 2006). SLH domains are not universal S-layer-anchoring modules, however. In *Geobacillus stearothermophilus* SbsC, an extended three-helix bundle is found as N-terminal glycan-binding domain (Pavkov et al. 2008), and in *Corynebacterium glutamicum* this role is taken by the C-terminal hydrophobic domain (Bahl et al. 1997; Chami et al. 1997). In Gram-negative bacteria, the S-layers attach to the OM LPS via direct or divalent cation-mediated charge interactions as in *Campylobacter fetus* or *Aeromonas salmonicida* (Garduno et al. 1992a, b), or by covalently bound fatty acids as in *Deinococcus radiodurans* Hpi (Peters et al. 1987).

Both bacterial and archaeal SLPs are frequently glycosylated, and S-layer glycoproteins (SLGPs) have provided a major impetus to the prokaryotic glycoprotein research. SLGPs have been described for halophilic archaeons such as *H. salinarum* (glycoprotein with a M_r of 200,000 and carbohydrate content of 10–12 %; Mescher and Strominger 1976), *Haloferax volcanii* (presence of O-glycosidic linkages like "Thr/Ser-Gal" and 1, 2-linked glucosyl-galactose as a structural element in S-layer; Eichler and Adams 2005; Sumper et al. 1990), hyperthermophilic methanogens such as *M. fervidus* (Brockl et al. 1991), *Methanothermus sociabilis* and *Methanococcus voltae* (Konisky et al., 1994) and the thermoacidophilic crenarchaeote *Sulfolobus acidocaldarius* (oligosaccharide is a complex, branched, six-membered glycan tree; Peyfoon et al. 2010). In Gram-positive bacteria, SLP glycosylation is

found in clostridia and bacilli such as *Thermoanaerobacter, Geobacillus, Aneurinibacillus, Paenibacillus* and *Lactobacillus* species, whereas in Gram-negative bacteria SLP glycosylation has only been described for *Tannerella forsythia* TfsA and TfsB (Posch et al. 2011; Schaffer and Messner 2004; Sleytr and Thorne 1976). The glycan chains can be branched, though in bacteria typically contain an extended linear stretch of repeating units (10–50 units). This is frequently capped by O-methylation in the 2′ or 3′ position of the nonreducing glycan and anchored to the protein via a core of two to four sugar residues and an *O*-glycosidic linkage (galactose–tyrosine, glucose–tyrosine, N-acetyl galactosamine–serine, N-acetyl galactosamine–threonine). Archaeal glycans are shorter and generally attached by an *N*-glycosidic bond to asparagine, though O-linked chains have also been observed (Altman et al. 1996; Messner 1997; Wugeditsch et al. 1999). The number of glycosylation sites can vary from two to four in Gram-positive SLPs, to up to 25 in archaeal SLPs (Lechner et al. 1986). Additional post-translational modifications of SLPs include sulphated glycan chains of *Halobacter halobium* to provide stability to the S-layer or phosphorylation of tyrosine residues in *Aeromonas hydrophila* to decrease the pI (6.7–4.6).

2.3 Functional Diversity of S-Layers

The primary function of S-layers is to stabilize cells against mechanical, thermal and osmotic stress (Engelhardt 2007a). From the accumulated data it is evident that S-layers exhibit high levels of physical and chemical stability, indicating they can act as protective and/or shape-maintaining exoskeleton (Engelhardt and Peters 1998). For example, experiments with *Halobacteria* found that the rod-like appearance was lost upon S-layer lattice degradation. (Engelhardt 2007a; Mescher and Strominger 1976). Even though S-layers can maintain and modify the cell morphology, the endoskeleton is the primary factor in determining shape. (Baumeister and Lembcke 1992; Engelhardt 2007a; Messner et al. 1986a; Peters et al. 1995; Pum et al. 1991). Another role of S-layers is to shield against environmental and biological factors. S-layers in Gram-negative bacteria such as *A. salmonicida*, *C. fetus* and *Caulobacter crescentus* can form a protective covering towards bacterial parasites like *Bdellovibrio bacteriovorous* (Koval 1988; Koval and Bayer 1997; Koval and Hynes 1991), though the S-layers did not provide a barrier for protozoans. S-layers have also been observed to attenuate host immune responses in the periodontal pathogen *T. forsythia* (Sekot et al. 2011). In the opportunistic pathogen *C. fetus,* the surface expression of SLPs prevented binding of complement component C3b, and in *A. salmonicida* the S-layer (A-layer) imparts high to moderate levels of anti-bactericidal activity against complement systems (Dworkin and Blaser 1997). The A-layer also imparts an adhesive property, able to bind laminins, fibronectins (Doig et al. 1992) and basement membrane protein collagen type IV (Trust et al. 1993). In other pathogens like *T. forsythia, C. difficile* and *B. anthracis,* the S-layers contribute to virulence by mediating host cell adhesion (Calabi et al. 2002; Kern and Schneewind 2010; Sakakibara et al. 2007).

Besides a supporting role in maintaining cell integrity or influencing bacterial virulence, several S-layers can also function as scaffold for the adhesion of other cellular components. Archaeal S-layers are composed of long hydrophobic protrusions entering the plasma membrane, which have been proposed to provide a contact zone for macromolecules that function in folding and export of proteins and/or nutrient degradation and transport mechanisms (Lechner and Sumper 1987). Similarly, in many Bacillaceae, S-layers provide adhesion sites for cell-associated exoenzymes (Sleytr et al. 1999). Well-documented examples include the high-molecular-weight amylases in *G. stearothermophilus* strains DSM 2358 and ATCC 12980 (Egelseer et al. 1995, 1996), endo-xylanase in *Thermoanaerobacterium thermohydrosulfurigen* strain JW/SL-YS 485 (Liu et al. 1996) and endo-glucanase in *Clostridium thermocellum* (Leibovitz et al. 1997). Finally, an interesting feature observed in the unicellular cyanobacterium *Synechococcus* strain GL24 (strain isolated from a meromictic Fayetteville Green Lake, New York, USA, with high levels of calcium and sulphate ions) is that the hexagonal S-layer acts as a template for sulphate and carbonate mineral formation over its surface (Schultzelam and Beveridge 1994a, b).

Thus, although a general function of an S-layer appears to be the provision of a structurally supporting 2D array outside the cell, various genetic and functional studies found that they are phylogenetically and structurally dissimilar and attain varied roles in cellular activities, leading to a high degree of functional heterogeneity.

2.4 Structural Biology of S-Layers

Over the past two decades, there has been a steady increase in the level of molecular and structural understanding of the surface layer proteins (Table 2.1). In the initial phase, S-layer structural biology was mainly based on freeze-etching, freeze-drying, negative staining followed by 2D and 3D transmission electron microscopy (TEM) and on scanning probe microscopy (Beveridge 1993; Beveridge et al. 1993; Firtel et al. 1994b). This was followed by efforts towards the 3D prediction of the building components using the mean force approach, and by simulations of self-assembly process by Monte-Carlo simulations (Horejs et al. 2008, 2011). Cryo-electron microscopy and tomography (cryo-EM, cryo-ET) in turn provided depth to the topographical information derived from the SLPs (Baumeister and Lembcke 1992; Kinns et al. 2010; Norville et al. 2007; Rachel et al. 1986; Shin et al. 2013; Smit et al. 1992; Figure 2.1). Atomic force microscopy (AFM) has provided dynamic views of the crystallization pathways during in vitro S-layer formation (Chung et al. 2010; Shin et al. 2012). The search for high resolution structural information by 3D crystallization of SLPs has long been plagued by the inherent tendency of SLPs to form 2D lattices. Nevertheless, in recent years, X-ray crystallography has started to reveal the molecular architecture of the SLPs and/or non-assembling SLP fragments (Baranova et al. 2012; Ethordic et al. 2012; Fagan et al. 2009; Jing et al. 2002; Kern et al. 2011; Pavkov et al. 2003, 2008; Stetefeld et al. 2000; Figures 2.2, 2.3, 2.4, 2.5, 2.6, 2.7, 2.8) and provide more molecular insights into the assembly of the supramolecular structures. In the following paragraphs, these recent advances in SLP structural biology are systematically reviewed. As common feature, bacterial SLPs

Table 2.1 Archaeal and bacterial members with characterized S-layers and methods employed to analyze the properties and structural characteristics of the S-layer lattice

Species	Methods employed	Reference
Acinetobacter sp. strain MJIT/F5/199A	EM	Thornley et al. (1973)
Aeromonas salmonicida A449-TM5	EM	Dooley et al. (1989); Garduno et al. (1992a, b); Stewart et al. (1986)
Aeromonas hydrophila TF7	EM	Al-Karadaghi et al. (1988); Dooley and Trust (1988); Murray et al. (1988)
Aneurinibacillus thermoaerophilus	Negative staining, thin-sectioning and immuno-gold labelling, EM	Kadurugamuwa et al. (1998)
Aneurinibacillus thermoaerophilus DSM 10155	Spectroscopy	Steindl et al. (2002)
Aquaspirillum serpens MW5	SAXS	Sekot et al. (2013)
Bacillus anthracis	EM	Etienne-Toumelin et al. (1995); Mesnage et al. (1997)
	X-ray crystallography	Kern et al. (2011)
Bacillus coagulans E38-66	Atomic force microscopy (AFM)	Dufrene (2001)
	EM	Sara et al. (1992)
	Freeze etching	Pum et al. (1989)
Bacillus pseudofirmus OF4	EM, 2D gel-electrophoresis	Gilmour et al. (2000)
Bacillus subtilis 168	EM	Graham and Beveridge (1994)
Bacillus sphaericus CCM2177	AFM	Gyorvary et al. (2003); Toca-Herrera et al. (2004)
	Scanning force microscopy (SFM)	Ohnesorge et al. (1992)
	Molecular recognition force spectroscopy (MRFS)	Tang et al. (2008)
	TEM, SAXS	Horejs et al. (2010)
	SPR	Huber et al. (2005)
	Cryo-EM, tomography, spectroscopy	Shin et al. (2013)
	Electron crystallography	Norville et al. (2007)
Bacillus sphaericus NCTC 9602	TEM and electron holography	Simon et al. (2004)
Bacillus stearothermophilus NRS2004/3a	EM	Kupcu et al. (1984); Messner et al. (1986a); Sleytr et al. (1986)
	Spectroscopy, mass spectrometry (MS)	Steiner et al. (2006)
Bacillus stearothermophilus PV72/p2	EM	Howorka et al. (2000); Sara et al. (1998)
	Spectroscopy	Runzler et al. (2004)
	Limited proteolysis, spectroscopy, Cryo-EM	Kinns et al. (2010)
Caulobacter crescentus	Negative staining, thin-section EM	Smit et al. (1992)
	Cryo-electron tomography (Cryo-ET) and statistical image processing	Amat et al. (2010)

Table 2.1 (continued)

Species	Methods employed	Reference
Clostridium difficile	MS and EM	Calabi et al. (2001)
Clostridium difficile CD630	X-ray crystallography and SAXS	Fagan et al. (2009)
Clostridium thermocellum	Immuno-blotting, EM	Leibovitz et al. (1997)
Clostridium thermohydrosulfuricum L111-69 *Clostridium thermosaccharolyticum* D120-70	Freeze etching, EM	Sara et al. (1988)
Corynebacterium glutamicum	AFM imaging, single molecule force spectroscopy (SMFS)	Scheuring et al. (2002)
	Freeze-etching, EM	Peyret et al. (1993)
	Cryo-electron microscopy of vitreous sections (CEMOVIS)	Zuber et al. (2008)
Deinococcus radiodurans	AFM	Karrasch et al. (1994); Lister and Pinhero (2001); Muller et al. (1996, 1999); Wiegrabe et al. (1991)
	Cryo-microscopy	Baumeister et al. (1986); Karrenberg et al. (1987); Rachel et al. (1986); Sleytr et al. (1973)
Desulfotomaculum nigrificans	EM	Sleytr et al. (1986)
Escherichia coli K29	EM	Koval and Bayer (1997)
Geobacillus stearothermophilus	X-ray crystallography and SAXS	Pavkov et al. (2003, 2008)
Geobacillus stearothermophilus ATCC 12980	SAXS	Sekot et al. (2013)
Geobacillus stearothermophilus NRS2004/3a	Spectroscopy, MS	Schaffer et al. (2002)
Geobacillus stearothermophilus PV72/p2	Spectroscopy, MS, electrospray spectrometry (ES)	Petersen et al. (2008)
	EM	Kinns et al. (2010)
	X-ray crystallography, cryo-EM and SAXS	Baranova et al. (2012)
Lactobacillus brevis ATCC 14869	EM	Jakava-Viljanen et al. (2002)
Lactobacillus buchneri CD034	MS	Anzengruber et al. (2013)
Lactobacillus helveticus CNRZ 892	Immuno-blotting, EM	Callegari et al. (1998)
Lactobacillus salivarus 16	Spectroscopy and thermal denaturation	Lighezan et al. (2012)
Lysinibacillus sphaericus	Cryo-EM, Cryo-ET	Shin et al. (2013)
Methanosarcina mazei	X-ray crystallography	Jing et al. (2002)
Methanosarcina acetivorans	X-ray crystallography	Arbing et al. (2012)
Methanospirillum hungatei Gp1	Scanning-tunnelling microscopy (STM) Thin sectioning, negative staining, platinum shadowing and image processing, EM	Blackford et al. (1994) Firtel et al. (1994a, b)

Table 2.1 (continued)

Species	Methods employed	Reference
Staphylococcus marinus	EM	Peters et al. (1955)
Staphylothermus marinus	X-ray crystallography	Stetefeld et al. (2000)
Tannerella forsythia	TEM, immune-fluorescence microscopy (IFM) and AFM	Oh et al. (2013); Sekot et al. (2011, 2012)
	Spectroscopy	Posch et al. (2011, 2013)
Thermococcus litoralis Z-1301	Thin-sectioning, freeze etching, EM	Kostyukova et al. (1999)
Thermoproteus tenax *Thermoproteus neutrophilus*	Freeze etching, freeze drying, negative staining, image enhancement, EM	Messner et al. (1986a)

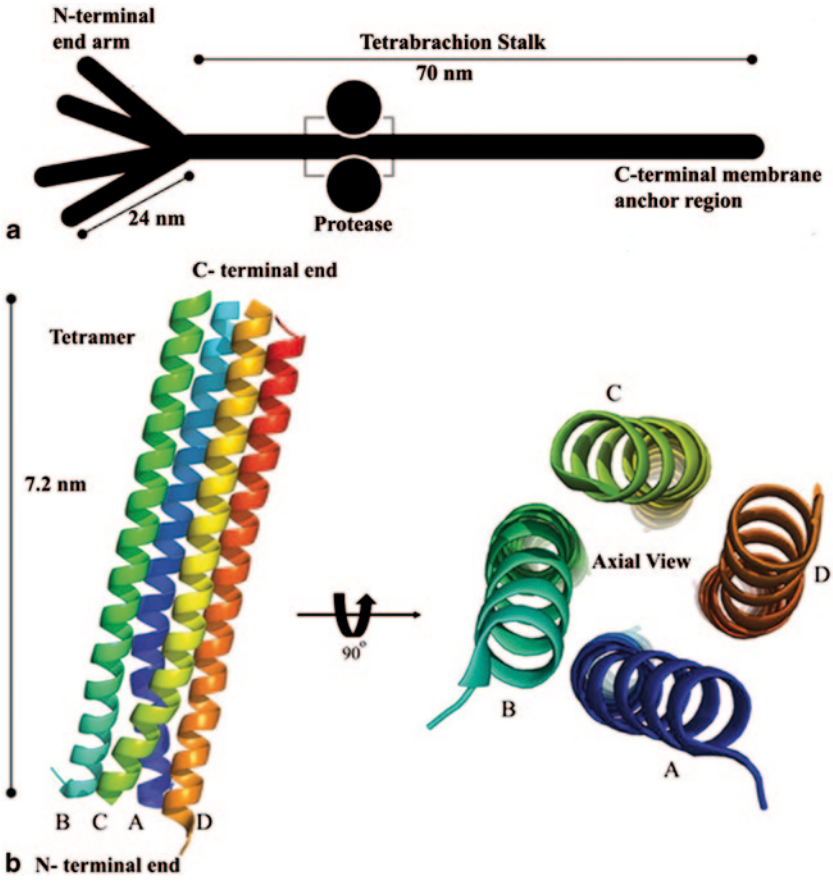

Fig. 2.2 **a** Schematic diagram of the *S. marinus* SLP which forms a filiform tetrameric unit called tetrabrachion (70 nm in length). The tetrabrachion is composed of an extended parallel-coiled coil stalk region with C-terminal membrane anchor region and four extending arms (24 nm each in length) at its N-terminal end (Peters et al. 1995). The tetrameric stalk contains a protease (represented as *globular structures*)-binding domain, the atomic structure of which (*grey boxed area*) is shown in panel **b**. **b** Crystal structure of the right-handed parallel coiled coil region (RHCC) (PDB code: 1FE6) corresponding to the protease-binding domain (*grey boxed area*), shown in lateral and axial view. (Stetefeld et al. 2000)

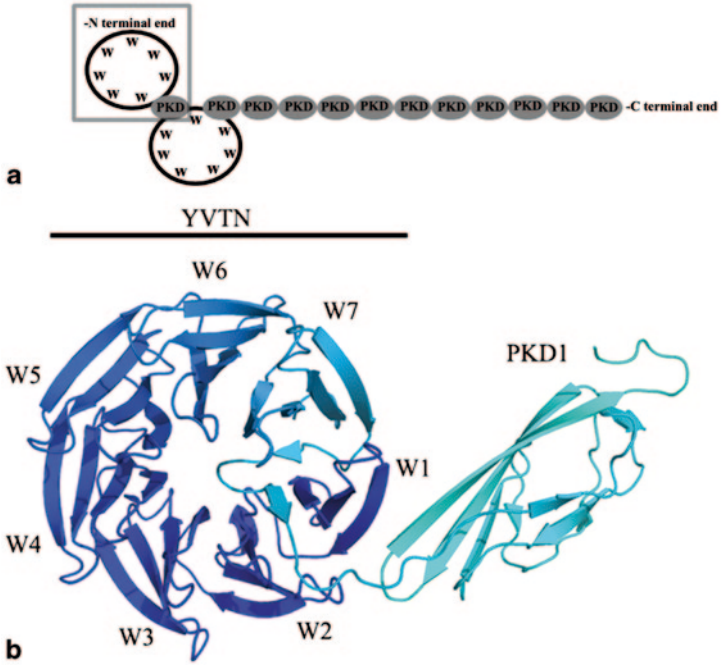

Fig. 2.3 **a** Schematic representation of the domain composition of the *M. mazei* SLP MA1904 (Jing et al. 2002). At its N-terminus, the SLP contains two "YVTN" β-propeller domains (each with seven blades composed of four-stranded β-sheets labelled *W*), followed by twelve (1+11) consecutive PKD domains. **b** Crystal structure of a 42 kDa N-terminal SLP fragment (*boxed area* in panel **a**) reveals the molecular structure of a "YVTN" β-propeller domain (blades labelled *W1 to W7*) and a single-polycystic-kidney disease (*PKD1*) domain (PDB code: 1L06)

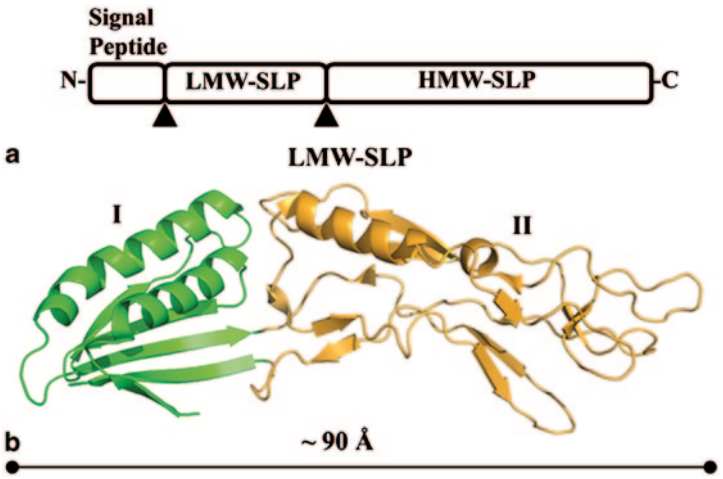

Fig. 2.4 **a** Domain architecture of the SlpA preprotein from *C. difficile* CD 630. The preprotein is proteolytically processed into a high- and low-molecular weight SLP (*HMW-* and *LMW-SLP*, resp.). Cleavage sites are represented by *small triangles*. **b** Crystal structure of LMW-SLP$_{1\text{-}262}$ (PDB code: 3CVZ) encompassing domains I and II, spanning ~90 Å in length

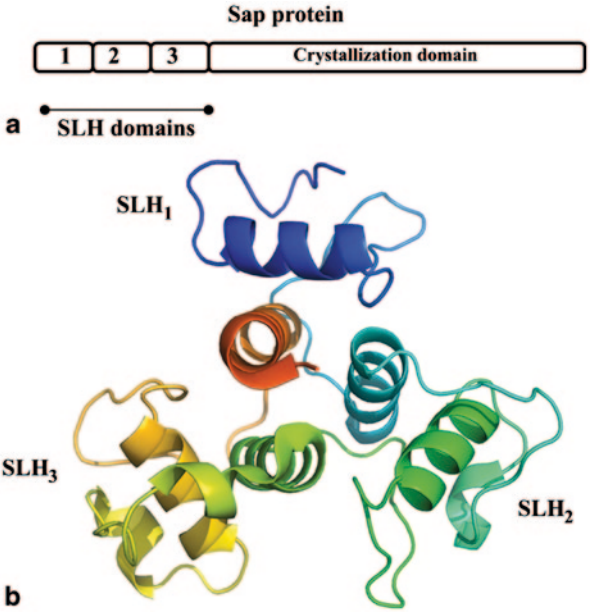

Fig. 2.5 **a** Schematic representation of the Sap protein from *B. anthracis*, indicating the N-terminal SLH domains and C-terminal crystallization domain. **b** Crystal structure of the cell-wall-anchoring domain of Sap (residues 31–210) (PDB code: 3PYW) with the SLH domains labelled as SLH_1, SLH_2 and SLH_3

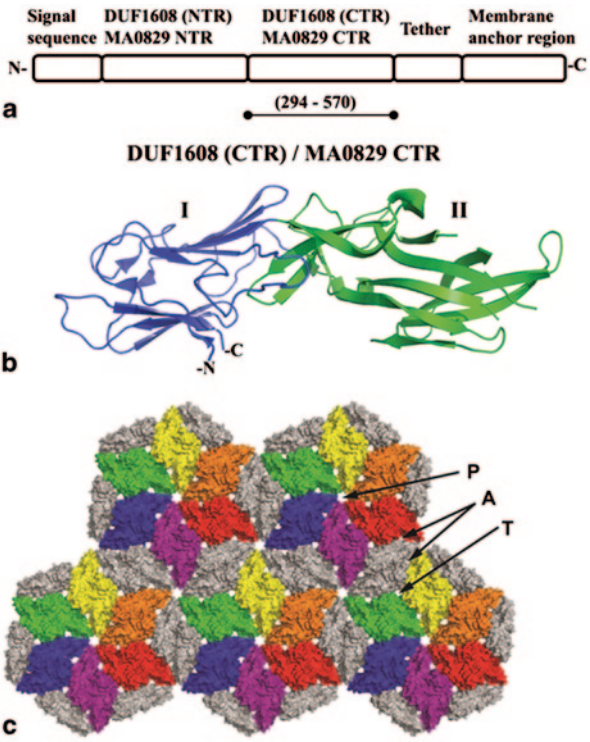

Fig. 2.6 **a** A schematic representation of the *M. acetivorans* MA0829 S-layer protein with N-terminal signal sequence, followed by a tandem repeat of DUF1608 domains (*NTR* and *CTR*), a tether sequence and finally, the C-terminal membrane-anchoring region. **b** The crystal structure of DUF1608 (CTR)/MA0829 CTR (294–570 residues) (PDB code: 3U2G) reveals two subdomains, domain I and II. **c** Putative model of the MA0829 S-layer lattice generated based on crystallographic dimers of the CTR. The model shows a semiporous lattice with three distinct pores, labelled *P* (primary), *A* (asymmetric) and *T* (trimer). (Image courtesy of Mark A. Arbing)

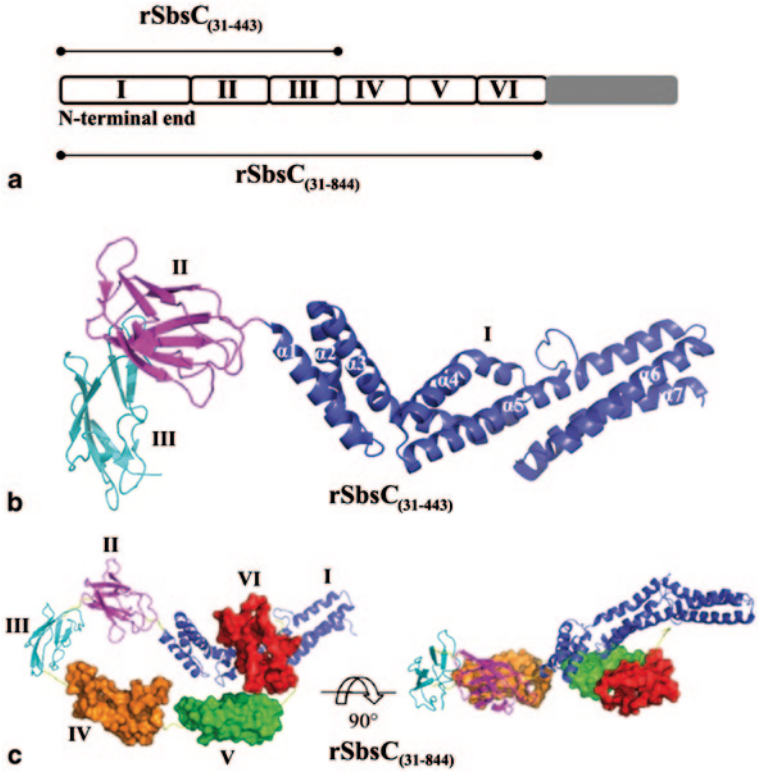

Fig. 2.7 **a** A schematic representation of domain composition of SbsC from *G. stearothermophilus* with experimentally observed domains labelled *I–VI,* followed by a C-terminal fragment of unknown domain structure, coloured grey. Domains I–III correspond to $rSbsC_{(31-443)}$ and domains I–VI correspond to $rSbsC_{(31-844)}$. **b** Crystal structure of $rSbsC_{(31-443)}$ (PDB code: 2RA1) revealing the N-terminal cell wall attachment domain (domain *I*, α1–α7) and partial C-terminal crystallization domains (*II* and *III*). **c** Crystal structure $rSbsC_{(31-844)}$ (adapted from Pavkov et al. 2008), with the modelled structure comprising the domains I, II and III shown in ribbon representation and the unmodelled density for domains IV, V and VI in surface representation. Domains II–VI form a planar, ring-like structure similar to that seen in SbsB (see Figure 2.8). Adjacent view is by a lateral rotation of 90°

appear to have the self-assembling or "crystallization domain" located in the C-terminal part of the protein, preceded by the cell-wall-anchoring domain(s), mostly SLH domains, at the N-terminus. The SLH domains are present in the majority of bacterial SLPs, though there are exceptions like SbsC in *G. stearothermophilus* (Pavkov et al. 2008).

2.4.1 Structure of SLP Fragment from Staphylothermus marinus

Staphylothermus marinus is a hyperthermophilic archaeobacterium. EM studies provided initial insight into its S-layer (Peters et al. 1995). The SLP subunits organize into ~70-nm-long filiform "tetrabrachions" (M_r 92,000) by tetramerization via

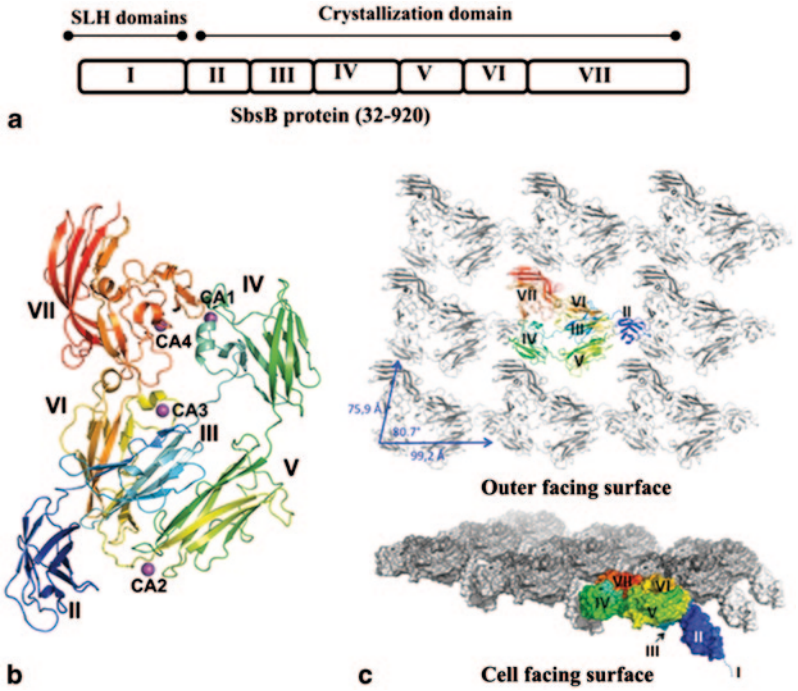

Fig. 2.8 **a** A schematic representation of domain composition of mature SbsB from *G. stearothermophilus* show the N-terminal cell wall attachment domain, domain I (composed of three SLH domains), and the C-terminal crystallization domain composed of domains II–VII that can self-assembly to form the S-layer lattice. **b** Crystal structure of $SbsB_{32-920}$ (PDB code: 4AQ1) in complex with the single domain antibody NbKB6 (not shown in the figure), with domains II–VII in a φ-shaped, disk-like quaternary structure. **c** Ribbon and space-filling representation of the calculated S-layer model in extracellular view (*top panel*) and side view, with the cell-wall facing surface pointing down (*lower panel*). For clarity, one protomer is coloured in *rainbow* from N- to C-terminus

a parallel, four-stranded α-helical structure (Figure 2.2). The presence of leucine and isoleucine throughout the hydrophobic core in the long α-helical stalk provides an extreme level of structural stability resistant to heating at 130 °C in the presence of 1 % (*w/v*) dodecyl sulphate or 6M guanidine (Peters et al. 1996). The 1.8 Å X-ray structure of a 52-amino-acid recombinant fragment encompassing a protease-binding region of the tetrabrachion (PDB code: 1FE6) shows a right-handed coiled coil structure (RHCC; with dimensions of ~ 72 Å length and ~ 25 Å in diameter, respectively; Stetefeld et al. 2000; Figure 2.2b). Three intra-helical (Glu 24—Lys27; Asp 10—Arg14 and Asp 21—Arg 22 pairs) and four inter-helical (Arg 33—Asp 35; Arg 36—Glu 38; Asp 20—Arg 22 and Asp 9—Arg 14 pairs) salt bridges provide electrostatic interactions in the coiled coil structure. The RHCC is further stabilized by a series of complex hydrophobic interactions between the four helices (Peters

et al. 1995, 1996). This RHCC crystal structure provides a deeper understanding of the stability of hyperthermophilic proteins and has helped inspire de novo design strategies for thermostable protein scaffolds.

2.4.2 Structure of SLP from M. mazei

The 2.4-Å resolution structure of an N-terminal fragment from the MA1904 SLP from the methanogenic archaeobacterium *M. mazei* provides structural information on an architecturally different class of archaeal SLPs (PDB code: 1L0Q; Jing et al. 2002). MA1904 is a 1564-residue mature protein has a repeating domain organization featuring two YVTA heptarepeat domains and a series of polycystic-kidney disease (PKD)-like domains (Figure 2.3a). Jing et al. (2002) crystallized a 42-kDa MA1904 fragment encompassing the N-terminal YVTN heptarepeat domain (residues 1–302) and the subsequent PKD domain (residues 303–391). The YVTN repeats give rise to a seven-bladed β-propeller, with each propeller blade composed of a four-stranded antiparallel β-sheet, while the PKD domain is formed of an eight-stranded β-sandwich (Figure 2.3b). Based on these domain structures, the full-length *M. mazei* SLP can be discerned to comprise 14 YVTN repeats grouped in two β-propeller domains and 12 PKD domains. Apart from MA1904, genome analysis of metazoans reveals similar six-bladed YWTN β-propeller domains in cell surface and extracellular matrix-associated proteins. These are sequentially similar to the YVTN β-propeller domain seen in the MA1904 structure and are expected to differ only at the position of a β-bulge in β-strand 4 (Jing et al. 2002) and the number of propeller blades. Along with these two domains, many SLPs in archaea also exhibit a third kind of repeat, which is predicted to form a right-handed parallel β-helix domain (Galagan et al. 2002).

2.4.3 Structure of SlpA from C. difficile

SlpA is a surface layer protein from the Gram-positive, spore-forming, anaerobic bacterium *C. difficile,* which causes opportunistic gastrointestinal tract infections called *C. difficile*–associated disease (CDAD; Fagan et al. 2009; Poxton et al. 2001). The *C. difficile* S-layer contains a 374-residue "high molecular weight SLP" (HMW-SLP) and a 321-residue "low molecular weight SLP" (LMW-SLP), which associate to form a tight non-covalent complex (H/L) that gives rise to an elongated particle, as revealed by small-angle X-ray scattering (SAXS) analysis (Fagan et al. 2009). A 3D crystal structure is available of a LMW-SLP (321 amino acid residues in length, 34.2 kDA without signal peptide) from *C. difficile* CD630 determined at 2.4 Å resolution (PDB code: 3CVZ). The crystal structure reveals that LMW-SLP is composed of two non-contiguous domains (Figure 2.4b; Fagan et al. 2009). Domain 1 encompasses residues 1–88 and 239–249 that form a two-layered sandwich

structure composed of a five-stranded mixed β-sheet that is packed against a pair of antiparallel α-helices. Domain 2 encompasses residues 89–238 and exhibits a novel fold with two β-hairpins (residues 150–170 and 211–227) and an elongated α-helix (residues 97–111), interspersed by extended loop regions. Mutagenesis studies show the C-terminal end of LMW-SLP to be involved in the formation of the LMW–HMW complex. Further, the HMW-SLP contains the "cell-wall-binding" motifs (PF04122; Calabi et al. 2001) that anchor the protein to the cell wall.

2.4.4 Structure of the SLH Domain of Sap from B. anthracis

Sap is an SLP in the Gram-positive, rod-shaped, spore-forming mammalian pathogen *B. anthracis*. As many other bacterial SLPs, Sap utilizes three consecutive surface-layer homology (SLH) repeats to be tethered to the secondary cell wall polysaccharide (SCWP) in the bacterial cell envelope (Mesnage et al. 2000). Kern et al. provided the first crystal structure of an SLH domain (Sap_{SLH}, residues 31–210, N-terminal His-tag), solved at a resolution of 1.8 Å (Kern et al. 2011; PDB code: 3PYW; Figure 2.5a, b). The 3D structure is defined to be a three-pronged spindle with each prong arising from a single SLH repeat. The spindle's base is formed by a three-helical bundle that is formed by the three SLH domains, each providing a single helix. Solvent-accessible surface area analysis revealed that each SLH repeat contains a small tunnel. The SLH domains (SLH_1, residues 31–90; SLH_2, residues 91–151; SLH_3, residues 152–209) exhibit a partially conserved ITRAE motif (not shown in figure). Both the tunnels and ITRAE motifs contribute positively charged residues to the surface structure of inter-prong grooves formed by all the three prongs of SLP. Kern et al. (2011) propose that these positively charged residues play a major role in binding of SLP to the pyruvyl-ketal of SCWP.

2.4.5 Structure of the DUF1608 Domain of Methanosarcina acetivorans

M. acetivorans is a methanogenic archaeon that has its cytoplasmic membrane surrounded by an S-layer composed of a single protein, MA0829. Depending on the environmental conditions, the S-layer may additionally be covered with a layer of heteropolysaccharide (methanochondroitin; Francoleon et al. 2009; Sowers et al. 1993a, b). Two crystal structures of the C-terminal DUF1608 domain of *M. acetivorans* MA0829 were reported at 2.3 and 2.36 Å resolutions, respectively (Arbing et al. 2012; PDB codes: 3U2H and 3U2G; Figure 2.6). The mature MA0829 (671 residues) consists of a signal sequence followed by an N-terminal DUF1608 domain (DUF1608 (NTR)/MA0829 NTR) and a C-terminal DUF1608 domain (DUF1608 (CTR)/MA0829 CTR; Arbing et al. 2012; Bateman et al. 2010). The crystal structure of MA0829 CTR exhibits two structurally related domains (rmsd:

3.1 Å, sequence identity: 3 %) comprising two antiparallel β-sheets that give rise to a β-sandwich fold. Both the N- and C-terminal ends are located nearer to the domain I. The polypeptide chain crosses domain I to domain II and folds back to form the bipartite CTR structure and, during the process, creates a connector domain (~40-amino-acid, three-stranded β-sheet). Domain II has an additional three-stranded β-sheet observed to be attached to one of the β-sheets.

The MA0829 CTR possesses a hexagonal lattice and is used to model the basic repeating unit of the S-layer (Figure 2.6b). Around a threefold crystallographic axis, three CTR dimers (trimeric unit) are arranged to form the repeating unit. Using this trimeric unit, a translation in two dimensions creates a sheet with sixfold symmetry that is similar to the architecture of hexagonal S-layers visualized by EM for archaea (Figure 2.6c). The 2D S-layer lattice is stabilized by a series of extensive intermolecular interactions including hydrogen bonds, salt bridges and van der Waals interactions. The modelled S-layer reveals three types of pores classified as P or primary pores (pores on sixfold axis; ~13 Å in diameter), T or trimer pores (pores on the three-fold axis at the center of trimer; ~8 Å in diameter) and A or asymmetric pores (pores at the interface of two trimers; 5 × 14 Å in dimensions). All these pores are expected to assist in the passage of small molecules nutrients, and due to large pore size; P pores may assist in passage of siderophores, oligos and lipids.

2.4.6 *Structures of SbsB and SbsC from G. stearothermophilus*

G. stearothermophilus is a Gram-positive, rod-shaped thermophilic bacterium encased in a rigid cell wall composed of peptidoglycan (A1-γ chemotype) and an SCWP composed of 2,3-diacetamido mannosamine uronic acid, N-acetyl glucosamine and glucose in wild-type strains; or N-acetyl glucosamine, N-acetyl mannosamine and pyruvic acid in variant strains (Egelseer et al. 1998; Mader et al. 2004; Schaffer et al. 1999). Five different SLPs have been identified in various strains of *G. stearothermophilus*, namely SbsA (wild-type strain PV72/p6, hexagonal lattice type; Kuen et al. 1994), SbsB (oxygen-induced variant strain PV72/p2, oblique lattice type; Scholz et al. 2001), SbsC (strain ATCC 12980, oblique lattice type; Jarosch et al. 2000, 2001), SbsD (strain ATCC 12980 under high temperatures of 67 °C, oblique lattice type; Egelseer et al. 2001) and SgsE (strain NRS 2004/3a, oblique lattice type; Schaffer et al. 2002; Pavkov et al. 2011). The N-terminal ends of SbsA, SbsC, SbsD and SgsE share higher sequence similarity and are capable of binding to the same SCWP (Egelseer et al. 2001; Pavkov et al. 2011; Schaffer et al. 2002). The C-terminal crystallization domains of these SLPs show little sequence conservation, except for SbsD and SgsE which share 94 % sequence identity. SbsB shows an overall low sequence similarity with SbsA, SbsC, SbsD and SgsE.

A partial crystal structure of SbsC was reported at 2.4 Å resolution, corresponding to a C-terminal truncation mutant spanning the first 412 residues of the mature protein ($rSbsC_{(31–443)}$; PDB code: 2RA1; Pavkov et al. 2008; Figure 2.7). The structure reveals an overall architecture that is composed of an α-helical N-terminal

domain corresponding to the cell-wall-anchoring domain, followed by a string of consecutive β-sandwich domains that are part of the C-terminal crystallization domain. The N-terminal domain of $rSbsC_{(31–443)}$ (domain I, residues 32–260) comprises seven α-helices organized into three three-helix bundles that give rise to a unique "banana-shaped" conformation (Figure 2.7a). The interface of the first and second triple-helical bundle is interspersed with aromatic residues, and the presence of kinks in α4 and α5 in the second triple-helical bundle due to larger residues (Tyr 130, Arg 167, Arg 184 and Lys188) results in an increased exposure of the hydrophobic core region between the α-helices. The third triple-helical bundle exhibits a canonical coiled-coil structure (Lupas and Gruber 2005; Pavkov et al. 2008). Surface plasmon resonance (SPR) studies revealed that specific binding of SCWP to SbsC is facilitated by the N-terminal end of the SbsC ($rSbsC_{(31–270)}$; Ferner-Ortner-Bleckmann et al. 2009). Binding experiments with SCWP and further biochemical analyses reveal that the N-terminal end stabilizes upon binding to the SCWP and this is ascribed to the presence of regularly spaced, positively charged residues on the putative ligand-binding surface matching the negatively charged residues on elongated SCWP. In the crystallization domain, domains II (residues 261–331; two anti-parallel β-sheets) and III (residues 332–443; three anti-parallel β-sheets) adopt immunoglobulin-like (Ig-like) folds (Figure 2.4b) and are believed to take part in intermolecular domain–domain interactions in the S-layer (Luo et al. 2000; Pavkov et al. 2008). The crystal structure of a larger SbsC fragment ($rSbsC_{(31–844)}$) reveals an elongated molecule with an additional three compact β-domains compared to $rSbsC_{(31–443)}$. Although poor electron density prevented model building for domains IV–VI, these can be seen to form a ring-like structure together with domains II and III (Figure 2.7c).

Subsequently, the crystal structure of full-length SbsB (residues 32–920 in mature SbsB) was reported at 2.4 Å (Figure 2.8) and provided the first structural insight into a full-length SLP (Baranova et al. 2012). To avoid the formation of S-layer self-assembly products, the protein was crystallized in complex with a single-domain antibody, or nanobody ($SbsB_{32–920}$:NbKB6). The mature SbsB comprises a functional N-terminal cell-wall-anchoring region with three SLH motifs and a C-terminal crystallization domain that can assemble in an oblique (p1 symmetry) 2D lattice with unit cell vectors $a = 104$ Å, $b = 79$ Å and base angle $\gamma = 81°$ (Moll et al. 2002). The crystal structure reveals seven domains of which the N-terminal domain (domain I, 32–201 residues) is not resolved due to poor electron density. The domains II–VII are arranged in a φ-shaped, disk-like quaternary structure that corresponds to the self-assembling crystallization domain of the protein (dimensions of 70 Å × 110 Å × 35 Å; Figure 2.8b). This arrangement creates a single plane (domains IV to VII) with an annular structure that encloses a cavity of ~24 Å in diameter. A nine-residue linker between domains IV and III (present at the rim of the ring) passes across the cavity and the domain II protruding away from the ring structure gives the final φ-shaped structure. The domains II and III correspond to C_1-type Ig folds, domains IV, V and VII correspond to I-type Ig fold, whereas the domain VII is a mixed fold with an Ig-like β-sandwich core along with a random-coil subdomain. The modular build-up of the crystallization domain by consecutive

Ig folds and their supramolecular organization is highly reminiscent of the ring-like architecture formed by domains II–VI in SbsC. Domains II and III in SbsB are structurally equivalent to those in SbsC, with rmsd values of 1.35 and 2.57 Å, respectively, suggesting that despite the low sequence identity SbsB and SbsC form a structurally similar SLP.

Chemically denatured SbsB refolds rapidly in the absence of a chaotropic agent and in the presence of Ca^{2+} ions (Runzler et al. 2004). The SbsB crystals structure reveals four bound Ca^{2+} ions that mediate inter-domain and intra-domain contacts (CA1 to CA3 ions; through a pentagonal bipyramidal coordination and CA4 ion through an octahedral coordination). CA1 is shared by domains IV and VII and is coordinated with a water molecule (W2063) along with the residues Gln 406, Thr 440 from domain IV and Asp 779, Asp 781 in domain VII. CA2 ion is at the interface of domains V and VI (located closer to domain V) and exhibits coordination with a water molecule (W2125) and residues from domain V (Asp517, Gln 518, Asp 592, Asn 624 and Val 625). CA3 ion shares coordination with two water molecules (W2153, W2154) and residues from domain VI (Ala 646, Thr 649, Ser 651 and Arg 654). Finally, CA4 ion is coordinated by the residues from domain VII (Glu 784, Gly 822, Asn 824, Asp 835, Glu 836 and Glu 837; Baranova et al. 2012). Circular dichroism and SAXS analysis showed the importance of Ca^{2+} ions for the adoption of the SbsB quaternary structure. Ethylenediaminetetraacetic acid (EDTA)-treated SbsB samples retained the secondary structure in the individual β-sandwich domains, but lost the φ-shaped quaternary structure and instead resulted in a dynamic beads-on-a-string architecture. Cryo-EM and chemical cross-linking data from SbsB S-layers showed that the φ-shaped conformers form the self-assembling species, which are juxtaposed in the plane of the disk-like crystallization domain (Baranova et al. 2012). The Ca^{2+}-triggered conformational reorganization of domains II–VII primes the SbsB protomers for self-assembly by prepositioning the interactive surfaces in the β-sandwich domains. In this way, a semi-porous monolayer is formed (Figure 2.8c). Intermolecular contacts are formed by domains IV and VII, and domains IV and II. The latter ducks underneath an adjacent monomer and connects the crystallization domain to the N-terminal cell wall attachment domain. Interestingly, the domain II position was not rigid throughout the recombinant SbsB S-layer, possibly providing a conformational hinge between the SLP lattice and the nonuniform topology of the supporting cell wall.

2.5 Applications

The intrinsic capability of SLPs to self-assemble into semi-porous monolayers with defined structural properties has raised interest from the fields of material sciences and biotechnology (Ilk et al. 2011; Pavkov et al. 2011). Ordered S-layer fragments can be extracted from their bacterial hosts, or can be produced by (re)crystallizing the isolated proteins directly in solution or more commonly at liquid–air, liquid–solid and liquid–lipid interfaces (reviewed in Pum et al. 2013). Due to the presence

of pores with identical shape and morphology, S-layers have been utilized as efficient isoporous ultrafiltration membranes (Sara and Sleytr 1996; Sleytr et al. 1997, 1999). Such S-layer ultrafiltration membranes (SUMs) have been created by the deposition of S-layer assembly products over microfiltration membranes (Weigert and Sara 1995, 1996). Integration of functional groups in S-layers has also enabled a broad spectrum of applications owing to the topological alignment of the introduced functionalities. In affinity matrices, this property helps in binding molecules with higher specificity and affinity (Sleytr et al. 1999). S-layer microparticles or SMPs are cell wall fragments with S-layers having both the outer and inner S-layer cross-linked by glutaraldehyde (Breitwieser et al. 1996; Kupcu et al. 1995, 1996). These SMPs are used as affinity particles for covalent attachment of biologically active macromolecules (Kupcu et al. 1995). Monoclonal antibodies from serum have been isolated and purified using SMPs that are covalently linked to protein A which allows affinity binding of the Fc portion of the majority of mammalian antibodies (Weiner et al. 1994a, b). Affinity microparticles of 1–2-μm size have been prepared from the hexagonal S-layer lattice of *Clostridium thermohydrosulfuricum* L111–69, and used to isolate and purify IgG from artificial IgG–human serum albumin mixtures by affinity cross-flow filtration (Weiner et al. 1994a, b). Furthermore, S-layers have been considered for S-layer vaccine technology, allowing a high density display of recombinantly or chemically introduced epitopes. Smith et al. (1993) observed that when tumour-associated glycans (T- or Lewis Y antigen) are coupled with glutaraldehyde-cross-linked SLPs of Gram-positive bacteria, they gave rise to a stronger hapten-specific delayed-type hypersensitivity (DTH) response (Smith et al. (1993). The availability of a number of immunologically non-cross-reactive S-layers that can be utilized as combined carrier/adjuvant system has been suggested to provide molecular tools for anti-allergic immunotherapy (Jahn-Schmid et al. 1996, 1997) and for therapeutic cancer vaccines (Smith et al. 1993). Recrystallizing S-layer subunits on liposomes and cross-linking with glutaraldehyde produced closed biomimetic structures that resemble archaeal cells (Kupcu et al. 1995, 1998). In particular, the S-layer subunits of *B. stearothermophilus* PV72/p2 has been recrystallized on liposomes and used as a matrix for binding and entrapping functional molecules (Mader et al. 1999, 2000).

In material sciences, S-layers have been used as patterning resists for the deposition of inorganic materials into regular 2D arrays (Allred et al. 2008; Shenton et al. 1997) The SLPs of *G stearothermophilus* have also been recrystallized using gold colloids, cross-linked to each other and applied as electrochemical sensing tools by wrapping them around single-walled carbon nanotubes (CNT) allowing novel approaches in nanoelectronic biosensor applications (Park et al. 2011). By recrystallizing the SbpA (*B. sphaericus*) on amorphous and semicrystalline polyactide derivatives, new bio-supramolecular structures could be fabricated (Lejardi et al. 2013). In the creation of biomimetic sensors that involve sensitive microelectronic devices attached to biological systems, an attached lipid membrane intact with integral proteins (natural/designed) offers a good platform to perform scientific studies. These lipid membranes can be supported by S-layer assembled on metal or semiconductor surfaces that can be used as a separating layer in order to retain the

fluidity and stability of the lipid membrane, thereby providing an ion reservoir and required space for the proteins within the membrane (Schuster et al. 2004).

Available examples demonstrate that the scaffolding and organizing properties of S-layers can be employed to devise distinct biomimetic structures in a wide range of applications. It is expected that the increasing understanding of the SLP structure and dynamics will further enhance their application.

References

Al-Karadaghi S, Wang DN, Hovmoller S (1988) 3-Dimensional structure of the crystalline surface-layer from *Aeromonas hydrophila*. J Ultra Mol Struct R 101:92–97

Albers SV, Meyer BH (2011) The archaeal cell envelope. Nat Rev Microbiol 9:414–426

Allred DB, Cheng A, Sarikaya M et al (2008) Three-dimensional architecture of inorganic nanoarrays electrodeposited through a surface-layer protein mask. Nano Lett 8:1434–1438

Altman E, Brisson JR, Messner P et al (1990) Chemical characterization of the regularly arranged surface layer glycoprotein of *Clostridium thermosaccharolyticum* D120–70. Eur J Biochem 188:73–82

Altman E, Schaffer C, Brisson JR et al (1996) Isolation and characterization of an amino sugar-rich glycopeptide from the surface layer glycoprotein of *Thermoanaerobacterium thermosaccharolyticum* E207–71. Carbohydr Res 295:245–253

Amat F, Comolli LR, Nomellini JF et al (2010) Analysis of the intact surface layer of caulobacter crescentus by cryo-electron tomography. J Bacteriol 192:5855–5865

Anzengruber J, Pabst M, Neumann L et al (2013) Protein O-glucosylation in *Lactobacillus buchneri*. Glycoconj J 32:117–131

Arbing MA, Chan S, Shin A et al (2012) Structure of the surface layer of the methanogenic archaean *Methanosarcina acetivorans*. Proc Natl Acad Sci U S A 109:11812–11817

Bahl H, Scholz H, Bayan N et al (1997) Molecular biology of S-layers. FEMS Microbiol Rev 20:47–98

Baranova E, Fronzes R, Garcia-Pino A et al (2012) SbsB structure and lattice reconstruction unveil Ca2+ triggered S-layer assembly. Nature 487:119–122

Bateman A, Coggill P, Finn RD (2010) DUFs: families in search of function. Acta Crystallogr F 66:1148–1152

Baumeister W, Lembcke G (1992) Structural features of archaebacterial cell envelopes. J Bioenerg Biomembr 24:567–575

Baumeister W, Barth M, Hegerl R et al (1986) 3-dimensional structure of the regular surface-layer (Hpi Layer) of *Deinococcus radiodurans*. J Mol Biol 187:241–253

Beveridge TJ (1993) Current trends and future-prospects in prokaryotic envelope research—a microscopists view. J Appl Bacteriol 74:S143–S153

Beveridge TJ, Stewart M, Doyle RJ et al (1985) Unusual stability of the *Methanospirillum hungatei* sheath. J Bacteriol 162:728–737

Beveridge TJ, Koval SF, Sleytr UB et al (1993) Advances in bacterial paracrystalline surface-layers. Nato Adv Sci Inst Se 252:323–327

Blackford BL, Xu W, Jericho MH et al (1994) Direct observation by scanning-tunneling-microscopy of the 2-dimensional lattice structure of the S-layer sheath of the archaeobacterium *Methanospirillum hungatei* Gp1. Scanning Microsc 8:507–512

Boot HJ, Kolen CP, Pouwels PH (1995) Identification, cloning, and nucleotide sequence of a silent S-layer protein gene of *Lactobacillus acidophilus* ATCC 4356 which has extensive similarity with the S-layer protein gene of this species. J Bacteriol 177:7222–7230

Breitwieser A, Kupcu S, Howorka S et al (1996) 2-D protein crystals as an immobilization matrix for producing reaction zones in dipstick-style immunoassays. BioTechniques 21:918–925

Brockl G, Behr M, Fabry S et al (1991) Analysis and nucleotide sequence of the genes encoding the surface-layer glycoproteins of the hyperthermophilic methanogens *Methanothermus fervidus* and *Methanothermus sociabilis*. Eur J Biochem 199:147–152

Calabi E, Ward S, Wren B et al (2001) Molecular characterization of the surface layer proteins from *Clostridium difficile*. Mol Microbiol 40:1187–1199

Calabi E, Calabi F, Phillips AD et al (2002) Binding of *Clostridium difficile* surface layer proteins to gastrointestinal tissues. Infect Immun 70:5770–5778

Callegari ML, Riboli B, Sanders JW et al (1998) The S-layer gene of *Lactobacillus helveticus* CNRZ 892: cloning, sequence and heterologous expression. Microbiology 144(Part 3):719–726

Chami M, Bayan N, Peyret JL et al (1997) The S-layer protein of *Corynebacterium glutamicum* is anchored to the cell wall by its C-terminal hydrophobic domain. Mol Microbiol 23:483–492

Chung S, Shin SH, Bertozzi CR, De Yoreo JJ (2010) Self-catalyzed growth of S layers via an amorphous-to-crystalline transition limited by folding kinetics. Proc Natl Acad Sci U S A., 107:16536–41

Doig P, Emody L, Trust TJ (1992) Binding of laminin and fibronectin by the trypsin-resistant major structural domain of the crystalline virulence surface array protein of *Aeromonas salmonicida*. J Biol Chem 267:43–49

Dooley JSG, Trust TJ (1988) Surface protein-composition of *Aeromonas hydrophila* strains virulent for fish—identification of a surface array protein. J Bacteriol 170:499–506

Dooley JSG, Engelhardt H, Baumeister W et al (1989) 3-dimensional structure of an open form of the surface-layer from the fish pathogen *Aeromonas salmonicida*. J Bacteriol 171:190–197

Dufrene YF (2001) Application of atomic force microscopy to microbial surfaces: from reconstituted cell surface layers to living cells. Micron 32:153–165

Dworkin J, Blaser MJ (1997) Molecular mechanisms of *Campylobacter fetus* surface layer protein expression. Mol Microbiol 26:433–440

Egelseer E, Schocher I, Sara M et al (1995) The S-layer from *Bacillus stearothermophilus* DSM 2358 functions as an adhesion site for a high-molecular-weight amylase. J Bacteriol 177:1444–1451

Egelseer EM, Schocher I, Sleytr UB et al (1996) Evidence that an N-terminal S-layer protein fragment triggers the release of a cell-associated high-molecular-weight amylase in *Bacillus stearothermophilus* ATCC 12980. J Bacteriol 178:5602–5609

Egelseer EM, Leitner K, Jarosch M et al (1998) The S-layer proteins of two *Bacillus stearothermophilus* wild-type strains are bound via their N-terminal region to a secondary cell wall polymer of identical chemical composition. J Bacteriol 180:1488–1495

Egelseer EM, Danhorn T, Pleschberger M et al (2001) Characterization of an S-layer glycoprotein produced in the course of S-layer variation of *Bacillus stearothermophilus* ATCC 12980 and sequencing and cloning of the sbsD gene encoding the protein moiety. Arch Microbiol 177:70–80

Eichler J, Adams MWW (2005) Posttranslational protein modification in Archaea. Microbiol Mol Biol R 69:393

Engelhardt H (2007a) Are S-layers exoskeletons? The basic function of protein surface layers revisited. J Struct Biol 160:115–124

Engelhardt H (2007b) Mechanism of osmoprotection by archaeal S-layers: a theoretical study. J Struct Biol 160:190–199

Engelhardt H, Peters J (1998) Structural research on surface layers: a focus on stability, surface layer homology domains, and surface layer cell wall interactions. J Struct Biol 124:276–302

Ethordic A, Egelseer EM, Tesarz M et al (2012) Crystallization of domains involved in self-assembly of the S-layer protein SbsC. Acta Crystallogr F 68:1511–1514

Etienne-Toumelin I, Sirard JC, Duflot E et al (1995) Characterization of the *Bacillus anthracis* S-layer: cloning and sequencing of the structural gene. J Bacteriol 177:614–620

Fagan RP, Fairweather NF (2014) Biogenesis and functions of bacterial S-layers. Nat Rev Microbiol 12:211–222

Fagan RP, Albesa-Jove D, Qazi O et al (2009) Structural insights into the molecular organization of the S-layer from *Clostridium difficile*. Mol Microbiol 71:1308–1322
Ferner-Ortner-Bleckmann J, Huber-Gries C, Pavkov T et al (2009) The high-molecular-mass amylase (HMMA) of *Geobacillus stearothermophilus* ATCC 12,980 interacts with the cell wall components by virtue of three specific binding regions. Mol Microbiol 72:1448–1461
Firtel M, Southam G, Harauz G et al (1994a) The organization of the paracrystalline multilayered spacer-plugs of *Methanospirillum hungatei*. J Struct Biol 112:160–171
Firtel M, Xu W, Southam G et al (1994b) Tip-induced displacement and imaging of a multilayered bacterial structure by scanning-tunneling-microscopy. Ultramicroscopy 55:113–119
Ford MJ, Nomellini JF, Smit J (2007) S-layer anchoring and localization of an S-layer-associated protease in *Caulobacter crescentus*. J Bacteriol 189:2226–2237
Francoleon DR, Boontheung P, Yang Y et al (2009) S-layer, surface-accessible, and concanavalin A binding proteins of *Methanosarcina acetivorans* and *Methanosarcina mazei*. J Proteome Res 8:1972–1982
Galagan JE, Nusbaum C, Roy A et al (2002) The genome of *M. acetivorans* reveals extensive metabolic and physiological diversity. Genome Res 12:532–542
Garduno RA, Lee EJY, Kay WW (1992a) S-layer-mediated association of *Aeromonas salmonicida* with murine macrophages. Infect Immun 60:4373–4382
Garduno RA, Phipps BM, Baumeister W et al (1992b) Novel structural patterns in divalent cation-depleted surface-layers of *Aeromonas salmonicida*. J Struct Biol 109:184–195
Gilmour R, Messner P, Guffanti AA et al (2000) Two-dimensional gel electrophoresis analyses of pH-dependent protein expression in facultatively alkaliphilic *Bacillus pseudofirmus* OF4 lead to characterization of an S-layer protein with a role in alkaliphily. J Bacteriol 182:5969–5981
Graham LL, Beveridge TJ (1994) Structural differentiation of the *Bacillus subtilis* 168 cell-wall. J Bacteriol 176:1413–1421
Gyorvary ES, Stein O, Pum D et al (2003) Self-assembly and recrystallization of bacterial S-layer proteins at silicon supports imaged in real time by atomic force microscopy. J Microsc 212:300–306
Horejs C, Pum D, Sleytr UB et al (2008) Structure prediction of an S-layer protein by the mean force method. J Chem Phys 128:065106
Horejs C, Pum D, Sleytr UB et al (2010) Surface layer protein characterization by small angle x-ray scattering and a fractal mean force concept: from protein structure to nanodisk assemblies. J Chem Phys 133:175102
Horejs C, Mitra MK, Pum D et al (2011) Monte Carlo study of the molecular mechanisms of surface-layer protein self-assembly. J Chem Phys 134:125103
Houwink AL (1953) A macromolecular mono-layer in the cell wall of *Spirillum* spec. Biochimica et Biophysica Acta 10:360–366
Houwink AL (1956) Flagella, gas vacuoles and cell-wall structure in *Halobacterium halobium*—an electron microscope study. J Gen Microbiol 15:146–150
Howorka S, Sara M, Wang Y et al (2000) Surface-accessible residues in the monomeric and assembled forms of a bacterial surface layer protein. J Biol Chem 275:37876–37886
Huber C, Ilk N, Runzler D et al (2005) The three S-layer-like homology motifs of the S-layer protein SbpA of *Bacillus sphaericus* CCM 2177 are not sufficient for binding to the pyruvylated secondary cell wall polymer. Mol Microbiol 55:197–205
Ilk N, Egelseer EM, Sleytr UB (2011) S-layer fusion proteins–construction principles and applications. Curr Opin Biotechnol 22:824–831
Jahn-Schmid B, Messner P, Unger FM et al (1996) Toward selective elicitation of TH1-controlled vaccination responses: vaccine applications of bacterial surface layer proteins. J Biotechnol 44:225–231
Jahn-Schmid B, Siemann U, Zenker A et al (1997) Bet v 1, the major birch pollen allergen, conjugated to crystalline bacterial cell surface proteins, expands allergen-specific T cells of the Th1/Th0 phenotype in vitro by induction of IL-12. Int Immunol 9:1867–1874
Jakava-Viljanen M, Avall-Jaaskelainen S, Messner P et al (2002) Isolation of three new surface layer protein genes (slp) from Lactobacillus brevis ATCC 14869 and characterization of the

change in their expression under aerated and anaerobic conditions. Journal of bacteriology 184:6786–6795

Janesch B, Koerdt A, Messner P et al (2013a) The S-layer homology domain-containing protein SlhA from *Paenibacillus alvei* CCM 2051(T) is important for swarming and biofilm formation. PloS One 8:e76566

Janesch B, Messner P, Schaffer C (2013b) Are the surface layer homology domains essential for cell surface display and glycosylation of the S-layer protein from *Paenibacillus alvei* CCM 2051T? J Bacteriol 195:565–575

Jarosch M, Egelseer EM, Mattanovich D et al (2000) S-layer gene sbsC of *Bacillus stearothermophilus* ATCC 12980: molecular characterization and heterologous expression in *Escherichia coli*. Microbiology 146(Part 2):273–281

Jarosch M, Egelseer EM, Huber C et al (2001) Analysis of the structure-function relationship of the S-layer protein SbsC of *Bacillus stearothermophilus* ATCC 12980 by producing truncated forms. Microbiology 147:1353–1363

Jing H, Takagi J, Liu JH et al (2002) Archaeal surface layer proteins contain beta propeller, PKD, and beta helix domains and are related to metazoan cell surface proteins. Structure 10:1453–1464

Kadurugamuwa JL, Mayer A, Messner P et al (1998) S-layered *Aneurinibacillus* and *Bacillus* spp. are susceptible to the lytic action of *Pseudomonas aeruginosa* membrane vesicles. J Bacteriol 180:2306–2311

Karrasch S, Hegerl R, Hoh JH et al (1994) Atomic force microscopy produces faithful high-resolution images of protein surfaces in an aqueous environment. Proc Natl Acad Sci U S A 91:836–838

Karrenberg FH, Wildhaber I, Baumeister W (1987) Surface-structure variants in *Deinococcus radiodurans*. Curr Microbiol 16:15–20

Kern J, Schneewind O (2010) BslA, the S-layer adhesin of *B. anthracis*, is a virulence factor for anthrax pathogenesis. Mol Microbiol 75:324–332

Kern J, Wilton R, Zhang RG et al (2011) Structure of surface layer homology (SLH) domains from *Bacillus anthracis* surface array protein. J Biol Chem 286:26042–26049

Kinns H, Badelt-Lichtblau H, Egelseer EM et al (2010) Identifying assembly-inhibiting and assembly-tolerant sites in the SbsB S-layer protein from *Geobacillus stearothermophilus*. J Mol Biol 395:742–753

Konisky J, Lynn D, Hoppert M et al (1994) Identification of the *Methanococcus voltae* S-layer structural gene. J Bacteriol 176:1790–1792

Kostyukova AS, Gongadze GM, Polosina YY et al (1999) Investigation of structure and antigenic capacities of Thermococcales cell envelopes and reclassification of "Caldococcus litoralis" Z-1301 as Thermococcus litoralis Z-1301. Extremophiles: life under extreme conditions 3:239–245

Koval SF (1988) Paracrystalline protein surface arrays on bacteria. Can J Microbiol 34:407–414

Koval SF, Hynes SH (1991) Effect of paracrystalline protein surface-layers on predation by *Bdellovibrio bacteriovorus*. J Bacteriol 173:2244–2249

Koval SF, Bayer ME (1997) Bacterial capsules: no barrier against *Bdellovibrio*. Microbiology (UK) 143:749–753

Kuen B, Sleytr UB, Lubitz W (1994) Sequence analysis of the sbsA gene encoding the 130-kDa surface-layer protein of *Bacillus stearothermophilus* strain PV72. Gene 145:115–120

Kupcu Z, Marz L, Messner P et al (1984) Evidence for the glycoprotein nature of the crystalline cell wall surface layer of *Bacillus stearothermophilus* strain NRS2004/3a. FEBS Lett 173:185–190

Kupcu S, Sara M, Sleytr UB (1995) Liposomes coated with crystalline bacterial cells surface protein (S-layer) as immobilization structures for macromolecules. Biochimica et Biophysica Acta 1235:263–269

Kupcu S, Sleytr UB, Sara M (1996) Two-dimensional paracrystalline glycoprotein S-layers as a novel matrix for the immobilization of human IgG and their use as microparticles in immunoassays. J Immunol Methods 196:73–84

Kupcu S, Lohner K, Mader C et al (1998) Microcalorimetric study on the phase behaviour of S-layer coated liposomes. Mol Membr Biol 15:69–74
Lechner J, Sumper M (1987) The primary structure of a prokaryotic glycoprotein—cloning and sequencing of the cell-surface glycoprotein gene of *Halobacteria*. J Biol Chem 262:9724–9729
Lechner J, Wieland F, Sumper M (1986) Sulfated dolicholphosphate oligosaccharides are transiently methylated during biosynthesis of Halobacterial glycoproteins. Syst Appl Microbiol 7:286–292
Leibovitz E, Ohayon H, Gounon P et al (1997) Characterization and subcellular localization of the *Clostridium thermocellum* scaffoldin dockerin binding protein SdbA. J Bacteriol 179:2519–2523
Lejardi A, Lopez AE, Sarasua JR et al (2013) Making novel bio-interfaces through bacterial protein recrystallization on biocompatible polylactide derivative films. J Chem Phys 139:121903
Lighezan L, Georgieva R, Neagu A (2012) A study of the thermal denaturation of the S-layer protein from *Lactobacillus salivarius*. Phys Scripta 86
Lister TE, Pinhero PJ (2001) In vivo atomic force microscopy of surface proteins on *Deinococcus radiodurans*. Langmuir 17:2624–2628
Liu SY, Gherardini FC, Matuschek M et al (1996) Cloning, sequencing, and expression of the gene encoding a large S-layer-associated endoxylanase from *Thermoanaerobacterium* sp strain JW/SL-YS 485 in *Escherichia coli*. J Bacteriol 178:1539–1547
Luo Y, Frey EA, Pfuetzner RA et al (2000) Crystal structure of enteropathogenic *Escherichia coli* intimin-receptor complex. Nature 405:1073–1077
Lupas AN, Gruber M (2005) The structure of alpha-helical coiled coils. Adv Protein Chem 70:37–78
Mader C, Kupcu S, Sara M et al (1999) Stabilizing effect of an S-layer on liposomes towards thermal or mechanical stress. Biochimica et Biophysica Acta 1418:106–116
Mader C, Kupcu S, Sleytr UB et al (2000) S-layer-coated liposomes as a versatile system for entrapping and binding target molecules. Biochimica et Biophysica Acta 1463:142–150
Mader C, Huber C, Moll D et al (2004) Interaction of the crystalline bacterial cell surface layer protein SbsB and the secondary cell wall polymer of *Geobacillus stearothermophilus* PV72 assessed by real-time surface plasmon resonance biosensor technology. J Bacteriol 186:1758–1768
Mayerhofer LE, Macario AJL, Demacario EC (1992) Lamina, a novel multicellular form of *Methanosarcina mazei* S-6. J Bacteriol 174:309–314
Mescher MF, Strominger JL (1976) Purification and characterization of a prokaryotic glycoprotein from cell-envelope of *Halobacterium salinarium*. J Biol Chem 251:2005–2014
Mesnage S, Tosi-Couture E, Mock M et al (1997) Molecular characterization of the *Bacillus anthracis* main S-layer component: evidence that it is the major cell-associated antigen. Mol Microbiol 23:1147–1155
Mesnage S, Fontaine T, Mignot T et al (2000) Bacterial SLH domain proteins are non-covalently anchored to the cell surface via a conserved mechanism involving wall polysaccharide pyruvylation. EMBO J 19:4473–4484
Messner P (1997) Bacterial glycoproteins. Glycoconj J 14:3–11
Messner P, Sleytr UB (1992) Crystalline bacterial cell-surface layers. Adv Microb Physiol 33:213–275
Messner P, Pum D, Sara M et al (1986a) Ultrastructure of the cell envelope of the archaebacteria *Thermoproteus tenax* and *Thermoproteus neutrophilus*. J Bacteriol 166:1046–1054
Messner P, Pum D, Sleytr UB (1986b) Characterization of the ultrastructure and the self-assembly of the surface layer of *Bacillus stearothermophilus* strain NRS 2004/3a. J Ultra Mol Struct R 97:73–88
Messner P, Allmaier G, Schaffer C et al (1997) Biochemistry of S-layers. FEMS Microbiol Rev 20:25–46
Messner P, Steiner K, Zarschler K et al (2008) S-layer nanoglycobiology of bacteria. Carbohydr Res 343:1934–1951

Moll D, Huber C, Schlegel B et al (2002) S-layer-streptavidin fusion proteins as template for nanopatterned molecular arrays. Proc Natl Acad Sci U S A 99:14646–14651

Muller DJ, Baumeister W, Engel A (1996) Conformational change of the hexagonally packed intermediate layer of *Deinococcus radiodurans* monitored by atomic force microscopy. J Bacteriol 178:3025–3030

Muller DJ, Baumeister W, Engel A (1999) Controlled unzipping of a bacterial surface layer with atomic force microscopy. Proc Natl Acad Sci U S A 96:13170–13174

Murray RGE, Dooley JSG, Whippey PW et al (1988) Structure of an S-layer on a pathogenic strain of *Aeromonas hydrophila*. J Bacteriol 170:2625–2630

Noonan B, Trust TJ (1995) Molecular analysis of an a-protein secretion mutant of *Aeromonas salmonicida* reveals a surface layer-specific protein secretion pathway. J Mol Biol 248:316–327

Norville JE, Kelly DF, Knight TF et al (2007) 7 angstrom projection map of the S-layer protein sbpA obtained with trehalose-embedded monolayer crystals. J Struct Biol 160:313–323

Oh YJ, Sekot G, Duman M et al (2013) Characterizing the S-layer structure and anti-S-layer antibody recognition on intact *Tannerella forsythia* cells by scanning probe microscopy and small angle X-ray scattering. JMR 26:542–549

Ohnesorge F, Heckl WM, Haberle W et al (1992) Scanning force microscopy studies of the S-layers from *Bacillus coagulans* E38–66, *Bacillus sphaericus* CCM2177 and of an antibody binding process. Ultramicroscopy 42–44(Part B):1236–1242

Park TJ, Lee SJ, Park JP et al (2011) Characterization of a bacterial self-assembly surface layer protein and its application as an electrical nanobiosensor. J Nanosci Nanotechnol 11:402–407

Pavkov T, Oberer M, Egelseer EM et al (2003) Crystallization and preliminary structure determination of the C-terminal truncated domain of the S-layer protein SbsC. Acta Crystallogr D 59:1466–1468

Pavkov T, Egelseer EM, Tesarz M et al (2008) The structure and binding behavior of the bacterial cell surface layer protein SbsC. Structure 16:1226–1237

Pavkov T, Howorka S, Keller W (2011) The structure of bacterial S-layer proteins. In Howorka S (ed) Progress in molecular biology and translational science, vol 103. Academic Press, Elsevier, Burlington, Massachusetts, US, pp 73–130

Peters J, Peters M, Lottspeich F et al (1987) Nucleotide-sequence analysis of the gene encoding the *Deinococcus radiodurans* surface protein, derived amino-acid-sequence, and complementary protein chemical studies. J Bacteriol 169:5216–5223

Peters J, Nitsch M, Kuhlmorgen B et al (1995) Tetrabrachion: a filamentous archaebacterial surface protein assembly of unusual structure and extreme stability. J Mol Biol 245:385–401

Peters J, Baumeister W, Lupas A (1996) Hyperthermostable surface layer protein tetrabrachion from the archaebacterium *Staphylothermus marinus*: evidence for the presence of a right-handed coiled coil derived from the primary structure. J Mol Biol 257:1031–1041

Petersen BO, Sara M, Mader C et al (2008) Structural characterization of the acid-degraded secondary cell wall polymer of *Geobacillus stearothermophilus* PV72/p2. Carbohydr Res 343:1346–1358

Peyfoon E, Meyer B, Hitchen PG et al (2010) The S-layer glycoprotein of the crenarchaeote *Sulfolobus acidocaldarius* is glycosylated at multiple sites with chitobiose-linked N-glycans. Archaea 2010: 754101

Peyret JL, Bayan N, Joliff G et al (1993) Characterization of the cspB gene encoding PS2, an ordered surface-layer protein in *Corynebacterium glutamicum*. Mol Microbiol 9:97–109

Posch G, Pabst M, Brecker L et al (2011) Characterization and scope of S-layer protein O-glycosylation in *Tannerella forsythia*. J Biol Chem 286:38714–38724

Posch G, Andrukhov O, Vinogradov E et al (2013) Structure and immunogenicity of the rough-type lipopolysaccharide from the periodontal pathogen *Tannerella forsythia*. CVI 20:945–953

Poxton IR, Mccoubrey J, Blair G (2001) The pathogenicity of *Clostridium difficile*. Clin Microbiol Infect 7:421–427

Pum D, Sara M, Sleytr UB (1989) Structure, surface charge, and self-assembly of the S-layer lattice from *Bacillus coagulans* E38–66. J Bacteriol 171:5296–5303

Pum D, Messner P, Sleytr UB (1991) Role of the S layer in morphogenesis and cell division of the archaebacterium *Methanocorpusculum sinense*. J Bacteriol 173:6865–6873

Pum D, Toca-Herrera JL, Sleytr UB (2013) S-layer protein self-assembly. Int J Mol Sci 14:2484–2501

Rachel R, Jakubowski U, Tietz H et al (1986) Projected structure of the surface protein of *Deinococcus radiodurans* determined to 8 a resolution by cryomicroscopy. Ultramicroscopy 20:305–316

Runzler D, Huber C, Moll D et al (2004) Biophysical characterization of the entire bacterial surface layer protein SbsB and its two distinct functional domains. J Biol Chem 279:5207–5215

Sakakibara J, Nagano K, Murakami Y et al (2007) Loss of adherence ability to human gingival epithelial cells in S-layer protein-deficient mutants of *Tannerella forsythensis*. Microbiology 153:866–876

Sara M, Sleytr UB (1996) Biotechnology and biomimetic with crystalline bacterial cell surface layers (S-layers). Micron 27:141–156

Sara M, Sleytr UB (2000) S-Layer proteins. J Bacteriol 182:859–868

Sara M, Kalsner I, Sleytr UB (1988) Surface properties from the S-layer of *Clostridium thermosaccharolyticum* D120–70 and *Clostridium thermohydrosulfuricum* L111–69. Arch Microbiol 149:527–533

Sara M, Pum D, Sleytr UB (1992) Permeability and charge-dependent adsorption properties of the S-layer lattice from *Bacillus coagulans* E38–66. J Bacteriol 174:3487–3493

Sara M, Dekitsch C, Mayer HF et al (1998) Influence of the secondary cell wall polymer on the reassembly, recrystallization, and stability properties of the S-layer protein from *Bacillus stearothermophilus* PV72/p2. J Bacteriol 180:4146–4153

Schaffer C, Messner P (2004) Surface-layer glycoproteins: an example for the diversity of bacterial glycosylation with promising impacts on nanobiotechnology. Glycobiology 14:31R–42R

Schaffer C, Messner P (2005) The structure of secondary cell wall polymers: how Gram-positive bacteria stick their cell walls together. Microbiology 151:643–651

Schaffer C, Kahlig H, Christian R et al (1999) The diacetamidodideoxyuronic-acid-containing glycan chain of *Bacillus stearothermophilus* NRS 2004/3a represents the secondary cell-wall polymer of wild-type *B. stearothermophilus* strains. Microbiology 145(Part 7):1575–1583

Schaffer C, Wugeditsch T, Kahlig H et al (2002) The surface layer (S-layer) glycoprotein of *Geobacillus stearothermophilus* NRS 2004/3a. Analysis of its glycosylation. J Biol Chem 277:6230–6239

Scheuring S, Stahlberg H, Chami M et al (2002) Charting and unzipping the surface layer of *Corynebacterium glutamicum* with the atomic force microscope. Mol Microbiol 44:675–684

Scholz HC, Riedmann E, Witte A et al (2001) S-layer variation in *Bacillus stearothermophilus* PV72 is based on DNA rearrangements between the chromosome and the naturally occurring megaplasmids. J Bacteriol 183:1672–1679

Schultzelam S, Beveridge TJ (1994a) Nucleation of celestite and strontianite on a cyanobacterial S-layer. Appl Environ Microbiol 60:447–453

Schultzelam S, Beveridge TJ (1994b) Physicochemical characteristics of the mineral-forming S-layer from the *Cyanobacterium synechococcus* strain Gl24. Can J Microbiol 40:216–223

Schuster B, Gufler PC, Pum D et al (2004) S-layer proteins as supporting scaffoldings for functional lipid membranes. IEEE T Nanobiosci 3:16–21

Sekot G, Posch G, Messner P et al (2011) Potential of the *Tannerella forsythia* S-layer to delay the immune response. J Dent Res 90:109–114

Sekot G, Posch G, Oh YJ et al (2012) Analysis of the cell surface layer ultrastructure of the oral pathogen *Tannerella forsythia*. Arch Microbiol 194:525–539

Sekot G, Schuster D, Messner P et al (2013) Small-angle X-ray scattering for imaging of surface layers on intact bacteria in the native environment. J Bacteriol 195:2408–2414

Shenton W, Pum D, Sleytr UB et al (1997) Synthesis of cadmium sulphide superlattices using self-assembled bacterial S-layers. Nature 389:585–587

Shin SH, Chung S, Sanii B, Comolli LR, Bertozzi CR, De Yoreo JJ (2012) Direct observation of kinetic traps associated with structural transformations leading to multiple pathways of S-layer assembly. Proc Natl Acad Sci U S A., 109:12968–73

Shin SH, Comolli LR, Tscheliessnig R et al (2013) Self-assembly of “S-bilayers”, a step toward expanding the dimensionality of S-layer assemblies. ACS Nano 7:4946–4953
Simon P, Lichte H, Wahl R et al (2004) Electron holography of non-stained bacterial surface layer proteins. Bba-Biomembranes 1663:178–187
Sleytr UB, Thorne KJ (1976) Chemical characterization of the regularly arranged surface layers of *Clostridium thermosaccharolyticum* and *Clostridium thermohydrosulfuricum*. J Bacteriol 126:377–383
Sleytr UB, Beveridge TJ (1999) Bacterial S-layers. Trends Microbiol 7:253–260
Sleytr UB, Kocur M, Glauert AM et al (1973) A study by freeze-etching of the fine structure of *Micrococcus radiodurans*. Arch Mikrobiol 94:77–87
Sleytr UB, Sara M, Kupcu Z et al (1986) Structural and chemical characterization of S-layers of selected strains of *Bacillus stearothermophilus* and *Desulfotomaculum nigrificans*. Arch Microbiol 146:19–24
Sleytr UB, Messner P, Pum D et al (1993) Crystalline bacterial cell surface layers. Mol Microbiol 10:911–916
Sleytr UB, Pum D, Sara M (1997) Advances in S-layer nanotechnology and biomimetics. Adv Biophys 34:71–79
Sleytr UB, Messner P, Pum D et al (1999) Crystalline bacterial cell surface layers (S layers): from supramolecular cell structure to biomimetics and nanotechnology. Angew Chem Int Edit 38:1035–1054
Smit J, Engelhardt H, Volker S et al (1992) The S-layer of *Caulobacter crescentus*: three-dimensional image reconstruction and structure analysis by electron microscopy. J Bacteriol 174:6527–6538
Smith RH, Messner P, Lamontagne LR et al (1993) Induction of T-cell immunity to oligosaccharide antigens immobilized on crystalline bacterial surface layers (S-layers). Vaccine 11:919–924
Sowers KR, Boone JE, Gunsalus RP (1993a) Disaggregation of *Methanosarcina* spp. and growth as single cells at elevated osmolarity. Appl Environ Microbiol 59:3832–3839
Sowers KR, Thai TT, Gunsalus RP (1993b) Transcriptional regulation of the carbon monoxide dehydrogenase gene (cdhA) in *Methanosarcina thermophila*. J Biol Chem 268:23172–23178
Steindl C, Schaffer C, Wugeditsch T et al (2002) The first biantennary bacterial secondary cell wall polymer and its influence on S-layer glycoprotein assembly. Biochem J 368:483–494
Steiner K, Pohlentz G, Dreisewerd K et al (2006) New insights into the glycosylation of the surface layer protein SgsE from *Geobacillus stearothermophilus* NRS 2004/3a. J Bacteriol 188:7914–7921
Stetefeld J, Jenny M, Schulthess T et al (2000) Crystal structure of a naturally occurring parallel right-handed coiled coil tetramer. Nat Struct Biol 7:772–776
Stewart M, Beveridge TJ, Sprott GD (1985) Crystalline order to high resolution in the sheath of *Methanospirillum hungatei*: a cross-beta structure. J Mol Biol 183:509–515
Stewart M, Beveridge TJ, Trust TJ (1986) 2 Patterns in the *Aeromonas salmonicida* a-layer may reflect a structural transformation that alters permeability. J Bacteriol 166:120–127
Sumper M, Berg E, Mengele R et al (1990) Primary structure and glycosylation of the S-layer protein of *Haloferax volcanii*. J Bacteriol 172:7111–7118
Takeoka A, Takumi K, Koga T et al (1991) Purification and characterization of S-layer proteins from *Clostridium difficile* Gai-0714. J Gen Microbiol 137:261–267
Tang J, Ebner A, Badelt-Lichtblau H et al (2008) Recognition imaging and highly ordered molecular templating of bacterial S-layer nanoarrays containing affinity-tags. Nano Letters 8:4312–4319
Thompson SA, Shedd OL, Ray KC et al (1998) Campylobacter fetus surface layer proteins are transported by a type I secretion system. J Bacteriol 180:6450–6458
Thornley MJ, Glauert AM, Sleytr UB (1973) Isolation of outer membranes with an ordered array of surface subunits from Acinetobacter. J Bacteriol 114:1294–1308
Toca-Herrera JL, Moreno-Flores S, Friedmann J et al (2004) Chemical and thermal denaturation of crystalline bacterial S-layer proteins: an atomic force microscopy study. Microsc Res Tech 65:226–234

Trust TJ, Kostrzynska M, Emody L et al (1993) High-affinity binding of the basement-membrane protein collagen type-IV to the crystalline virulence surface protein array of *Aeromonas salmonicida*. Mol Microbiol 7:593–600

Tsuboi A, Uchihi R, Tabata R et al (1986) Characterization of the genes-coding for 2 major cell-wall proteins from protein-producing *Bacillus brevis* 47—complete nucleotide-sequence of the outer wall protein gene. J Bacteriol 168:365–373

Weigert S, Sara M (1995) Surface modification of an ultrafiltration membrane with crystalline-structure and studies on interactions with selected protein molecules. J Membrane Sci 106:147–159

Weigert S, Sara M (1996) Ultrafiltration membranes prepared from crystalline bacterial cell surface layers as model systems for studying the influence of surface properties on protein adsorption. J Membrane Sci 121:185–196

Weiner C, Sara M, Dasgupta G et al (1994a) Affinity cross-flow filtration: purification of IgG with a novel protein a affinity matrix prepared from two-dimensional protein crystals. Biotechnol Bioeng 44:55–65

Weiner C, Sara M, Sleytr UB (1994b) Novel protein a affinity matrix prepared from two-dimensional protein crystals. Biotechnol Bioeng 43:321–330

Wiegrabe W, Nonnenmacher M, Guckenberger R et al (1991) Atomic force microscopy of a hydrated bacterial surface protein. J Microsc (Oxf) 163:79–84

Wugeditsch T, Zachara NE, Puchberger M et al (1999) Structural heterogeneity in the core oligosaccharide of the S-layer glycoprotein from *Aneurinibacillus thermoaerophilus* DSM 10155. Glycobiology 9:787–795

Zhao GS, Ali E, Sakka M et al (2006) Binding of S-layer homology modules from *Clostridium thermocellum* SdbA to peptidoglycans. Appl Microbiol Biotechnol 70:464–469

Zuber B, Chami M, Houssin C et al (2008) Direct visualization of the outer membrane of mycobacteria and corynebacteria in their native state. J Bacteriol 190:5672–5680

Chapter 3
Magnetotactic Bacteria, Magnetosomes, and Nanotechnology

Dennis A. Bazylinski, Christopher T. Lefèvre and Brian H. Lower

3.1 Introduction and Historical Perspective

In the early 1960s, Salvatore Bellini microscopically observed large numbers of bacteria swimming in a consistent, single, northward direction in drops of water samples collected from freshwater environments near Pavia, Italy. He referred to these organisms as magnetosensitive bacteria and postulated that the magnetic behavior of the cells was caused by an internal "magnetic compass." For many years, Bellini's findings went unnoticed as they were published in an obscure journal in 1963. These papers have now been translated and were republished in 2009 (Bellini 2009a, b). Magnetic behavior in prokaryotes was rediscovered in 1974 and described in 1975 by Richard P. Blakemore (1975), who coined the terms magnetotaxis for the behavior and magnetotactic bacteria for the organisms that exhibited it. He was also the first to demonstrate that Bellini's internal "magnetic compass" were unique organelles he referred to as magnetosomes (Blakemore 1975).

Magnetotactic bacteria are defined as motile prokaryotes whose swimming direction is guided by magnetic fields, including the Earth's geomagnetic field (Bazylinski and Frankel 2004; Lower and Bazylinski 2013). As implied earlier, this behavior, magnetotaxis, is a result of the presence of magnetosomes which are composed of a magnetic mineral crystal, either an iron oxide or iron sulfide, surrounded by a lipid bilayer membrane known as the magnetosome membrane (Bazylinski and Frankel 2004; Lower and Bazylinski 2013).

D. A. Bazylinski (✉)
School of Life Sciences, University of Nevada at Las Vegas, 4505 S. Maryland Pkwy, Las Vegas, NV 89154-4004, USA
e-mail: dennis.bazylinski@unlv.edu

C. T. Lefèvre
CEA/CNRS/Aix-Marseille Université, Biologie Végétale et Microbiologie Environnementales, Laboratoire de Bioénergétique Cellulaire, Saint Paul lez Durance, France

B. H. Lower
School of Environment and Natural Resources, The Ohio State University, Columbus, OH, USA

L. L. Barton et al. (eds.), *Nanomicrobiology,* DOI 10.1007/978-1-4939-1667-2_3

Magnetotactic bacteria exhibit a great diversity in their cell morphology, physiology, and phylogeny (Lefèvre and Bazylinski 2013). Most known species are microaerophiles, some of which may also be facultatively anaerobic, or obligate anaerobes. In general, these organisms are gradient loving and are found at the transition where oxygen becomes depleted in aquatic or sedimentary habitats (Bazylinski and Frankel 2004; Lefèvre and Bazylinski 2013). Because of the chemical (e.g., oxygen concentration) and redox gradients often required for their growth, the isolation and cultivation of magnetotactic bacteria is difficult due to their fastidious nature and the lack of suitable enrichment media. However, in the past two decades, there has been a great deal of progress in the isolation of new strains of magnetotactic bacteria, in the development of genetic techniques for manipulating these strains, and in the ever-increasing amount of genomic data from these organisms. This has profoundly impacted our understanding of magnetosome biomineralization processes at the molecular, genetic, and (bio)chemical levels and paved the way for the use of magnetosomes and magnetotactic bacteria in nanotechnology. The purpose of this chapter is to briefly review this recent progress to describe the importance of magnetosomes in nanotechnology.

3.2 Diversity of Magnetotactic Bacteria

Magnetotactic bacteria do not represent a well-defined taxonomic group of prokaryotes, and their diverse nature was obvious to researchers even in early studies as numerous, varying cell morphologies of magnetotactic bacteria were commonly observed in water/sediment samples from natural environments. Commonly observed morphotypes include coccoid to ovoid cells, rods, vibrios, and spirilla as well as multicellular forms referred to as multicellular magnetotactic prokaryotes or MMPs (Abreu et al. 2007; Bazylinski and Frankel 2004; Lefèvre and Bazylinski 2013). The assumption that magnetotactic bacteria are very diverse based on morphology was confirmed in later studies involving their physiology and phylogeny.

Despite this great diversity, all known magnetotactic bacteria share several consistent traits. They are motile by means of flagella, possess a Gram-negative type of cell wall, are negatively impacted by atmospheric levels of oxygen, and have the ability to biomineralize magnetosomes (Bazylinski and Frankel 2004; Lefèvre and Bazylinski 2013).

Phylogenetic studies based on 16S ribosomal RNA gene (16S rDNA) sequences of cultured and uncultured magnetotactic bacteria reveal an extensive biodiversity of these microorganisms. Currently, recognized species are affiliated with five major lineages within the domain *Bacteria* with three belonging to the *Proteobacteria* phylum. Most known cultured and uncultured magnetotactic bacteria belong to these latter three groups which include the *Alpha-, Gamma-,* and *Deltaproteobacteria* classes of the *Proteobacteria* (Lefèvre and Bazylinski 2013). Some uncultured species are associated with the *Nitrospirae* phylum (Amann et al. 2007; Flies et al. 2005; Lefèvre and Bazylinski 2013; Lefèvre et al. 2011a; Lin and Pan

2012; Lin et al. 2011), and one with the candidate division OP3, part of the *Planctomycetes–Verrucomicrobia–Chlamydiae* (PVC) superphylum (Kolinko et al. 2011). Although no magnetotactic bacterium has yet been found to be phylogenetically affiliated with the *Archaea,* there is no known reason why this is not possible. While magnetotactic bacteria of the five groups biomineralize iron oxides, some in the *Deltaproteobacteria* also synthesize iron sulfides either exclusively or with iron oxides.

Magnetotactic bacteria are common in chemically- and redox-stratified water columns and sediments of almost all types of aquatic habitats and are cosmopolitan in distribution (Bazylinski and Frankel 2004; Lefèvre and Bazylinski 2013). Their presence in most situations appears to be dependent on opposing concentration gradients of oxygen from the surface and reducing compounds from the anoxic zone (e.g., sulfide) with a concomitant redox gradient in sediments or water columns resulting in an oxic–anoxic interface (OAI; sometimes referred to as the oxic–anoxic transition zone or OATZ; Lefèvre and Bazylinski 2013). While the highest total number of magnetotactic bacteria is at the OAI (Moskowitz et al. 2008), different species of magnetotactic bacteria appear to occupy different positions within the OAI that are dependent on specific chemical/redox conditions. For example, iron oxide-producing magnetotactic bacteria are generally found at the OAI proper, while iron sulfide-producing species are mostly present in the sulfidic, anoxic zone below the OAI (Lefèvre and Bazylinski 2013; Moskowitz et al. 2008).

Studies have shown that magnetotactic bacteria are not restricted to habitats with pH values near neutrality at ambient temperatures as several cultured and uncultured extremophilic species have recently been described. Moderately thermophilic uncultured species have been found in several hot springs in northern Nevada with a probable upper growth limit of about 63 °C (Lefèvre et al. 2010) and in California (Nash 2008). In addition, three strains of obligately alkaliphilic, sulfate-reducing magnetotactic bacteria have been isolated from highly alkaline aquatic habitats in California (Lefèvre et al. 2011b). These latter alkaliphilic isolates appear to be strains of the dissimilatory sulfate-reducing bacterium *Desulfonatronum thiodismutans* (Pikuta et al. 2003), which does not display magnetotaxis, and have an optimal growth pH of about 9.0 (Lefèvre et al. 2011b). Magnetotactic bacteria have never been found in strongly acidic habitats.

Physiologies and some metabolic pathways of known magnetotactic bacteria have been determined experimentally with cultured strains as well as from genomic data. Some physiological traits of several uncultured magnetotactic bacteria have also been inferred from ecological and genomic information and from elemental analyses of cells. For example, the presence of intracellular, sulfur-rich globules in a magnetotactic bacterial cell would suggest that it is capable of sulfide oxidation.

All known magnetotactic bacteria are obligate microaerophiles, facultatively anaerobic microaerophiles, or obligate anaerobes (Bazylinski and Frankel 2004; Lefèvre and Bazylinski 2013). With regard to temperature, all cultured strains are mesophilic with optimal growth temperatures ~30 °C although, as previously stated, two uncultured, moderately thermophilic species have been identified (Lefèvre et al. 2010; Nash 2008).

Different general types of metabolism are present in magnetotactic bacteria, including chemoorganoheterophy, chemolithoautotrophy, and even chemoorganoautotrophy (Bazylinski and Williams 2007). Metabolism is obligately respiratory in all species with one exception, *Desulfovibrio magneticus* is able to couple growth with the fermentation of pyruvate to acetate and hydrogen (Bazylinski and Williams 2007; Sakaguchi et al. 2002). A respiratory form of metabolism may be essential in magnetosome synthesis as a strong correlation exists between oxygen respiration and magnetite biomineralization: the terminal oxidase cbb_3 required for simultaneous denitrification and aerobic respiration in microaerobic conditions appears to also be involved in magnetite biomineralization in *Magnetospirillum gryphiswaldense* (Li et al. 2014).

Magnetotactic bacteria are known to mediate numerous, important, environmental biogeochemical transformations of key elements, including sulfur, nitrogen, carbon, as well as iron. Many species metabolize sulfur compounds. Many alpha- and gammaproteobacterial magnetotactic bacteria oxidize sulfide and thiosulfate as electron donors which supports chemolithoautotrophy in these species (Bazylinski et al. 2004, 2013a, b; Geelhoed et al. 2010; Lefèvre et al. 2012; Williams et al. 2006, 2012). Autotrophy in these organisms is mediated through the Calvin–Benson–Bassham cycle for the most part in the *Alpha-* and *Gammaproteobacteria* (Bazylinski et al. 2004, 2013b; Lefèvre et al. 2012; Williams et al. 2012), while one, *Magnetococcus marinus,* an alphaproteobacterium, utilizes the reverse tricarboxylic acid cycle (Bazylinski et al. 2013a; Williams et al. 2006). Autotrophic growth also occurs in the alkaliphilic, hydrogen-oxidizing, sulfate-reducing strains of magnetotactic bacteria phylogenetically similar to *Desulfonatronum thiodismutans* (Lefèvre et al. 2011a) although the pathway has not yet been determined. Several magnetotactic species in the *Deltaproteobacteria* reduce sulfate as a terminal electron acceptor to sulfide (Lefèvre et al. 2011b, c; Sakaguchi et al. 2002).

Nitrogenous compounds are also metabolized by many magnetotactic bacteria. The *Alphaproteobacteria, Magnetospirillum* species, and *Magnetovibrio blakemorei* respire using nitrate as a terminal electron acceptor with *Magnetospirillum* species capable of denitrification, reducing nitrate to dinitrogen gas (Bazylinski and Blakemore 1983; Bazylinski et al. 2013b; Li et al. 2012). A strong positive correlation appears to exist between nitrate reduction, denitrification, and magnetite synthesis in *Magnetospirillum* species (Blakemore et al. 1985; Li et al. 2012, 2013a). The periplasmic nitrate reductase *nap* and the cytochrome *cd*1 nitrite reductase NirS have been shown to be required by *M. gryphiswaldense* for anaerobic growth and are involved in redox control of magnetite biomineralization (Li et al. 2012, 2013a). Almost all known cultured magnetotactic bacteria are capable of nitrogen fixation (Bazylinski and Williams 2007; Bazylinski et al. 2000, 2013a, b; Lefèvre et al. 2012; Williams et al. 2012), except strain SS-5 of the *Gammaproteobacteria* (Lefèvre et al. 2012) and *Magnetospira* strain QH-2 (Ji et al. 2014).

3.3 The Bacterial Magnetosome

Magnetosomes are intracellular, membrane-bounded crystals consisting of a magnetic iron oxide, the mineral magnetite (Fe_3O_4), or an iron sulfide, the mineral greigite (Fe_3S_4) (Bazylinski and Frankel 2004; Lefèvre and Bazylinski 2013; Lins et al. 2007; Lower and Bazylinski 2013). Most known magnetotactic bacteria biomineralize only one magnetosome mineral, while some are capable of synthesizing both minerals (Bazylinski et al. 1993b, 1995; Lefèvre et al. 2011c). Magnetosomal magnetite is of high chemical purity usually lacking other metal ions although trace amounts of some (e.g., titanium) have been found in some uncultured magnetotactic bacteria (Towe and Moench 1981), while significant amounts of copper have been found in greigite magnetosome crystals of some uncultured magnetotactic bacteria (Bazylinski et al. 1993a).

Regardless of mineral composition, almost all individual magnetosomes crystals lie within the stable single-magnetic-domain size range (Bazylinski and Frankel 2004; Frankel et al. 1998; Lefèvre and Bazylinski 2013) which is approximately between 35 and 120 nm in diameter (Butler and Banerjee 1975; Diaz-Ricci and Kirschvink 1992). Single-magnetic-domain crystals of magnetite and greigite are the smallest particles consisting of these minerals that retain a permanent magnetic dipole at ambient temperature. So-called superparamagnetic crystals, those that are smaller than this size range, do not possess stable, remanent magnetization (the magnetic induction or magnetism remaining in a material in a zero magnetic field after exposure to a strong external magnetic field) at ambient temperature. Thus, they are only magnetic in the presence of a strong magnetic field (the Earth's geomagnetic field is not strong enough) and could therefore not function in bacterial magnetotaxis. Multiple domains tend to form in crystals larger than single magnetic domains, thus reducing the remanent magnetization of the crystal. Amazingly, through the biomineralization of single-magnetic-domain crystals, magnetotactic bacteria have maximized the magnetic remanence per unit volume of mineral (Frankel and Blakemore 1980; Frankel and Moskowitz 2003).

Magnetosomes are generally present in the cell as one or more chains (Bazylinski and Frankel 2004; Frankel et al. 1998; Lefèvre and Bazylinski 2013; Frankel and Moskowitz 2003). Although magnetic interactions between individual magnetic magnetosomes within the chain are thought to be important in prompting each magnetosome moment to orient parallel to one another, thereby minimizing the magnetostatic energy of the chain and maximizing the magnetic dipole moment of the bacterial cell (Frankel and Moskowitz 2003), cytoskeletal elements appear to also be important in magnetosome chain formation and anchoring the chain within the cell (Komeili et al. 2006; Katzmann et al. 2010). When magnetosomes are in the chain motif, the total magnetic dipole moment of the cell is the sum of the moments of the individual magnetosomes which ultimately causes magnetotactic cells to passively align along the Earth's geomagnetic field lines as they swim (Frankel and Blakemore 1980; Frankel and Moskowitz 2003).

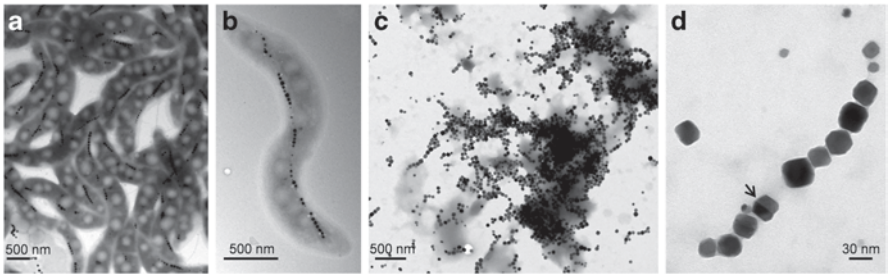

Fig. 3.1 **a, b** Transmission electron microscope (TEM) images of cells *Magnetospirillum magneticum* strain AMB-1 grown in a fermenter showing chains of magnetite magnetosomes that traverse the cell along its long axis. **c, d** TEM images of purified magnetosomes from the same organism. The magnetite crystals are cuboctahedral in morphology. **d** *Arrow* denotes magnetosome membrane which envelopes each crystal

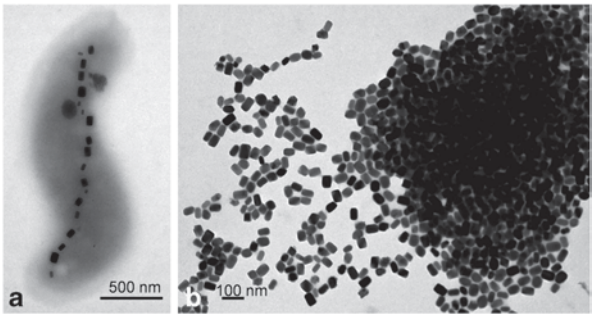

Fig. 3.2 **a** TEM images of a cell and **b** purified magnetite magnetosomes of *Magnetovibrio blakemorei* strain MV-1 grown in a fermenter. The magnetite crystals in this organism are elongated hexahedrons

Magnetosome magnetite crystal morphology is generally consistent within a single species of magnetotactic bacterium (Bazylinski and Frankel 2004; Lefèvre et al. 2013a). While seemingly also true of some uncultured greigite-producing species, several different morphologies of greigite have been observed in some cells. Regardless of composition, three general magnetosome crystal morphologies have been characterized, which include: (1) cuboctahedral (equidimensional; Figure 3.1), (2) elongated prismatic (Figure 3.2), and (3) bullet- or tooth-shaped (anisotropic having properties that differ according to direction or are directionally dependent; Bazylinski and Frankel 2004; Lefèvre et al. 2011d). Bullet-shaped magnetosome magnetite crystals are further subdivided into those with one pointed end and one flat end (flat-top shaped, fts) and those pointed at each end (double-triangular shaped, dts) which appear as two isosceles triangles sharing a common base (Lefèvre et al. 2011d). Although the projected triangles in dts crystals appear to have the same width, one triangle is often longer.

The cuboctahedral, equilibrium form of magnetite is known to occur in inorganically chemically formed magnetites (Palache et al. 1944). However, the occurrence of elongated prismatic and anisotropic habits in magnetosome crystals indicates anisotropic growth conditions such as a temperature or chemical concentration

gradient, or an anisotropic ion flux, any of which could cause these crystals to grow at faster rate in one direction than another, i.e., growth of these crystals is not centrosymmetric (Mann and Frankel 1989).

It is important to note that the chemical purity of magnetosome crystals, the intracellular arrangement of magnetosomes in the cell, as well as the strict control over the size and crystal morphology are characteristic features of a biologically controlled mineralization (Bazylinski and Frankel 2003). The non-equidimensional forms, the elongated prismatic and bullet-shaped crystals, of magnetite found in ancient sediments on Earth and in extraterrestrial materials such as meteorites have been used as evidence for the past presence of magnetotactic bacteria and are known as magnetofossils (Bazylinski and Frankel 2003; Jimenez-Lopez et al. 2010; Thomas-Keprta et al. 2000, 2001, 2002).

The organic component of the magnetosome, the magnetosome membrane (Figure 3.1d), appears to be the locus of control over the biomineralization of magnetosomes in magnetotactic bacteria (Schüler 2008). The magnetosome membrane is similar to the outer and cytoplasmic membranes of other Gram-negative prokaryotes in that it consists of fatty acids, glycolipids, sulfolipids, phospholipids, and proteins (Gorby et al. 1988; Grünberg et al. 2004). Based on fatty acid similarities and electron cryoelectrontomography studies, the magnetosome membrane originates as an invagination of the cytoplasmic membrane (Grünberg et al. 2004; Komeili et al. 2006; Tanaka et al. 2006). However, many specific proteins are only present in the magnetosome membrane, and these represent the proteins thought to mediate magnetosome biomineralization.

3.4 The First Magnetosomes and Origin of Greigite Magnetosome Biomineralization

A significant correlation between phylogenetic groups of magnetotactic bacteria and their magnetosome mineral composition and crystal morphology exists that might have important evolutionary implications. All known species within the most deeply branching phylogenetic groups in the domain Bacteria containing magnetotactic bacteria which include the candidate division OP3, the *Nitrospirae,* and the *Deltaproteobacteria* biomineralize only bullet-shaped crystals of magnetite in their magnetosomes (Kolinko et al. 2011; Lefèvre et al. 2011a, b, c) although some species in the *Deltaproteobacteria* also produce greigite (Lefèvre et al. 2011b; Lins et al. 2007) or only greigite (Abreu et al. 2007). Magnetotactic bacteria in the later diverging groups, the *Alpha-* and *Gammaproteobacteria*, biomineralize only cuboctahedral and elongated prismatic crystals of magnetite and never bullet-shaped crystals (Bazylinski and Williams 2007; Lefèvre et al. 2012; Schüler and Baeuerlein 1997). This finding suggests, given this correlation and the large amount of variation and number of crystal flaws in bullet-shaped magnetite crystals in general, that the composition of the first magnetosome crystals was magnetite and the first

magnetosome mineral morphology was bullet-shaped (Abreu et al. 2011; Lefèvre et al. 2013a). It will be interesting and exciting if geological studies of magnetosomes support this hypothesis.

Greigite biomineralization in magnetosomes seems to have originated in the *Deltaproteobacteria* since every recognized magnetotactic bacterium that produces this iron sulfide mineral belongs to this phylogenetic group (Lefèvre et al. 2011c). A separate set of genes may be responsible for greigite biomineralization as the only cultured magnetotactic bacterium that produces greigite also produces magnetite and contains two sets or cassettes of magnetosome genes (see latter section on genomics of magnetotactic bacteria). Specific individual genes are quite similar which might suggest that the second set of genes possibly involved in greigite biomineralization might have arisen from gene duplication and subsequent mutation (Lefèvre et al. 2013a).

3.5 Function of Magnetosomes

Magnetosome chains impart a permanent magnetic dipole moment to a magnetotactic bacterium which causes it to experience a torque in a magnetic field tending to align the cell along the Earth's geomagnetic field lines while it swims (Blakemore 1975). In a magnetic field, cells therefore behave like miniature, motile compass needles (Frankel and Blakemore 1980; Frankel and Moskowitz 2003). The suffix "-taxis" is a misnomer in the magnetotaxis context because cells do not swim towards or away from a magnetic field. This is quite different from bacterial phototaxis or chemotaxis in which cells move either towards or away from light or concentrations of different chemical molecules, respectively.

Although it is widely accepted that the Earth's geomagnetic field has direction (e.g., north and south), the actual direction of the Earth's geomagnetic field lines at any given location is the vectorial sum of the horizontal and vertical components of the geomagnetic field. The geomagnetic field lines are flat at the equator because there is no vertical component to the field which only includes the horizontal component. At any specific location away from the equator towards either pole, geomagnetic field lines deviate from the horizontal at an angle (known as the angle of dip) which increases to 90° at the poles where only the vertical component is present. Thus, geomagnetic field lines are inclined on most of Earth. While several models have been proposed on how magnetotaxis functions in nature, the most widely accepted model suggests that magnetotaxis aids cells locating and maintain an optimal position in vertical chemical and redox gradients by making chemotaxis more efficient (Frankel et al. 1997, 2007).

Two forms of magnetotaxis are currently recognized (Frankel et al. 1997, 2007). The term axial magneto-aerotaxis is used for cells that lack a polar preference in their swimming direction and that swim in both directions in a magnetic field under

oxic conditions, thus using the magnetic field as an axis. In contrast, polar magneto-aerotaxis describes the behavior of cells that swim in a preferred direction in a magnetic field under oxic conditions. Polar magnetotactic bacteria are either north- or south-seeking depending on which magnetic pole they swim towards under oxic conditions. In the northern hemisphere, north-seeking cells swim downward because of the Earth's inclined geomagnetic field lines and vice versa. Those that swim downward are thought to be selected for as those that swim upward would die from exposure to toxic concentrations of oxygen.

Cells of both axial and polar cultured magnetotactic bacteria grow as microaerophilic bands of cells in semisolid oxygen gradient media and are capable of reversing their swimming direction. This reversal in swimming direction for both appears to be dependent on aerotaxis, although each type appears to utilize a different mechanism of aerotaxis (Frankel et al. 1997, 2007). Regardless of whether cells use axial or polar magneto-aerotaxis, once cells are aligned along the Earth's inclined magnetic field lines, locating an optimal position in a vertical chemical/redox gradient is reduced from a three-dimensional search problem, which would apply to motile nonmagnetotactic bacteria, to one of a single dimension. Thus, the passive alignment of motile cells along geomagnetic field lines in magnetotaxis increases the efficiency of chemotaxis (in this case aerotaxis; Frankel et al. 1997, 2007). This model suits some magnetotactic bacteria very well, especially sulfide-oxidizing species that use hydrogen sulfide and oxygen as the electron donor and acceptor, respectively, as both compounds are available to the cells at the OAI in many aquatic environments. However, this model does not explain certain observations. These include the presence of large numbers of south-seeking polar magnetotactic bacteria in natural habitats of the northern hemisphere (Shapiro et al. 2011; Simmons et al. 2004, 2006) and the presence of significant amounts of south-seeking cells in cultures of polar magnetotactic bacteria grown in the northern hemisphere. In both cases, in the magneto-aerotaxis model described above, south-seeking cells would presumably continue to swim southward/upward towards the oxygen-rich surface of the northern hemisphere and die and thus be selected against.

There are other observations and results that remain to be explained. For example, why do magnetotactic bacteria require magnetosomes to locate the OAI when many obligately microaerophilic, nonmagnetotactic bacteria do so apparently successfully without them? Why do cells of *Magnetospirillum* species continue to produce magnetosomes when grown anaerobically and respiring nitrate in homogenous growth medium lacking a gradient? While it is certainly possible that there are physiological explanations for magnetosome biomineralization that might include energy conservation through iron oxidation/reduction (Guerin and Blakemore 1992), detoxification of free iron ions in the cell, and decomposition of toxic oxygen radicals produced during respiration (Blakemore 1982; Guo et al. 2012b), no strongly convincing physiological function for magnetosomes has yet been characterized and widely accepted.

3.6 Genomics of Magnetotactic Bacteria

The complete or nearly complete genome sequences of a number of cultured and uncultured magnetotactic bacteria are available for examination. Magnetosome biomineralization- and magnetotaxis-related genes have now been identified using two different strategies: (1) performing reverse genetics using amino acid sequences of isolated magnetosome membrane proteins to obtain the gene sequences that encode these proteins and (2) cross-comparing complete and partial genomes of different magnetotactic bacteria using various genomic techniques. This latter type of genome analyses has provided valuable insight into how magnetosome genes are organized in different magnetotactic bacteria as well as to the identification of magnetosome genes common to groups of magnetotactic bacteria as well as how these genes evolved (Richter et al. 2007; Jogler et al. 2009; Lefèvre et al. 2013b).

Magnetosome-related genes are referred to as the *mam* (magnetosome membrane) and *mms* (magnetic particle membrane specific) genes, and a significant number of these genes and perhaps organism-specific magnetosome genes have been found in the genomes of every magnetotactic bacterium whose genome has been sequenced. The *Mam* and *mms* genes are arranged as clusters that are in relatively close proximity to one another within the genomes of almost all magnetotactic bacteria studied (Lefèvre and Bazylinski 2013). These clusters are further organized as a larger unit, sometimes as a genomic magnetosome island (MAI), in some organisms. Typical characteristics of genomic islands include the presence of mobile elements (e.g., insertion sequences) and transfer RNA (tRNA) genes that act as insertion sites for integrases (Blum et al. 1994; Mahillon and Chandler 1999; Mahillon et al. 1999; Reiter and Palm 1990; Reiter et al. 1989) and a different guanine + cytosine content compared to the rest of the genome (Dobrindt et al. 2004). For example, in *M. gryphiswaldense,* the putative MAI is about 130 kb in size, contains three tRNA genes upstream of the *mms* operon, has a slightly different guanine + cytosine content to that of the rest of the genome, and contains 42 mobile elements that include transposases of the insertion sequence type and integrases (Ullrich et al. 2005). Putative MAIs have been found in the genomes of other magnetotactic bacteria, including other *Magnetospirillum* species, *M. blakemorei,* and *Desulfovibrio magneticus* (Jogler et al. 2009; Matsunaga et al. 2005; Nakazawa et al. 2009). However, an MAI may not be present in all magnetotactic bacteria as the clusters of magnetosome genes in some species, such as *M. marinus, Candidatus Desulfamplus* magnetomortis strain BW-1, or *Magnetospira* sp. QH-2 lack some or many of the features typical of genomic islands (Ji et al. 2014; Lefèvre et al. 2013b; Schübbe et al. 2009).

Some evidence suggests that genomic islands are transferred between different bacteria through a process referred to as horizontal gene transfer (HGT). In addition, because of the, oftentimes, many mobile elements between genes in genomic islands, they are known to undergo frequent gene rearrangements some believe are a major mechanism for the evolution of bacterial genomes (Juhas et al. 2009). Transfer of the MAI through HGT could explain the great phylogenetic diversity

of the magnetotactic bacteria, while variations of the MAI in different magnetotactic bacteria might result from rearrangements within the MAI occurring over time (Bazylinski and Frankel 2004; Lefèvre and Bazylinski 2013).

In sequenced *Magnetospirillum* species, magnetosome genes comprise three clusters, including the *mamAB, mamGFDC,* and *mms* operons (Ullrich et al. 2005). Although these three operons are conserved in all magnetotactic *Alphaproteobacteria* (Jogler and Schüler 2009), only the *mamAB* cluster is present in other phylogenetic groups of magnetotactic bacteria (Lefèvre and Wu 2013; Lefèvre et al. 2013b). Gene deletion studies in *M. magneticum* and *M. gryphiswaldense* show that only the *mamAB* cluster is essential for the biomineralization of magnetite magnetosomes (Lohße et al. 2011; Murat et al. 2010; Ullrich and Schüler 2010). Additional operons or genes in magnetotactic bacteria, some of which are specific to phylogenetic groups of magnetotactic bacteria, appear to have accessory functions in controlling the size and morphology of magnetite magnetosome crystals (Katzmann et al. 2010; Lohße et al. 2011; Murat et al. 2010; Ullrich and Schüler 2010). Two examples include the *mamGFDC* and *mms* operons in the magnetotactic *Alphaproteobacteria* (Scheffel et al. 2008) and the recently described *mad* (magnetosome-associated deltaproteobacterial) genes in the magnetotactic *Deltaproteobacteria* and *Nitrospirae* (Lefèvre et al. 2013b).

The *mamAB* operon contains all the genetic determinants responsible for the minimal set of functions required for magnetosome chain formation in all magnetotactic bacteria. This operon contains ten genes (*mamABEIKLMOPQ*) that are conserved in all magnetite-producing magnetotactic bacteria while nine of these genes (*mamABEIKMOPQ*) are also conserved in greigite-producing species (Abreu et al. 2011; Lefèvre et al. 2013b; Lohße et al. 2011). Thus, identifying the function of the proteins that these genes encode appears to be the key to elucidating the magnetosome biomineralization process. Putative functions for many of these proteins have been predicted and/or assigned based on comparisons of similar proteins through mutagenesis experiments and basic local alignment search tool (BLAST) searches.

The proteins MamI and MamL are specific to magnetotactic bacteria and have no known homologues in nonmagnetotactic species (Richter et al. 2007). They do not contain known domains or obvious sequence patterns. Experimental evidence suggests that they might be involved in the invagination of the cell membrane to form the magnetosome vesicle (Murat et al. 2010).

Other proteins in the core set encoded by genes in the *mamAB* operon contain functional domains identified through in silico and/or experimental evidence. These include (1) one tetratricopeptide repeat (TPR) in MamA, a protein that appears to participate in assembly of the magnetosome membrane through protein–protein interaction (Komeili et al. 2004; Zeytuni et al. 2011, 2012); (2) at least one cation diffusion facilitator (CDF) domain necessary for iron transport and magnetosome membrane assembly, present in both MamB and MamM (Uebe et al. 2011); (3) PDZ (named after three proteins: postsynaptic density (PSD95) protein, *Drosophila* disc large tumor suppressor (Dlg1), and zonula occludens-1 protein (zo-1) (Beuming et al. 2005)) domains that mediate protein–protein interactions (two are present in MamE and one in MamP; Jogler and Schüler 2009; Murat et al. 2010; Quinlan et al.

2011); (4) a LemA domain, present in MamQ, whose function is unknown (Lohße et al. 2011; Murat et al. 2010); (5) at least four magnetochrome domains (two in MamP, two in MamE and/or MamT) that putatively ensure redox control and the stoichiometry of Fe(II)/Fe(III) (Siponen et al. 2012); and (6) one or two actin-like domains, present in MamK, involved in magnetosome chain assembly and its positioning inside the cell (Katzmann et al. 2010; Komeili et al. 2006). Several proteins contain multiple domains such as the proteases MamE which contains trypsin, magnetochrome, and PDZ domains or MamO which contains one trypsin and one TauE domain (Lohße et al. 2011; Murat et al. 2010). The roles of some of these proteins in magnetosome biomineralization are presented in greater detail in the next section.

3.7 Magnetosome Biomineralization

Little is known regarding the biomineralization of greigite magnetosomes except that several nonmagnetic iron sulfide minerals have been identified in greigite-producing magnetotactic bacteria, including mackinawite (tetragonal FeS) and a cubic form of FeS, both of which are thought to be precursors to greigite (Pósfai et al. 1998a, b). Therefore, this section is mainly focused on the biomineralization of magnetite magnetosomes.

The magnetite magnetosome biomineralization process in magnetotactic bacteria is complex and consists of a number of steps which must occur simultaneously within the cell (Bazylinski and Frankel 2004; Komeili 2012; Lefèvre and Bazylinski 2013; Lower and Bazylinski 2013; Schüler 2008). Magnetite biomineralization has been mainly studied in *Magnetospirillum* species, a group of *Alphaproteobacteria* that produce cuboctahedral crystals of magnetite (Bazylinski and Frankel 2004; Lefèvre and Bazylinski 2013; Schüler and Baeuerlein 1997), because growing these organisms is relatively simple and because there are tractable and efficient genetic systems for species of this genus (Komeili et al. 2004; Matsunaga et al. 1992; Murat et al. 2010; Schultheiss and Schüler 2004; Schultheiss et al. 2004). A summary of the proteins believed to be involved in magnetite biomineralization and their putative function is shown in Table 3.1.

In *Magnetospirillum,* the first stage in magnetite magnetosome synthesis involves invagination of the cytoplasmic membrane and formation of a membrane vesicle, presumably by pinching off of some of the cell membrane (Komeili et al. 2006). Whether the invagination truly pinches off to form a true membrane vesicle has not been unequivocally resolved (Komeili et al. 2006; Katzmann et al. 2010). Magnetosome proteins important in magnetosome invagination/vesicle formation include MamB, MamI, MamL, and MamQ which appear to be essential for the formation of the magnetosome membrane in *M. magneticum* (Murat et al. 2010). Some may also be important in bending and shaping of the magnetosome membrane (Komeili 2012). The *mamA* gene, present in the genomes of all known magnetotactic bacteria, encodes a protein that displays high amino acid sequence similarity to proteins of the TPR protein family as stated in the previous section (Okuda et al. 1996).

Table 3.1 Magnetosome proteins and their putative function

Protein	Function	Reference
MamA, Mam22, Mam24	Serve as scaffold proteins to coordinate assembly of functional protein complexes within the magnetosome	Abreu et al. 2011; Grünberg et al. 2001; Komeili et al. 2004; Matsunaga et al. 2005; Nakazawa et al. 2009; Okuda et al. 1996; Schübbe et al. 2009; Taoka et al. 2006; Yamamoto et al. 2010
MamB, MamM, MamN, MamP, MamV	Transport iron into the magnetosome, initiate magnetite crystal growth, form protein–protein complexes with each other	Abreu et al. 2011; Grass et al. 2005; Grünberg et al. 2001; Haney et al. 2005; Matsunaga et al. 2005; Murat et al. 2010; Nakazawa et al. 2009; Schübbe et al. 2009; Uebe et al. 2011; Siponen et al. 2013
MamC/Mms12/Mms13, MamD/Mms7, MamF MamG/Mms5, Mms6, MamR, MamS, MamT, MamX, MamZ	Control nanocrystal size, morphology, and maturation	Arakaki et al. 2003; Ding et al. 2010; Fukuda et al. 2006; Grünberg et al. 2004; Murat et al. 2010; Prozorov et al. 2007; Raschdorf et al. 2013; Taoka et al. 2006; Valverde-Tercedor et al. 2014; Yang et al. 2013
MamE, MamO	Proper localization and arrangement of proteins within the magnetosome membrane	Grünberg et al. 2001; Murat et al. 2010; Quinlan et al. 2011; Yang et al. 2010
MamI, MamL, MamQ	Catalyze initial step in magnetosome membrane formation and invagination	Murat et al. 2010
MamJ, MamK	Assembly of the magnetosome chain	Katzmann et al. 2010, 2011; Komeili et al. 2006; Schübbe et al. 2003; Scheffel et al. 2006; Scheffel and Schüler 2007
FeoB1, FeoB2, Fur protein, FtsZm	Cellular iron uptake, prevent oxidative stress, iron homeostasis, magnetosome formation, redox control	Müller et al. 2014; Qi et al. 2012; Rong et al. 2008, 2012; Uebe et al. 2010

Multiple copies of TPRs are known to form scaffolds within proteins to mediate protein–protein interactions and to coordinate the assembly of proteins into multisubunit complexes (Ponting and Phillips 1996). Therefore, MamA might function as a scaffolding protein in the coordination of the assembly of oligomeric protein complexes which could occur during magnetosome biomineralization and construction of the magnetosome chain (Zeytuni et al. 2011, 2012).

The next stage of magnetosome biomineralization involves the apparently continual uptake of iron. Cultured magnetotactic bacteria are facile with regard to iron uptake and can consist of greater than 3 % iron on a dry weight basis, an amount sev-

eral orders of magnitude over nonmagnetotactic bacterial species (Blakemore 1982; Heyen and Schüler 2003; Schüler and Baeuerlein 1998). Both Fe(II) and Fe(III) are taken up by cells of *Magnetospirillum* for magnetite synthesis (Matsunaga and Arakaki 2007; Schüler and Baeuerlein 1998; Suzuki et al. 2006) and the process appears to occur relatively quickly (Heyen and Schüler 2003; Schüler and Baeuerlein 1997, 1998). The specific details regarding iron uptake by magnetotactic bacteria for magnetosome synthesis are not known, but it seems likely that several iron uptake systems function in each magnetotactic bacterial species, as has been found in other nonmagnetotactic bacteria (Calugay et al. 2003; Dubbels et al. 2004; Paoletti and Blakemore 1986). Siderophores, low molecular weight iron chelators (Neilands 1995), have been implicated in iron uptake by some magnetotactic bacteria (Calugay et al. 2003; Dubbels et al. 2004; Paoletti and Blakemore 1986) but not others (Schüler and Baeuerlein 1996; Zhang et al. 2013) although their role in magnetosome synthesis has never been clearly established. Other studies have proposed different possible mechanisms for iron uptake in magnetotactic bacteria, including a copper-dependent iron uptake system in *M. blakemorei* (Dubbels et al. 2004) and an accessory role for *feoB1,* a gene encoding the ferrous iron transport protein B, in magnetosome formation in *M. gryphiswaldense* (Rong et al. 2008). However, comparative genomic analyses showed that in most genomes of magnetotactic bacteria, a second copy of the operon *feoAB* is specific to them and might be involved in ferrous iron uptake for magnetite and/or greigite biomineralization (Lefèvre et al. 2013b). Rong et al. (2012) recently provided evidence that FeoB2 functions in magnetosome formation and oxidative stress protection in *M. gryphiswaldense*.

After iron has been taken up by the cell, it is transported to the interior of the magnetosome invagination/vesicle. A number of magnetosome membrane proteins are thought to be involved in this process. MagA was originally thought to play a significant role in iron transport to the magnetosome membrane vesicle in *M. magneticum* (Nakamura et al. 1995) although recent evidence suggests that it is not involved in magnetosome biomineralization (Uebe et al. 2012). MamB and MamM (and MamV in some species), homologous proteins that function as CDF transporters that mediate the influx or efflux of cadmium, iron and zinc in some bacteria, (Grass et al. 2005; Haney et al. 2005; Paulsen et al. 1997) are thought to be responsible for the transport of iron to the magnetosome membrane vesicle/invagination (Grünberg et al. 2001). The genes that encode MamB and MamM are present in the genomes of all magnetotactic bacteria examined thus far, while *mamV* has only been found in *Magnetospirillum magnetotacticum* and *M. magneticum* (Abreu et al. 2011; Grünberg et al. 2001; Matsunaga et al. 2005; Nakazawa et al. 2009; Schübbe et al. 2009).

Considering how much iron is taken up by magnetotactic bacteria, the regulation of iron uptake genes might differ greatly from nonmagnetotactic prokaryotes. In one study (Suzuki et al. 2006), it was shown that the genes encoding ferrous iron transporter proteins were upregulated during magnetite biomineralization by cells of *M. magneticum,* while those encoding ferric iron transporter proteins were downregulated. Interestingly, there was no observable change in the expression patterns of the CDF proteins MamB and MamM. These proteins form heterodimers and

interact with other magnetosome proteins, suggesting that magnetosome formation involves coordinated interactions between many proteins and genes (Uebe et al. 2011). The Fur (ferric uptake regulator) protein has been shown to be involved in global iron homeostasis in *M. gryphiswaldense,* possibly by balancing competing requirements for iron in essential biochemical reactions (in enzymes) and magnetite biomineralization (Qi et al. 2012; Uebe et al. 2010).

Finally, in the last stage, magnetite biomineralization occurs which likely involves redox reactions of iron (i.e., reduction and/or oxidation) and the controlled nucleation and maturation of the magnetite crystal within the magnetosome invagination/vesicle. Results from Mössbauer spectroscopic analysis of magnetotactic bacteria and magnetosomes suggested that magnetite precipitation in magnetotactic bacteria occurred through the reduction of hydrated ferric oxide(s) (Faivre et al. 2007; Frankel et al. 1979, 1983). This now seems unlikely because cells of *M. gryphiswaldense* shifted from iron-limited to iron-sufficient conditions show no delay in magnetite production (Heyen and Schüler 2003) which implies that there are no mineral precursors to magnetite in this organism (Faivre et al. 2007; Heyen and Schüler 2003) during biomineralization or that they are unstable and transform to magnetite extremely rapidly. Iron reduction may still be important in the process as Zhang et al. (2013) found six ferric reductase isoenzymes in *M. gryphiswaldense,* two of which (the bifunctional FeR5 and FeR6), when their genes were deleted, resulted in the loss of magnetosome magnetite synthesis. However, deletion of one or the other alone showed no significant loss of magnetite synthesis in the organism, suggesting that these enzymes play complementary roles in magnetite magnetosome synthesis.

A ferritin-like protein was identified in the membrane fraction of cells of *M. gryphiswaldense* during magnetite biomineralization using Mössbauer spectroscopy (Faivre et al. 2007). No other intermediates were observed. Ferritins, ubiquitous intracellular proteins that store iron, release their stored iron in a controlled fashion when required by the cell (Theil 1987). It is possible that iron contained within this ferritin-like protein co-precipitates soluble ferrous iron to form magnetite crystals in the cell membrane, which are then transported into the magnetosome invagination/vesicle (Faivre et al. 2007). In a recent study, in which X-ray absorption spectroscopy at cryogenic temperatures and transmission electron microscopic imaging techniques were used to chemically characterize and spatially resolve the mechanism of magnetite biomineralization in magnetotactic bacteria, it was shown that magnetite forms through phase transformation from a highly disordered phosphate-rich ferric hydroxide phase, consistent with prokaryotic ferritins, through transient nanometric ferric (oxyhydr)oxide intermediates within the magnetosome vesicle (Baumgartner et al. 2013).

Two phases of iron, ferrihydrite and magnetite, were identified and quantified in a magnetic and structural study of magnetosomes of *M. gryphiswaldense* that used a combination of iron K-edge X-ray absorption near edge structure (XANES) and high-resolution transmission electron microscopy (Fdez-Gubieda et al. 2013). Results from this work suggest that indeed ferrihydrite is the source of iron ions for magnetite biomineralization in *M. gryphiswaldense*. Two steps were characterized

in the magnetite biomineralization process: First, iron accumulates in the cell in the form of ferrihydrite, and second, magnetite is rapidly biomineralized from ferrihydrite. The XANES analysis suggests that the origin of the ferrihydrite is bacterial ferritin cores that are characterized by high phosphorus content and a poorly crystalline structure (Fdez-Gubieda et al. 2013).

If ferrihydrite and/or ferritins are indeed precursors to magnetite in magnetotactic bacteria, specific proteins involved in their synthesis have not been clearly identified. The magnetosome protein MamP contains a self-plugged PDZ domain fused to two magnetochrome domains and has recently been shown to possess iron oxidase activity that contributes to the formation of iron(III) ferrihydrite possibly required for magnetite crystal growth in vivo as described above (Siponen et al. 2013). Thus, magnetochrome domains in the proteins MamE, MamP, and MamX may play an important role in iron biomineralization processes (Siponen et al. 2013).

Specific magnetosome proteins appear to be implicated in magnetosome magnetite crystal maturation. The tubulin-like protein FtsZ, a ubiquitous cytosolic protein in prokaryotes, is known to polymerize into an oligomeric structure that forms the initial ring at midcell and plays an essential role in cytokinesis (cell division; Errington et al. 2003). A similar gene, referred to as *ftZ*-like, is present in the MAI of *Magnetospirillum* species, and like FtsZ, the FtsZ-like protein forms guanosine triphosphate (GTP)-dependent filaments in vitro (Ding et al. 2010). Although cell division was unaffected when *ftZ*-like was deleted in *M. gryphiswaldense,* cells were nonmagnetotactic and contained magnetite crystals that were significantly smaller than those of the wild-type strain (Ding et al. 2010). It was recently shown in *M. gryphiswaldense* that FtsZ-like interacts in vitro, when expressed in *Escherichia coli,* with its homolog FtsZ and forms distinct structures localized at midcell and at the cell pole (Müller et al. 2014). It was demonstrated in this study that deletion of *Ftsz*-like has a strong effect on magnetite formation when cells are grown under microaerobic conditions, suggesting that this protein plays a role in redox control during magnetite crystallization (Müller et al. 2014). In contrast, deletion of this gene in *M. magneticum* did not result in changes in the size of magnetosome magnetite crystals (Murat et al. 2010).

Some magnetosome membrane proteins, including MamC (equivalent to Mms12 and Mms13), MamD (Mms7), MamF, MamG (Mms5), MamX, and Mms6, appear to control the shape and size of the crystals during magnetosome magnetite crystal maturation (Arakaki et al. 2003; Fukuda et al. 2006; Grünberg et al. 2004; Taoka et al. 2006; Yang et al. 2013). Of all magnetosome membrane proteins, MamC, MamD, and MamG appear to be the most abundant, comprising about 35 % of all proteins present in this structure (Scheffel et al. 2008). The amphiphilic protein Mms6 consists of an N-terminal leucine–glycine-rich hydrophobic region and a C-terminal hydrophilic region containing numerous acidic amino acids (Arakaki et al. 2003; Prozorov et al. 2007). It has iron-binding capabilities and appears to influence the morphology of magnetite crystals precipitated chemically in vitro (Arakaki et al. 2003; Prozorov et al. 2007). The MamX protein appears to play a significant role in controlling magnetosome magnetite crystal size, maturation, and crystal form and is highly conserved in *Magnetospirillum* species. Deletion mutants of *mamX* in

M. gryphiswaldense, like those of *ftsZ-like* deletion mutants described earlier, exhibit a very weak magnetotactic response and biomineralize very small, irregularly shaped, superparamagnetic magnetosome magnetite particles (Yang et al. 2013). Recently, however, it has been shown that MamX, as well as MamZ and MamH, are involved in redox control of magnetite biomineralization in *M. gryphiswaldense* (Raschdorf et al. 2013), thereby possibly affecting magnetosome magnetite crystal size and maturation.

3.8 Mass Cultivation of Magnetotactic Bacteria

A major challenge to the use of materials from magnetotactic bacteria for virtually all commercial and medical applications is obtaining the high yields of magnetotactic bacterial cells and magnetosomes required for these applications. Cells of the desired strain must thus be grown in mass culture under conditions where growth and magnetite biomineralization is optimized. The focus of these studies generally involves modifications of growth media and the conditions under which cultures are incubated. The model organisms used in almost all these studies are *Magnetospirillum* species because they appear to be the magnetotactic bacteria that are the simplest to grow. It is important to note that when examining studies of this type, it is difficult to compare growth and magnetosome yields directly; yields are reported in different units in different studies. In addition, some studies only report magnetosome yields, and it is unclear whether magnetosome membranes are included in the yield values.

Two general approaches have been used in studies involving mass culture of magnetotactic bacteria. They include (1) the simple scaling up of batch cultures and (2) growing cells in a fermenter where the oxygen concentration is precisely controlled. Microaerobic or anaerobic conditions are absolutely required for magnetite synthesis in magnetotactic bacteria (Bazylinski and Frankel 2004; Lefèvre and Bazylinski 2013), and thus controlling the level of oxygen is very important. Redox potential of the growth medium is also important as most magnetotactic bacteria require not only low or no oxygen but also a reducing agent added to the growth medium. The selection of a reducing agent used to poise the redox potential of the growth medium is also very important as some are known to be toxic and/or may also have an effect on magnetosome production (Li et al. 2013a). *Magnetospirillum* species, which biomineralize cuboctahedral crystals of magnetite, were the model magnetotactic bacteria in these studies (Bazylinski and Frankel 2004; Lefèvre and Bazylinski 2013). A problem using *Magnetospirillum* species solely in these studies is that many magnetotactic bacteria synthesize elongated prismatic magnetite crystals which might be more suitable or have properties that are more advantageous than cuboctahedra in specific applications but have not been tested because of the lack of growth experiments on these latter organisms.

Matsunaga et al. (1990) grew cells of *M. magneticum* strain AMB-1 in a 1000 l fermenter and obtained the highest magnetosome yield yet achieved of 2.6 mg/L

of culture. The same group performed culture optimization experiments using fed-batch cultures of the same organism but did not obtain higher yields of cells or magnetosomes (Matsunaga et al. 1996, 2000). A recombinant strain of *M. magneticum* harboring the plasmid pEML was grown in a pH-regulated fed-batch culture system where the addition of fresh nutrients was feedback controlled as a function of the pH of the culture (Yang et al. 2001a). In this study, magnetosome yield was boosted by adjusting the rate of addition of the major iron source, ferric quinate at 15.4 mg/min, resulting in a magnetosome yield of 7.5 mg/L. The use of different iron sources and the addition of various nutrients and chemical reducing agents (e.g., L-cysteine, yeast extract, polypeptone) also had significant effects on magnetosome yield by *M. magneticum* grown in fed-batch culture (Yang et al. 2001b).

Use of an oxygen-controlled fermenter has allowed for more rigorous control over the growth of and magnetosome production by *Magnetospirillum* species (Heyen and Schüler 2003; Lang and Schüler 2006). Three species were grown using this technique, *M. gryphiswaldense, M. magnetotacticum,* and *M. magneticum,* and magnetite yields of 6.3, 3.3, and 2.0 mg/L/day were obtained from each species, respectively (Heyen and Schüler 2003). A different group, using a similar type of fermenter where the dissolved oxygen was controlled to an optimal level using the change of cell growth rate rather than from a direct measurement from the sensitive oxygen electrode, obtained a cell density measured as an optical density at 565 nm (OD_{595}) of 7.24 for *M. gryphiswaldense* after 60 h of culture incubation (Sun et al. 2008). The cell yield (dry weight) was 2.17 g/L, and the yield of magnetosomes (dry weight) was 41.7 mg/L and 16.7 mg/L/day. In a similar study, Liu et al. (2010) decreased the amount of carbon and electron source (lactate) in the same fermenter and reported growth and magnetosome yields of OD_{595} of 12 and 55.49 mg/L/day, respectively, after 36 h of culture, using *M. gryphiswaldense*. The presence of iron-chelating agents such as rhodamine B and EDTA also appear to stimulate growth of and magnetosome production by *M. magneticum* (Alphandéry et al. 2012a).

A strategy different from those described above was used to obtain optimal growth and magnetosome yields in mass culture of the marine magnetotactic bacterium *M. blakemorei* (Silva et al. 2013). In this case, a statistics-based experimental factorial design approach was used to determine the key components and amounts in growth medium for maximum yields. This study is significant for several reasons, including: (1) *M. blakemorei* biomineralizes elongated prismatic magnetite crystals which could be superior to the cuboctahedral produced by *Magnetospirillum* species in certain applications, and (2) it represents the first attempt at mass culture of a marine magnetotactic bacterium. Using the optimized growth medium in this study, maximum magnetite yields of 64.3 mg/L in batch cultures and 26 mg/L in a fermenter were obtained (Silva et al. 2013).

A challenge for many years was to have magnetosomes synthesized by a non-magnetotactic organism with a short generation time such as *E. coli*. This was recently achieved by Kolinko et al. (2014) with the introduction and expression of all the *mam* genes of *M. gryphiswaldense* in one of the closest, nonmagnetotactic, phylogenetic relatives of the *Magnetospirillum* species, the photosynthetic *Rhodospirillum rubrum*. The biomineralization of magnetosomes in a nonmagnetotactic

recipient of the *mam* genes represent an important step not only towards the production of magnetosomes to high yield but also towards the endogenous magnetization of various organisms by synthetic biology (Kolinko et al. 2014).

3.9 Purification of Magnetosomes

Another major challenge to acquiring enough magnetosomes for specific applications is their efficient purification. Several reports have been published that describe purification of magnetite magnetosomes from magnetotactic bacterial cells and all involve magnetic separation (Bazylinski et al. 1994; Gorby et al. 1988). The extensive washing of magnetosomes is a relatively tedious task in these purification strategies. There is one study reporting a more rapid procedure for magnetosome purification (Guo et al. 2011).

3.10 Applications of Magnetotactic Bacteria and Magnetosomes in Nanotechnology

Chemically and biologically produced nanoparticles of numerous compositional and morphological types have been shown to be very useful in many scientific, commercial, and medical applications (Cameotra and Dhanjal 2010; Musarrat et al. 2011). Due to their physical properties, magnetic nanoparticles in particular have proven to be essential in numerous medical applications (Ramanujan and Narayan 2009; Trahms 2009). In this section, we examine how magnetosome magnetic crystals might or have been exploited in specific applications.

Cells of magnetite-producing magnetotactic bacteria, their magnetosomes, and magnetosome crystals have unusual and, sometimes, unique magnetic, physical, and optical properties that make them employable in numerous scientific, commercial, and other applications. The applications presented in this section focus on magnetite magnetotactic bacteria and magnetosomes since there are few cultured greigite-producing strains and the mass synthesis of greigite by magnetotactic bacteria has not yet been achieved.

Magnetotactic bacterial cells, living or not, have proven useful in medical, magnetic, and environmental applications. They are very effective in cell sorting and separation because of the ease in which the resultant magnetic cells can be manipulated using magnetic techniques (Matsunaga et al. 1989). Magnetotactic bacteria can act as biosorbents for heavy metals (Zhou et al. 2012). This and the fact that the cells can be relatively easily removed magnetically from a suspension, the use of magnetotactic bacteria in the uptake and remediation of heavy metals, and radionuclides from wastewater has been discussed (Arakaki et al. 2002; Cameotra and Dhanjal 2010; Bahaj et al. 1993, 1998a, b, c).

Polar magnetotactic bacteria, those that display a clear preferred direction of swimming under oxic conditions, are useful in applications in which the cells can be guided to a target area magnetically. For example, they are useful in determining south magnetic poles in meteorites and rocks containing fine-grained (< 1 mm) magnetic minerals (Funaki et al. 1989, 1992) and for nondestructive magnetic domain analysis on soft magnetic materials (Harasko et al. 1993, 1995). One of the most interesting applications of magnetotactic bacteria is their use as microrobots (e.g., Martel 2008, 2012). Cells of the polar magnetotactic cocci, *M. marinus* (Bazylinski et al. 2013) and strain MO-1 (Lefèvre et al. 2009), have been used to transport 2–3 mm diameter microbeads efficiently and towards a specific area through microfluidic channels (Ma et al. 2012; Martel 2012; Felfoul and Martel 2013). These studies demonstrate possible uses of magnetotactic bacteria in chemical analyses and medical diagnoses using biochips, as well as in nano/microscale transport of, for example, drugs. The behavior of polar magnetotactic bacteria has even inspired the creation of nonbiological magnetic microengines or robots for applications (Zhao et al. 2012).

The magnetic and physical features of magnetosomes, i.e., they are membrane-enveloped, single magnetic domain crystals, make them useful and effective in many applications. Magnetosomes, like cells of magnetotactic bacteria, are also useful in magnetic cell separation (Kuhara et al. 2004). The phospholipid magnetosome membrane that envelopes the magnetic crystals allows for the attachment of different types of biological molecules on their surfaces, thus making them particularly suitable in many applications. For example, magnetite magnetosomes have proven useful in the immobilization of various enzymes (Matsunaga and Kamiya 1987) and in the formation of magnetic antibodies useful in various fluoroimmunoassays (Matsunaga et al. 1990) involving the detection of allergens (Nakamura and Matsunaga 1993) and squamous cell carcinoma cells (Matsunaga 1991) and the quantification of immunoglobulin G (Nakamura et al. 1991). Fluorescein isothiocyanate-conjugated monoclonal antibodies immobilized on magnetosome membranes have been used in the detection and removal of *E. coli* cells (Nakamura et al. 1993). Trypsin conjugates immobilized to *M. gryphiswaldense* magnetite magnetosomes exhibited stability at relatively high temperature and were reusable in protein digestion (Pečová et al. 2013). Magnetite magnetosomes have also been used to detect single-nucleotide polymorphism based on a fluorescence resonance energy transfer technique in which double-stranded labeled DNA synthesized by polymerase chain reaction (PCR) and immobilized to the magnetosomes hybridizes to target DNA and a fluorescence signal is detected (Maruyama et al. 2004; Nakayama et al. 2003; Ota et al. 2003; Tanaka et al. 2003; Yoshino et al. 2003). Magnetosomes, when conjugated to other molecules, have been used as sensors for *Staphylococcus enterotoxin* B in milk (Wu et al. 2013) and for the simultaneous detection of the drugs Pefloxacin and Microcystin-LR in seafood (Sun et al. 2013).

Specific magnetosome membrane proteins are very effective as anchor molecules and have been used as protein displays for the assembly of foreign proteins on the membrane surface of magnetite magnetosomes (Matsunaga and Takeyama 1998; Matsunaga et al. 2002; Yoshino and Matsunaga 2005, 2006). Magnetosome

membrane proteins, fused to the chemiluminescent protein luciferase (Matsunaga et al. 2000, 2002; Yoshino and Matsunaga 2006), were used to determine stability of the anchor proteins. The most stable of the proteins tested was Mms13 (equivalent to MamC, Mam12 in some species), whose fusion resulted in 400–1000 times the luminescence activity observed for other magnetosome protein fusions such as those using Mms16 or MagA (Yoshino and Matsunaga 2005) although its use in the expression of a number of human proteins was relatively low (Matsunaga et al. 2002). To improve expression levels of human proteins on magnetosomes, an *mms13* deletions mutant strain of *M. magneticum* was constructed. This strain biomineralized magnetosomes with a significantly higher expression of two human proteins, including thyroid-stimulating hormone receptor (TSHR) and the class II major histocompatibility complex (MHC II) molecules (Kanetsuki et al. 2012). It thus seems likely that magnetotactic bacterial strains that do not show high levels of specific protein expression can be genetically modified to overcome this problem. The poor expression of recombinant human proteins on magnetosomes might be due to proteolytic degradation by endogenous proteases (Kanetsuki et al. 2013). This problem was obviated by use of a strain of *M. magneticum* in which the *lon* protease gene was deleted (*Δlon*). Expression of the human proteins tested, including TSHR and MHC II, of the mutant *Δlon* was similar to that of the wild-type strain although protein expression levels in the *Δlon* transformants were significantly increased over wild-type cells. This strategy resulted in improved concentrations of the two proteins on magnetosomes (Kanetsuki et al. 2013). Functional expression of TSHR was also achieved on magnetosomes of *M. magneticum* (Sugamata et al. 2013). Oligomeric proteins were expressed by gene fusion to the MamC protein in *M. gryphiswaldense* (Ohuchi and Schüler 2009).

The magnetosome membrane protein MamC has been used as an anchor for a paraoxonase, resulting in magnetosomes that display phosphohydrolase activity effective in the degradation of ethyl-paraoxon, an organophosphate pesticide (Ginet et al. 2011). This finding has led to the production of functionalized magnetic nanoparticles efficient as a reusable nanobiocatalyst for pesticide bioremediation in contaminated effluents (Ginet et al. 2011).

Magnetosomes have been used effectively in the isolation of nucleic acids. Modified magnetosomes, using compounds such as hyperbranched polyamidoamine dendrimers, amino silanes, or oligo(dT), have been used for the extraction of DNA (Yoza et al. 2002, 2003a, b) and mRNA (Sode et al. 1993).

Chemically produced magnetic nanocrystals are relatively inexpensive to synthesize, particularly compared to the synthesis of magnetosomes, and are useful in numerous medical applications. The specificity, affinity, and binding capacity of these nanoparticles are the main characteristics that dictate how well these particles function in many applications. These characteristics, in turn, are dependent on the size, form, dispersion, and surface chemistry of the nanoparticles. These types of particles, when conjugated to antibodies, can enhance magnetic resonance imaging (MRI) sensitivity for the detection of cancer markers, particularly when compared with other types of probes currently available (Lee et al. 2007), and of acute brain inflammation that occurs in diseases like multiple sclerosis (McAteer et al. 2007).

While magnetosomes have been employed in and/or modeled for MRI in several studies (Benoit et al. 2009; Goldhawk et al. 2012; Hartung et al. 2007; Herborn et al. 2003; Lisy et al. 2007), important questions remain such as whether magnetosomes are superior chemically produced magnetite particles for specific or perhaps even all applications and will their use be cost effective.

Magnetosomes may be useful as gene and/or drug carriers for the treatment of cancer and perhaps other diseases. "Nanobodies," functional antibody fragments, have been coupled in vivo to magnetosomes via genetic fusion (Pollithy et al. 2011). Conjugated magnetic nanoparticles such as these can also be coupled to drugs or genes which could then be used as carriers of these molecules for targeted therapy of tumors (Chertok et al. 2007; Deng et al. 2013; Guo et al. 2012a; Sun et al. 2007; Zhao et al. 2010) or as vaccine delivery systems (Tang et al. 2012a).

Interestingly, and of some importance, heat is generated when magnetic nanoparticles are placed in the presence of an oscillating (alternating) magnetic field (Duguet et al. 2006; Dutz et al. 2007a, b; Gloeckl et al. 2006), thought to be a result of hysteresis losses (Dutz et al. 2007b; Hergt et al. 1998). This observation has led many to believe that magnetic nanoparticles can be effective in the destruction of tumors through magnetic hyperthermia or thermoablation (Ciofani et al. 2009; Hilger and Kaiser 2006; Hilger et al. 2001, 2005; Ito et al. 2006). Even bacterial magnetite magnetosomes display this characteristic (Alphandéry et al. 2013; Hergt et al. 2005, 2006; Liu et al. 2012) when the magnetite has oxidized to the less magnetic mineral maghemite (Alphandéry et al. 2011a, b, 2012b). Magnetosomes might even be more effective than synthetic magnetite nanoparticles in magnetic hyperthermia and thermoablation according to a model that was recently published (Martinez-Boubeta et al. 2013). Chemically synthesized greigite particles between 50 and 100 nm in size were also shown to be effective in hyperthermia therapy against cancerous cells of a human lung adenocarcinoma epithelial cell line (Chang et al. 2011). Now that a cultured greigite-producing magnetotactic bacterium, designated strain BW-1, is available for study (Lefèvre et al. 2011c), it should be possible to obtain enough magnetosomal greigite to investigate whether they are useful in this and other applications and whether they are superior to chemically produced greigite particles in these applications.

Few studies have addressed the toxicity of magnetosomes and magnetosome crystals as well as chemically synthesized magnetite and greigite in medical procedures in humans, an issue that must be addressed before magnetosomes can be used commercially for medical purposes. Magnetosome membrane proteins, like other proteins in general, will likely behave as strong antigens, and thus, it is also likely patients injected with magnetosomes will mount an immune response. Preliminary toxicity studies, however, suggest that purified, sterilized magnetosomes from magnetotactic bacteria are nontoxic for mouse fibroblasts in vitro (Xiang et al. 2007). Chains of magnetosomes administered directly in xenografted breast tumors of a mouse were shown to progressively depart from the tumors during a 14-day period following their administration and were then eliminated mainly in the feces (Alphandéry et al. 2013). Purified magnetosomes from *M. gryphiswaldense* were

labeled with the fluorescence dye 1,1(-dioctadecyl-3,3,3(,3(-tetramethylindocarbocianin perchlorate and injected into the tail vein of nude mice, where they were tracked using a whole-body fluorescence imaging system (Tang et al. 2012b). Magnetosome membranes did not appear to decompose in the body during the duration of this study which may represent another desirable quality of magnetosomes in medical applications.

3.11 Future Directions

It has now been a little over 50 years since Bellini described the unusual behavior of magnetotactic bacteria. In these 50 years, this simple observation has had major impacts in almost every field of science. These include microbiology, cell and molecular biology, microbial ecology, biogeography and microbial genetics and genomics, geology, (bio)geochemistry, biomineralization, mineralogy, chemistry, physics and geophysics, paleomagnetism, and astrobiology.

The magnetosome chain in magnetotactic bacteria is a masterpiece of microbial engineering. Through the molecular and physical assembly of an intracellular chain or chains of single-magnetic-domain magnetic crystals, these prokaryotic microorganisms have maximized and presumably optimized the magnetic dipole moment of each individual magnetosome crystal as well as that of the cell itself. The biologically controlled process of magnetosome biomineralization, which includes control over the mineral composition and the size and morphology of the crystals as well as their position within the cell, has been refined in the course of evolution. This is an amazing achievement considering that the process probably started as cells first taking up huge amounts of iron for some reason that is not yet known. At some point, the genes for magnetosome membrane proteins developed, leading to the biomineralization of a specific magnetic magnetosome mineral crystal, ultimately leading to the creation of the first magnetotactic bacterium. After this point, magnetosome genes appear to have evolved somewhat independently in magnetotactic bacteria of different phylogenetic groups, resulting in different magnetosome crystal compositions and morphologies. Finally, phylogenetic group specific genes, presumably with accessory functions, appeared to have evolved, thus leading to the overall great diversity of magnetotactic bacteria.

We hope, based on the amount progress on magnetotactic bacteria made in these first 50 years, that the next 50 years will prove to be just as exciting!

Acknowledgments We thank F. Abreu, D. Faivre, R. B. Frankel U. Lins, and D. Schüler for continual collaboration and extensive discussions. We have been supported by US National Science Foundation (NSF) Grants EAR-0920718 and EAR-0920299. DAB is currently supported by subcontract SC-12–384 from US Department of Energy contract DE-AC02–07CH11358 to the Ames Laboratory at Iowa State University. CTL is supported by the French national research agency ANR on the call-for-project P2 N (project MEFISTO).

References

Abreu F, Martins JL, Silveira TS, Keim CN, Lins de Barros HGP, Filho FJG, Lins U (2007) '*Candidatus* Magnetoglobus multicellularis', a multicellular, magnetotactic prokaryote from a hypersaline environment. Int J Syst Evol Micr 57:1318–1322

Abreu F, Cantão ME, Nicolás MF, Barcellos FG, Morillo V, Almeida LG, do Nascimento FF, Lefèvre CT, Bazylinski DA, de Vasconcelos ATR, Lins U (2011) Common ancestry of iron oxide- and iron-sulfide-based biomineralization in magnetotactic bacteria. ISME J 5:1634–1640

Alphandéry E, Faure S, Raison L, Duguet E, Howse PA, Bazylinski DA (2011a) Heat production by bacterial magnetosomes exposed to an oscillating magnetic field. J Phys Chem C 115:18–22

Alphandéry E, Faure S, Seksek O, Guyot F, Chebbi I (2011b) Chains of magnetosomes extracted from AMB-1 magnetotactic bacteria for application in alternative magnetic field cancer therapy. ACS Nano 5:6279–6296

Alphandéry E, Amor M, Guyot F, Chebbi I (2012a) The effect of iron-chelating agents on *Magnetospirillum magneticum* strain AMB-1: stimulated growth and magnetosome production and improved magnetosome heating properties. Appl Microbiol Biot 96:663–670

Alphandéry E, Guyot F, Chebbi I (2012b) Preparation of chains of magnetosomes, isolated from *Magnetospirillum magneticum* strain AMB-1 magnetotactic bacteria, yielding efficient treatment of tumors using magnetic hyperthermia. Int J Pharm 434:444–452

Alphandéry E, Chebbi I, Guyot F, Durand-Dubief M (2013) Use of bacterial magnetosomes in the magnetic hyperthermia treatment of tumours: a review. Int J Hyperther 29:801–809

Amann R, Peplies J, Schüler D (2007) Diversity and taxonomy of magnetotactic bacteria. In: Schüler D (ed) Magnetoreception and magnetosomes in bacteria, microbiology monographs. Springer, Berlin, pp 25–36

Arakaki A, Takeyama H, Tanaka T, Matsunaga T (2002) Cadmium recovery by a sulfate-reducing magnetotactic bacterium, *Desulfovibrio magneticus* RS-1, using magnetic separation. Appl Biochem Biotech 98:833–840

Arakaki A, Webb J, Matsunaga T (2003) A novel protein tightly bound to bacterial magnetic particles in *Magnetospirillum magneticum* strain AMB-1. J Biol Chem 278:8745–8750

Bahaj AS, James PAB, Ellwood DC, Watson JHP (1993) Characterization and growth of magnetotactic bacteria: implications of clean up of environmental pollution. J Appl Phys 73:5394–5396

Bahaj AS, Croudace IW, James PAB, Moeschler FD, Warwick PE (1998a) Continuous radionuclide recovery from wastewater using magnetotactic bacteria. J Magn Magn Mater 184:241–244

Bahaj AS, James PAB, Moeschler FD (1998b) Low magnetic-field separation system for metal-loaded magnetotactic bacteria. J Magn Magn Mater 177:1453–1454

Bahaj AS, James PAB, Moeschler FD (1998c) Wastewater treatment by bio-magnetic separation: a comparison of iron oxide and iron sulphide biomass recovery. Water Sci Technol 38:311–317

Baumgartner J, Morin G, Menguy N, Perez Gonzalez T, Widdrat M, Cosmidis J, Faivre D (2013) Magnetotactic bacteria form magnetite from a phosphate-rich ferric hydroxide via nanometric ferric (oxyhydr)oxide intermediates. P Natl Acad Sci U S A 110:14883–14888

Bazylinski DA, Blakemore RP (1983) Denitrification and assimilatory nitrate reduction in *Aquaspirillum magnetotacticum*. Appl Environ Microbiol 46:1118–1124

Bazylinski DA, Frankel RB (2003) Biologically controlled mineralization in prokaryotes. Rev Mineral 54:95–114

Bazylinski DA, Frankel RB (2004) Magnetosome formation in prokaryotes. Nat Rev Microbiol 2:217–230

Bazylinski DA, Williams TJ (2007) Ecophysiology of magnetotactic bacteria. In: Schüler D (ed) Magnetoreception and magnetosomes in bacteria, microbiology monographs. Springer, Berlin, pp 37–75

Bazylinski DA, Garratt-Reed AJ, Abedi A, Frankel RB (1993a) Copper association with iron sulfide magnetosomes in a magnetotactic bacterium. Arch Microbiol 160:35–42

Bazylinski DA, Heywood BR, Mann S, Frankel RB (1993b) Fe_3O_4 and Fe_3S_4 in a bacterium. Nature 366:218

Bazylinski DA, Garratt-Reed AJ, Frankel RB (1994) Electron microscopic studies of magnetosomes in magnetotactic bacteria. Microsc Res Techniq 27:389–401

Bazylinski DA, Frankel RB, Heywood BR, Mann S, King JW, Donaghay PL, Hanson AK (1995) Controlled biomineralization of magnetite (Fe_3O_4) and greigite (Fe_3S_4) in a magnetotactic bacterium. Appl Environ Microbiol 61:3232–3239

Bazylinski DA, Dean AJ, Schüler D, Phillips EJP, Lovley DR (2000) N_2-dependent growth and nitrogenase activity in the metal-metabolizing bacteria, *Geobacter* and *Magnetospirillum* species. Environ Microbiol 2:266–273

Bazylinski DA, Dean AJ, Williams TJ, Kimble-Long L, Middleton SL, Dubbels BL (2004) Chemolithoautotrophy in the marine, magnetotactic bacterial strains MV-1 and MV-2. Arch Microbiol 182:373–387

Bazylinski DA, Williams TJ, Lefèvre CT, Berg RJ, Zhang CL, Bowser SS, Dean AJ, Beveridge TJ (2013a) *Magnetococcus marinus* gen. nov., sp. nov., a marine, magnetotactic bacterium that represents a novel lineage (*Magnetococcaceae* fam. nov.; *Magnetococcales* ord. nov.) at the base of the *Alphaproteobacteria*. Int J Syst Evol Micr 63:801–808

Bazylinski DA, Williams TJ, Lefèvre CT, Trubitsyn D, Fang J, Beveridge TJ, Moskowitz BM, Ward B, Schübbe S, Dubbels BL, Simpson B (2013b) *Magnetovibrio blakemorei*, gen. nov. sp. nov., a new magnetotactic bacterium (*Alphaproteobacteria: Rhodospirillaceae*) isolated from a salt marsh. Int J Syst Evol Micr 63:1824–1833

Bellini S (2009a) On a unique behavior of freshwater bacteria. Chin J Oceanol Limn 27:3–5

Bellini S (2009b) Further studies on "magnetosensitive bacteria". Chin J Oceanol Limn 27:6–12

Benoit M, Mayer D, Barak Y, Chen IY, Hu W, Cheng Z, Wang SX, Spielman DM, Gambhir SS, Matin A (2009) Visualizing implanted tumors in mice with magnetic resonance imaging using magnetotactic bacteria. Clin Cancer Res 15:5170–5177

Beuming T, Skrabanek L, Niv MY, Mukherjee P, Weinstein H (2005) PDZBase: a protein-protein interaction database for PDZ-domains. Bioinformatics 21:827–828

Blakemore RP (1975) Magnetotactic bacteria. Science 190:377–379

Blakemore RP (1982) Magnetotactic bacteria. Annu Rev Microbiol 36:217–238

Blakemore RP, Frankel RB, Kalmijn AJ (1980) South-seeking magnetotactic bacteria in the southern- hemisphere. Nature 286:384–385

Blakemore RP, Short KA, Bazylinski DA, Rosenblatt C, Frankel RB (1985) Microaerobic conditions are required for magnetite synthesis within *Aquaspirillum magnetotacticum*. Geomicrobiol J 4:53–71

Blum G, Ott M, Lischewski A, Ritter A, Imrich H, Tschäpe H, Hacker J (1994) Excision of large DNA regions termed pathogenicity islands from tRNA-specific loci in the chromosome of an *Escherichia coli* wild-type pathogen. Infect Immun 62:606–614

Butler RF, Banerjee SK (1975) Theoretical single-domain grain size range in magnetite and titanomagnetite. J Geophys Res 80:4049–4058

Calugay RJ, Miyashita H, Okamura Y, Matsunaga T (2003) Siderophore production by the magnetic bacterium *Magnetospirillum magneticum* AMB-1. FEMS Microbiol Lett 218:371–375

Cameotra SS, Dhanjal S (2010) Environmental nanotechnology: nanoparticles for bioremediation of toxic pollutants. In: Fulekar MH (ed) Bioremediation technology; recent advances. Springer, Dordrecht, pp. 348–374

Chang Y-S, Savitha S, Sadhasivam S, Hsu C-K, Lin F-H (2011) Fabrication, characterization, and application of greigite nanoparticles for cancer hyperthermia. J Colloid Interf Sci 363:314–319

Chertok B, David AE, Huang Y, Yang C (2007) Glioma selectivity of magnetically targeted nanoparticles: a role of abnormal tumor hydrodynamics. J Control Release 122:315–323

Ciofani G, Riggio C, Raffa V, Menciassi A, Cuschieri A (2009) A bi-modal approach against cancer: magnetic alginate nanoparticles for combined chemotherapy and hyperthermia. Med Hypotheses 73:80–82

Deng Q, Liu Y, Wang S, Xie M, Wu S, Chen A, Wu W (2013) Construction of a novel magnetic targeting anti-tumor drug delivery system: cytosine arabinoside-loaded bacterial magnetosome. Materials 6:3755–3763

Diaz-Ricci JC, Kirschvink JL (1992) Magnetic domain state and coercivity predictions for biogenic greigite (Fe_3S_4): a comparison of theory with magnetosome observations. J Geophys Res 97:17309–17315

Ding J, Li J, Liu J, Yang J, Jiang W, Tian J, Li Y, Pan Y, Li J (2010) Deletion of the *ftsZ*-like gene results in the production of superparamagnetic magnetite magnetosomes in *Magnetospirillum gryphiswaldense*. J Bacteriol 192:1097–1105

Dobrindt U, Hochhut B, Hentschel U, Hacker J (2004) Genomic islands in pathogenic and environmental microorganisms. Nat Rev Microbiol 2:414–424

Dubbels BL, DiSpirito AA, Morton JD, Semrau JD, Neto JNE, Bazylinski DA (2004) Evidence for a copper-dependent iron transport system in the marine, magnetotactic bacterium strain MV-1. Microbiology 150:2931–2945

Duguet E, Vasseur S, Mornet S, Devoisselle J-M (2006) Magnetic nanoparticles and their applications in medicine. Nanomedicine-UK 1:157–168

Dutz S, Andrä W, Hergt R, Hilger I, Müller R, Töpfer J, Zeisberger M, Bellemann ME (2007a) Biomedical heating applications of magnetic iron oxide nanoparticles. In: Kim SI, Suh TS (eds) World congress on medical physics and biomedical engineering 2006, vol 14, parts 1–6. Springer, Berlin, pp. 271–274

Dutz S, Hergt R, Muerbe J, Müller R, Zeisberger M, Andrä W, Töpfer J, Bellemann ME (2007b) Hysteresis losses of magnetic nanoparticle powders in the single domain size range. J Magn Magn Mater 308:305–312

Errington J, Daniel RA, Scheffers DJ (2003) Cytokinesis in bacteria. Microbiol Mol Biol Rev 67:52–65

Faivre D, Bottger LH, Matzanke BF, Schüler D (2007) Intracellular magnetite biomineralization in bacteria proceeds by a distinct pathway involving membrane-bound ferritin and an iron(II) species. Angew Chem Int Edit 46:8495–8499

Fdez-Gubieda ML, Muela A, Alonso J, García-Prieto A, Olivi L, Fernández-Pacheco R, Barandiarán JM (2013) Magnetite biomineralization in *Magnetospirillum gryphiswaldense*: time-resolved magnetic and structural studies. ACS Nano 7:3297–3305

Felfoul O, Martel S (2013) Assessment of navigation control strategy for magnetotactic bacteria in microchannel: toward targeting solid tumors. Biomed Microdevices 15:1015–1024

Flies CB, Peplies J, Schüler D (2005) Combined approach for characterization of uncultivated magnetotactic bacteria from various aquatic environments. Appl Environ Microbiol 71:2723–2731

Frankel RB, Blakemore RP (1980) Navigational compass in freshwater magnetotactic bacteria. J Magn Magn Mater 15–18:1562–1564

Frankel RB, Moskowitz BM (2003) Biogenic magnets. In: Miller JS, Drillon M (eds) Magnetism: molecules to materials IV. Wiley, Weinheim, pp. 205–231

Frankel RB, Blakemore RP, Wolfe R (1979) Magnetite in freshwater magnetotactic bacteria. Science 203:1355–1356

Frankel RB, Papaefthymiou GC, Blakemore RP, O'Brien W (1983) Fe_3O_4 precipitation in magnetotactic bacteria. Biochim Biophys Acta 763:147–159

Frankel RB, Bazylinski DA, Johnson MS, Taylor BL (1997) Magneto-aerotaxis in marine coccoid bacteria. Biophys J 73:994–1000

Frankel RB, Bazylinski DA, Schüler D (1998) Biomineralization of magnetic iron minerals in magnetotactic bacteria. Supramol Sci 5:383–390

Frankel RB, Williams TJ, Bazylinski DA (2007) Magneto-aerotaxis. In: Schüler D (ed) Magnetoreception and magnetosomes in bacteria, microbiology monographs. Springer, Berlin, pp. 1–24

Fukuda Y, Okamura Y, Takeyama H, Matsunaga T (2006) Dynamic analysis of a genomic island in *Magnetospirillum* sp. strain AMB-1 reveals how magnetosome synthesis developed. FEBS Lett 580:801–812

Funaki M, Sakai H, Matsunaga T (1989) Identification of the magnetic poles on strong magnetic grains from meteorites using magnetotactic bacteria. J Geomagn Geoelectr 41:77–87

Funaki M, Sakai H, Matsunaga T, Hirose S (1992) The S-pole distribution on magnetic grains in pyroxenite determined by magnetotactic bacteria. Phys Earth Planet In 70:253–260

Geelhoed JS, Kleerebezem R, Sorokin DY, Stams AJM, van Loosdrecht MCM (2010) Reduced inorganic sulfur oxidation supports autotrophic and mixotrophic growth of *Magnetspirillum* strain J10 and *Magnetospirillum gryphiswaldense*. Environ Microbiol 12:1031–1040

Ginet N, Pardoux R, Adryanczyk G, Garcia D, Brutesco C, Pignol D (2011) Single-step production of a recyclable nanobiocatalyst for organophosphate pesticides biodegradation using functionalized bacterial magnetosomes. PLoS One 6:e21442

Gloeckl G, Hergt R, Zeisberger M, Dutz S, Nagel S, Weitschies W (2006) The effect of field parameters, nanoparticle properties and immobilization on the specific heating power in magnetic particle hyperthermia. J Phys-Condens Mat 18:S2935–S2949

Goldhawk DE, Rohani R, Sengupta A, Gelman N, Prato FS (2012) Using the magnetosome to model effective gene-based contrast for magnetic resonance imaging. WIREs Nanomed Nanobiotechnol 4:378–388

Gorby YA, Beveridge TJ, Blakemore RP (1988) Characterization of the bacterial magnetosome membrane. J Bacteriol 170:834–841

Grass G, Otto M, Fricke B, Haney CJ, Rensing C, Nies DH, Munkhelt D (2005) FieF (YiiP) from *Escherichia coli* mediates decreased cellular accumulation of iron and relieves iron stress. Arch Microbiol 183:9–18

Grünberg K, Wawer C, Tebo BM, Schüler D (2001) A large gene cluster encoding several magnetosome proteins is conserved in different species of magnetotactic bacteria. Appl Environ Microbiol 67:4573–4582

Grünberg K, Müller EC, Otto A, Reszka R, Linder D, Kube M, Reinhardt R, Schüler D (2004) Biochemical and proteomic analysis of the magnetosome membrane in *Magnetospirillum gryphiswaldense*. Appl Environ Microbiol 70:1040–1050

Guerin WF, Blakemore RP (1992) Redox cycling of iron supports growth and magnetite synthesis by *Aquaspirillum magnetotacticum*. Appl Environ Microbiol 58:1102–1109

Guo F, Liu Y, Chen Y, Tang T, Jiang W, Li Y, Li J (2011) A novel rapid and continuous procedure for large-scale purification of magnetosomes from *Magnetospirillum gryphiswaldense*. Appl Microbiol Biot 90:1277–1283

Guo L, Huang J., Zheng L-M (2012a) Bifunctional bacterial magnetic nanoparticles for tumor targeting. Nanoscale 4:879–884

Guo FF, Yang W, Jiang W, Geng S, Peng T, Li JL (2012b) Magnetosomes eliminate intracellular reactive oxygen species in *Magnetospirillum gryphiswaldense* MSR-1. Environ Microbiol 14:1722–1729

Haney CJ, Grass G, Franke S, Rensing C (2005) New developments in the understanding of the cation diffusion facilitator family. J Ind Microbiol Biot 32:215–226

Harasko G, Pfutzner H, Rapp E, Futschik K, Schüler D (1993) Determination of the concentration of magnetotactic bacteria by means of susceptibility measurements. Jpn J Appl Phys 32:252–260

Harasko G, Pfutzner H, Futschik K (1995) Domain analysis by means of magnetotactic bacteria. IEEE T Magn 31:938–949

Hartung A, Lisy R, Herrmann KH, Hilger I, Schüler D, Lang C, Bellemann ME, Kaiser WA, Reichenbach JR (2007) Labeling of macrophages using bacterial magnetosomes and their characterization by magnetic resonance imaging. J Magn Magn Mater 311:454–459

Herborn C, Papanikolaou N, Reszka R, Grünberg K, Schüler D, Debatin JF (2003) Magnetosomen als biologisches modell der eisenbindung: messung der relaxivitat in der MRT. Fortschr Rontg Neuen 175:830–834

Hergt R, Andrä W, d'Ambly GC, Hilger I, Kaiser WA, Richter U, Schmidt HG (1998) Physical limits of hyperthermia using magnetite fine particles. IEEE T Magn 34:3745–3754

Hergt R, Hiergeist R, Zeisberger M, Schüler D, Heyen U, Hilger I, Kaiser WA (2005) Magnetic properties of bacterial magnetosomes as potential diagnostic and therapeutic tools. J Magn Magn Mater 293:80–86

Hergt R, Dutz S, Müller R, Zeisberger M (2006) Magnetic particle hyperthermia: nanoparticle magnetism and materials development for cancer therapy. J Phys-Condens Mat 18:S2919–S2934

Heyen U, Schüler D (2003) Growth and magnetosome formation by microaerophilic *Magnetospirillum* strains in an oxygen-controlled fermentor. Appl Microbiol Biot 61:536–544

Hilger I, Kaiser WA (2006) Magnetic thermoablation. Eur Radiol 16:E47

Hilger I, Andrä W, Hergt R, Hiergeist R, Schubert H, Kaiser WA (2001) Electromagnetic heating of breast tumors in interventional radiology: *in vitro* and *in vivo* studies in human cadavers and mice. Radiology 218:570–575

Hilger I, Hergt R, Kaiser WA (2005) Use of magnetic nanoparticle heating in the treatment of breast cancer. IEE P-Nanobiotechnol 152:33–39

Ito A, Honda H, Kobayashi T (2006) Cancer immunotherapy based on intracellular hyperthermia using magnetite nanoparticles: a novel concept of 'heat-controlled necrosis' with heat shock protein expression. Cancer Immunol Immun 55:320–328

Ji B, Zhang S-D, Arnoux P, Rouy Z, Alberto F, Philippe N, Murat D, Zhang W-J, Rioux J-B, Ginet N, Sabaty M, Mangenot S, Pradel N, Tian J, Yang J, Zhang L, Zhang W, Pan H, Henrissat B, Coutinho PM, Li Y, Xiao T, Médigue C, Barbe V, Pignol D, Talla E, Wu L-F (2014) Comparative genomic analysis provides insights into the evolution and niche adaptation of marine *Magnetospira* sp. QH-2 strain. Environ Microbiol 16:525–544

Jimenez-Lopez C, Romanek CS, Bazylinski DA (2010) Magnetite as a prokaryotic biomarker: a review. J Geophys Res-Biogeo 115:G00G03

Jogler C, Schüler D (2009) Genomics, genetics, and cell biology of magnetosome formation. Annu Rev Microbiol 63:501–521

Jogler C, Kube M, Schübbe S, Ullrich S, Teeling H, Bazylinski DA, Reinhardt R, Schüler D (2009) Comparative analysis of magnetosome gene clusters in magnetotactic bacteria provides further evidence for horizontal gene transfer. Environ Microbiol 11:1267–1277

Juhas M, van der Meer JR, Gaillard M, Harding RM, Hood DW, Crook DW (2009) Genomic islands: tools of bacterial horizontal gene transfer and evolution. FEMS Microbiol Rev 33:376–393

Kanetsuki Y, Tanaka M, Tanaka T, Matsunaga T, Yoshino T (2012) Effective expression of human proteins on bacterial magnetic particles in an anchor gene deletion mutant of *Magnetospirillum magneticum* AMB-1. Biochem Bioph Res Co 426:7–11

Kanetsuki Y, Tanaka T, Matsunaga T, Yoshino T (2013) Enhanced heterologous protein display on bacterial magnetic particles using a *lon* protease gene deletion mutant in *Magnetospirillum magneticum* AMB-1. J Biosci Bioeng 116:65–70

Katzmann E, Scheffel A, Gruska M, Plitzko JM, Schüler D (2010) Loss of the actin-like protein MamK has pleiotropic effects on magnetosome formation and chain assembly in *Magnetospirillum gryphiswaldense*. Mol Microbiol 77:208–224

Katzmann E, Müller F, Lang C, Messerer M, Winklhofer M, Plitzko JM, Schüler D (2011) Magnetosome chains are recruited to cellular division sites and split by asymmetric septation. Mol Microbiol 82:1316–1329

Kolinko S, Jogler C, Katzmann E, Wanner G, Peplies J, Schüler D (2011) Single-cell analysis reveals a novel uncultivated magnetotactic bacterium within the candidate division OP3. Environ Microbiol 14:1709–1721

Kolinko I, Lohße A, Borg S, Raschdorf O, Jogler C, Tu Q, Pósfai M, Tompa E, Plitzko JM, Brachmann A, Wanner G, Müller R, Zhang Y, Schüler D (2014) Biosynthesis of magnetic nanostructures in a foreign organism by transfer of bacterial magnetosome gene clusters. Nat Nanotechnol 9:193–197

Komeili A (2012) Molecular mechanisms of compartmentalization and biomineralization in magnetotactic bacteria. FEMS Microbiol Rev 36:232–255

Komeili A, Vali H, Beveridge TJ, Newman DK (2004) Magnetosome vesicles are present before magnetite formation, and MamA is required for their activation. P Natl Acad Sci U S A 101:3839–3844

Komeili A, Li Z, Newman DK, Jensen GJ (2006) Magnetosomes are cell membrane invaginations organized by the actin-like protein MamK. Science 311:242–245

Kuhara M, Takeyama H, Tanaka T, Matsunaga T (2004) Magnetic cell separation using antibody binding with protein A expressed on bacterial magnetic particles. Anal Chem 76:6207–6213

Lang C, Schüler D (2006) Biogenic nanoparticles: production, characterization, and application of bacterial magnetosomes. J Phys-Condens Mat 18:S2815–S2828

Lee J-H, Huh Y-M, Jun Y, Seo J, Jang J, Song H-T, Kim S, Cho EJ, Yoon HG, Suh JS, Cheon J (2007) Artificially engineered magnetic nanoparticles for ultra-sensitive molecular imaging. Nat Med 13:95–99

Lefèvre CT, Bazylinski DA (2013) Magnetotactic bacteria: ecology, diversity and evolution. Microbiol Mol Biol R 77:497–526

Lefèvre CT, Wu LF (2013) Evolution of the bacterial organelle responsible for magnetotaxis. Trends Microbiol 21:534–543

Lefèvre CT, Bernadac A, Yu-Zhang K, Pradel N, Wu L-F (2009) Isolation and characterization of a magnetotactic bacterial culture from the Mediterranean Sea. Environ Microbiol 11:1646–1657

Lefèvre CT, Abreu F, Schmidt ML, Lins U, Frankel RB, Hedlund BP, Bazylinski DA (2010) Moderately thermophilic magnetotactic bacteria from hot springs in Nevada USA. Appl Environ Microbiol 76:3740–3743

Lefèvre CT, Frankel RB, Abreu F, Lins U, Bazylinski DA (2011a) Culture-independent characterization of a novel, uncultivated magnetotactic member of the *Nitrospirae* phylum. Environ Microbiol 13:538–549

Lefèvre CT, Frankel RB, Pósfai M, Prozorov T, Bazylinski (2011b) Isolation of obligately alkaliphilic magnetotactic bacteria from extremely alkaline environments. Environ Microbiol 13:2342–2350

Lefèvre CT, Menguy N, Abreu F, Lins U, Pósfai M, Prozorov T, Pignol D, Frankel RB, Bazylinski DA (2011c) A cultured greigite-producing magnetotactic bacterium in a novel group of sulfate-reducing bacteria. Science 334:1720–1723

Lefèvre CT, Pósfai M, Abreu F, Lins U, Frankel RB, Bazylinski DA (2011d) Morphological features of elongated-anisotropic magnetosome crystals in magnetotactic bacteria of the *Nitrospirae* phylum and the *Deltaproteobacteria* class. Earth Planet Sci Lett 312:194–200

Lefèvre CT, Viloria N, Schmidt ML, Pósfai M, Frankel RB, Bazylinski DA (2012) Novel magnetite-producing magnetotactic bacteria belonging to the *Gammaproteobacteria*. ISME J 6:440–450

Lefèvre CT, Trubitsyn D, Abreu F, Kolinko S, de Almeida LGP, de Vasconcelos ATR, Lins U, Schüler D, Ginet N, Pignol D, Bazylinski DA (2013a) Monophyletic origin of magnetotaxis and the first magnetosomes. Environ Microbiol 15:2267–2274

Lefèvre CT, Trubitsyn D, Abreu F, Kolinko S, Jogler C, de Almeida LGP, de Vasconcelos ATR, Kube M, Reinhardt R, Lins U, Pignol D, Schüler D, Bazylinski DA, Ginet N (2013b) Comparative genomic analysis of magnetotactic bacteria from the *Deltaproteobacteria* provides new insights into magnetite and greigite magnetosome genes required for magnetotaxis. Environ Microbiol 15:2712–2735

Li Y, Katzmann E, Borg S, Schüler D (2012) The periplasmic nitrate reductase *nap* is required for anaerobic growth and involved in redox control of magnetite biomineralization in *Magnetospirillum gryphiswaldense*. J Bacteriol 194:4847–4856

Li Y, Bali S, Borg S, Katzmann E, Ferguson SJ, Schüler D (2013a) Cytochrome cd_1 nitrite reductase NirS is involved in anaerobic magnetite biomineralization in *Magnetospirillum gryphiswaldense* and requires NirN for proper *d*1 heme assembly. J Bacteriol 195:4297–4309

Li X, Wang Q, Xue Y (2013b) On the change in bacterial growth and magnetosome formation for *Magnetospirillum* sp. strain AMB-1 under different concentrations of reducing agents. J Nanosci Nanotechno 13:1392–1398

Li Y, Raschdorf O, Silva KT, Schüler D (2014) The terminal oxidase cbb3 functions in redox control of magnetite biomineralization in *Magnetospirillum gryphiswaldense.* J Bacteriol (in press). doi:10.1128/JB.01652–14

Lin W, Jogler C, Schüler D, Pan Y (2011) Metagenomic analysis reveals unexpected subgenomic diversity of magnetotactic bacteria within the phylum *Nitrospirae*. Appl Environ Microbiol 77:323–326

Lin W, Li J, Pan Y (2012) Newly isolated but uncultivated magnetotactic bacterium of the phylum *Nitrospirae* from Beijing, China. Appl Environ Microbiol 78:668–675

Lins U, Keim CN, Evans FF, Farina M, Buseck PR (2007) Magnetite (Fe_3O_4) and greigite (Fe_3S_4) crystals in multicellular magnetotactic prokaryotes. Geomicrobiol J 24:43–50

Lisy MR, Hartung A, Lang C, Schüler D, Richter W, Reichenbach JR, Kaiser WA, Hilger I (2007) Fluorescent bacterial magnetic nanoparticles as bimodal contrast agents. Invest Radiol 42:235–241

Liu R, Liu J, Tong J, Tang T, Kong W-C, Wang X, Li Y, Tang J (2012) Heating effect and biocompatibility of bacterial magnetosomes as potential materials used in magnetic fluid hyperthermia. Prog Nat Sci 22:31–39

Liu Y, Li GR, Guo FF, Jiang W, Li Y, Li LJ (2010) Large-scale production of magnetosomes by chemostat culture of *Magnetospirillum gryphiswaldense* at high cell density. Microb Cell Fact 9:99

Lohße A, Ullrich S, Katzmann E, Borg S, Wanner G, Richter M, Voigt B, Schweder T, Schüler D (2011) Functional analysis of the magnetosome island in *Magnetospirillum gryphiswaldense*: the *mamAB* operon is sufficient for magnetite biomineralization. PLoS ONE 6:e25561

Lower BH, Bazylinski DA (2013) The bacterial magnetosome, a unique prokaryotic organelle. J Mol Microbiol Biotechnol 23:63–80

Ma Q, Chen C, Wei S, Chen C, Wu L-F, Song T (2012) Construction and operation of a microrobot based on magnetotactic bacteria in a microfluidic chip. Biomicrofluidics 6:24107–24112

Mahillon J, Chandler M (1998) Insertion sequences. Microbiol Mol Biol Rev 62:725–774

Mahillon J, Leonard C, Chandler M (1999) IS elements as constituents of bacterial genomes. Res Microbiol 150:675–687

Mann S, Frankel RB (1989) Magnetite biomineralization in unicellular organisms. In: Mann S, Webb J, Williams RJP (eds) Biomineralization: chemical and biochemical perspectives. VCH, Weinheim, pp. 389–426

Martel S (2008) Nanorobots for microfactories to operations in the human body and robots propelled by bacteria. Facta Univ Ser Mech Automat Control Robot 7:1–8

Martel S (2012) Bacterial microsystems and microrobots. Biomed Microdevices 14:1033–1045

Martinez-Boubeta C, Simeonidis K, Makridis A, Angelakeris M, Iglesias O, Guardia P, Cabot A, Yedra L, Estradé S, Peiró F, Saghi Z, Midgley PA, Conde-Leborán I, Serantes D, Baldomir D (2013) Learning from nature to improve the heat generation of iron-oxide nanoparticles for magnetic hyperthermia applications. Sci Rep 3:1652

Maruyama K, Takeyama H, Nemoto E, Tanaka T, Yoda K, Matsunaga T (2004) Single nucleotide polymorphism detection in aldehyde dehydrogenase 2 (ALDH2) gene using bacterial magnetic particles based on dissociation curve analysis. Biotechnol Bioeng 87:687–694

Matsunaga T (1991) Applications of bacterial magnets. Trends Biotechnol 9:91–95

Matsunaga T, Arakaki A (2007) Molecular bioengineering of bacterial magnetic particles for biotechnological applications. In: Schüler D (ed) Magnetoreception and magnetosomes in bacteria, microbiology monographs. Springer, Berlin/Heidelberg, pp. 227–254

Matsunaga T, Kamiya S (1987) Use of magnetic particles isolated from magnetotactic bacteria for enzyme immobilization. Appl Microbiol Biot 26:328–332

Matsunaga T, Takeyama H (1998) Biomagnetic nanoparticle formation and application. Supramol Sci 5:391–394

Matsunaga T, Hashimoto K, Nakamura N, Nakamura K, Hashimoto S (1989) Phagocytosis of bacterial magnetite by leukocytes. Appl Microbiol Biot 31:401–405

Matsunaga T, Tadokoro F, Nakamura N (1990) Mass culture of magnetic bacteria and their application to flow type immunoassays. IEEE T Magn 26:1557–1559

Matsunaga T, Nakamura C, Burgess JG, Sode K (1992) Gene-transfer in magnetic bacteria: transposon mutagenesis and cloning of genomic DNA fragments required for magnetosome synthesis. J Bacteriol 174:2748–2753

Matsunaga T, Tsujimura N, Kamiya S (1996) Enhancement of magnetic particle production by nitrate and succinate fed-batch culture of *Magnetospirillum* sp. AMB-1. Biotechnol Tech 10:495–500

Matsunaga T, Togo H, Kikuchi T, Tanaka T (2000) Production of luciferase-magnetic particle complex by recombinant *Magnetospirillum* sp. AMB-1. Biotechnol Bioeng 70:704–709

Matsunaga T, Arakaki A, Takahoko M (2002) Preparation of luciferase-bacterial magnetic particle complex by artificial integration of MagA-luciferase fusion protein into the bacterial magnetic particle membrane. Biotechnol Bioeng 77:614–618

Matsunaga T, Okamura Y, Fukuda Y, Wahyudi AT, Murase Y, Takeyama T (2005) Complete genome sequence of the facultative anaerobic magnetotactic bacterium *Magnetospirillum* sp. strain AMB-1. DNA Res 12:157–166

McAteer MA, Sibson NR, von zur Muhlen C, Schneider JE, Lowe AS, Warrick N, Channon KM, Anthony DC, Choudhury RP (2007) *In vivo* magnetic resonance imaging of acute brain inflammation using microparticles of iron oxide. Nat Med 13:1253–1258

Moskowitz BM, Bazylinski DA, Egli R, Frankel RB, Edwards KJ (2008) Magnetic properties of marine magnetotactic bacteria in a seasonally stratified coastal pond (Salt Pond, MA, USA). Geophys J Int 174:75–92

Müller FD, Raschdorf O, Nudelman H, Messerer M, Katzmann E, Plitzko JM, Zarivach R, Schüler D (2014) The FtsZ-like protein FtsZm of *Magnetospirillum gryphiswaldense* likely interacts with its generic homolog and is required for biomineralization under nitrate deprivation. J Bacteriol 196:650–659

Murat D, Quinlan A, Vali H, Komeili A (2010) Comprehensive genetic dissection of the magnetosome gene island reveals the step-wise assembly of a prokaryotic organelle. P Natl Acad Sci U S A 107:5593–5598

Musarrat J, Dwivedi S, Singh BR, Saquib Q, Al-Khedhairy AA (2011) Microbially synthesized nanoparticles: scope and applications. In: Ahmad I, Ahmad F, Pichtel R (eds) Microbes and microbial technology: agricultural and environmental ppplications. Springer, New York, pp. 101–126

Nakamura N, Matsunaga T (1993) Highly sensitive detection of allergen using bacterial magnetic particles. Anal Chim Acta 281:585–589

Nakamura N, Hashimoto K, Matsunaga T (1991) Immunoassay method for the determination of immunoglobulin G using bacterial magnetic particles. Anal Chem 63:268–272

Nakamura N, Burgess JG, Yagiuda K, Kudo S, Sakaguchi T, Matsunaga T (1993) Detection and removal of *Escherichia coli* using fluorescein isothiocyanate conjugated monoclonal antibody immobilized on bacterial magnetic particles. Anal Chem 65:2036–2039

Nakamura C, Burgess JG, Sode K, Matsunaga T (1995) An iron-regulated gene, *MagA*, encoding an iron transport protein of *Magnetospirillum* sp. strain AMB-1. J Biol Chem 270:28392–28396

Nakayama N, Arakaki A, Maruyama K, Takeyama H, Matsunaga T (2003) Single-nucleotide polymorphism analysis using fluorescence resonance energy transfer between DNA-labeling fluorophore, fluorescein isothiocyanate, and DNA intercalator, POPO-3, on bacterial magnetic particles. Biotechnol Bioeng 84:96–102

Nakazawa H, Arakaki A, Narita-Yamada S, Yashiro I, Jinno K, Aoki A, Tsuruyama A, Okamura Y, Tanikawa S, Fujita N, Takeyama H, Matsunaga T (2009) Whole genome sequence of *Desulfovibrio magneticus* strain RS-1 revealed common gene clusters in magnetotactic bacteria. Genome Res 19:1801–1808

Nash C (2008) Mechanisms and evolution of magnetotactic bacteria. Ph.D. thesis, California Institute of Technology

Neilands JB (1995) Siderophores: structure and function of microbial iron transport compounds. J Biol Chem 270:26723–26726

Ohuchi S, Schüler D (2009) *In vivo* display of a multisubunit enzyme complex on biogenic magnetic nanoparticles. Appl Environ Microbiol 75:7734–7738

Okuda Y, Denda K, Fukumori Y (1996) Cloning and sequencing of a gene encoding a new member of the tetratricopeptide protein family from magnetosomes of *Magnetospirillum magnetotacticum*. Gene 171:99–102

Ota H, Takeyama H, Nakayama H, Katoh T, Matsunaga T (2003) SNP detection in transforming growth factor-beta 1 gene using bacterial magnetic particles. Biosens Bioelectron 18:683–687

Palache C, Berman H, Frondel C (1944) Dana's system of mineralogy. Wiley, New York

Paoletti LC, Blakemore RP (1986) Hydroxamate production by *Aquaspirillum magnetotacticum*. J Bacteriol 167:73–76

Paulsen IT, Park JH, Choi PS Jr, Saier HH (1997) A family of Gram-negative bacterial outer membrane factors that function in the export of proteins, carbohydrates, drugs and heavy metals from Gram-negative bacteria. FEMS Microbiol Lett 156:1–8

Pečová M, Šebela M, Marková Z, Poláková Z, Čuda J, Šafářová K, Zbořil R (2013) Thermostable trypsin conjugates immobilized to biogenic magnetite show a high operational stability and remarkable reusability for protein digestion. Nanotechnology 24:125102

Pikuta EV, Hoover RB, Bej AK, Marsic D, Whitman WB, Cleland D, Krader P (2003) *Desulfonatronum thiodismutans* sp. nov., a novel alkaliphilic, sulfate-reducing bacterium capable of lithoautotrophic growth. Int J Syst Evol Micr 53:1327–1332

Pollithy A, Romer T, Lang C, Müller FD, Helma F, Leonhardt H, Rothbauer U, Schüler D (2011) Magnetosome expression of functional camelid antibody fragments (nanobodies) in *Magnetospirillum gryphiswaldense*. Appl Environ Microbiol 77:6165–6171

Ponting CCP, Phillips C (1996) Rapsyn's knobs and holes: eight tetratrico peptide repeats. Biochem J 314:1053–1054

Pósfai M, Buseck PR, Bazylinski DA, Frankel RB (1998a). Reaction sequence of iron sulfide minerals in bacteria and their use as biomarkers. Science 280:880–883

Pósfai M, Buseck PR, Bazylinski DA, Frankel RB (1998b) Iron sulfides from magnetotactic bacteria: structure, compositions, and phase transitions. Am Mineral 83:1469–1481

Prozorov T, Mallapragada SK, Narasimhan B, Wang L, Palo P, Nilsen-Hamilton M, Williams TJ, Bazylinski DA, Prozorov R, Canfield PC (2007) Protein-mediated synthesis of uniform superparamagnetic magnetite nanocrystals. Adv Funct Mater 17:951–957

Qi L, Li J, Zhang W, Liu J, Rong C, Li Y, Wu L-F (2012) Fur in *Magnetospirillum gryphiswaldense* influences magnetosomes formation and directly regulates the genes involved in iron and oxygen metabolism. PLoS ONE 7:e29572

Quinlan A, Murat D, Vali H, Komeili A (2011) The HtrA/DegP family protease MamE is a bifunctional protein with roles in magnetosome protein localization and magnetite biomineralization. Mol Microbiol 80:1075–1087

Ramanujan RV (2009) Magnetic particles for biomedical applications. In: Narayan R (ed) Biomedical materials. Springer, New York, pp. 477–491

Raschdorf O, Müller FD, Pósfai M, Plitzko JM, Schüler D (2013) The magnetosome proteins MamX, MamZ and MamH are involved in redox control of magnetite biomineralization in *Magnetospirillum gryphiswaldense*. Mol Microbiol 89:872–886

Reiter W-D, Palm P (1990) Identification and characterization of a defective SSV1 genome integrated into a tRNA gene in the archaebacterium *Sulfolobus* sp. B12. Mol Gen Genet 221:65–71

Reiter W-D, Palm P, Yeats S (1989) Transfer RNA genes frequently serve as integration sites for prokaryotic genetic elements. Nucleic Acids Res 17:1907–1914

Richter M, Kube M, Bazylinski DA, Lombardot T, Glöckner FO, Reinhardt R, Schüler D (2007) Comparative genome analysis of four magnetotactic bacteria reveals a complex set of group-specific genes implicated in magnetosome biomineralization and function. J Bacteriol 189:4899–4910

Rong C, Huang Y, Zhang W, Jiang W, Li Y, Li J (2008) Ferrous iron transport protein B gene (*feoB1*) plays an accessory role in magnetosome formation in *Magnetospirillum gryphiswaldense* strain MSR-1. Res Microbiol 159:530–536

Rong C, Zhang C, Zhang Y, Qi L, Yang J, Guan G, Li Y, Li J (2012) FeoB2 functions in magnetosome formation and oxidative stress protection in *Magnetospirillum gryphiswaldense* strain MSR-1. J Bacteriol 194:3972–3976

Sakaguchi T, Arakaki A, Matsunaga T (2002) *Desulfovibrio magneticus* sp. nov., a novel sulfate-reducing bacterium that produces intracellular single-domain-sized magnetite particles. Int J Syst Evol Micr 52:215–221

Scheffel A, Gruska M, Faivre D, Linaroudis A, Plitzko JM, Schüler D (2006) An acidic protein aligns magnetosomes along a filamentous structure in magnetotactic bacteria. Nature 440:110–114

Scheffel A, Schüler D (2007) The acidic repetitive domain of the *Magnetospirillum gryphiswaldense* MamJ protein displays hypervariability but is not required for magnetosome chain assembly. J Bacteriol 189:6437–6446

Scheffel A, Gärdes A, Grünberg K, Wanner G, Schüler D (2008) The major magnetosome proteins MamGFDC are not essential for magnetite biomineralization in *Magnetospirillum gryphiswaldense* but regulate the size of magnetosome crystals. J Bacteriol 190:377–386

Schübbe S, Kube M, Scheffel A, Wawer C, Heyen U, Meyerdierks A, Madkour MH, Mayer F, Reinhardt R, Schüler D (2003) Characterization of a spontaneous nonmagnetic mutant of *Magnetospirillum gryphiswaldense* reveals a large deletion comprising a putative magnetosome island. J Bacteriol 185:5779–5790

Schübbe S, Williams TJ, Xie G, Kiss HE, Brettin TS, Martinez D, Ross CA, Schüler D, Cox BL, Nealson KH, Bazylinski DA (2009) Complete genome sequence of the chemolithoautotrophic marine magnetotactic coccus strain MC-1. Appl Environ Microbiol 75:4835–4852

Schüler D (2008) Genetics and cell biology of magnetosome formation in magnetotactic bacteria. FEMS Microbiol Rev 32:654–672

Schüler D, Baeuerlein E (1996) Iron-limited growth and kinetics of iron uptake in *Magnetospirillum gryphiswaldense*. Arch Microbiol 166:301–307

Schüler D, Baeuerlein E (1997) Iron transport and magnetite crystal formation of the magnetic bacterium *Magnetospirillum gryphiswaldense*. J Phys IV 7:647–650

Schüler D, Baeuerlein E (1998) Dynamics of iron uptake and Fe_3O_4 biomineralization during aerobic and microaerobic growth of *Magnetospirillum gryphiswaldense*. J Bacteriol 180:159–162

Schultheiss D, Schüler D (2003) Development of a genetic system for *Magnetospirillum gryphiswaldense*. Arch Microbiol 179:89–94

Schultheiss D, Kube M, Schüler D (2004) Inactivation of the flagellin gene *flaA* in *Magnetospirillum gryphiswaldense* results in nonmagnetotactic mutants lacking flagellar filaments. Appl Environ Microbiol 70:3624–3631

Shapiro OH, Hatzenpichler R, Buckley DH, Zinder SH, Orphan VJ (2011) Multicellular photomagnetotactic bacteria. Environ Microbiol Rep 3:233–238

Silva KT, Leão PE, Abreu F, López JA, Gutarra ML, Farina M, Bazylinski DA, Freire DMG, Lins U (2013) Optimized magnetosome production and growth by the magnetotactic vibrio *Magnetovibrio blakemorei* strain MV-1 using statistical experimental design. Appl Environ Microbiol 79:2823–2827

Simmons SL, Sievert SM, Frankel RB, Bazylinski DA, Edwards KJ (2004) Spatiotemporal distribution of marine magnetotactic bacteria in a seasonally stratified coastal salt pond. Appl Environ Microbiol 70:6230–6239

Simmons SL, Bazylinski DA, Edwards KJ (2006) South seeking magnetotactic bacteria in the Northern Hemisphere. Science 311:371–374

Siponen MI, Adryanczyk G, Ginet N, Arnoux P, Pignol D (2012) Magnetochrome: a *c*-type cytochrome domain specific to magnetotatic bacteria. Biochem Soc T 40:1319–1323

Siponen, MI, Legrand P, Widdrat M, Jones SR, Zhang W-J, Chang MCY, Faivre D, Arnoux P, Pignol D (2013) Structural insight into magnetochrome-mediated magnetite biomineralization. Nature 30:681–684

Sode K, Kudo S, Sakaguchi T, Nakamura N, Matsunaga T (1993) Application of bacterial magnetic particles for highly selective messenger-RNA recovery-system. Biotechnol Tech 7:688–694

Sugamata Y, Uchiyama R, Honda T, Tanaka T, Matsunaga T, Yoshino T (2013) Functional expression of thyroid-stimulating hormone receptor on nano-sized bacterial magnetic particles in *Magnetospirillum magneticum* AMB-1. Int J Mol Sci 14:14426–14438

Sun J-B, Duan J-H, Dai S-L, Reri J, Zhang Y-D, Tian J-S, Li Y (2007) *In vitro* and *in vivo* antitumor effects of doxorubicin loaded with bacterial magnetosomes (DBMs) on H22 cells: the magnetic bionanoparticles as drug carriers. Cancer Lett 258:109–117

Sun J-B, Zhao F, Tang T, Jiang W, Tian J, Li Y, Li LJ (2008) High-yield growth and magnetosome formation by *Magnetospirillum gryphiswaldense* MSR-1 in an oxygen-controlled fermentor supplied solely with air. Appl Microbiol Biot 79:389–397

Sun X, Wu L, Ji J, Jiang D, Zhang Y, Li Z, Zhang G, Zhang H (2013) Longitudinal surface plasmon resonance assay enhanced by magnetosomes for simultaneous detection of Pefloxacin and Microcystin-LR in seafoods. Biosens Bioelectron 47:318–323

Suzuki T, Okamura Y, Calugay RJ, Takeyama H, Matsunaga T (2006) Global gene expression analysis of iron-inducible genes in *Magnetospirillum magneticum* AMB-1. J Bacteriol 188:2275–2279

Tanaka M, Okamura Y, Arakaki A, Tanaka T, Takeyama H, Matsunaga T (2006) Origin of magnetosome membrane: proteomic analysis of magnetosome membrane and comparison with cytoplasmic membrane. Proteomics 6:5234–5247

Tanaka T, Maruyama K, Yoda K, Nemoto E, Udagawa Y, Nakayama H, Takeyama H, Matsunaga T (2003) Development and evaluation of an automated workstation for single nucleotide polymorphism discrimination using bacterial magnetic particles. Biosens Bioelectron 19:325–330

Tang T, Zhang L, Gao R, Dai Y, Meng F, Li Y (2012b) Fluorescence imaging and targeted distribution of bacterial magnetic particles in nude mice. Appl Microbiol Biot 94:495–503

Tang Y-S, Wang D, Zhou C, Ma W, Zhang Y-Q, Liu B, Zhang S (2012a) Bacterial magnetic particles as a novel and efficient gene vaccine delivery system. Gene Ther 19:1187–1195

Taoka A, Asada R, Sasaki H, Anzawa K, Wu L-F, Fukumori Y (2006) Spatial localizations of Mam22 and Mam12 in the magnetosomes of *Magnetospirillum magnetotacticum*. J Bacteriol 188:3805–3812

Theil E (1987) Ferritin—structure, gene-regulation, and cellular function in animals, plants, and microorganisms. Annu Rev Biochem 56:289–315

Thomas-Keprta KL, Bazylinski DA, Kirschvink JL, Clemett SJ, McKay DS, Wentworth SJ, Vali H, Gibson EK Jr, Romanek CS (2000) Elongated prismatic magnetite crystals in ALH84001 carbonate globules: potential Martian magnetofossils. Geochim Cosmochim Acta 64:4049–4081

Thomas-Keprta KL, Bazylinski DA, Kirschvink JL, Clemett SJ, McKay DS, Wentworth SJ, Vali H, Gibson EK Jr, McKay MF, Romanek CS (2001) Truncated hexa-octahedral magnetite crystals in ALH84001: presumptive biosignatures. P Natl Acad Sci U S A 98:2164–2169

Thomas-Keprta KL, Clemett SJ, Bazylinski DA, Kirschvink JL, McKay DS, Wentworth SJ, Vali H, Gibson EK Jr, Romanek CS (2002) Magnetofossils from ancient Mars: a robust biosignature in the Martian meteorite ALH84001. Appl Environ Microbiol 68:3663–3672

Towe KM, Moench TT (1981) Electron-optical characterization of bacterial magnetite. Earth Planet Sci Lett 52:213–220

Trahms L (2009) Biomedical applications of magnetic nanoparticles. Lect Notes Phys 763:327–358

Uebe R, Voigt B, Schweder T, Albrecht D, Katzmann E, Lang C, Böttger L, Matzanke B, Schüler D (2010) Deletion of a *fur*-like gene affects iron homeostasis and magnetosome formation in *Magnetospirillum gryphiswaldense*. J Bacteriol 192:4192–4204

Uebe R, Junge K, Henn V, Poxleitner G, Katzmann E, Plitzko JM, Zarivach R, Kasama T, Wanner G, Pósfai M, Böttger L, Matzanke B, Schüler D (2011) The cation diffusion facilitator proteins MamB and MamM of *Magnetospirillum gryphiswaldense* have distinct and complex functions, and are involved in magnetite biomineralization and magnetosome membrane assembly. Mol Microbiol 82:818–835

Uebe R, Henn V, Schüler D (2012) The MagA protein of magnetospirilla is not involved in bacterial magnetite biomineralization. J Bacteriol 194:1018–1023

Ullrich S, Schüler D (2010) Cre-lox-based method for generation of large deletions within the genomic magnetosome island of *Magnetospirillum gryphiswaldense*. Appl Environ Microbiol 76:2439–2444

Ullrich S, Kube M, Schübbe S, Reinhardt R, Schüler D (2005) A hypervariable 130-kilobase genomic region of *Magnetospirillum gryphiswaldense* comprises a magnetosome island which undergoes frequent rearrangements during stationary growth. J Bacteriol 187:7176–7184

Valverde-Tercedor C, Abadía-Molina F, Martinez-Bueno M, Pineda-Molina E, Chen L, Oestreicher Z, Lower BH, Lower SK, Bazylinski DA, Jimenez-Lopez C (2014) Subcellular localization

of the magnetosome protein MamC in the marine magnetotactic bacterium *Magnetococcus marinus* strain MC-1 using immunoelectron microscopy. Arch Microbiol (in press). doi:10.1007/s00203–014-0984–0

Williams TJ, Zhang CL, Scott JH, Bazylinski DA (2006) Evidence for autotrophy via the reverse tricarboxylic acid cycle in the marine magnetotactic coccus strain MC-1. Appl Environ Microbiol 72:1322–1329

Williams TJ, Lefèvre CT, Zhao W, Beveridge TJ, Bazylinski DA (2012) *Magnetospira thiophila*, gen. nov. sp. nov., a new marine magnetotactic bacterium that represents a novel lineage within the *Rhodospirillaceae* (*Alphaproteobacteria*). Int J Syst Evol Micr 62:2443–2450

Wu L, Gao B, Zhang F, Sun X, Zhang Y, Li Z (2013) A novel electrochemical immunosensor based on magnetosomes for detection of staphylococcal enterotoxin B in milk. Talara 106:360–366

Xiang L, Wei J, Jianbo S, Guili W, Feng G, Ying L (2007) Purified and sterilized magnetosomes from *Magnetospirillum gryphiswaldense* MSR-1 were not toxic to mouse fibroblasts *in vitro*. Lett Appl Microbiol 45:75–81

Yamamoto D, Taoka A, Uchihashi T, Sasaki H, Watanabe H, Ando T, Fukumori Y (2010) Visualization and structural analysis of the bacterial magnetic organelle magnetosome using atomic force microscopy. P Natl Acad Sci U S A 107:9382–9387

Yang CD, Takeyama H, Tanaka T, Hasegawa A, Matsunaga T (2001a) Synthesis of bacterial magnetic particles during cell cycle of *Magnetospirillum magneticum* AMB-1. Appl Biochem Biotech 91–93:155–160

Yang CD, Takeyama H, Tanaka T, Matsunaga T (2001b) Effects of growth medium composition, iron sources and atmospheric oxygen concentrations on production of luciferase-bacterial magnetic particle complex by a recombinant *Magnetospirillum magneticum* AMB-1. Enzyme Microb Tech 29:13–19

Yang W, Li R, Peng T, Zhang Y, Jiang W, Li Y, Li J (2010) *MamO* and *mamE* genes are essential for magnetosome crystal biomineralization in *Magnetospirillum gryphiswaldense* MSR-1. Res Microbiol 161:701–705

Yang Y, Li S, Huang X, Li J, Li L, Pan Y, Li Y (2013) MamX encoded by the *mamXY* operon is involved in control of magnetosome maturation in *Magnetospirillum gryphiswaldense* MSR-1. BMC Microbiol 13:203

Yoshino T, Matsunaga T (2005) Development of efficient expression system for protein display on bacterial magnetic particles. Biochem Bioph Res Co 338:1678–1681

Yoshino T, Matsunaga T (2006) Efficient and stable display of functional proteins on bacterial magnetic particles using Mms13 as a novel anchor molecule. Appl Environ Microbiol 72:465–471

Yoshino T, Tanaka T, Takeyama H, Matsunaga T (2003) Single nucleotide polymorphism genotyping of aldehyde dehydrogenase 2 gene using a single bacterial magnetic particle. Biosens Bioelectron 18:661–666

Yoza B, Matsumoto M, Matsunaga T (2002) DNA extraction using modified bacterial magnetic particles in the presence of amino silane compound. J Biotechnol 94:217–224

Yoza B, Arakaki A, Maruyama K, Takeyama H, Matsunaga T (2003a) Fully automated DNA extraction from blood using magnetic particles modified with a hyperbranched polyamidoamine dendrimer. J Biosci Bioeng 95:21–26

Yoza B, Arakaki A, Matsunaga T (2003b) DNA extraction using bacterial magnetic particles modified with hyperbranched polyamidoamine dendrimer. J Biotechnol 101:219–228

Zeytuni N, Ozyamak E, Ben-Harush K, Davidov G, Levin M, Gat Y, Moyal T, Brik A, Komeili A, Zarivach R (2011) Self-recognition mechanism of MamA, a magnetosome-associated TPR-containing protein, promotes complex assembly. P Natl Acad Sci U S A 108:E480–E487

Zeytuni N, Baran D, Davidov D, Zarivach R (2012) Inter-phylum structural conservation of the magnetosome-associated TPR-containing protein, MamA. J Struct Biol 180:479–487

Zhang C, Meng X, Li N, Wang W, Sun Y, Jiang W, Guan G, Li Y (2013) Two bifunctional enzymes with ferric reduction ability play complementary roles during magnetosome synthesis in *Magnetospirillum gryphiswaldense* MSR-1. J Bacteriol 195:876–885

Zhao M, Liang C, Li A, Chang J, Wang H, Yan R, Zhang J, Tai J (2010) Magnetic paclitaxel nanoparticles inhibit glioma growth and improve the survival of rats bearing glioma xenografts. Anticancer Res 30:2217–2223

Zhao G, Sanchez S, Schmidt OG, Pumera M (2012) Micromotors with built-in compasses. Chem Commun 48:10090–10092

Zhou W, Zhang Y, Ding X, Liu Y, Shen F, Zhang X, Deng S, Xiao H, Yang G, Peng H (2012) Magnetotactic bacteria: promising biosorbents for heavy metals. Appl Microbiol Biot 95:1097–1104

Chapter 4
Carboxysomes and Their Structural Organization in Prokaryotes

Sabine Heinhorst, Gordon C. Cannon and Jessup M. Shively

4.1 Introduction

Following their discovery in the early 1970s, carboxysomes, the CO_2-fixing organelles of many autotrophic bacteria, were largely regarded as oddities, specific to the metabolism of autotrophs and therefore of limited interest to the greater scientific community. After leading an existence in relative obscurity for decades, the genetic potential to form polyhedral protein inclusions related to carboxysomes was discovered throughout the bacterial kingdom. Once the structural similarity of the building blocks from which all of these bacterial microcompartments (BMCs) are constructed was elucidated, the tremendous potential of carboxysomes and related BMCs for synthetic biology and a variety of biotechnological applications was recognized. The ensuing flurry of research activities designed to elucidate and manipulate their structure, function, and biogenesis has led to considerable advances that are documented in several recent reviews (Bobik 2006; Cheng et al. 2008; Yeates et al. 2008; Kerfeld et al. 2010; Yeates et al. 2011; Rae et al. 2013; Yeates et al. 2013). This contribution will concentrate on areas that have not been covered exhaustively, such as insights gained from recent ultrastructural and cell biological approaches, and will focus on structural and functional comparisons between the α-carboxysomes found in many marine cyanobacteria and chemoautotrophs and the β-carboxysomes that occur mainly in freshwater cyanobacteria.

In accordance with the earliest models of carboxysome contribution to autotrophic metabolism, these polyhedral structures constitute a separate compartment within the bacterial cell, in which the important final step of the carbon dioxide-concentrating mechanism (CCM) takes place. The ability to accumulate inorganic

S. Heinhorst (✉) · G. C. Cannon
Department of Chemistry and Biochemistry, The University of Southern Mississippi, 118 College Drive #5043, Hattiesburg, MS 39406-0001, USA
e-mail: Sabine.heinhorst@usm.edu

J. M. Shively
Department of Genetics and Biochemistry, Clemson University, Clemson, SC 29634, USA

L. L. Barton et al. (eds.), *Nanomicrobiology,* DOI 10.1007/978-1-4939-1667-2_4

carbon intracellularly allows autotrophic bacteria to grow efficiently at the low concentrations of available dissolved carbon they encounter in their environment (reviewed in Heinhorst et al. 2006). Carboxysomes, which contain the CO_2-fixing enzyme ribulose 1,5-bisphosphate carboxylase/oxygenase (RubisCO), enhance the catalytic performance of this rather inefficient enzyme by a molecular mechanism that, although not completely understood, relies on contributions of their protein shell and of the carboxysomal carbonic anhydrase to concentrate the RubisCO substrate CO_2 within their interior. Underscoring the importance of carboxysomes for autotrophic metabolism are the numerous mutants that harbor structurally or functionally deficient organelles; the great majority of them have a *h*igh CO_2-*r*equiring or *hcr* phenotype, i.e., they require supplementation with additional CO_2 to achieve growth rates that approach wild-type levels.

4.2 Ultrastructure of Carboxysomes and Their Cellular Associations

The ultrastructure of carboxysomes and their cellular environment have been documented and refined repeatedly since the function of these microcompartments was elucidated in 1973 (Shively et al. 1973a). The early literature is largely based on observations made with thin sections of cells and with isolated carboxysomes that had been fixed and stained in preparation for transmission electron microscopy (TEM). Surprisingly, in spite of the drawbacks and artifacts associated with the harsh treatments to which the specimen were subjected, most of the conclusions reached about shape and diameter of carboxysomes, their number per cell, and the arrangement of RubisCO holoenzymes within the particles have withstood the test of time.

The higher resolution capabilities of modern electron microscopy techniques and instrumentation, combined with milder specimen preparation methods, have since revealed unprecedented ultrastructural details. Of particular importance in this regard has been the ability to obtain three-dimensional images of cellular structures and supramolecular assemblies by cryo-electron tomography (CET). Specimens are frozen rapidly in vitreous ice, a procedure that minimizes damage and preserves molecular structures in a near-in vivo, hydrated state. A series of images, taken at different tilt angles, subsequently forms the basis for the computer-aided reconstruction of biological structures in three dimensions (Tocheva et al. 2010).

In a landmark publication, Nierzwicki-Bauer et al. (1983) reported the three-dimensional ultrastructure of the β-carboxysome-containing unicellular cyanobacterium *Synechococcus* sp. PCC 7002, reconstructed from high-voltage transmission electron micrographs of serial cell sections. Van der Meene et al. (2006) later used a combination of electron microscopy and tomography to establish a three-dimensional model of the β-cyanobacterium *Synechocystis* PCC 6803. Both of these studies, as well as more recent electron tomography work (Ting et al. 2007; Liberton et al. 2011), confirmed the observations that carboxysomes in unicellular cyanobacteria are exclusively located in the central cytoplasm, which is devoid of thylakoid membranes and contains the bacterial DNA and the majority of the ribosomes.

Grouping of carboxysomes was observed in the cyanobacteria *Synechococcus* sp. PCC 7002 (Nierzwicki-Bauer et al. 1983), *Cyanothece* sp. ATCC 51142 (Liberton et al. 2011), *Anabaena* PCC 7119 (Orus et al. 2001), and two *Prochlorococcus* strains (Ting et al. 2007), as well as in the chemoautotrophic sulfur oxidizers *Halothiobacillus neapolitanus,Thiomicrospira crunogena,* and *Thiomonas intermedia* (Iancu et al. 2010). Although the significance of this clustering is not known, Ting et al. (2007) speculated that the close proximity of multiple carboxysomes may allow CO_2 that has diffused out of one carboxysome to be taken up by a neighboring organelle and contribute to efficient CO_2 fixation. Indeed, an increase in nonrandom distribution of carboxysomes was observed in several cyanobacterial species that were placed under carbon limitation conditions (McKay et al. 1993; Orus et al. 2001). Iancu et al. (2010) offered the alternative possibility that carboxysome grouping may reflect a common biogenesis site in the cell or may simply be the consequence of molecular crowding.

Most species have been reported to harbor between 1 and 20 carboxysomes per cell, with average numbers ranging from four to ten (Shively et al. 1973b; Nierzwicki-Bauer et al. 1983; van der Meene et al. 2006; Iancu et al. 2010); in a chemostat culture of the deep sea chemoautotroph *Thiomicrospira crunogena,* more than 80 carboxysomes were observed in some cells (Iancu et al. 2010). Changes in the number of carboxysomes per cell are well documented in the literature for chemo- and photoautotrophic bacteria. In keeping with their role in the CCM, carboxysome numbers increase during carbon limitation and decrease when the bacteria are supplied with elevated levels of CO_2 (Purohit et al. 1976; Beudeker et al. 1980; Pronk et al. 1990; McKay et al. 1993; Orus et al. 2001). For some but not all bacteria, the number of carboxysomes per cell increases significantly during stationary growth phase (Shively et al. 1970; Purohit et al. 1976). Likewise, a correlation of carboxysome numbers with cell size, i.e., the cell division cycle, has been reported (Shively et al. 1973b; Iancu et al. 2010).

4.2.1 Carboxysome Association with Polyphosphate Granules

In transmission electron micrographs of *Synechococcus* sp. PCC 7002 cell thin sections, carboxysomes are seen aligned along the longitudinal cell axis, where they are interspersed and sometimes in direct contact with electron dense, spherical cytoplasmic inclusions (Nierzwicki-Bauer et al. 1983). Elemental analysis by energy dispersive X-ray spectrometry of *Synechococcus leopoliensis* thin sections led to the conclusion that these structures, which are found in many bacteria and some archaea, are polyphosphate (also known as volutin) granules (Tang et al. 1995). Liberton et al. (2011) likewise observed a close association of carboxysomes with polyphosphate bodies in *Cyanothece* sp. ATCC 51142. A recent CET study of three chemoautotrophic sulfur bacteria revealed that their carboxysomes also cluster around cytoplasmic polyphosphate granules (Figure 4.1a), often through direct physical connections that appear to be mediated by unique lattice and string structures emanating from the granules (Iancu et al. 2010). In *H. neapolitanus,* 40 % of

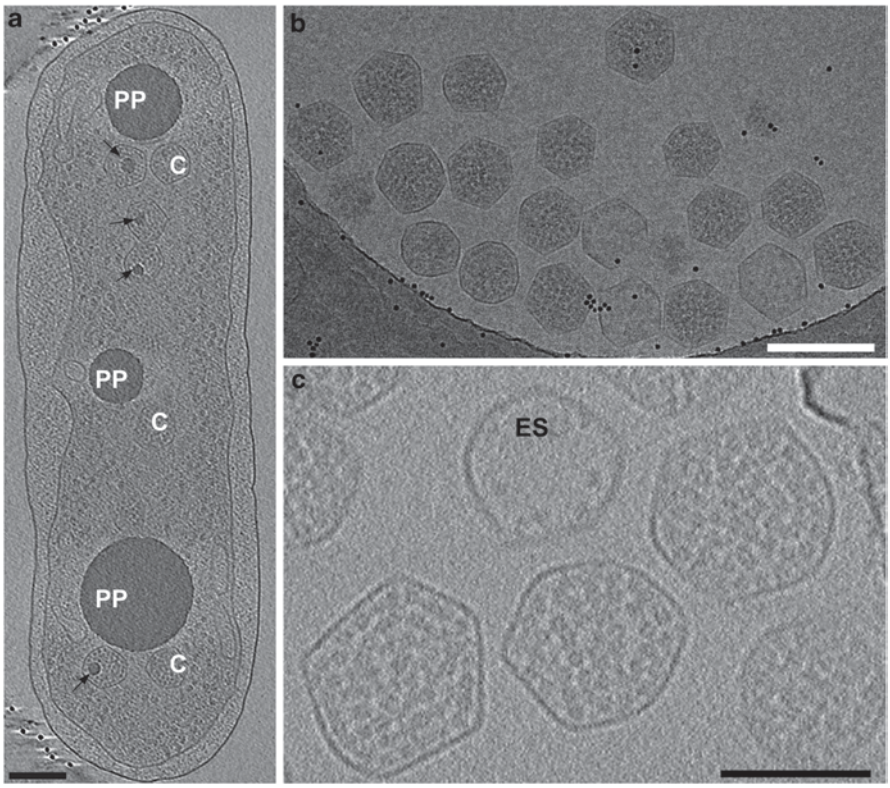

Fig. 4.1 Cryo-electron tomograms. **a** *H. neapolitanus* cell containing several carboxysomes (*C*) and polyphosphate granules (*PP*); some of the carboxysomes have polyphosphate inclusions (*small black arrows*); scale bar = 200 nm. **b** Tomogram of purified *H. neapolitanus* carboxysomes that illustrate the size heterogeneity among individual particles; scale bar = 100 nm. **c** Tomogram of carboxysomes that illustrate the arrangement of individual RubisCO molecules inside; *ES* = empty shell with just a few remaining RubisCO holoenzyme molecules; scale bar = 100 nm. (Images courtesy of Cristina Iancu and Grant J. Jensen)

the cellular carboxysomes were found to be associated with polyphosphate bodies. Interestingly, smaller inclusions of similar densities as the cytoplasmic polyphosphate granules also reside within the carboxysomes of several cyanobacteria (Tang et al. 1995; and references therein) and chemoautotrophs (Figure 4.1a; Iancu et al. 2010). Like their cytoplasmic counterparts, the intra-carboxysomal granules of *Synechococcus leopoliensis* are enriched in phosphorus and contain Ca^{2+}, and probably Mg^{2+} and K^{+} counterions (Tang et al. 1995). To date, a functional relationship between polyphosphate granules and carboxysomes has not been established. Since only a fraction of the carboxysomes within a cell contains polyphosphate inclusions (Tang et al. 1995; Iancu et al. 2010), a direct effect on CO_2 fixation can probably be excluded. Instead, a role as a phosphorus or divalent metal store has

been suggested, particularly in light of the documented decrease in size and abundance of the granules in response to sulfur and phosphate deprivation (Tang et al. 1995; Iancu et al. 2010). *Synechococcus leopoliensis* cells exposed to heavy metals contain an increased number of carboxysomes with polyphosphate granules, which indicates a possible connection to the stress response in this bacterium (Tang et al. 1995). Although not all carboxysomes in a cell harbor polyphosphate granules, considering the importance of phosphorylated intermediates in metabolism, the physiological significance of the observed association of α- as well as β-carboxysomes with polyphosphate bodies begs to be addressed experimentally.

4.2.2 Carboxysome Size Heterogeneity

Compared to the considerable size variations observed among α-carboxysomes in cells of chemoautotrophic bacteria (Figure 4.1a; Iancu et al. 2010), purified particles exhibit only moderate size heterogeneity, with diameters of individual *H. neapolitanus* (Figure 4.1b, c) and *Synechococcus* WH 8102 carboxysomes ranging from less than 100 to more than 160 nm (Schmid et al. 2006; Iancu et al. 2007; Iancu et al. 2010). Using scanning electron microscopy, Schmid et al. (2006) documented mass heterogeneity (100–350 MDa) among purified carboxysomes from *H. neapolitanus*. The extremes of that mass range deviate considerably from the calculated 280 MDa derived from the weight percentages of individual polypeptides in carboxysomes (Cannon and Shively 1983) and from geometric calculations (Shively and English 1991), and are indicative of significant variations in shell composition and/or packaging density of RubisCO between individual particles. Regardless of the observed size and mass heterogeneity, the CET studies (Schmid et al. 2006; Iancu et al. 2007) firmly established an icosahedral geometry for purified α-carboxysomes and resolved the long-standing question regarding their shape (icosahedron vs. pentagonal dodecahedron) that had persisted in the literature for several decades (Peters 1974; Holthuijzen et al. 1986; Shively and English 1991).

The polyhedral shape of carboxysomes led some investigators to suggest early on that they might be related to bacteriophages (Bock et al. 1974; Peters 1974; Westphal and Bock 1974). However, there is no bioinformatic or structural evidence that would indicate a phylogenetic link between carboxysomes and viruses (Kerfeld et al. 2010). Likewise, size and shape heterogeneity of carboxysomes (Figure 4.1; Schmid et al. 2006; Iancu et al. 2007; Iancu et al. 2010) suggests a high degree of compositional flexibility that differs starkly from the monodispersity of virus particles. Careful consideration of shell thickness as a percentage of particle diameter yields a significantly lower number for carboxysomes than for typical viral capsids (Tsai et al. 2007). The thickness of *H. neapolitanus* and *Nitrobacter winogradsky* carboxysome shells is less than 5 % of their particle diameter; by comparison, the corresponding value for cowpea chlorotic mottle virus is approximately 14 % (Shepherd et al. 2006).

4.3 Stability Differences Between Carboxysome Types

While α-carboxysomes can be purified, are stable in vitro, and therefore lend themselves to detailed ultrastructural (Figure 4.1b, c; Schmid et al. 2006; Iancu et al. 2007; Iancu et al. 2010), compositional (Cannon and Shively 1983; Baker et al. 1999, 2000), and functional analysis (Dou et al. 2008; Menon et al. 2008, 2010; Cai et al. 2009; Menon et al. 2010), the same cannot be said for β-carboxysomes. Fractions enriched in β-carboxysomes can be obtained via a Percoll-based coprecipitation method (Price et al. 1992), but the resulting preparations do not appear to be homogeneous and do not lend themselves to exhaustive ultrastructural analysis by electron microscopic methods, such as negative staining TEM or CET, that require large sample numbers to yield meaningful information. In our hands (authors' unpublished observations), electron microscopic analysis of fractions obtained during the purification of carboxysomes from *Thermosynechococcus elongatus* suggests that β-carboxysomes lose their polyhedral structure soon after lysis of the cell. While occasionally an intact β-carboxysome is observed without prior fixation, sample sizes large enough to yield definitive compositional information and draw solid ultrastructural conclusions are not obtained. In contrast, α-carboxysomes appear to be quite robust; sterile samples of *H. neapolitanus* carboxysomes retain their shape and enzymatic activity for at least 5 years when stored at 4 °C. Furthermore, the literature contains numerous examples of electron micrographs in which multiple, apparently homogeneous, intact α-carboxysomes are visible per microscope field. Likewise, 100–200 individual α-carboxysomes were analyzed for CET studies (Figure 4.1b, 4.1c) (Schmid et al. 2006; Iancu et al. 2007; Iancu et al. 2010). To date, comparable studies of intact, purified β-carboxysomes do not exist.

4.4 The Carboxysome Shell

The predominant proteins of the carboxysome shell are small (8–10 kDa) polypeptides that contain a BMC domain (Pfam00936) of approximately 80 amino acids consisting of three α-helices and four β-strands (Kerfeld et al. 2005). The single-BMC-domain proteins, termed CsoS1 in α-carboxysomes and CcmK in β-carboxysomes, self-assemble into hexamers that, in turn, tessellate to form the arrays thought to give rise to the facets of the icosahedral shell (Figure 4.2; (Kerfeld et al. 2005; Tsai et al. 2007; Tsai et al. 2009; Kinney et al. 2011). The tandem-BMC-domain proteins, which are low-abundance shell components, assemble into trimers (pseudohexamers) that are stacked (Figure 4.2; Klein et al. 2009; Kinney et al. 2011; Cai et al. 2013). With the exception of the small marine cyanobacterium *Prochlorococcus marinus* MED4, which is unique in that it utilizes only one single-BMC-domain (CsoS1) and one tandem-BMC-domain (CsoS1D) protein in its carboxysome shell (Figure 4.3; Roberts et al. 2012), the genomes of all other known carboxysome-containing bacteria carry multiple paralogs for single-BMC-domain proteins and at least one gene for a tandem-BMC-domain polypeptide (Figure 4.3)

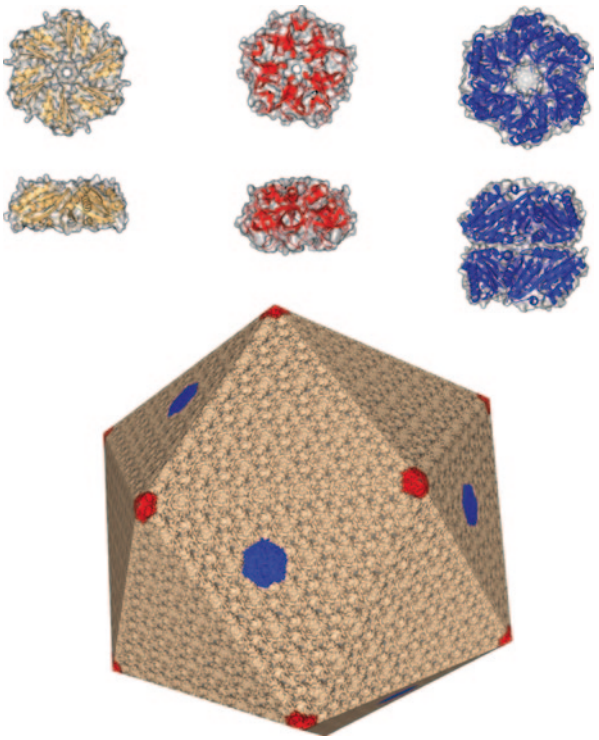

Fig. 4.2 The known building blocks of the carboxysome shell. Hexamers of pfam00936 single-BMC-domain proteins (*wheat*) are the main shell components, thought to form the facets of the icosahedral particles. Pentamers of pfam03319 proteins (*red*) are believed to occupy the vertices. Pseudohexamers of pfam00936 tandem-BMC-domain proteins (*blue*), some of which assemble into stacked dimers of trimers, are low-abundance shell constituents. Shown are models based on α-carboxysome shell components (from left to right 2G13, 2RCF, and 3F56). (Image courtesy of Fei Cai and Cheryl Kerfeld)

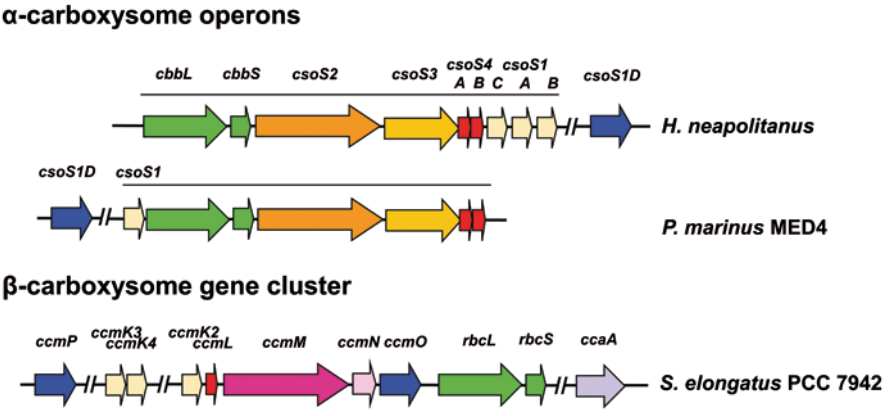

Fig. 4.3 Gene clusters encoding proteins of α- and β-carboxysomes. Shown are the *cso* operons of *Prochlorococcus marinus* MED 4 and *Halothiobacillus neapolitanus* including the *csoS1D* genes that are not part of the operons, and the carboxysome gene clusters of *Synechococcus elongatus* PCC 7942. The colors of the genes encoding the major shell components are the same as those in Figure 4.2 (*wheat, red,* and *blue*). The genes for the large and small subunits of Form I RubisCO are *green*

(Kinney et al. 2011). Members of an additional shell protein family (Pfam03319) are the constituents of the pentamers thought to occupy the vertices of the polyhedral carboxysomes (Figures 4.2 and 4.3; Tanaka et al. 2008; Kinney et al. 2011). Orthologous genes encoding these two protein families are found throughout many bacterial lineages in approximately one fifth of all sequenced bacterial genomes. Some of these bacteria have been shown to form BMCs of similar structure, but unrelated function, that encapsulate enzymes necessary for the catabolism of certain carbon sources (reviewed in Kerfeld et al. 2010). Clearly, protein shell-based compartmentalization of the enzymes that catalyze selected biochemical reactions appears to be a widespread metabolic strategy among the bacteria.

4.4.1 Single Pfam00936 Shell Proteins

The *cso* operons of *H. neapolitanus,Thiomonas intermedia,* and *Thiomicrospira crunogena* each encode three single-BMC-domain proteins (CsoS1) that share a high degree of sequence similarity and differ in only a few residues throughout the length of their common regions (Figure 4.3). The CsoS1B protein of *H. neapolitanus* features a C-terminal extension of 12 amino acids that is not present in its CsoS1A and CsoS1C paralogs (Cannon et al. 2003) and may be important for carboxysome assembly and/or interaction with proteins located on the interior face of the shell (see below).

The genomes of the model β-cyanobacteria *Synechocystis* sp. PCC6803 and *Synechococcus elongatus* PCC7942 (Figure 4.3) harbor genes for four and three single-BMC-domain paralogs, respectively. Individual CcmK paralogs, like their α-carboxysomal orthologs, have very similar core sequences but differ in their C-termini (Tanaka et al. 2009). Although the protein complement of β-carboxysomes has not been unequivocally determined, proteomic analysis of fractions highly enriched in β-carboxysome proteins (Long et al. 2005, Long et al. 2007, Long et al. 2010) and the phenotypes of various mutants (Savage et al. 2010; Rae et al. 2012 and references therein) have permitted an assessment of the likely shell constituents. In *Synechococcus elongatus* PCC 7942, CcmK2 appears to be the most abundant single-BMC-domain protein that is consistently identified in enriched fractions (Long et al. 2005, Long et al. 2007; Long et al. 2010). Furthermore, *ΔccmK2* mutants are devoid of carboxysomes, a phenotype that establishes this protein as an essential constituent of the β-carboxysome shell (Rae et al. 2012; Cameron et al. 2013). Fluorescently tagged CcmK4 protein of *Synechococcus elongatus* PCC7942 localizes to the punctate structures thought to represent individual carboxysomes (Savage et al. 2010). This protein and its paralog CcmK3 do not seem to be structurally important components of the β-carboxysome shell but rather contribute to organelle function (Zhang et al. 2004; Rae et al. 2012).

Whether the carboxysome shell in those bacteria that express multiple single-BMC-domain proteins contains homo-hexamers consisting of only one type of monomer or is comprised of hexamers that feature combinations of different

paralogs is not known. Hexamers formed by individual β-carboxysomal CcmK paralogs are nearly identical in shape and are easily superimposable, with the exception of the C-terminal extensions found in some paralogs (Tanaka et al. 2009). Although they do not address the homo-versus hetero-hexamer question, the fluorescence resonance energy transfer (FRET) approaches employed by Samborska and Kimber (Samborska and Kimber 2012) are the first to directly probe interactions between pairs of BMC-domain protein paralogs. The authors showed that *Thermosynechococcus elongatus* CcmK2 preferentially interacts with itself. The CcmK1 and CcmK4a proteins, however, have higher affinity for specific paralogs than for themselves. Whether this result is indicative of interactions within hetero-hexamers or between homohexamers of different paralogs is not clear. One can speculate that hetero-hexamers would expand the repertoire of potential contacts and attachment points for cargo proteins within the carboxysome, and/or with extra-organellar structures on the cytosolic side that might be relevant for carboxysome function and/or intracellular distribution.

Based on molecular models derived from crystallographic data, each hexamer possesses a convex and a concave side of different surface charge (reviewed in Kinney et al. 2011). All hexamers are predicted to be oriented in the same manner in the shell (Tanaka et al. 2008), but the sidedness of the arrays is an as-yet unresolved question. The surface that presents itself to the cytosolic side is likely important for the recruitment of metabolites to the carboxysome, their transfer across the shell, and interactions with other cellular structures, while the inward-facing surface engages in contact with the encapsulated proteins. Direct experimental evidence is needed to determine which side of the BMC-domain protein assemblies faces the inside and the outside of the carboxysome to advance our understanding of the way in which shell structure and architecture are related to function.

Each shell protein hexamer contains a central pore of a diameter that varies from 4 to 7 Å, depending on the monomer constituent (Figure 4.2; reviewed in Kinney et al. 2011). Given the tight interactions between individual subunits within a hexamer and between neighboring hexamers and the invariably positive surface charge of the openings, the pores have been proposed to represent the main route for the flux of the negatively charged RubisCO substrates and products into and out of the carboxysome (Kerfeld et al. 2005; Tsai et al. 2007; Tanaka et al. 2008). If this assumption is proven to be correct, the pore structure/function relationship forms the basis for the selective shell permeability that appears to be a crucial determinant of carboxysome function in the bacterial CCM (Reinhold et al. 1989; Kaplan and Reinhold 1999; Dou et al. 2008). Although sulfate (Kerfeld et al. 2005; Tsai et al. 2007; Samborska and Kimber 2012) and glycerol (Samborska and Kimber 2012) can be trapped in crystals of single-BMC-domain protein crystals, the molecular mechanism by which the pores might provide the requisite selective permeability and impede the diffusion of CO_2 is not obvious. It is tempting to suggest that metabolite transfer might operate through a protein channel-like mechanism reminiscent of that found in aquaporins (de Groot and Grubmuller 2005). One may also speculate that the monomer composition of individual hexamers could exert an effect on the characteristics of the pore. Although the residues that line the pores are

highly conserved among paralogs, the presence of different paralogs in a hexamer may lead to subtle yet significant variations in pore structure; these could broaden the range of small molecules able to cross the carboxysome shell or, alternatively, restrict access of certain metabolites to the carboxysome interior. A complicating factor in proposing a convincing mechanism for metabolite transfer across the carboxysome shell is the small size of the hexamer pores. Although wide enough for the passage of bicarbonate and Mg^{2+}, it is difficult to envision how the considerably larger RubP and 3-phosphoglyceric acid (3-PGA) molecules could effectively traverse the shell through such narrow passages, despite some apparent structural flexibility of the pore (Samborska and Kimber 2012).

4.4.2 Tandem Pfam00936 Shell Proteins

Recently, the tandem-BMC-domain proteins have emerged as possible candidates that might mediate passage of larger metabolites across the carboxysome shell. Discovered originally in the genome of *P. marinus* MED4, the gene encoding such a protein was termed *csoS1D* to indicate the structural relationship of its product to the single-BMC-domain proteins (Figure 4.3). Orthologs exist in all cyanobacteria (Klein et al. 2009; Cai et al. 2013) and in carboxysome-forming chemoautotrophs (Roberts et al. 2012; Figure 4.3). Interestingly, the *csoS1D* genes of α-carboxysome-forming bacteria are not part of their *cso* operons (Figure 4.3); however, expression of *csoS1D* appears to respond to carbon availability in the same manner as the canonical carboxysome genes in *P. marinus* MED4 (Klein et al. 2009).

The two BMC domains of CsoS1D and its orthologs, although bearing little amino acid sequence similarity, are structurally almost identical and assemble into stacked dimers of pseudohexameric trimers (Figure 4.2; Klein et al. 2009; Cai et al. 2013). The pores of the trimers are considerably larger (14–15 Å diameter) than those of the hexamers formed by single-BMC-domain proteins and could easily accommodate the larger RubisCO substrate and product molecules (Klein et al. 2009; Cai et al. 2013). Furthermore, the CcmP protein was recently shown to have some affinity for 3-PGA (Cai et al. 2013), a finding that supports a role for tandem-BMC-domain proteins as conduits for the transfer of larger metabolites across the shell. Roberts et al. (2012) identified the CsoS1D protein in purified *P. marinus* MED4 α-carboxysomes and showed that it is tightly associated with the shell, as had been predicted based on models that revealed a tight fit of CsoS1D trimers within CsoS1 hexamer arrays (Figure 4.2; Klein et al. 2009). Cai and coworkers (Cai et al. 2013) solved the structure of the CcmP protein and, using fluorescently tagged protein, showed that CcmP colocalizes with RubisCO to the β-carboxysomes of *Synechococcus elongatus* PCC7942 (Figure 4.4).

Carboxysome tandem-BMC domain protein assemblies have two intriguing structural features with potentially important implications for the mechanism by which carboxysomes communicate and exchange small molecules with their

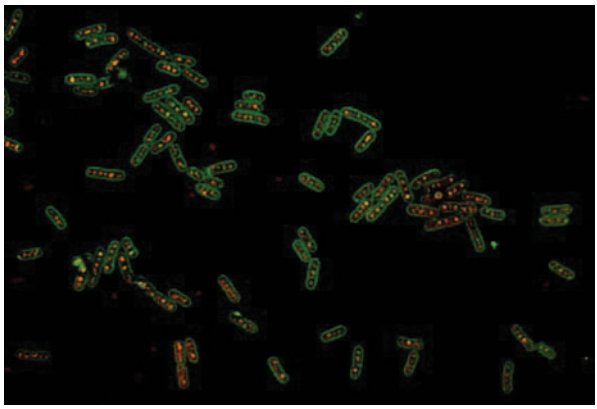

Fig. 4.4 Fluorescently labeled β-carboxysomes in *Synechococcus elongatus* PCC 7942. The cells express fusions of the large subunit of RubisCO with cyan fluorescent protein (*CFP*; *pseudo-color red*) and of shell protein CcmP with yellow fluorescent protein (*YFP*; *pseudo-color green*). Both fluorescent fusion proteins colocalize to bright punctae that are spaced evenly along the long axes of the cells and believed to represent individual carboxysomes. (Image courtesy of Fei Cai and Cheryl Kerfeld)

exterior. The first is an interior channel of predominantly positive surface potential that was first observed in the stacked dimers of *P. marinus* MED4 CsoS1D trimers (Figure 4.3; Klein et al. 2009). Structural analysis of CcmP revealed the existence of a similar nanocompartment within the assembly of this protein; its cavity was also shown to display weak affinity for the product of the RubisCO reaction, 3-PGA (Cai et al. 2013). Secondly, the large trimer pores of tandem BMC-domain proteins can exist in two different states through alternative side-chain conformations of two absolutely conserved residues (Glu and Arg) that that are found in all tandem-BMC proteins identified bioinformatically (Figure 4.3; Klein et al. 2009; Cai et al. 2013). These two amino acids are responsible for gating the two pores of the stacked trimers, one of which tends to be closed while the other one is in the open state in CsoS1D and CcmP crystals (Klein et al. 2009; Cai et al. 2013). Considering the metabolic steps downstream from the carboxylation reaction catalyzed by RubisCO, these nanocompartments within the carboxysome shell could act as temporary reservoirs for RubP and/or 3-PGA. Import into and/or release from the carboxysome of these metabolites could be regulated through gating of the pores in response to the metabolic state (e.g., energy charge, redox poise) of the cell. The one important caveat to this elegant model is the very low abundance of the CsoS1D protein in the *P. marinus* MED4 carboxysome, which is estimated to contain 12 trimers or 6 dimers of stacked trimers that correspond to only 6 nanocompartments with 12 gated pores per particle (Roberts et al. 2012). Each carboxysome has an estimated 740 to more than 1000 pores for bicarbonate (Iancu et al. 2007; Tanaka et al. 2008) provided by the single-BMC domain hexamers. Whether a sufficiently high flux of RubP and/or 3-PGA through the predicted tandem-BMC domain "transporters" can be achieved to support the enzymatic activity of the ~270 fully activated RubisCO holoenzyme molecules in the interior awaits experimental evidence.

4.4.3 *Pfam03319 Shell Proteins*

The geometric requirement for 12 pentamers to close the 20 facets of an icosahedron is believed to be satisfied in both α- and β-carboxysomes by proteins belonging to Pfam03319. The CsoS4 paralogs in α-carboxysomes and CcmL in β-carboxysomes are low-abundance components of the shell that self-associate into pentamers (Figure 4.2). In models of the icosahedral carboxysome shell, the molecular dimensions of the pentamers, calculated from crystallographic data, fit precisely into the proposed vertices (Tanaka et al. 2008). Mutants that do not express vertex proteins have the *hcr* phenotype and produce an increased number of elongated carboxysomes in addition to many particles of apparently normal icosahedral shape (Price et al. 1993; Cai et al. 2009; Rae et al. 2012; Cameron et al. 2013). Since most of the carboxysomes purified from a *H. neapolitanus csoS4A/csoS4B* null mutant appear morphologically similar to wild-type particles, the remaining (Pfam00936) shell proteins appear to be able to close the hexamer arrays of the facets into a three-dimensional icosahedron (Cai et al. 2009).

4.4.4 *Is the Shell Single- or Double-Layered?*

Most ultrastructural studies of carboxysomes have concluded that the bounding shell is a 3–4-nm-thick protein monolayer (Shively et al. 1973; Peters 1974; Holthuijzen et al. 1986; Schmid et al. 2006). However, recent structural analysis of *Thermosynechococcus elongatus* CcmK2 assemblies, combined with elegant FRET analyses, revealed that the concave faces of two of its hexamers associate to form a double-layered dodecamer in vitro (Samborska and Kimber 2012). Since CcmK2 is the only paralog present in all β-carboxysome-forming cyanobacteria, the BMC domain protein that is consistently recovered in β-carboxysome-enriched fractions and an essential carboxysome component (Rae et al. 2012; Cameron et al. 2013), models of the β-carboxysome shell that take into account these hexamer interactions suggest that its facets might consist of a double layer formed by CcmK2 dodecamers (Samborska and Kimber 2012). However, consideration of the fit of the CcmP trimer in the hexamer arrays of CcmK2, on the other hand, favors a single-layered β-carboxysome shell (Cai et al. 2013). Whether the CcmK2 dodecamers observed in vitro reflect the organization of this protein in the carboxysome shell in vivo or possibly represent an early assembly intermediate, as was offered as an alternative suggestion (Samborska and Kimber 2012), awaits further experimental evidence.

4.5 Shell-Associated Proteins

4.5.1 *Shell-Associated Proteins of α-Carboxysomes*

When purified α-carboxysomes are subjected to mild denaturants or mechanical shear, a fraction of the shells breaks and releases the carboxysomal RubisCO into

the surrounding buffer. Although no longer intact, the broken shells tend to retain their shape and can be separated from unbroken carboxysomes and free RubisCO by density gradient centrifugation. This fraction consistently contains the stoichiometric amounts of CsoS1 and CsoS4 paralogs expected from the polypeptide pattern of purified carboxysomes (reviewed in Heinhorst et al. 2006), as well as the CsoS2A and CsoS2B polypeptides and the carbonic anhydrase CsoSCA. In addition, approximately 20 % of the total carboxysomal RubisCO protein complement usually remains with the broken shell fraction and is not released by additional washes (Heinhorst et al. 2006; Schmid et al. 2006; Iancu et al. 2010), suggesting that the outermost RubisCO layer engages in strong interactions with the shell.

The *csoS3* gene of the *cso* operon encodes the CsoSCA protein, the apparently sole CA of α-carboxysomes (reviewed in Cannon et al. 2010). The protein is a unique β-class enzyme whose identity had long remained obscure because of an almost complete lack of primary structure homology to other CAs (Sawaya et al. 2006; Cannon et al. 2010; Kerfeld et al. 2010). Of the three distinct domains revealed in its crystal structure, the middle and C-terminal domains appear to have arisen by an ancient gene duplication event but have since diverged considerably. Only the C-terminal domain carries a binding site for the obligatory zinc ion found in β-CAs and has catalytic activity (Sawaya et al. 2006). The likely in vivo form of CsoSCA is a dimer, which is present in the carboxysome in an estimated 40 copies (Heinhorst et al. 2006). The CsoSCA protein is tightly associated with the shell (Baker et al. 2000; So et al. 2004; Heinhorst et al. 2006; Dou et al. 2008) and, to be stripped from isolated shells, requires increasingly harsh denaturing conditions that release enzymatically inactive CsoSCA protein only as the entire shell dissolves (Heinhorst et al. 2006).

The structural basis for the strong association of CsoSCA with other shell components and the identity of its interaction partners are unknown. There is no obvious fit of the CsoSCA dimers within the tight CsoS1 hexamer arrays or at the vertices of the carboxysome. Since recombinant CsoSCA supplied externally to purified *H. neapolitanus ΔcsoS3* carboxysomes does not rescue the compromised CO_2 fixation ability of the mutant organelles, the enzyme likely faces inward (Dou et al. 2008), as predicted also for the β-carboxysomal CAs CcaA and CcmM (see below; Long et al. 2007; Cot et al. 2008). Although CsoSCA clearly is an important functional component of the α-carboxysome, a significant role of this protein in carboxysome biogenesis and shell structure can be excluded because the carboxysomes of a *H. neapolitanus ΔcsoS3* mutant are indistinguishable from wild-type particles in morphology and protein content, other than lacking the CsoSCA protein (Dou et al. 2008).

Like CsoSCA, the CsoS2 protein of α-carboxysomes does not have an ortholog in β-carboxysomes (Cannon et al. 2002). The largest known constituent of α-carboxysomes remains associated with the shell upon carboxysome disruption and is released only under conditions that lead to disintegration of the entire shell structure (Baker et al. 1999; Heinhorst et al. 2006). The CsoS2 protein has several unique properties. In some bacteria, including *H. neapolitanus,* the protein exists in two forms that share the same N-terminus but may be differentially glycosylated (Baker et al. 1999). The primary structure of the protein features multiple repeat

motifs consisting of three and seven or eight amino acids, as well as a series of conserved Cys residues (Cannon et al. 2003). Since expression of soluble recombinant CsoS2 protein has proven difficult (authors' unpublished observations), no crystal structure is available to date. Its high pI (>9) distinguishes CsoS2 from the remaining known α-carboxysome proteins and suggests that the protein might participate in the transfer of the negatively charged substrate and/or products across the carboxysome shell. However, to date, there is no experimental evidence for a role of CsoS2 in metabolite flux. Given the size of the protein and its unusually high pI, it is tempting to speculate that CsoS2 might be arranged inside the shell, where it could act as molecular "glue" that reinforces the thin layer of BMC-domain protein hexamers. In addition or alternatively, CsoS2 may connect the proximal layer of RubisCO, which remains attached to broken shells (Heinhorst et al. 2006; Iancu et al. 2010) to the inside of the single-BMC domain protein hexamer arrays.

4.5.2 Shell-Associated Proteins of β-Carboxysomes

Contrary to α-carboxysomes, β-carboxysomes are yet to be purified to homogeneity. Since their composition and the stoichiometric ratios of their protein components are not known, their internal organization has been inferred from a combination of genetic, biochemical, and proteomic approaches. The protein encoded by the *ccmM* gene, which does not have a homolog in α-carboxysome forming bacteria, is a crucial component of β-carboxysomes. Gene knockouts yield Δ*ccmM* mutants that do not form carboxysomes and have an absolute requirement for elevated CO_2 (*hcr* phenotype; Ludwig et al. 2000; Berry et al. 2005; Long et al. 2011). The gene encodes at least two protein products in vivo (Price et al. 1998; Long et al. 2005): The full-length polypeptide consists of an N-terminal domain with homology to the γ-carbonic anhydrase Cam from *Methanosarcina thermophila* (Alber and Ferry 1994) and of a C-terminal region featuring multiple repeats with similarity to the small subunit of RubisCO (RbcS; Price et al. 1993; Ludwig et al. 2000). A second, shorter protein product consisting of only the C-terminal RbcS-like repeats is translated from an internal start codon (Long et al. 2007; Long et al. 2011), is present in higher copy number than the full-length version in carboxysome protein-enriched cellular fractions (Long et al. 2011), and is also needed for the assembly of functional carboxysomes in *Synechococcus elongatus* PCC 7942 (Long et al. 2010). Yeast two-hybrid analysis with recombinant proteins that are predicted to be components of the *Synechocystis* sp. PCC 6803 carboxysome revealed interactions between the N-terminal domain of CcmM, the CcmN protein, and CcaA (Cot et al. 2008) and led the authors to propose the existence of a bicarbonate dehydration complex in β-carboxysomes. An assembly consisting of CcmM trimers, CcaA dimers, and CcmN is thought to interact with the outermost RubisCO layer via the C-terminal RbcS-like repeats of CcmM and to rapidly equilibrate entering bicarbonate with CO_2. This model was confirmed by additional protein interaction studies and was subsequently expanded to include a role of the shorter form of CcmM as an organizer of RubisCO in the carboxysome interior (Long et al. 2007, 2010, 2011; Cot

et al. 2008; Peña et al. 2010). Kinney et al. (2012), however, did not find evidence for the presence of CcaA in complexes of CcmM, RubisCO, and the carboxysome protein CcmN the authors isolated using similar immunoprecipitation experiments.

The *ccaA* (*icfA*) gene, which is found in many, but not all, β-carboxysome-containing cyanobacteria, encodes a β-CA that co-purifies with other β-carboxysome proteins during enrichment procedures (So and Espie 1998; So et al. 2002; Cot et al. 2008). Like its α-carboxysomal counterpart CsoSCA, the CcaA protein does not seem to be an important structural component of β-carboxysomes; however, its enzymatic activity is essential for organelle function. Although its carboxysomes are indistinguishable from wild-type organelles in transmission electron micrographs of cell thin sections, *ccaA* null mutants exhibit an *hcr* phenotype (So et al. 2002). The N-terminal portion of CcaA harbors its catalytic domain, which requires dimerization via the C-terminal domain for enzymatic activity and for interaction of CcaA with CcmM (So et al. 2002; Cot et al. 2008).

The absence of a *ccaA* gene from the genomes of several β-carboxysome forming cyanobacteria begged the question whether another carbonic anhydrase exists that is present in all β-carboxysomes. Catalytic activity of the obvious candidate, CcmM, had eluded detection in assays of purified recombinant protein and of *Escherichia coli* extracts expressing CcmM from several cyanobacteria (Cot et al. 2008). Peña et al. (2010) solved the structure of a CcmM fragment from *Thermosynechococcus elongatus* BP-1 that consists of the first 209 amino acids. The authors showed that the CA activity of the protein depends on the oxidized state of a crucial disulfide bond in the catalytic domain. A reducing environment like the cytosol disrupts the structure of the trimeric enzyme and prompts the suggestion that the carboxysome interior is able to maintain an oxidizing milieu in which CcmM is active. A recent study of β-carboxysome biogenesis lends support to this hypothesis by providing evidence for the oxidation of the carboxysome interior as the organelle ages (Chen et al. 2013). Although the CcmM protein appears to be a universal organizing component of all β-carboxysomes, its CA activity seems to have been replaced by that of CcaA in those cyanobacteria that also carry a *ccaA* gene (Peña et al. 2010).

Another gene unique to β-cyanobacteria, *ccmN,* is part of the cluster that includes *ccmM,ccmL,ccmO,ccmK2,* and the RubisCO genes in *Synechococcus elongatus* PCC 7942 (Figure 4.3). Like the *Δ*ccmM mutant, the *ccmN* knockout does not grow at ambient CO_2 concentration (*hcr* phenotype) and, instead of carboxysomes, contains a large polar body that is thought to consist of aggregated protein (Kinney et al. 2012). Fluorescently tagged CcmN protein colocalizes with RubisCO to the distinct punctate structures in the cell thought to represent individual carboxysomes (Kinney et al. 2012). A bioinformatic analysis of CcmN orthologs revealed that the protein contains two conserved regions. The N-terminal portion, which consists of six bacterial hexapeptide repeats (Pfam00132), is predicted to be structurally similar to the CcmM N-terminal region (Peña et al. 2010; Kinney et al. 2012) and was shown to interact with CcmM in pulldown assays that feature CcmN as bait. A conserved C-terminal peptide of 18 amino acids, which is connected to the N-terminal region of CcmN through a variable Pro- and Ser-rich linker, interacts with the shell protein CcmK2. A mutant of *Synechococcus elongatus* PCC 7942 producing CcmN

that is devoid of these 18 amino acids has a similar phenotype as the *ccmN* null mutant, emphasizing the importance of this portion of the protein for carboxysome formation (Kinney et al. 2012). Interestingly, a search for bacterial genomes that carry orthologs of the common BMC shell genes (Pfam00936 and Pfam03319) identified peptides similar to the C-terminal peptide of CcmN in many proteins thought to be targeted to the interior of BMCs. This finding raises the interesting possibility that BMC proteins carrying such a peptide may recruit other proteins to the nascent organelle or contribute to the assembly of the BMC shell itself through interactions with conserved structural elements of shell components (Kinney et al. 2012).

4.6 Shell Permeability

Throughout the evolution of a working model for carboxysome function, various permeability properties have been attributed to the protein shell that could support the proposed role of the carboxysome in the CCM (reviewed in Heinhorst et al. 2006). Clearly, the enzymatic action of the carboxysomal carbonic anhydrase plays a pivotal role in providing the encapsulated RubisCO with a sufficiently high concentration of its substrate CO_2 to ensure efficient CO_2 fixation. Carbon dioxide fixation assays performed with purified *ΔcsoS3* mutant carboxysomes of *H. neapolitanus* revealed a requirement of the encapsulated RubisCO for elevated inorganic carbon levels that was not observed in assays performed with broken mutant organelles. These kinetic measurements provided direct experimental evidence that the shell impedes diffusion of CO_2 (Dou et al. 2008), as had been predicted in the original CCM model (Reinhold et al. 1989). Likewise, carbonic anhydrase activity assays performed with intact purified carboxysomes devoid of the vertex proteins CsoS4A and CsoS4B established that their shells, although of apparently normal polyhedral appearance, are much more permeable to CO_2 than those of wild-type carboxysomes, a functional deficiency that explains the requirement of the mutant for elevated CO_2 levels and lends further support to the proposed role of the shell as a CO_2 diffusion barrier (Cai et al. 2009).

In an attempt to reconcile the common building principles of all BMC shells with a universal function of these bacterial organelles, Penrod and Roth proposed that the interior of all BMCs might provide an environment with a lower pH than that of the cytosol (Penrod and Roth 2006). In the carboxysome interior, a lower pH would benefit CO_2 fixation by shifting the equilibrium between bicarbonate and CO_2 in favor of the RubisCO substrate, and could explain at least in part the advantage RubisCO derives from compartmentalization. However, experiments employing a fusion protein that consists of a pH-sensitive GFP variant and the small subunit of RubisCO did not reveal a pH differential between the inside of the organelle and the cytosol. Unlike the lipid bilayer-based borders that separate eukaryotic cell compartments, the protein shell of the carboxysome is freely permeable to protons (Menon et al. 2010).

4.7 The Arrangement of RubisCO Within the Carboxysome

Transmission electron micrographs presented in the earliest reports of carboxysomes (Gantt and Conti 1969; Shively et al. 1973b) suggested that some particles contain a core of highly ordered RubisCO that is arranged in what was termed a paracrystalline array. However, perusal of a large number of TEM images, each containing many negatively stained, purified α-carboxysomes per field, suggests that paracrystalline structures are rather rare (authors' unpublished observations). Likewise, exhaustive CET analysis of α-carboxysomes, both purified and within intact cells, does not support the paracrystalline model as the most prevalent and biologically significant packing of RubisCO in the icosahedral particles (Figure 4.1; Schmid et al. 2006; Iancu et al. 2007, 2010). Instead, most of the RubisCO holoenzyme molecules were found to be arranged in a layer abutting the inside of the shell. The remaining enzyme molecules occupy two or three additional concentric layers, with RubisCO packing becoming less tight and ordered towards the center of the carboxysome (Figure 4.2). A preferential orientation of individual RubisCO molecules, as one would expect to see in a paracrystalline array, was not discernible. The basis for the rare occurrence of regular RubisCO arrays in α-carboxysome preparations is a mystery that might, however, be related to the tendency of carboxysomal RubisCO molecules to orient themselves on electron microscope grids in highly concentrated preparations (Shively et al. 1973b); Orus et al. 1995; and authors' unpublished observations). Since carboxysomes that are filled to varying degrees with RubisCO are well documented (Schmid et al. 2006; Iancu et al. 2007, 2010), maybe the regular array of RubisCO seen in the occasional carboxysome reflects a particle with particularly densely packed contents.

The arrangement of RubisCO in the interior of β-carboxysomes may be different. Gantt and Conti (Gantt and Conti 1969) reported that some polyhedral bodies observed in negatively stained, cell-free preparations of *Synechococcus elongatus* (formerly *Anacystis nidulans*) appeared as crystalline bodies. More recently, Kaneko et al. (2006) employed Hilbert differential contrast electron microscopy to examine rapidly frozen cells of *Synechococcus elongatus* PCC 7942 and stated about the resulting micrographs: "Occasionally the paracrystalline arrangement of particles could be recognized." It is difficult to assess the proportion of the cellular carboxysomes that contain regularly packed RubisCO and the extent to which the paracrystalline RubisCO arrangement represents the carboxysome interior. Perhaps the highly ordered structures seen in the Hilbert images represent only the outermost layer of RubisCO that is attached to the inside of the shell. Unfortunately, current CET methods do not allow high-resolution studies of intact bacterial cells as large as most cyanobacteria that contain β-carboxysomes; elucidation of RubisCO packaging in these carboxysomes awaits the development of a purification method.

4.8 Carboxysome Assembly

In contrast to the moderate size and mass heterogeneity exhibited by populations of purified α-carboxysomes, CET revealed a considerably greater variation in size and shape among particles within intact cells of the chemoautotrophs *H. neapolitanus,Thiomonas intermedia,* and *Thiomicrospira crunogena* (Iancu et al. 2010) that are suggestive of a considerable structural flexibility of the shell. Occasionally, moderately to greatly elongated carboxysomes, as well as irregularly shaped microcompartments can be seen in cells next to normal icosahedral particles (Gantt and Conti 1969; Shively et al. 1970, 1973b; Iancu et al. 2010). It is not yet known how these aberrantly shaped carboxysomes come to be or, for that matter, how the regular icosahedral shape of carboxysomes arises during biogenesis. Whether the observed misshapen variants are functionally impaired assembly "accidents" or represent intermediates that await processing to regular icosahedra remains to be determined. Mutants of α- and β-carboxysome containing bacteria that do not express the proposed vertex proteins are enriched in elongated carboxysomes (Price and Badger 1989, 1991; Price et al. 1993; Cai et al. 2009). Likewise, overexpression of a single shell protein of the Pdu BMC in *Salmonella enterica* cells leads to the production of normal as well as abnormally shaped particles (Havemann et al. 2002). Similar results were also reported in expression studies of the *pdu* operon of *Citrobacter freundii* in *E. coli* (Parsons et al. 2008). The BMCs of aberrant size and shape that are formed under these conditions suggest that a certain ratio of structural components is a crucial factor in the pathway that leads to the assembly of microcompartments of proper shape and size. Clearly, the expression of individual carboxysome proteins is closely regulated in vivo. In *H. neapolitanus,* a tight correlation exists between transcript levels for individual carboxysome proteins encoded by genes of the *cso* operon, and the abundance of each protein in the organelle (Cai et al. 2008).

4.8.1 Assembly Intermediates

Structures that likely represent α-carboxysome assembly intermediates were identified in a CET study of frozen, hydrated cells of *H. neapolitanus* (Iancu et al. 2010). The structures resemble partial shells at various stages of assembly; some, but not all of them, appear to be connected to one or more layers of RubisCO holoenzyme molecules on their concave sides. A structure that might be interpreted as a preassembled RubisCO core was not seen in any of the numerous cells examined in that study. Instead, the observed structures and the arrangement of the encapsulated RubisCO support a biogenesis pathway for α-carboxysome in which shell formation and the filling of nascent particles with RubisCO take place simultaneously. This model of carboxysome biogenesis is further supported by the polyhedral shells that are formed in a *H. neapolitanus* RubisCO knockout mutant and can be purified by sucrose gradient centrifugation (Menon et al. 2008). Although α-carboxysome shell

assembly and packaging of RubisCO are clearly independent processes (Menon et al. 2008), in vivo both must be coordinated and take place concomitantly during carboxysome formation. It is interesting that only one partially assembled carboxysome structure per cell was observed by Iancu et al. (2010), suggesting that a rate-determining nucleation event governs shell assembly and/or that the energetics of autotrophic metabolism limit the synthetic potential of the cell and the number of microcompartments that can be assembled at any given time.

In contrast to the single intermediates evident in *H. neapolitanus* cells, multiple small ring structures were seen in fixed and stained thin sections of the filamentous cyanobacterium *Anabaena variabilis* M3 (Price and Badger 1991). Their electron-translucent interior led to the suggestion that RubisCO and presumably also the carboxysomal carbonic anhydrase(s) enter a preassembled shell during carboxysome biogenesis in this cyanobacterium. For the unicellular cyanobacterium *Synechococcus elongatus* PCC 7942, an alternative model was proposed. Orus et al. (1995) found TEM evidence for supramolecular RubisCO assemblies that suggest shell formation occurs around an existing RubisCO core. This latter assembly model has gained support recently through a series of elegant genetic, biochemical, and cell biological studies that have established the pathway of β-carboxysome biogenesis in this cyanobacterium (Cameron et al. 2013).

4.8.2 The β-Carboxysome Assembly Pathway

Making use of an inducible shell protein operon in combination with fluorescently tagged individual shell proteins and RubisCO (Figure 4.4), Cameron et al. (2013) generated a series of single gene mutants that provided experimental evidence for the role of the major β-carboxysome proteins in organelle biogenesis. The progression of carboxysome assembly in vivo and the fate of newly formed organelles were followed by time lapse fluorescence microscopy. As in the α-carboxysome-forming chemoautotroph *H. neapolitanus* (Iancu et al. 2010), only one new carboxysome is formed per *Synechococcus elongatus* PCC 7942 cell, beginning with a preassembled RubisCO core (termed pro-carboxysome) that, in most cells, is located at one of the poles (Cameron et al. 2013; Chen et al. 2013). These studies further concluded that precursors of new carboxysomes bud off the pro-carboxysome (Cameron et al. 2013) and/or are generated adjacent to a recently formed organelle (Chen et al. 2013). With time, the new carboxysomes migrate closer to the center of the cell and seem to persist beyond a single cell division cycle (Jain et al. 2012).

The proposed assembly mechanism for β-carboxysomes in *Synechococcus elongatus* PCC 7942 (Cameron et al. 2013) is shown in Figure 4.5. Crucial for the formation of the RubisCO nucleus of the pro-carboxysome is the presence of CcmM. The RbcS-like domains of its C-terminal portion are thought to stabilize the RubisCO assembly. Whether RubisCO is arranged in a paracrystalline array, as is favored in the current model (Cameron et al. 2013; Chen et al. 2013), remains to be determined. In accordance with prior biochemical evidence (Long et al. 2007,

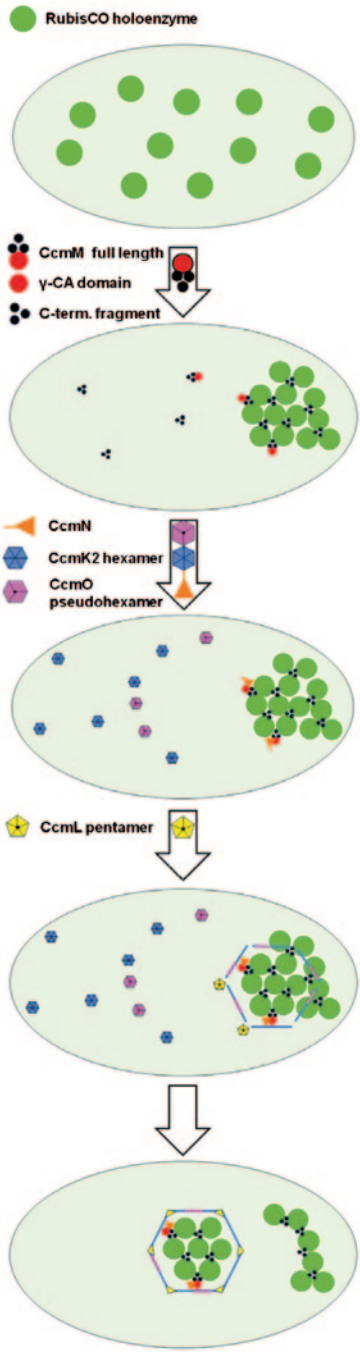

Fig. 4.5 The assembly pathway of β-carboxysomes. Carboxysome biogenesis begins with the assembly of a pro-carboxysome consisting of RubisCO and the CcmM full-length and C-terminal polypeptides. The CcmN protein recruits the shell proteins that self-assemble into the icosahedral carboxysome shell. Once completed, the newly generated carboxysome migrates towards the center of the cell. (Cameron et al. 2013)

2011; Cot et al. 2008; Kinney et al. 2012), the N-terminal domain of the full-length CcmM polypeptide binds to CcmN, which in turn recruits the Pfam00936 shell proteins CcmO and CcmK2 to the assembly, probably through interactions with its C-terminal peptide (Kinney et al. 2012). Incorporation of additional Pfam00936 proteins leads to formation of the hexamer arrays that constitute the shell facets. Addition of CcmL pentamers closes the shell at the vertices and is followed by the liberation of the completed carboxysome and its migration from its biogenesis site at the pole towards the center of the cell.

It is reasonable to assume that RubisCO must engage in specific contacts with shell component(s) during biogenesis of α- and β-carboxysomes, regardless of the assembly path. Although ultrastructural evidence obtained with purified α-carboxysomes could not unequivocally establish such interactions (Schmid et al. 2006; Iancu et al. 2007), the fact that only the Form IA RubisCO that is encoded by the *cso* operon of *Thiomicrospira crunogena*, but not its very similar non-carboxysomal paralog, can be encapsulated in *H. neapolitanus* carboxysomes (Menon et al. 2008) supports the existence of specific contacts with other carboxysome proteins. The large subunit of the enzyme has emerged as the determining factor for RubisCO encapsulation in α-carboxysomes. *H. neapolitanus* mutants expressing chimeric and foreign Form IA RubisCO species incorporate the enzyme into carboxysomes as long as the large subunit is derived from a carboxysomal RubisCO ortholog (Menon et al. 2008). Interestingly, α-carboxysomes can also accommodate Form IB RubisCO of β-carboxysomes (Menon et al. 2009), suggesting that any interactions of RubisCO with the shell transcend differences between the two carboxysome classes. It is noteworthy that extensive comparisons did not identify a sequence motif in the primary structure of carboxysomal RubisCOs that might target the enzymes into the carboxysome interior, such as the peptide that directs lumenal enzymes into the Pdu BMC (Fan et al. 2012). Regardless of the mechanism by which the carboxysomal RubisCO is sequestered into the organelle interior, there seems to be considerable flexibility regarding the nature of the cargo protein(s), since a GFP variant fused to the small subunit of RubisCO is readily incorporated into α-carboxysomes *H. neapolitanus* (Menon et al. 2010) and localizes to the punctuate fluorescent structures that are thought to represent individual β-carboxysomes in *Synechococcus elongatus* PCC 7942 when fused to the large subunit (RbcL; Savage et al. 2010; Cameron et al. 2013).

4.9 Carboxysome Segregation

The close to even distribution of carboxysomes within the two halves of dividing *H. neapolitanus* cells suggested the existence of an active distribution mechanism that ensures adequate CO_2 fixation potential in both daughter cells (Iancu et al. 2010). Although the exact molecular basis for such a mechanism is currently unknown, components of the bacterial cytoskeleton, which organize and/or move intracellular

structures (Jensen 1984; Gitai 2005), were considered likely candidates. Considering the close proximity of carboxysomes to DNA fibrils, which was noted in several bacteria (Mahoney and Edwards 1966; Gantt and Conti 1969; Shively et al. 1970, 1973; Purohit et al. 1976), it is not surprising that a protein implicated in DNA segregation was shown to play a role in partitioning carboxysomes among the daughter cells upon cell division. In *Synechococcus elongatus* PCC7942, in vivo tracking of fluorescently labeled carboxysomes revealed that carboxysomes are regularly interspersed with the multiple chromosome copies along the longitudinal cell axis of this bacterium (Jain et al. 2012). Mutants lacking the cytoskeletal protein ParA maintain the regular chromosome spacing (Jain et al. 2012), but their carboxysomes are not aligned like those in the wild type (Savage et al. 2010; Jain et al. 2012). These observations led the authors to suggest that ParA may utilize the ordered chromosomes to position carboxysomes in the cell or that, alternatively, chromosome spacing may restrict and therefore dictate the cellular locations of carboxysomes (Jain et al. 2012).

Following division, carboxysomes are not evenly apportioned to the two daughter cells in the Δ*par*A mutant, giving rise to cell subpopulations of normal fitness as well as those with reduced CO_2 fixation ability because they received an insufficient number of carboxysomes (Savage et al. 2010). The underlying molecular mechanism of ParA action is not known at present, and additional cytoskeletal components, such as MreB, also appear to participate in carboxysome organization and distribution (Savage et al. 2010). The frequent clustering and less regular intracellular spacing of carboxysomes seen in many chemo- and photoautotrophic bacteria raise the possibility that multiple organelle organization and segregation mechanisms may exist among the bacteria. It is noteworthy in this context that a *par*A homolog is present downstream from the *cso* operon of *H. neapolitanus* and of many other chemoautotrophs; whether its product plays a role in carboxysome ordering and movement remains to be elucidated.

4.10 Concluding Remarks

The wide range of fresh and increasingly sophisticated experimental approaches that have been applied to carboxysome research in recent years have produced considerable advances in the field. Our knowledge base of the relationship between structure and function of the organelle has greatly expanded; however, many of the questions that were summarized in a recent review (Kerfeld et al. 2010) still remain unanswered despite these great strides made towards gaining a complete understanding of carboxysome biology.

Similarities and differences between carboxysomes of the α- and β-type have become evident, thanks to novel insights into the roles and interactions of protein components that are unique to each type. It is clear that the two types of carboxysomes arose from different evolutionary events, and that they represent morphologically similar but compositionally different solutions to the problem of concentrating

CO_2 around the catalytically challenged RubisCO. Since the shell architecture of carboxysomes and other BMCs is very similar, comparative studies of BMC properties are needed that can elucidate unifying functions of BMCs and the principles of metabolic organization to which BMCs contribute.

For decades, the composition of α-carboxysomes, which can be purified to homogeneity, was assumed to have been elucidated. However, the recent discovery that the CsoS1D protein, which is not encoded in the canonical *cso* operon, is a low abundance shell component raises the possibility that other, as yet unknown proteins may be present and/or play a role in function, biogenesis, or regulation of both carboxysome types. Determination of structure and function of these, as well as other, less tractable carboxysome components is needed. An example of a still poorly understood component of α-carboxysomes is CsoS2, the largest and highly abundant shell protein. Technical difficulties related to its unusual characteristics have so far prevented elucidation of CsoS2 structure and role in the organelle.

For both carboxysome types, details of their shell properties remain to be resolved. To validate the proposed differential permeability of the shell to gases, experiments that directly address gas flux across the shell are required. Preferential CO_2 sequestration into the carboxysome interior and exclusion of O_2, the competitive inhibitor of the RubisCO-catalyzed carboxylation reaction, are elements of the prevailing working model and its variants. However, the molecular details of the proposed selective shell permeability and of metabolite transfer across the protein boundary remain a mystery.

Acknowledgments The authors are grateful to Drs. Fei Cai, Cheryl Kerfeld, Cristina Iancu, and Grant Jensen for the images they provided and their help with various figures in this review. We truly appreciate the many stimulating discussions we have had throughout the years of our respective collaborations. SH and GCC acknowledge the generous funding of their carboxysome research from the National Science Foundation (current awards: MCB-0851070 and MCB-1244534).

References

Alber BE, Ferry JG (1994) A carbonic anhydrase from the archaeon Methanosarcina thermophila. Proc Natl Acad Sci USA 91:6909–6913

Baker SH, Lorbach SC, Rodriguez-Buey M, Williams DS, Aldrich HC, Shively JM (1999) The correlation of the gene csoS2 of the carboxysome operon with two polypeptides of the carboxysome in Thiobacillus neapolitanus. Arch Microbiol 172:233–239

Baker SH, Williams DS, Aldrich HC, Gambrell AC, Shively JM (2000) Identification and localization of the carboxysome peptide CsoS3 and its corresponding gene in Thiobacillus neapolitanus. Arch Microbiol 173:278–283

Berry S, Fischer JH, Kruip J, Hauser M, Wildner GF (2005) Monitoring cytosolic pH of carboxysome-deficient cells of Synechocystis sp. PCC 6803 using fluorescence analysis. Plant Biol (Stuttg) 7:342–347

Beudeker RF, Cannon GC, Kuenen JG, Shively JM (1980) Relations between d-ribulose-1,5-bisphosphate carboxylase, carboxysomes, and CO_2 fixing capacity in the obligate chemolithotroph Thiobacillus neapolitanus grown under different limitations in the chemostat. Arch Microbiol 124:185–189

Bobik TA (2006) Polyhedral organelles compartmenting bacterial metabolic processes. Appl Microbiol Biotechnol 70:517–525

Bock E, Duval D, Peters KR (1974) Charakterisierung eines phagenähnlichen Partikels aus Zellen von Nitrobacter. I. Wirstpartikelbeziehung und Isolierung. Arch Microbiol 97:115–127

Cai F, Heinhorst S, Shively J, Cannon G (2008) Transcript analysis of the Halothiobacillus neapolitanus cso operon. Arch Microbiol 189:141–150

Cai F, Menon BB, Cannon GC, Curry KJ, Shively JM, Heinhorst S (2009) The pentameric vertex proteins are necessary for the icosahedral Carboxysome shell to function as a CO_2 leakage barrier. PLoS ONE 4:e7521

Cai F, Sutter M, Cameron JC, Stanley DN, Kinney JN, Kerfeld CA (2013) The structure of CcmP, a tandem bacterial microcompartment domain protein from the beta-carboxysome, forms a subcompartment within a microcompartment. J Biol Chem 288:16055–16063

Cameron JC, Wilson SC, Bernstein SL, Kerfeld CA (2013) Biogenesis of a bacterial organelle: the carboxysome assembly pathway. Cell 155:1131–1140

Cannon GC, Shively JM (1983) Characterization of a homogenous preparation of carboxysomes from Thiobacillus neapolitanus. Arch Microbiol 134:52–59

Cannon GC, Heinhorst S, Bradburne CE, Shively JM (2002) Carboxysome genomics: a status report. Funct Plant Biol 29:175–182

Cannon GC, Baker SH, Soyer F, Johnson DR, Bradburne CE, Mehlman JL, Davies PS, Jiang QL, Heinhorst S, Shively JM (2003) Organization of carboxysome genes in the thiobacilli. Curr Microbiol 46:115–119

Cannon GC, Heinhorst S, Kerfeld CA (2010) carboxysomal carbonic anhydrases: structure and role in microbial CO_2 fixation. Biochim Biophys Acta 1804:382–392

Chen AH, Robinson-Mosher A, Savage DF, Silver PA, Polka JK (2013) The bacterial carbon-fixing organelle is formed by shell envelopment of preassembled cargo. PLoS ONE 8:e76127

Cheng S, Liu Y, Crowley CS, Yeates TO, Bobik TA (2008) Bacterial microcompartments: their properties and paradoxes. Bioessays 30:1084–1095

Cot SS-W, So AK-C, Espie GS (2008) A multiprotein bicarbonate dehydration complex essential to carboxysome function in cyanobacteria. J Bacteriol 190:936–945

Dou Z, Heinhorst S, Williams EB, Murin CD, Shively JM, Cannon GC (2008) CO_2 fixation kinetics of *Halothiobacillus neapolitanus* mutant carboxysomes lacking carbonic anhydrase suggest the shell acts as a diffusional barrier for CO_2. J Biol Chem 283:10377–10384

Fan C, Cheng S, Liu Y, Escobar CM, Crowley CS, Jefferson RE, Yeates TO, Bobik TA. (2012) Short N-terminal sequences package proteins into bacterial microcompartments. Proc Natl Acad Sci USA 107:7509–7514

Gantt E, Conti SF (1969) Ultrastructure of blue-green algae. J Bacteriol 97:1486–1493

Gitai Z (2005) The new bacterial cell biology: moving parts and subcellular architecture. Cell 120:577–586

de Groot BL, Grubmuller H (2005) The dynamics and energetics of water permeation and proton exclusion in aquaporins. Curr Opin Struct Biol 15:176–183

Havemann GD, Sampson EM, Bobik TA (2002) PduA is a shell protein of polyhedral organelles involved in coenzyme B(12)-dependent degradation of 1,2-propanediol in *Salmonella enterica* serovar typhimurium LT2. J Bacteriol 184:1253–1261

Heinhorst S, Cannon GC, Shively JM (2006) Carboxysomes and carboxysome-like inclusions. In: Shively JM (ed) Complex intracellular structures in prokaryotes, vol 2. Springer, Berlin, pp 141–164

Heinhorst S, Williams EB, Cai F, Murin CD, Shively JM, Cannon GC (2006) Characterization of the carboxysomal carbonic anhydrase CsoSCA from *Halothiobacillus neapolitanus*. J Bacteriol 188:8087–8094

Holthuijzen YA, Breemen JFL, Konings WN, Bruggen EFJ (1986) Electron microscopic studies of carboxysomes of *Thiobacillus neapolitanus*. Arch Microbiol 144:258–262

Iancu CV, Ding HJ, Morris DM, Dias DP, Gonzales AD, Martino A, Jensen GJ (2007) The structure of isolated synechococcus strain WH8102 Carboxysomes as revealed by electron cryotomography. J Mol Biol 372:764–773

Iancu CV, Morris DM, Dou Z, Heinhorst S, Cannon GC, Jensen GJ (2010) Organization, structure, and assembly of [alpha]-carboxysomes determined by electron cryotomography of intact cells. J Mol Biol 396:105–117

Jain IH, Vijayan V, O'Shea EK (2012) Spatial ordering of chromosomes enhances the fidelity of chromosome partitioning in cyanobacteria. Proc Natl Acad Sci USA 109:13638–13643

Jensen TE (1984) Cyanobacterial cell inclusions of irregular occurrence: systematic and evolutionary implications. Cytobios 39:35–62

Kaneko Y, Danev R, Nagayama K, Nakamoto H (2006) Intact carboxysomes in a cyanobacterial cell visualized by hilbert differential contrast transmission electron microscopy. J Bacteriol 188:805–808

Kaplan A, Reinhold L (1999) CO_2 concentrating mechanisms in photosynthetic microorganisms. Annu Rev Plant Physiol Plant Mol Biol 50:539–570

Kerfeld CA, Sawaya MR, Tanaka S, Nguyen CV, Phillips M, Beeby M, Yeates TO (2005) Protein structures forming the shell of primitive bacterial organelles. Science 309:936–938

Kerfeld CA, Heinhorst S, Cannon GC (2010) Bacterial microcompartments. Annu Rev Microbiol 64:391–408

Kinney J, Axen S, Kerfeld CA (2011) Comparative analysis of carboxysome shell proteins. Photosynth Res 109:21–32

Kinney JN, Salmeen A, Cai F, Kerfeld CA (2012) Elucidating essential role of conserved carboxysomal protein CcmN reveals common feature of bacterial microcompartment assembly. J Biol Chem 287:17729–17736

Klein MG, Zwart P, Bagby SC, Cai F, Chisholm SW, Heinhorst S, Cannon GC, Kerfeld CA (2009) Identification and structural analysis of a novel carboxysome shell protein with implications for metabolite transport. J Mol Biol 392:319–333

Liberton M, Austin JR, Berg RH, Pakrasi HB (2011) Unique thylakoid membrane architecture of a unicellular N_2-fixing cyanobacterium revealed by electron tomography Plant Physiol 155:1656–1666

Long BM, Price GD, Badger MR (2005) Proteomic assessment of an established technique for carboxysome enrichment from Synechococcus PCC7942. Can J Bot 83:746–757

Long BM, Badger MR, Whitney SM, Price GD (2007) Analysis of carboxysomes from Synechococcus PCC7942 reveals multiple RubisCO complexes with carboxysomal proteins CcmM and CcaA. J Biol Chem 282:29323–29335

Long BM, Tucker L, Badger MR, Price GD (2010) Functional cyanobacterial β-carboxysomes have an absolute requirement for both long and short forms of the CcmM protein. Plant Physiol 153:285–293

Long BM, Rae BD, Badger MR, Price GD (2011) Over-expression of the β-carboxysomal CcmM protein in Synechococcus PCC7942 reveals a tight co-regulation of carboxysomal carbonic anhydrase (CcaA) and M58 content. Photosynth Res 109:33–45

Ludwig M, Sültemeyer D, Price GD (2000) Isolation of ccmKLMN genes from the marine cyanobacterium Synechococcus sp. PCC7002 and evidence that CcmM is essential for carboxysome assembly. J Phycol 36:1109–1118

Mahoney RP, Edwards MR (1966) Fine structure of *Thiobacillus thiooxidans*. J Bacteriol 92: 487–495

McKay RML, Gibbs SP, Espie GS (1993) Effect of dissolved inorganic carbon on the expression of carboxysomes, localization of RubisCO and the mode of carbon transport in cells of the cyanobacterium Synechococcus UTEX 625. Arch Microbiol 159:21–29

Menon BB, Dou Z, Heinhorst S, Shively JM, Cannon GC (2008) *Halothiobacillus neapolitanus* carboxysomes sequester heterologous and chimeric RubisCO species. PLoS ONE 3:e3570

Menon BB, Dou Z, Milam J, Shively JM, Heinhorst S, Cannon GC (2009) Phenotypic analysis of a Halothiobacillus neapolitanus mutant harboring beta-cyanobacterial form IB RubisCO. In: Amercian society for microbiology 109th general meeting Philadelphia, PA. K–066

Menon BB, Heinhorst S, Shively JM, Cannon GC (2010) The carboxysome shell is permeable to protons. J Bacteriol 192:5881–5886

Nierzwicki-Bauer S, Balkwill D, Stevens S Jr (1983) Three-dimensional ultrastructure of a unicellular cyanobacterium. J Cell Biol 97:713–722

Orus MI, Rodriguez ML, Martinez F, Marco E (1995) Biogenesis and ultrastructure of carboxysomes from wild type and mutants of Synechococcus sp. strain PCC 7942. Plant Physiol 107:1159–1166

Orus MI, Rodriguez-Buey ML, Marco E, Fernandez-Valiente E (2001) Changes in carboxysome structure and grouping and in photosynthetic affinity for inorganic carbon in Anabaena strain PCC 7119 (Cyanophyta) in response to modification of CO_2 and Na^+ supply. Plant Cell Physiol 42:46–53

Parsons JB, Dinesh SD, Deery E et al (2008) Biochemical and structural insights into bacterial organelle form and biogenesis. J Biol Chem 283:14366–14375

Peña KL, Castel SE, de Araujo C, Espie GS, Kimber MS (2010) Structural basis of the oxidative activation of the carboxysomal gamma-carbonic anhydrase, CcmM. Proc Natl Acad Sci USA 107:2455–2460

Penrod JT, Roth JR (2006) Conserving a volatile metabolite: a role for carboxysome-like organelles in *Salmonella enterica*. J Bacteriol 188:2865–2874

Peters K-R (1974) Characterisierung eines phagenaehnlichen Partikels aus Zellen von Nitrobacter. Arch Microbiol 97:129–140

Price GD, Badger MR (1989) Isolation and characterization of high CO_2-requiring-mutants of the cyanobacterium Synechococcus PCC 7942: two phenotypes that accumulate inorganic carbon but are apparently unable to generate CO_2 within the carboxysome. Plant Physiol 91:514–525

Price GD, Badger MR (1991) Evidence for the role of carboxysomes in the cyanobacterial CO_2-concentrating mechanism. Can J Bot 69:963–973

Price GD, Coleman JR, Badger MR (1992) Association of carbonic anhydrase activity with carboxysomes isolated from the cyanobacterium Synechococcus PCC7942. Plant Physiol 100:784–793

Price GD, Howitt S, Harrison K, Badger MR (1993) Analysis of a genomic DNA region from the cyanobacterium Synechococcus sp. strain PCC7942 involved in carboxysome assembly and function. J Bacteriol 175:2871–2879

Price GD, Sültemeyer D, Klughammer B, Ludwig M, Badger MR (1998) The functioning of the CO_2 concentrating mechanism in several cyanobacterial strains: a review of general physiological characteristics, genes, proteins and recent advances. Can J Bot 76:973–1002

Pronk JT, Meulenberg R, van den Berg DJ, Batenburg-van der Vegte W, Bos P, Kuenen JG (1990) Mixotrophic and autotrophic growth of *Thiobacillus acidophilus* on glucose and thiosulfate. Appl Environ Microbiol 56:3395–3401

Purohit K, McFadden BA, Shaykh MM (1976) D-Ribulose-1,5-bisphosphate carboxylase and polyhedral inclusion bodies in *Thiobacillus intermedius*. J Bacteriol 127:516–522

Rae BD, Long BM, Badger MR, Price GD (2012) Structural determinants of the outer shell of β-carboxysomes in *Synechococcus elongatus* PCC 7942: roles for CcmK2, K3-K4, CcmO, and CcmL. PLoS ONE 7:e43871

Rae BD, Long BM, Badger MR, Price GD (2013) Functions, compositions, and evolution of the two types of carboxysomes: polyhedral microcompartments that facilitate CO_2 fixation in cyanobacteria and some proteobacteria. Microbiol Mol Biol Rev 77: 357–379

Reinhold L, Zviman M, Kaplan A (1989) A quantitative model for carbon fluxes and photosynthesis in cyanobacteria. Plant Physiol Biochem 27:945–954

Roberts EW, Cai F, Kerfeld CA, Cannon GC, Heinhorst S (2012) Isolation and characterization of the prochlorococcus carboxysome reveal the presence of the novel shell protein CsoS1D. J Bacteriol 194:787–795

Samborska B, Kimber MS (2012) A dodecameric CcmK2 structure suggests beta-carboxysomal shell facets have a double-layered organization. Structure 20:1353–1362

Savage DF, Afonso B, Chen AH, Silver PA (2010) Spatially ordered dynamics of the bacterial carbon fixation machinery. Science 327:1258–1261

Sawaya MR, Cannon GC, Heinhorst S, Tanaka S, Williams EB, Yeates TO, Kerfeld CA (2006) The structure of β-carbonic anhydrase from the carboxysomal shell reveals a distinct subclass with one active site for the price of two. J Biol Chem 281:7546–7555

Schmid MF, Paredes AM, Khant HA, Soyer F, Aldrich HC, Chiu W, Shively JM (2006) Structure of *Halothiobacillus neapolitanus* carboxysomes by cryo-electron tomography. J Mol Biol 364:526–535

Shepherd CM, Borelli IA, Lander G, Natarajan P, Siddavanahalli V, Bajaj C, Johnson JE, Brooks CL 3rd, Reddy VS (2006) VIPERdb: a relational database for structural virology. Nucl Acids Res 34:D386–389

Shively JM, English RS (1991) The carboxysome, a prokaryotic organelle: a mini review. Can J Bot 69:957–962

Shively JM, Decker GL, Greenawalt JW (1970) Comparative ultrastructure of the thiobacilli. J Bacteriol 101: 618–627

Shively JM, Ball F, Brown DH, Saunders RE (1973a) Functional organelles in prokaryotes: polyhedral inclusions (carboxysomes) of *Thiobacillus neapolitanus*. Science 182:584–586

Shively JM, Ball FL, Kline BW (1973b) Electron microscopy of the carboxysomes (polyhedral bodies) of *Thiobacillus neapolitanus*. J Bacteriol 116:1405–1411

So AK-C, Espie GS (1998) Cloning, characterization and expression of carbonic anhydrase from the cyanobacterium Synechocystis PCC6803. Plant Mol Biol 37:205–215

So AK-C, John-McKay M, Espie GS (2002) Characterization of a mutant lacking carboxysomal carbonic anhydrase from the cyanobacterium Synechocystis PCC6803. Planta 214:456–467

So AK-C, Espie GS, Williams EB, Shively JM, Heinhorst S, Cannon GC (2004) A novel evolutionary lineage of carbonic anhydrase (epsilon class) is a component of the carboxysome shell. J Bacteriol 186:623–630

Tanaka S, Kerfeld CA, Sawaya MR, Cai F, Heinhorst S, Cannon GC, Yeates TO (2008) Atomic-level models of the bacterial carboxysome shell. Science 319:1083–1086

Tanaka S, Sawaya MR, Phillips M, Yeates TO (2009) Insights from multiple structures of the shell proteins from the beta-carboxysome. Protein Sci 18:108–120

Tang M, Jensen TE, Corpe WA (1995) The occurrence of polyphosphate bodies in polyhedral bodies (carboxysomes) in *Synechococcus leopoliensis* (Cyanophyceae). Microbios 81:59–66

Ting CS, Hsieh C, Sundararaman S, Mannella C, Marko M (2007) Cryo-electron tomography reveals the comparative three-dimensional architecture of Prochlorococcus, a globally important marine cyanobacterium. J Bacteriol 189:4485–4493

Tocheva EI, Li Z, Jensen GJ (2010) Electron cryotomography. Cold Spring Harb Perspect Biol 2:a003442

Tsai Y, Sawaya MR, Cannon GC, Cai F, Williams EB, Heinhorst S, Kerfeld CA, Yeates TO (2007) Structural analysis of CsoS1A and the protein shell of the *Halothiobacillus neapolitanus* carboxysome. PLoS Biol 5:e144

Tsai Y, Sawaya MR, Yeates TO (2009) Analysis of lattice-translocation disorder in the layered hexagonal structure of carboxysome shell protein CsoS1C. Acta Crystallogr D Biol Crystallogr 65:980–988

van der Meene AML, Hohmann-Marriott MF, Vermaas WFJ, Roberson RW (2006) The three-dimensional structure of the cyanobacterium Synechocystis sp. PCC 6803. Arch Microbiol 184:259–270

Westphal K, Bock E (1974) Charakterisierung eines phagenähnlichen Partikels aus Zellen von Nitrobacter III. Nachweis von DNS. Arch Microbiol 101:121–130

Yeates TO, Kerfeld CA, Heinhorst S, Cannon GC, Shively JM (2008) Protein-based organelles in bacteria: carboxysomes and related microcompartments. Nat Rev Microbiol 6:681–691

Yeates TO, Thompson MC, Bobik TA (2011) The protein shells of bacterial microcompartment organelles. Curr Opin Struct Biol 21:223–231

Yeates TO, Jorda J, Bobik TA (2013) The shells of BMC-type microcompartment organelles in bacteria. J Mol Microbiol Biotechnol 23:290–299

Zhang S, Laborde SM, Frankel LK, Bricker TM (2004) Four novel genes required for optimal photoautotrophic growth of the cyanobacterium Synechocystis sp. strain PCC 6803 identified by in vitro transposon mutagenesis. J Bacteriol 186:875–879

Chapter 5
Bacterial Organization at the Smallest Level: Molecular Motors, Nanowires, and Outer Membrane Vesicles

Larry L. Barton

5.1 Introduction

From early microscopic evaluations, it was apparent that the prokaryotic cell lacks the structural organization found in larger plant and animal cells. Due to the lack of internal membranes in bacterial cells, a simplistic view was to consider that the bacterial cell was regarded as a collection of enzymes without organization. Over many decades, bacterial physiologists have dissected the microbial cell and have characterized numerous subcellular structures (Saier 2013). The genetic material, nucleoid, in bacteria appears to be dispersed throughout the cell; however, the architectural configuration and condensation of the nucleoid is highly complex and the specific chemical processes accounting for these physical rearrangements have not been reported. The prokaryotic 70S ribosomes have a complex organization required to facilitate protein synthesis and while self-assembly of the ribosomal reveals a precise organization (Noller and Nomura 1987), the movement of ribosomes along the messenger ribonucleic acid (mRNA) are an interesting mechanical feature. A plasma membrane encompasses the cytoplasm of the prokaryotic cell and while it is an obligatory structure, the construction of the plasma membrane poses many physical challenges to bacterial and archaeal cells. Almost all prokaryotic cells have walls to maintain cell shape and chemical differences are observed with various bacteria and Archaea. The topics of microbial nucleoid, ribosomes, sulfur globules, polyphosphate granules, polyhydroxylanoate granules, gas vacuoles, bacterioferritin, and proteasomes have been addressed in recent reviews and these will not be covered here. Several microbial nanostructures (motors of gliding bacteria, S-layer of prokaryotes, carobxysomes, magnetosomes, and metallo-particles) are covered in considerable detail in other chapters of this book. This chapter will focus on molecular motors of flagella and adenosine triphosphate (ATP) synthase as well as physiological activities of nanowires and outer membrane vesicles.

L. L. Barton (✉)
Department of Biology, University of New Mexico,
MSCO3 2020, Albuquerque, NM 87131-0001, USA
e-mail: lbarton@unm.edu

L. L. Barton et al. (eds.), *Nanomicrobiology,* DOI 10.1007/978-1-4939-1667-2_5

5.2 Molecular Motors

Throughout cellular biology, there are molecules that are dedicated to perform in mechanical processes and many of these activities are described as molecular motors or biological nanomachines (Saier 2013; Nelson et al. 2013; Bustamante et al. 2004). Just as machines perform specified work with the input of energy, there are many subcellular examples where proteins become energized and function as molecular motors to achieve a specific mechanical event. There are several examples of prokaryotic and eukaryotic molecular motors and some of these are listed in Table 5.1. In terms of molecular movement, biological nanomotors represent three different types of systems: (1) rotating motors, (2) linear movement, and (3) revolving movement. Nanomotors are common in all bacterial cells and it may be that nanomotors not only enhance growth but are an obligatory requirement for bacterial viability as well. Each bacterial cell may have hundreds of nanomotors representing several different specific examples which act independently or collectively respond to a molecular switch to facilitate cell growth. A common theme of nanomotor activity is that energy is used to move a protein or several proteins organized into a specific unit. These motors may be enzymes that are energized by ATP hydrolysis or in some instances, nanomotors in the plasma membrane are energized by proton (in some cases Na^+) movement across membranes. From a theoretical perspective, various models have been developed to describe motor-protein concepts involved in converting chemical energy into mechanical work (Kolomeisky and Fisher 2007). In order to study these molecular motors, new methods have been developed and these include magnetic tweezers (De Vlaminck and Dekker 2012), optical tweezers (Reid 2008), neutron spin echo spectroscopy (Armstrong et al. 2013), and fluorescence methods (Didenko 2001; Haustein and Schwille 2007; Mattheyses et al. 2010) to measure individual molecules in a living cell on a nanosecond time scale. Just as nanomotor technology is evolving in biology, it should be emphasized that not all biological movement is attributed to molecular motors, but in some instances molecular movement is attributed to supramolecular springs and rachets (Mahadevan and Matsudaira 2000).

5.2.1 Flagellar Rotation Is a Nanomotor

Microorganisms have various types of motility and swimming is the result of flagellar activity. Flagella are found on Gram-positive, Gram-negative, and spirochete bacteria as well as on archaeal cells, and the number of flagella varies with the species. Discussion here will focus on the flagellum of the Gram-negative bacteria, such as *Escherichia coli* and *Salmonella typhimurium,* because they have been most extensively examined. The bacterial flagellum is stabilized in the plasma membrane and as the flagella rotate, the cell is propelled through the aqueous environment. The hallmark paper of Berg and Anderson (1973) alerted the scientific community

Table 5.1 Examples of molecular motors in biology

Linear motors in eukaryotic cells
Muscle contraction by myocins (Lodish et al. 2000)
Kinesin moves molecules along microtubles inside cells (Verhey et al. 2011)
Dynein promotes beating of cilia and flagella (Roberts et al. 2013)
Polymerization of actin (Lodish et al. 2000; Pierobon 2009)
Polymerization of microtubles (Desai and Mitchison 1997)
Dynamin fusion of membranes (Hinshaw 2000)
DNA polymerase as a nucleic acid motor turns single-stranded DNA into dsDNA (Hubscher et al. 2002)
Linear motors in prokaryotic cells
Sec pathway for general secretion of proteins (de Keyzer et al. 2003)
RNA polymerase drives DNA segregation (Dworkin and Losick 2002)
Rotary motors in prokaryotic and eukaryotic cells
F_1F_0 ATP synthase (Yoshida et al. 2001; Tsunoda et al. 2001; Weber and Senior 2003; Kolomeisky and Fisher 2007; Gaspard and Gerritsma 2007)
Rotary motor of bacteria
Flagella rotation (Minamino et al. 2008)
Revolving motor in viruses
Packaging dsDNA inside phi29 bacterial virus by a process similar to the earth revolving around the sun (Smith et al. 2001; Geng et al. 2011; Schwartz et al. 2013; Liu et al. 2014)

to the observation that bacteria swim by flagellar rotation. With *E. coli,* which typically has eight flagella per cell, each flagellum makes about 270 revolutions per second (rps) while the single flagellum of *Vibrio alginolyticus* rotates at about 1100 rps (Willey et al. 2014). Rates for flagellar rotation is species specific with *E. coli* moving at a velocity of 16.5 μm/s which is about 8 cell lengths/s while *Pseudomonas aeruginosa* moves at 55.8 μm/s or 37 cell lengths/s (Barton 2005). The power output for each flagellar motor may approach 10–16 W of power and 0.1 % of total energy used by the growing cell may be required to operate the flagellar motors (Macnab 1987).

The structures of the flagella from the Gram-negative *E. coli* and *S. typhimurium,* as established by electron microscopy, are relatively similar but differ from the Gram-positive *Bacillus subtilis* at the point of attachment to the cell wall (DePamphilis and Adler 1971a, b, c; Macnab and Aizawa 1984). Approximately 50 genes for flagellar synthesis are clustered in numerous regions on the bacterial chromosome and this would include genes for the physical structure as well as genes for transport across the cell envelope required for synthesis of the flagellum, and this would include chaperone and scaffolding proteins (Silverman and Simon 1974; Macnab 1992). The flagellum from *E. coli* and *S. typhimurium* has a unique structure (see Figure 5.1) that has three major segments: (1) a basal body consisting of a series of rings to stabilize the flagellum into the bacterial cell surface, (2) a rigid curved protein often referred to as the hook which connects to the basal body, and (3) a filament which extends from the hook.

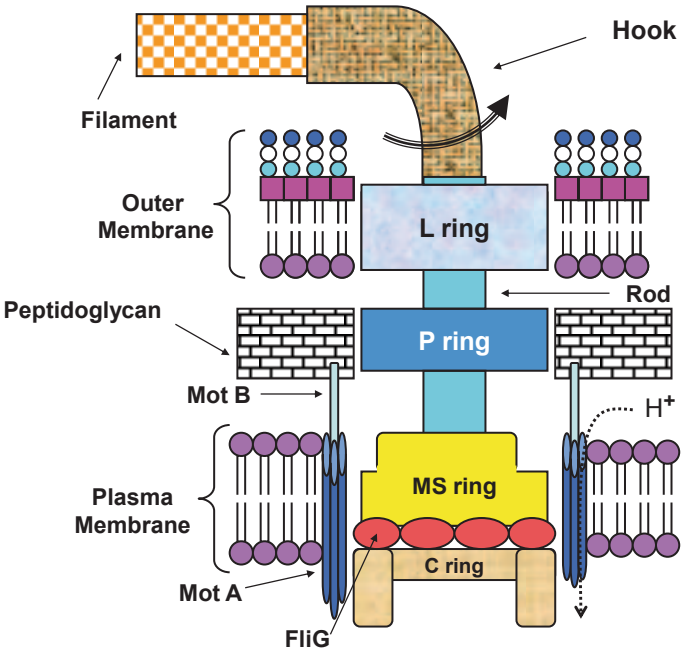

Fig. 5.1 Anatomy of flagellum in *Escherichia coli* and *Salmonella* sp. Dimensions of structures are from DePamphilis and Adler (1971b). Diameter of filament is 13.5 nm, diameter of hook is 17 nm, external diameter of rings is 22.5 nm, distance between *L* and *P* rings is 9 nm, diameter of rod is 7 nm, distance from *MS* ring to *L* ring is 27 nm, and internal diameter of filament is 30 Å

In the Gram-negative bacteria, the basal body originates at the plasma membrane and extends through the outer membrane (Figure 5.1). The bacterial flagellum has often been likened to rotary motors which have a rotor and a stator. The MS ring is attached into the plasma membrane and the C ring is in the cytoplasm. The motor (Mot) proteins surround the MS and C rings in the plasma membrane and serve as the stator to generate the rotational power. The P ring is stabilized into the peptidoglycan and serves as the rotor along with the MS and C rings. The L ring is secured into the lipopolysaccharide of the outer membrane of Gram-negative bacteria. In *E. coli,* the L, P, and MS rings have an external diameter of 22.5 nm and a central rod with a diameter of 7 nm attaches the basal body to the hook (DePamphilis and Adler 1971b). The distance between the MS ring and the P ring is 12 nm while there is 9 nm between the P and L rings. The hook is a rigid protein structure that attaches at one end to the rod of the basal body and the other end to the flagellum filament. In *E. coli,* the hook is 17–20 nm in diameter and about 80 nm in length (Macnab 2003). The filament of *E. coli* flagellum is 20 nm in diameter and is not straight but forms a helical wave of 2–2.5 nm and the helical diameter is about 0.4–0.5 nm. The helical character of the filament varies with the bacterial variants and the length of the filament ranges from 5 to 10 μm. The flagellar filament consists of protein subunits of about 55 kDa which are arranged in a cylindrical lattice consisting of 11

columns where the subunits are at a 45° angle to the filament axis (Berg 2003). In *S. typhimurium,* a series of protein rings are in association with the unit extending from the cell surface. One protein occurs between the rod and the hook, two rings are present between the hook and the filament, and a protein cap is at the distal end of the filament. For synthesis of the flagellum in Gram-negative bacteria, the rings and rod are first inserted into the membranes and the synthesis of the filament is at the tip with the protein subunits migrating through the hollow filament.

Bacterial locomotion is attributed to the rotation of the flagellum as published by Berg (1974, 1996). This rotation can be readily observed by tethering a bacterial flagellum with a filament-specific antibody to a glass microscope slide and observing the rotation of an individual cell. Mitchell (1956, 1972) was the first to propose that flagellar motor was driven by proton motor force and the chemiosmotic coupling of proton uptake with flagellar rotation is discussed by Harold and Maloney (1996). Cells, such as *E. coli* with an active metabolism, have a charge across the plasma membrane with the internal side of the plasma membrane being negative, attributed to the collection of hydroxyl ions, and the external side of the plasma membrane being positive as a result of proton accumulation. The localization on the exterior of the plasma membrane results from bacterial respiration where protons are pumped outward across the plasma membrane as a result of electron flow from a metabolic donor to a final electron acceptor. For bacteria that are growing in an elevated salt environment, Na^+ from the environment drives flagellar rotation and uptake of sodium ions is regulated by chemiosmotic energy coupling across the plasma membrane (Harold and Maloney 1996).

The motility protein B (MotB) extends from the plasma membrane into the periplasm where it is anchored to the peptidoglycan and four motility protein A (MotA) proteins which extend from the plasma membrane into the cytoplasm are bound to MotB to form a proton (or sodium ion) channel (Berg 2000). Thus, the stator consisting of MotA and MotB proteins are connected to the rigid peptidoglycan and enable a torque to be transferred to the filament.

The C ring consists of two proteins, FilM and FilN, which are found primarily in the cytoplasm and are involved in a switch mechanism to change the direction of flagellar rotation (see Figure 5.1). The switch complex consists of a series of non-basal body proteins that interface between the sensory transduction system and the energy-transducing mechanism. Flagella rotate clockwise (CW) or counterclockwise (CCW) in response to activities of chemotaxis-related proteins. The C ring is attached to the MS ring by a series of FliG proteins.

The mechanism of flagellar rotation has eluded scientists for many years; however, several models have been proposed to explain how proton reentry across the plasma membrane would account for flagellar rotation. Consistent in the models is the rotation of the MS ring, rod, hook, and filament while the Mot proteins are imbedded in the plasma membrane and do not rotate. As reviewed by Berry (2000) and by Elston and Oster (1997), there are three popular theories for rotation of the flagellar motor and these are represented in Figure 5.2a–c. The “proton turbine” model, described by Kleutsch and Laüger (1990) and Elston and Oster (1997), employs an electrostatic force resulting from the positive charge on the Mot proteins

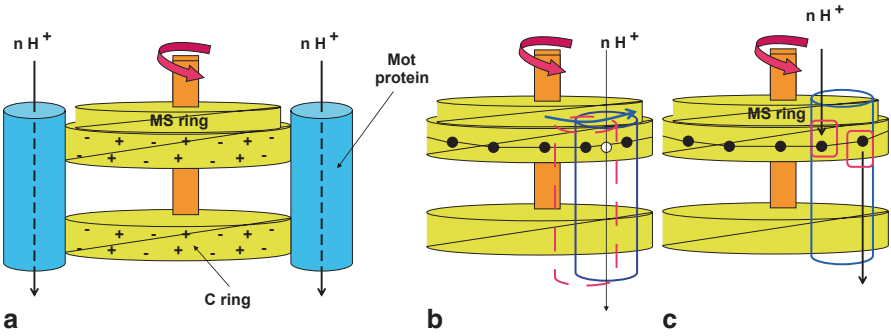

Fig. 5.2 Proposed mechanisms for proton-driven rotary motors. **a** Electrostatic proton turbine where positive charges passing through the stator (*Mot protein*) attracts the negative charges on the rotor. **b** Model of mechanical movement attributed to conformational changes between the stator and the MS ring due to passage of protons. **c** Model of a turnstile-type movement with rotation attributed to conformational changes on the *MS ring* attributed to the passage of protons through it

(stator) interfacing with negative/positive charges on the MS ring (rotor). Charges on the rotor would need to be tilted with respect to the positive charge on the stator. Another popular theory is the "turnstile" model of Khan and Berg (1983) where the flow of protons (or sodium ions) would be by a two-channel system in the stator. In this system, there are two separate events: Protons are carried by the stator and deposited on the rotor and this is followed by use of a second-ion channel on the stator to move the rotor and release the proton into the cell. An electrostatic repulsion/attraction would move the rotor and in this respect it would be similar to the proton turbine model. With the inward flow of protons, there is a series of protination of amino acids followed by deprotination and this would generate the torque needed to rotate the flagellum. As reviewed by Berg (2000), a cyclic process involving protination–deprotination would promote rotation of the MS ring attributed to conformational changes of the Mot proteins. A third model was proposed by Oosawa and Hayashi (1986) and it is similar to the proton turbine model except the protons move across the stator by a mobile carrier and does not use an ion channel. To better understand the mechanism behind the bacterial flagellar motor, further molecular characterizations are required.

5.2.2 F_1F_0-ATP Synthase Is a Rotary Nanomotor

The F_1F_0-ATP synthase is broadly distributed throughout biology and its function as a nanomotor has been widely examined. While eukaryotic systems have the F_1F_0-ATP synthase in the mitochondrial inner membrane and in chloroplast membranes, bacteria have this unit present in the plasma membrane. A similar structure with slightly different proteins is found as V_1V_0-ATP synthase in membranes of Archaea and vacuoles in eukaryotes. This review will focus on the activities of the F_1F_0-ATP synthase of bacteria and the activities of archaeal V_1V_0-ATP synthase are reviewed

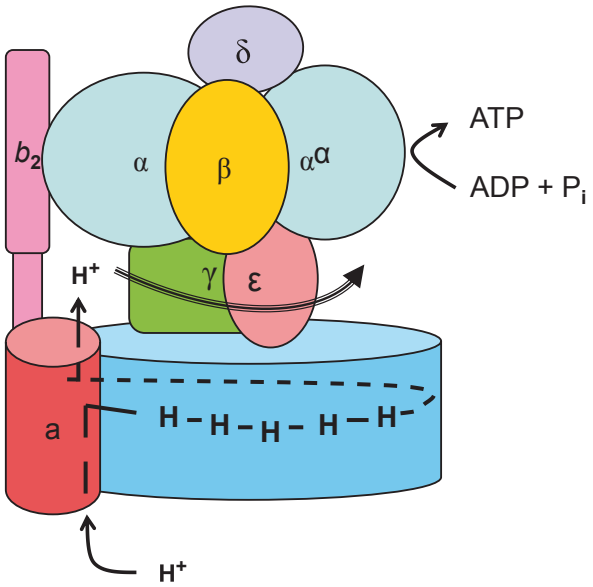

Fig. 5.3 Model of ATP synthase of *Escherichia coli*. Stator interfaces are between b_2 and *a* proteins. The stator functions to counteract rotor torque. Model of possible path for proton movement that drives the ATP synthase

elsewhere (Barton 2005). When proton gradients are generated across the plasma membranes of bacteria, the uptake of protons through the F_1F_0-ATP synthase results in the production of ATP from adenosine diphosphate (ADP) and inorganic phosphate; however, in the absence of respiration, protons may be exported by the F_1F_0-ATP synthase with the hydrolysis of ATP. One may consider the F_1F_0-ATP synthase a bidirectional revolving door driven with proton flow coupled to an electrochemical gradient or ATP hydrolysis as driving forces. Bacteria growing in saline environments may use sodium ions instead of protons to drive ATP synthesis but here we will focus on proton-coupled ATP synthesis. For ATP synthesis, proton movement induces rotation of a protein subunit and this is the central issue in F_1F_0-ATP synthase as a molecular motor.

The F_1F_0-ATP synthase throughout bacteria has a highly conserved structure consisting of eight subunits as $\alpha_3\beta_3\gamma\delta\varepsilon ab_2c_n$ (see review by Weber and Senior 2003). The lipophilic F_0 unit is imbedded in the plasma membrane and consists of the ab_2c_n subunits with "*n*" being 10 for *E. coli* but for some species of bacteria it may be 10–14. The F_1 unit in the cytoplasm consists of $\alpha_3\beta_3\gamma\delta\varepsilon$ and sits on top of the F_0 unit. The δ and γ proteins form the rotor stalk that interfaces the F_1 to the F_0, and the F_0 is stabilized by the stator stalk which consists of the b_2 and δ proteins, see Figure 5.3. Protons enter through a channel in the a protein subunit of F_0 and cycle through the ring of c proteins before exiting to the cytoplasm. It appears that the protons move through the c proteins on asparagine and arginine residues and the protonation of these amino acids induces a rotation of the C-terminal helix which energizes the helical rotation of F_1 (Rastogi and Girvin 1999).

Nanomotors associated with motility are found in Archaea and spirochete organisms. A molecular motor functions in the synthesis of ATP in species of Archaea;

however, the number and characteristics of the proteins are different from those found in bacteria and eukaryotic systems. In spirochetes, the flagella do not extend from the cell surface but are folded back from the poles of the cell to form an endoflagella. This endoflagellum occurs between the cell wall of the spirochete and an outer sheath which tightly adheres to the surface of the spirochete cell. The structure of the endoflagella in spirochete cells and the proteins present in the ATP synthase of Archaea are reviewed by Barton (2005).

5.2.3 Rotational DNA Motor

The packaging of double-stranded DNA (dsDNA) into viruses has been of interest because a mechanism must be employed that prevents coiling of dsDNA. While it had been considered that a rotational process was involved, recent models predict that packing of dsDNA into viruses is by a rotation mechanism (Schwartz et al. 2013). A model system to study rotational motors is the bacterial virus named phi29. This nanomotor in phi29 consists of a protein channel, the DNA packaging ATPase, and a packaging ring consisting of six RNA molecules (Geng et al. 2011). A protein forms the channel that regulates dsDNA to control the entry or exit of genomic dsDNA in the protein covering of the virus. During packaging, approximately two ATP are required for every two base pair of DNA and in phi29 considerable energy would be required because the dsDNA genome is 19.3 kb. Twelve protein subunits form a tapering channel which is widest inside the virus capsid. The direction for DNA travel can be controlled by conformational changes of the channel induced by electrical changes on the protein. ATP hydrolysis is used to energize the rotation motor resulting in uptake of DNA into the viral capsid and the protein accounting for this is a member of a class of proteins belonging to the ATPase associated with diverse cellular activities (AAA^+). Because of the many potential uses of a rotating motor for biomedical treatments, there has been considerable interest in development of an autonomous DNA nanomotor powered by DNA (Chen et al. 2004).

5.2.4 Linear Molecular Motors

While the best-known systems of linear nanomotors in eukaryotic biology involve myocin, kinesin, actin, and dynamin, considerable attention is being given to linear systems in bacteria (Table 5.1). The separation of DNA in bacteria prior to cell division is an area where a molecular motor may be involved and there are several proteins that form the “Z-ring” and the septum of dividing cells (Romberg and Levin 2003). One of the proteins, FtsZ, has been proposed to function in cell division by a process similar to the eukaryotic actin–myosin system (Erickson 2007). There is

some evidence that bacterial FtsZ is a homolog of eukaryotic tubulin and the polymerization of the FtsZ proteins could provide a mechanism to constrict bacterial cells at the time of division (Mingorance et al. 2011). Mechanical process of constriction has been displayed by FtsZ rings which had been inserted into liposomes (Osawa et al. 2009). While there is no motor protein associated with FtsZ, future research is needed to determine if FtsZ does function as a linear molecular motor in bacteria.

5.2.4.1 RNA Polymerase

The separation of daughter chromosomes of bacteria prior to cell division has long been associated with the passive process of DNA attaching to the cell wall and as the cell elongated, the chromosomes would separate. As reviewed by Dworkin and Losick (2002), chromosomal segregation in bacteria is not dependent on cell growth and could be attributed to a molecular motor involving RNA polymerase. RNA polymerase can pull DNA with a force of > 30 pN which is five times greater than myosin and would make this a significant molecular motor (Wang et al. 1998). With *E. coli* having over 10,000 copies of RNA polymerase, considerable pulling force on DNA could occur especially if these RNA polymerase molecules were coordinated (Dworkin and Losick 2002).

5.2.4.2 Export of Biomolecules

Secretion systems in bacteria are a result of biomolecules, usually protein, migrating from the cytoplasm to regions outside of the plasma membrane, and these are referred to as an example of a molecular motor (Peña and Arechaga 2013). About 20 % of proteins produced by bacteria are either inserted into the plasma membrane, outer membrane, periplasm or released from the cell. The energy supplied for this translocation comes from hydrolysis of ATP and in a few cases may be attributed to proton-motive force on the plasma membrane. Based on the export of proteins and the amount of energy required, it has been speculated that hydrolysis of one ATP accounts for the export of 20 amino acid residues across the plasma membrane. Motor-like molecules for the export of proteins across the plasma membrane are associated with the plasma membrane and although the molecular motors have received some interest, details on the mechanics have not been established (Peña and Arechaga 2013; Mizushima and Tokuda 1990). There are six secretion systems used by Gram-negative bacteria for secretion of biomolecules (Table 5.2) and several for Gram-positive bacteria. A feature of these secretion systems is the physical movement of a protein, DNA, or polymerized sugar molecules from the cytoplasm to the exterior of the cell. Models for export of biomolecules in Gram-negative bacteria are given in Figures 5.4–5.6.

Table 5.2 Characteristics of major secretory systems in Gram-negative bacteria

The type I secretory system consists of three protein units: An ABC protein which is in the plasma membrane and binds ATP which is hydrolyzed and provides energy for the translocation of proteins. A membrane fusion protein (MFP) provides a conduit across the periplasm to enable the protein to be exported by a single stem. A trimeric protein or outer membrane protein (OMP) establishes an avenue for the protein to travel across the outer membrane (Figure 5.5). Proteins of 800 kDa or smaller may be rapidly transported by this system. A 50 amino acid residue sequence provides the signal for export of unfolded proteins by type I secretion. Biomolecules exported by this system include: colicin V from *Escherichia coli,* LapA adhesion protein from *Pseudomonas aeruginosa,* toxins, lipases, glucans and polysaccharides from diverse bacteria (Holland et al. 2005)
The type II system consists of 12–16 proteins which are inserted into the plasma and outer membranes. A large protein complex initiated in the periplasm and extending through the outer membrane is referred to as the secreton (Figure 5.5). There are two types of transporters in the plasma membrane and these are the Sec transport system which exports unfolded proteins while the Tat export system transports proteins that are folded and may contain cofactors (Liang et.al. 2009; Lycklama et al. 2012). Proteins may be targeted for export by the type II secretion system by either co-translational or posttranslational mechanisms. Specific amino acid sequences near the N-terminus of the protein to be exported are used as signals for type II export. If the signal sequence interacts with proteins of the type II secretory system while synthesis occurs on the ribosome, this would constitute co-translational mechanism. If the protein for export is released into the cytoplasm, it is stabilized as a linear protein by chaperone proteins and this is referred to as the posttranslational mechanism. To energize the translocation of unfolded protein across the plasma membrane, traffic ATPase is required and this protein extends from the inner side of the plasma membrane into the cytoplasm. The type II traffic ATPases of the Sec system are similar to the proteins in type IV secretion system and both are members of a traffic ATPase super family (AAA^+). While the molecules for ATP hydrolysis are identified in Type II secretion, the mechanisms for mechanical translocation remain unclear (Sikora 2013; Douzi et al. 2012; Tseng 2009; Bolhuis 2004). The Tat translocation mechanism recognizes a signal sequence containing arginine residues on the protein and it is often called the twin-arginine translocation system. Energy for the Tat system is attributed to proton-motive force on the plasma membrane (Natale et al. 2008)
The type III secretory system has a structure referred to as the injectosome which resembles a molecular syringe used for the injection of proteins into host cells. The protein complex is similar to that of the basal body of bacterial flagella. Protein structures of the type III secretion system include a large ring in the plasma membrane, connector that traverses the periplasm, a series of outer membrane rings, and an extracellular needle (Figure 5.6). Proteins targeted for export by the type III system generally have a secretion signal which are the first 20 amino acids at the N-terminus of the protein to be exported. There is an ATPase at the base of the type III secretion system; however, it is unknown if it is involved in energizing the protein export (Guttman and McCann 2008; Medini et al. 2006; Saier 2004; Hueck 1998)
The type IV secretion system is used for the export of protein and export of DNA in conjugation activities (Lawley et al. 2003). A protein channel results from 11 to 13 subunits being incorporated in the plasma membrane and outer membrane (Figure 5.6). Located on the cytoplasmic side of the secretion channel are hexameric traffic ATPase enzymes that are members of the AAA^+ secretion protein superfamily. These traffic ATPases interact with substrate-specific proteins that function as molecular motors. The hydrolysis of ATP promotes the biosynthesis of pilus structures through polymerization of protein subunits, or in the case of conjugation energizes the export of DNA. Details of how these molecular motors work have not yet been produced (Ripoll-Rozada et al. 2013; Alvarez-Martinez and Christie 2009; Cabezon and de la Cruz 2006; Frank et al. 2005)

Table 5.2 (continued)

Type V secretion system is a two-component system for protein transport where the first activity uses the Sec system for transmovement across the plasma membrane and the second is a β-barrel configuration in the outer membrane (Figure 5.7). The C-terminus of the transported protein is incorporated into the outer membrane and forms the barrel structure with the passenger domain being released to the extracellular region. This secretion system has often been referred to as the autotransporter system. Molecular motor activity for type V secretion involves the traffic ATPase of the Sec system (Henderson et al. 2004)
Type VI secretion system functions as a defense mechanism used by bacteria against eukaryotic predators and potentially against other bacteria (Pukatzki et al. 2006; Mougous et al. 2006). It is broadly distributed in the bacterial world and requires 15–20 proteins for the construction of rigid protein system that resembles the tail of bacteriophages (Figure 5.7; Silverman et al. 2012). The energetics of this translocation of proteins has not been established

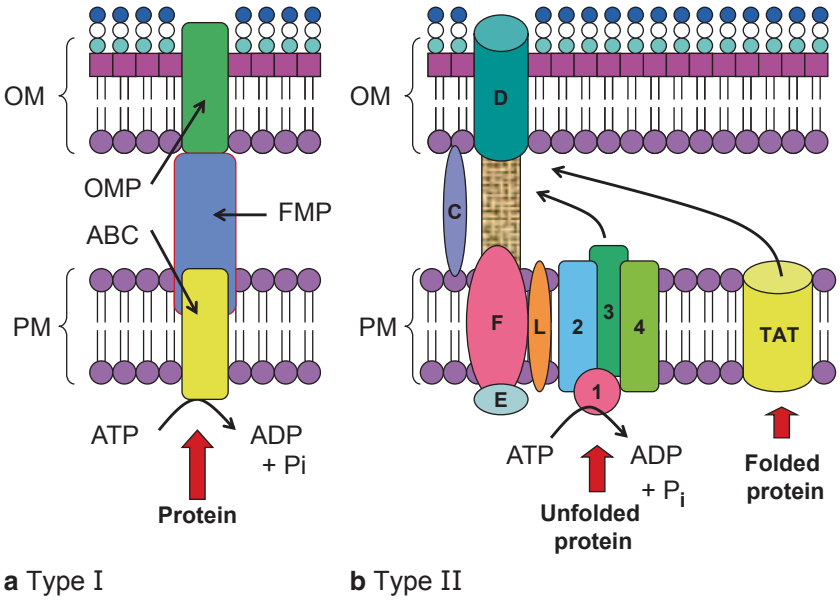

Fig. 5.4 Type I and type II secretion systems in Gram-negative bacteria. **a** Abbreviations in type I: *ABC* ATP binding protein, *MFP* membrane fusion protein, *OMP* outer membrane protein, *OM* outer membrane, *PM* plasma membrane. **b** Identification of proteins in type II: *1* SecA, *2* SecE, *3* SecY, *4* SecG, *TAT* complex formed by TatA, TatB, TatC, *C* GspC, *D* GapD, *E* GspE, *F* GspF, *G* GspG, *L* GspL, *M* GspM

5.2.5 *Micromechanical Devices Powdered by Microorganisms*

There is an interest in using microorganisms as motors for construction of microrobots (Vale and Milligan 2000; Balzani et al. 2000). In one report, bacterial carpets have been constructed by attaching flagellated cells of *Serratia marcescens,* a

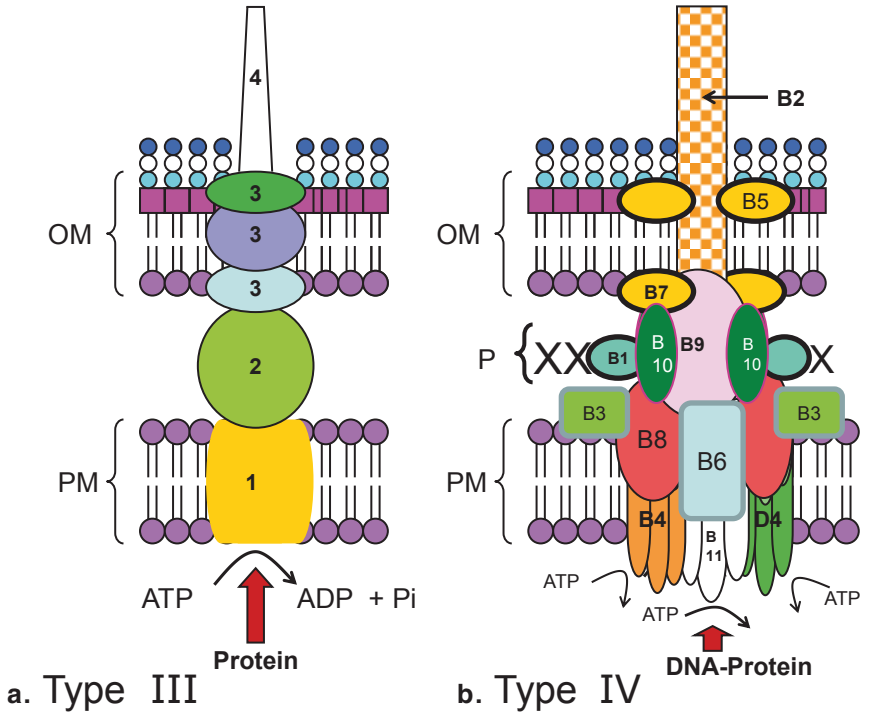

Fig. 5.5 Type III and type IV secretion systems in Gram-negative bacteria. **a** Type III. Proteins identified: *1* plasma membrane ring, *2* connector, *3* outer membrane rings, *4* needle. **b** Type IV. Proteins identified using the nomenclature of Ananiadou et al. (2011): *B1* T pilus formation, *B2* major T pillus for sutransfer, *B3* attachment to inner membrane, *B4* ATP hydrolysis with pilin dislocation, *B5* T pilus subunit for adhesion to outer membrane, *B6* channel for substrate transfer, *B7* pore structure, *B8* channel for substrate transfer, *B9* pore structure for substrate transfer, *B10* channel formation for pore structure, *B11* ATP hydrolysis for substrate transfer, *D4* substrate recognition and ATP hydrolysis, *P* peptidoglycan layer

Gram-negative bacterium, onto polystyrene forming a monolayer with the flagella exposed and free to rotate (Darnton et al. 2004). The bacterial carpet promotes fluid mixing and could be extremely applicable as a micropump or micromixer with motion controlled by coordinated rotation of flagella. Another application employed biflagellated *Chalmydomonas reinhardti* to move microscale loads by phototaxis (Weibel et al. 2005). When polystyrene beads of 3-μm diameter are attached to cells of *C. reinhardti,* the algae beads can be moved by photoexposure at a velocity of ~100 μm/s over a distance of 20 cm and the bead could be potentially uncoupled from the cell by remote hydrolysis of the molecule linking the bead to the cell.

An intriguing system is the microrotary motor using *Mycoplasma mobile,* a cell wall-less form of bacteria. This bacterium is only about 1 μm long and it moves along a solid surface at 2–5 μm/s. *M. mobile* moves by gliding and a review on the mechanics of gliding is covered in a previous chapter in this book. *M. mobile* is an oblong-shaped cell and gliding activity is attributed to proteins at the "neck"

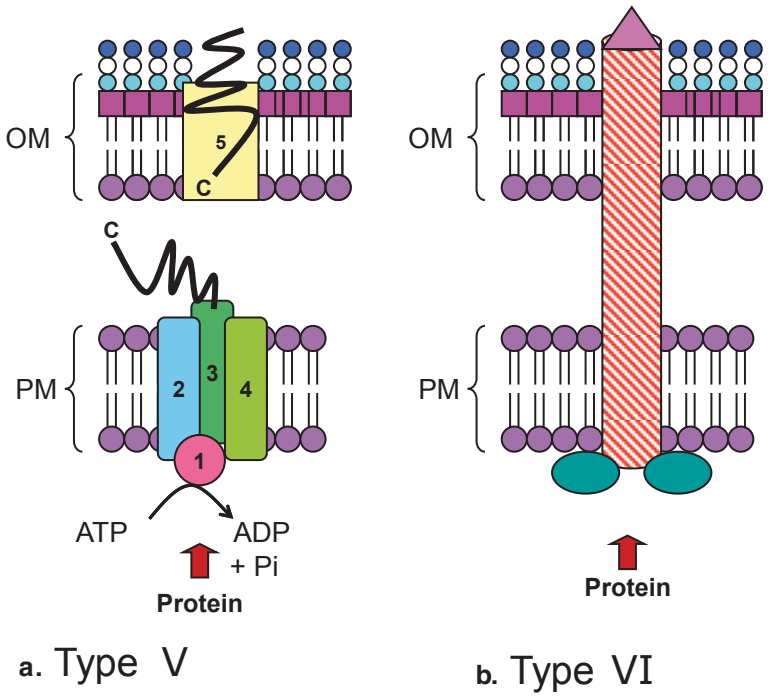

Fig. 5.6 Type V and type VI secretion systems in Gram-negative bacteria. **a** Identification of proteins for type V secretion: *1* SecA, *2* SecE, *3* SecY, *4* SecG, *5* autotransporter protein complex that either diverts the protein into the outer membrane or into the extracellular region. **b** Type VI secretion

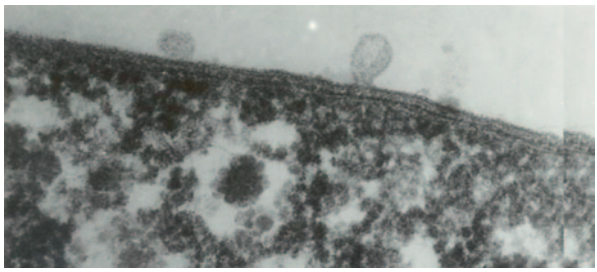

Fig. 5.7 The Gram-negative bacterium *Desulfovibrio gigas* with outer membrane vesicles. Cells were stained with uranyl acetate and lead citrate. Magnification is 60,000

of the cell which are energized by ATP hydrolysis. These proteins in *M. mobile* are Gli123, Gli349, and Gli521 which have a molecular mass of 123 kDa, 349 kDa, and 521 kDa, respectively (Uenoyama and Miyata 2006). The Gil349 protrudes from the cell and act like a leg and moves the cell by repeatedly attaching to a solid surface and releasing from it. Using a circular track etched into a solid silicon (Si) surface, Hiratsuka et al. (2006) introduced cells of *M. mobile* into the track along with a silicon dioxide (SiO_2) rotor which fits inside the track. Several bacterial cells were

bound to each rotor by biotin–streptavidin interactions. Bacteria were able to exceed the frictional forces of the system which were estimated to be 1.8×10^{-16} N/m and pull the rotor at a linear velocity of 1.2–2.1 μm/s.

5.3 Nanowires

Nanowires are linear appendages from bacterial cells that have electron-transfer characteristics. An impetus for study of nanowires has been the capability of extracellular electron transport by bacteria for oxidation of solid phase minerals such as iron and manganese, development of bacterial biofilm communities, and application in microbial fuel cells.

Most of the information about bacterial nanowires is from studies with *Shewanella* and *Geobacter* cultures. Cells of *Geobacter sulfurreducens,* an anaerobic chemolithotrophic bacterium grows with Fe (III) oxides as the electron donor and the transfer of electrons from the insoluble ferric oxide to the cell is by a pilus-like structure (Reguera et al. 2005). The reduction of uranyl (UIV) to uraninite (UVI), by *G. sulfurreducens* is accomplished by catalytic activity of conductive pili and this may be a process that is beneficial to the cell by preventing cellular uptake of soluble hexavalent uranium (Cologgi et al. 2011). The electron conductive activity of the nanowire pili was established through the use of a conducting-probe atomic force microscope (Reguera et al. 2005) and mutants lacking these pili were incapable of using ferric minerals as the electron source in support of growth. As determined by tunneling spectroscopy, electrically conductive pili or nanowires were produced by *Shewanella oneidensis* strain MR-1, a facultative anaerobe, when electron acceptors become limiting in the environment (Gorby et al. 2006). However, not all cells with appendages of 50–150 nm in diameter are nanowires because nonconductive appendages were demonstrated in mutants of *S. oneidensis* lacking genes for cytochrome expression (Gorby et al. 2006). While the conductivity studies of the nanowires were initially limited to electron measurements across the diameter of the appendage, El-Naggar et al. (2011) observed that electron transport along the length of the nanowires was at a rate of 10.9 per second at 100 mV with a resistance of 1 Ω/cm. The presence of electrically conductive nanowires is not restricted to *Geobacter* and *Shewanella* species but has also been demonstrated in the aerobic cyanobacterium *Synechocystis* PCC 6803 when CO_2 is limiting and the fermentative *Pelotomaculum thermoproionicum* when grown syntrophically with *Methanothermobacter thermoautotrophicus* (Gorby et al. 2006).

The mechanism of electron transfer has mystified scientists for some time and there are two viable hypotheses that attempt to explain this activity (Boesen and Nielsen 2013). The metal-like conductivity hypothesis has the nanowire moving electrons along the pilus-like structure with cytochromes transferring electrons to the electron acceptor. In the second hypothesis, electrons jump between heme groups since c-type cytochrome OmcS are located along the pilus-like nanowire of *G. sulfurreducens* (Leang et al. 2010). Using *G. sulfurreducens* strain Aro-5 with

mutations in aromatic amino acid residues of the nanowire, Vargas et al. (2013) observed that electron conductivity was diminished with the loss of aromatic amino acid residues in the pilus. However, Boesen and Nielsen (2013) caution that the mutated nanowires may have lost structural integrity and secondarily, the pili have diminished electron conductivity. Clearly, additional research is needed to understand the mechanism of electron conductivity of nanowires.

Biofilm development may benefit from nanowire formation which extends between cells in the microbial community (Rabaey and Rozendal 2010). Through a network of nanowires, cells at the interior of the biofilms may transfer electrons to surface bacteria which interact with oxygen as the final electron acceptor of metabolism. The biofilm matrix consists of exopolysaccharides and in the case of *Geobacter* sp. may also contain electrically conductive pili (Magnuson 2011). Also, biofilm formation is important for fuel cells where the nanowires from bacteria at the anode transmit electrons to an exterior load before being carried to the cathode (Reguera et al. 2006).

5.4 Outer Membrane Vesicles

Gram-negative bacteria have a unique outer membrane structure which constitutes the outer surface of the cell. Many Gram-negative bacteria produce vesicles or blebs that have originated from the outer membrane (Figure 5.7). The biogenesis of these outer membrane vesicles (OMV) occurs with complete release of OMV from the outer membrane (Scherizer and Whiteley 2012; Kulp and Kuehn 2010). These outer membrane vesicles are about 50–250 nm in diameter with a chemical composition similar to outer membranes. The membranous structure of these nanostructures is the same as outer membranes with lipopolysaccharides on the outer side and phospholipids on the inner side. The production of OMV has been demonstrated for many Gram-negative bacteria (Chatterjee and Chaudhuri 2012; Kuehn and Kesty 2005; Li et al. 1998) and it may be that most Gram-negative bacteria are capable of releasing these lipid vesicles. OMV are produced as a stress-induced response (MacDonald and Kuehn 2013) as well as bacterial cultures growing under normal conditions. Recently, a new structure has been identified in *Delftia,* a Gram-negative bacterium, and it is termed a nanopod (Shetty et al. 2011). The nanopod are $\geq$6 μm in length and is formed from OMV imbedded in a glycosylated protein, Nanopod protein A (NpdA). With the NpdA related to S-layer proteins, the nanopod is a product of OMV and S-layer synthesis. Specific strains of *Delftia* respond to environmental chemicals with the production of nanopods (Shetty and Hickey 2014).

The OMV are of considerable benefit to the bacteria which produce them because the OMV potentially carry various types of biomolecules (Table 5.3). As enumerated by Chatterjee and Chaudhuri (2012), virulence factors consisting of toxins, enzymes, cell-specific proteins, and adhesions have been isolated from OMV of pathogenic bacteria. In the same review, the proteins associated with the OMV could be classified into the following families: (1) porins, (2) enzymes responsible

Table 5.3 Biomolecules carried by outer membrane vesicles produced by *Bacteroides fragilis, Escherichia coli,* and *Pseudomonas aeruginosa*

Bacterium	Biomolecules carried	References
Bacteroides fragilis	Hemagglutin, alkaline phosphatase, acid phosphatase, lipase, phosphohydrolase, α- and β-galactosidases, β-glucosidase, glucosaminidase	Patrick et al. (1996)
Escherichia coli	Cytolysin, shiga toxin, heat-labile enterotoxin, α-Hemolysin, cytolethal decending toxin, heme and iron-binding proteins	Kolling and Matthews (1999); Wai et al. (2003); Yokoyama et al. (2000) Horstman and Kuehn (2000) Balsalobre et al. (2006)
Pseudomonas aeruginosa	Alkaline phosphatase, hemolysin, protease, phospholipase C, β-lactamase, peptido-glycan hydrolyases, cystic fibrosis, transmembrane regulator, and inhibitory factor	Bauman and Kuehn (2006); Cota-Gomez et al. (1997); Ciofu et al. (2000); Kadurugamuwa and Beveridge (1998); MacEachran et al. (2007); Li et al. (1998); Mashburn and Whiteley (2005); Bomberger et al. (2009); Wai et al. (2003)

for hydrolysis of the peptidoglycan, (3) multidrug efflux pumps, (4) ABC transporters, (5) protease/chaperones, and (6) proteins associated with motility or pili structure. With this diversity of biological molecules that may be contained in OMV, it should not be a surprise that OMV have several activities and some of these are listed in Table 5.4.

OMV are also produced by chemolithotrophic or phototrophic bacteria. The OMV of *Prochlorococcus,* a marine cyanobacterium, have been found to contain DNA and RNA in addition to proteins (Pérez-Cruz et al. 2013). OMVs of *Desulfovibrio gigas,* a sulfate-reducing anaerobe, contain 1 % of the periplasmic formate dehydrogenase (Haynes et al. 1995). The OMV of *Shewanella* contain redox-active proteins and these may be located on the surface of the cell, in the extracellular menstruum, and in some conditions attached to the cell surface by nanowires (Gorby et al. 2008). A unique double-bilayer OMV has been reported for *Shewanella vesiculosa* M7 and this has been designated as an outer-inner membrane vesicle (O-IMV; Pérez-Cruz et al. 2013). OMV from *Shewanella* are redox active and capable of metal reduction (Gorby et al. 2008). *Shewanella decolorationis* S12 reduces azo dyes with membrane fractions and by OMV (Hong et al. 2006). To underscore the great interest in OMV, especially in biomedical areas, a new publication, *Journal of Extracellular Vesicles,* specifically addresses this area of research. Several commercial applications have been proposed for OMV and a few of these are presented in Table 5.4.

Table 5.4 Activities and commercial applications associated with outer membrane vesicles produced by bacteria

Processes	References
Activities	
Lateral gene transfer	Pérez-Cruz et al. (2013)
Nutrient reserve in marine environment	Pérez-Cruz et al. (2013)
Lysis of Gram-negative and Gram-positive bacteria	Li et al. (1998)
Host-pathogen interaction	Kuehn and Kesty (2005); Scherizer and Whiteley (2013)
Periodontitis	Nakao et al. (2014)
Shedding encrusted surface of bacteria and preventing encrustation of bacteria by precipitated metals	Shao et al. (2014)
Applications	
Bioengineered to deliver anticancer drugs	Gujrati et al. (2014)
Vaccine production	Collins (2011); Bartolini et al. (2013)
As immunogens	Alaniz et al. (2007)
Bioremediation	Shetty and Hickey (2014)

5.5 Summary and Perspective

Bacterial cells display considerable organization at the molecular level as is apparent from the study of nanomotors, nanowires, and OMV. Mechanical processes are present in bacteria, and in export activities convert chemical energy, which usually comes from ATP hydrolysis, into translocation of protein or other biopolymers. Rotary molecular motors are present in ATP synthase as well as in basal structure of the flagellum, and energy for rotational processes are from proton or Na^+ transport processes. The mechanisms for molecular motor processes in bacteria appear to be attributed to conformational changes in proteins as a result of activation by proton (or Na^+) or ATP. Details of how these proteins perform specific work events remain to be established. However, it should be noted that the ATP synthase molecular motor is not restricted to bacteria but transcends biological systems. On the other hand, nanowires, conductive protein appendages from the bacterial cell are found only in the prokaryotic world and this system of extracellular electron transport is favored by bacteria in the mineralization of insoluble compounds, reduction of soluble toxic metals, and transfer of electrons to adjacent cells in a biofilm. OMV are a lipid-based structure originating from the outer membrane and are highly effective packaging systems that move biomaterial from a Gram-negative bacterial cell to adjacent prokaryotic or eukaryotic cells. Clearly, nanowires and OMV provide a benefit to bacteria that produce them and scientists are just starting to understand some of their activities. Bacteria have considerable molecular organization that affords the cells with responses to the changing environment and enables them to persist. Novel applications of the nanomotors, nanowires, and OMV are being considered for future biotechnology initiatives.

References

Alaniz RC, Deatherage BL, Lara JC, Cookston BT (2007) Membrane vesicles are immunogenic facsimiles of *Salmonella typhimurium* that potentially activate dendritic cells, prime B and Tcell responses and stimulate protective immunity in vivo. J Immunol 179:7692–7701

Alvarez-Martinez CE, Christie PJ (2009) Biological diversity of prokaryotic type IV secretion systems. Microbiol Mol Biol Rev 73:775–808

Ananiadou S, Sullivan D, Black W, Levow G-A, Gillespie JJ, Mao C, Pysalo S, Kollluru B, Tsujii J, Sobral B (2011) Named entry recognition for bacterial type IV secretion system. PLoS ONE 6:e14780. doi:10.1371/journal.pone0014780

Armstrong CL, Toppozini L, Dies H, Faraone A, Nagao M, Rheinstädter MC (2013) Incoherent neutron spin-echo spectroscopy as an option to study long-range lipid diffusion. ISRN Biophys 2013(2013):9. Article ID 439758. http://dx.doi.org/10.1155/2013/439758

Balsalobre C, Silvan JM, Berglund S, Mizunoe Y, Uhlin BE, Wai SN (2006) Release of type-I secreted alpha-hemolysin via outer membrane vesicles from *Escherichia coli*. Mol Microbiol 59:99–112

Balzani V, Credi A, Raymo FM, Stoddart JF (2000) Artificial molecular machines. Angew Chem Int Ed 39:3349–3391

Bartolini E, Ianni E, Frigimelica E, Petracca R, Galli G, Scorza BF, Norais N, Laera D, Giusti F, Pierleoni A, Donati M, Cevenini R, Finco D, Grande G, Grifantini R (2013) Recombinant outer membrane vesicles carrying *Chlamydia muridarum* HtrA induce antibodies that neutralize chlamydial infection in vivo. J Extracell Vesicles 2:20181

Barton LL (2005) Structural and functional relationships in prokaryotes. Springer, New York

Bauman SJ, Kuehn MJ (2006) Purification of outer membrane vesicles from *Pseudomonas aeruginosa* and their activities of an IL-8 response. Microbes Infect 8:2400–2408

Berg HC (1974) Dynamic properties of bacterial flagellar motors. Nature 249:77–79

Berg HC (1996) Symmetries in bacterial motility. Proc Natl Acad Sci U S A 93:14225–14228

Berg HC (2000) Constraints on models for the flagellar rotary motor. Phil Trans R Soc Lond B Biol Sci 355:491–501

Berg HC (2003) The rotary motor of bacterial flagella. Ann Rev Biochem 72:19–54

Berg HC, Anderson RA (1973) Bacteria swim by rotating their flagellar filaments. Nature 245:380–382

Berry RM (2000) Theories of rotary motors. Philos Trans R Soc Lond B Biol Sci 355:503–509

Boesen T, Nielsen LP (2013) Molecular dissection of bacterial nanowires. mBio 4(3):e00270-13. doi:10.1128/mBio.00270-13

Bolhuis A (2004) The archaeal sec-dependent protein translocation pathway. Philos Trans R Soc Lond B Biol Sci 359:919–927

Bomberger JM, Maceachran DP, Coutermarsh BA, Ye S, O'Toole GA, Stanton BA (2009) Long distance delivery of bacterial virulence factors by *Pseudomonal aeruginosa* outer membrane vesicles. PLoS Pathog 5:e1000382

Bustamante C, Chemla YR, Forde NR, Izhaky D (2004) Mechanical processes in biochemistry. Annu Rev Biochem 73:704–748

Cabezon E, de la Cruz F (2006) TrwB: an F(1)-ATPase-like molecular motor envolved in DNA transport during bacterial conjugation. Rev Microbiol 157:299–305

Chatterjee NS, Chaudhuri K (2012) Outer membrane vesicles of bacteria. SpringerBriefs in microbiology. Springer, New York

Chen Y, Wang M, Mao C (2004) An autonomous DNA nanomotor powered by a DNA enzyme. Agnew Chem Int Ed 43:3554–3557

Ciofu O, Beveridge TJ, Kadurugamuwa J, Walther-Rasmussen J, Hoiby N (2000) Chromosomal beta-lactamase is packaged into membrane vesicles and secreted from *Pseudomonas aeruginosa*. J Antimicrob Chemother 45:9–13

Collins BS (2011) Gram-negative outer membrane vesicles in vaccine development. Discov Med 12:7–15

Cologgi DL, Lampa-Pastirk S, Speers AM, Kelly SD, Reguera G (2011) Extracellular reduction of uranium via *Geobacter* conductive pili as a protective cellular mechanism. Proc Natl Acad Sci U S A 108:15248–15252

Cota-Gomez A, Vasil AL, Kadurugamuwa J, Beveridge TJ, Schweizer HP, Vasil ML (1997) PicR1 and PicR2 are putative calcium binding proteins required for secretion of the hemolytic phospholipase C of *Pseudomonas aeruginosa*. Infect Immun 65:2904–2913

Darnton N, Turner L, Breuer K, Berg HC (2004) Moving fluid with bacterial carpets. Biophys J 86:1863–1870

DePamphilis ML, Adler J (1971a) Purification of intact flagella from *Escherichia coli* and *Bacillus subtilis*. J Bacteriol 105:376–383

DePamphilis ML, Adler J (1971b) Fine structure and isolation of the hook-basal body complex of flagella from *Escherichia coli* and *Bacillus subtilis*. J Bacteriol 105:384–395

DePamphilis ML, Adler J (1971c) Attachment of flagellar basal bodies to the cell envelope: specific attachment to the outer, lipopolysaccharide membrane and the cytoplasmic membrane. J Bacteriol 105:396–407

Desai A, Mitchison TJ (1997) Microtubule polymerization dynamics. Annu Rev Cell Dev Biol 13:83–117. doi:10.1146/annurev.cellbio.13.1.83

de Keyzer J, van der Does C, Driessen AJ (2003) The bacterial translocase: a dynamic protein channel complex. Cell Mol Life Sci 60:2034–2052

De Vlaminck I, Dekker C (2012) Recent advances in magnetic tweezers. Annu Rev Biophys 41:453–472

Didenko VV (2001) DNA probes using fluorescence resonance energy transfer (FRET): designs and applications. Biotechniques 31:1106–1121

Douzi B, Filloux A, Voulhoux R (2012) On the path to uncover the bacterial type II secretion system. Philos Trans R Soc B 367:1059–1072

Dworkin J, Losick R (2002) Does RNA polymerase help drive chromosome segregation in bacteria? Proc Natl Acad Sci U S A 99:14089–14094

El-Naggar M, Wanger G, Leung KM, Yuzvinsky TD, Southam G, Yang J, Lau WM, Nealson KH, Gorby YA (2011) Electrical transport along bacterial nanowires from *Shewanella oneidensis* MR-1. Prod Natl Acad Sci U S A 107:18127–18131

Elston TC, Oster G (1997) Protein turbines I: the bacterial flagellar motor. Biophys J 73:703–721

Erickson HP (2007) Evolution of the cytoskeleton. Bioessays 29:668–677

Frank AC, Alsmark CM, Thollesson M, Andersson SG (2005) Functional divergence and horrizontal transfer of type IV secretion systems. Mol Biol Evol 22:1325–1336

Gaspard P, Gerritsma E (2007) The stochastic chemomechanics of the F_1–ATP ase molecular motor. J Theor Biol 247:672–686

Geng J, Fang H, Haque F, Zhang L, Guo P (2011) Three reversible and controllable discrete steps of channel gating of a viral DNA packaging motor. Biomaterials 32:8234–8242

Gorby YA, Yanina S, McLean JS, Rosso KM, Moyles D, Dohnalkova A, Beveridge TJ, Shang IS, Kim BH, Kim KS, Culley DE, Reed SB, Romine MF, Saffarini DA, Hill EA, Shi L, Elias DA, Kennedy DW, Pinchuk G, Wantanable K, Ishii S, Logan B, Nealson KH, Fredrickson JK (2006) Electrically conductive bacterial nanowires produced by *Shewanella oneidensis* strain MR-1 and other microorganisms. Proc Natl Acad Sci U S A 103:11358–11363

Gorby Y, McLean J, Korenevsky A, Rosso K, El-Naggar MY, Beveridge TJ (2008) Redox active membrane vesicles produced by *Shewanella*. Geobiol 6:232–241

Gujrati V, Kim S, Kim S-H, Min JJ, Choy HE, Kim SC, Jon S (2014) Bioengineered bacterial outer membrane vesicles as cell-specific drug-delivery vehicles for cancer therapy. ACS Nano 8:1525–1537

Guttman D, McCann H (2008) Evolution of the type III secretion system and its effectors in plant-microbe interactions. New Phytol 117:33–47

Harold FM, Maloney PC (1996) Energy transduction by ion currents. In: Neidhardt FC, Curtiss R, Ingraham JL, Lin ECC, Low KB, Magasanik B, Rezenikoff WS, Riley M, Schaechter M, Umbarger HE (eds) *Escherichia coli* and *Salmonella*: cellular and molecular biology, vol 1. American Society for Microbiology, Washington, pp 283–306

Haustein E, Schwille P (2007) Fluorescence correlation spectroscopy: novel variations of an established technique. Annu Rev Biophys Biomol Struct 36:151–169. doi:10.1146/annurev.biophys.36.040306.132612

Haynes TS, Klemm DJ, Rucco JJ, Barton LL (1995) Formate hedydrogenase activity in cells and outer membrane blebs of *Desulfobvibrio gigas*. Anaerobe 1:175–182

Henderson IR, Navarro-Garcia F, Desvaux M, Fernandez RC, Ala'Aldeen D (2004) Type V protein secretion pathway: the autotransporter store. Microbiol Mol Biol Rev 68:692–744

Hinshaw JE (2000) Dynamin and its role in membrane fission. Annu Rev Cell Dev Biol 16:483–519

Hiratsuka Y, Miyata M, Tada T (2006) A microrotary motor powered by bacteria. Proc Natl Acad Sci U S A 103:13613–13623

Holland IB, Schmitt L, Young J (2005) Type I protein secretion in bacteria, the ABC-transporter dependent pathway. Mol Membr Biol 22:29–39 (review)

Hong Y, Xu M, Guo J, Xu Z, Chen X, Sum G (2006) Respiration and growth of *Shewanella decolorationis* S12 with an azo compound as the sole electrón aceptor. Appl Environ Microbiol 73:64–72

Horstman AL, Kuehn MJ (2000) Enterotoxogenic *Ecsherichia coli* secretes active heat-labile enterotoxin via outer membrane vesicles. J Biol Chem 274:12489–12496

Hubscher U, Maga G, Spadari S (2002) Eukaryotic DNA polymerases. Annu Rev Biochem 71:133–163

Hueck CJ (1998) Type III protein secretion systems in bacterial pathogens of animals and plants. Microbiol Mol Biol Rev 62:379–435

Kadurugamuwa JL, Beveridge TJ (1998) Delivery of the non-membrane-permeative antibiotic gentamicin into mamalian cells by using *Shigella flexneri* membrane vesicles. Antimicrob Agents Chemother 42:1476–1483

Khan S, Berg HC (1983) Isotope and thermal effects in chemiosmotic coupling to the flagellar motor of *Streptococcus*. Cell 32:913–919

Kleutsch B, Laüger P (1990) Coupling of proton flow and rotation in the bacterial flagella motor: stochastic simulation of a microscopic model. Eur Biophys J 18:175–191

Kolling GL, Matthews KR (1999) Export of virulence genes and shiga toxin by membrane vesicles of *Escherichia coli* O157:H7. Appl Environ Microbiol 65:1843–1848

Kolomeisky RK, Fisher ME (2007) Molecular motors: a theorist's perspective. Annu Rev Phys Chem 58:675–695

Kuehn MJ, Kesty NC (2005) Bacterial outer membrane vesicles and the host-pathogen interaction. Genes Dev 19:2645–2655

Kulp A, Kuehn MJ (2010) Biological functions and biogenesis of secreted bacterial outer membrane vesicles. Annu Rev Microbiol 64:163–184

Lawley TD, Klimke WA, Gubbins MJ, Frost LS (2003) F factor conjugation is a true type IV secretion system. FEMS Microbiol Lett 224:1–15

Leang C, Qian X, Mester T, Lovley DR (2010) Alignment of the c-type cytochrome OmcS along pili of *Geobacter sulfurreducens*. Appl Environ Microbiol 76:4080–4084

Liang F-C, Bageshwar UK, Musser SM (2009) Bacterial sec protein transport is rate-limited by precursor length: a single turnover. Mol Biol Cell 20:4256–4266

Li Z, Clarke AJ, Beveridge TJ (1998) Gram-negative bacteria produce membrane vesicles which are capable of killing other bacteria. J Bacteriol 180:5478–5483

Liu S, Chistol G, Hetherington CL, Tafoya S, Aathavan K, Schnitzbauer J, Grimes S, Jardine PJ, Bustamante C (2014) A viral packaging motor varies its DNA rotation and step size to preserve subunit coordination as the capsid fills. Cell 157:702–713

Lodish H, Berk A, Zipursky SL et al (2000) Molecular cell biology, 4th edn. W. H. Freeman, New York. http://www.ncbi.nlm.nih.gov/books/NBK21724/

Lycklama A Nijeholt JA, Driessen AJM (2012) The bacterial sec-translocase: structure and mechanism. Phylos Trans R Soc B Biol Sci 367:1016–1028

MacDonald IA, Kuehn MJ (2013) Stress-induced outer membrane vesicle production by *Pseudomonas aeruginosa*. J Bacteriol 195:2971–2981

MacEachran DP, Ye S, Bomberger JM, Hogan DA, atecka-Urban A, Stanton BA, O'Toole GA (2007) The *Pseudomonas aeruginosa* secreted protein PA2934 decreases apical membrane expression of the cystic fibrosis transmembrane conductance regulator. Infect Immun 75:3902–3912

Macnab RM (1987) Flagella. In: Neidhardt FC, Ingraham JL, Low KB, Magasanik B, Schaechter M, Umbarger HE (eds) *Escherichia coli* and *Salmonella*: cellular and molecular biology, vol 1. American Society for Microbiology, Washington, pp 70–83

Macnab RM (1992) Genetics and biogenesis of bacterial flagella. Annu Rev Genet 26:131–158. doi:10.1016/j.tim.2004.09.002

Macnab RM (2003) How bacteria assemble flagella. Annu Rev Microbiol 57:77–100

Macnab RM, Aizawa S-I (1984) Bacterial motility and the bacterial flagellar motor. Annu Rev Biophys Bioeng 13:51–83

Magnuson TS (2011) How the *xap* locus put electrical "zap" in *Geobacter sulfurreducens* biofilms. J Bacteriol 193:1021–1022

Mahadevan L, Matsudaira P (2000) Motility powered by supramolecular springs and ratchets. Science 288:95–99

Mashburn LM, Whiteley M (2005) Membrane vesicles traffic signals and facilitate group activites in prokaryotes. Nature 437:422–435

Mattheyses AL, Simon SM, Rappoport JZ (2010) Imaging with total internal reflection fluorescence microscopy for the cell biologist. J Cell Sci 123:3621–3628

Medini D, Covacci A, Donati C (2006) Protein homology network families reveals step-wise diversification of type III and type IV secretion systems. PloS Comput Biol 2:1543–1551

Minamino T, Imada K, Namba K (2008) Molecular motors of the bacterial flagella. Curr Opin Struct Biol 18:693–701

Mingorance J, Rivas G, Vélez M, Gómez-Puertas P, Vicente M (2011) Strong FtsZ is with the force: mechanisms to constrict bacteria. Trends Microbiol 18:348–356

Mitchell P (1956) Hypothetical thermokinetic and electrokinetic mechanisms of locomotion in micro-organisms. Proc R Phys Soc Edinb 25:32–34

Mitchell P (1972) Self-electrophoretic locomotion in micro-organisms: bacterial flagella as giant ionophores. FEBS Lett 28:1–4

Mizushima S, Tokuda H (1990) In vivo translocation of bacterial secretory proteins and energy requirements. J Bioenerg Biomembr 22:389–399

Mougous JD, Cuff ME, Raunser S, Shen A, Zhou M, Gifford CA, Goodman AL, Joachimiak G, Ordoñez CL, Lory S, Walz T, Joachimiak A, Mekalanos JJ (2006) A virulence locus pf *Pseudomonas aeruginosa* encodes a protein secretion apparatus. Science 312:1526–1530

Nakao R, Takashiba S, Kosono S, Yoshida M, Watanabe H, Ohnishi M, Senpuku H (2014) Effect of *Porphyromonas gingivalis* outer membrane vesicles on gingipain-mediated detachment of cultured oral epithelial cells and immune response. Microbes Infect 16:6–16

Natale P, Brüser T, Drissen AJM (2008) Sec- and tat-mediated protein secretion across the bacterial cytoplasmic membrane—distinct translocases and mechanisms. Biochem Biophys Acta Biomembr 1778:1735–1756

Nelson P, Radosavljievic M, Bromberg S (2013) Biological physics. W. H. Freeman, New York

Noller HF, Nomura M (1987) Ribosomes. In: Neidhardt FC, Ingraham JL, Low KB, Magasanik B, Schaechter M, Umbarger HE (eds) *Escherichia coli* and *Salmonella*: cellular and molecular biology, vol 1. American Society for Microbiology, Washington, pp 104–125

Oosawa F, Hayashi S (1986) Coupling between flagellar motor rotation and proton flux in bacteria. J Physiol Soc Jpn 52:4019–4028

Osawa M, Anderson DE, Erickson HP (2009) Reconstruction of contractile FtsZ rings in liposomes. Science 320:792–794

Patrick S, McKenna JP, O'Hagan S, Dermott E (1996) A comparison of the haemogglutinating and enzyme activities of *Bacteroides fragilis* whole cells and outer membrane vesicles. Microb Pathog 20:191–202

Peña A, Arechaga I (2013) Molecular motors in bacterial secretion. J Mol Microbiol Biotechnol 23:357–369

Pérez-Cruz C, Carrión O, Delgado L, Martinez G, López-Iglesias C, Mercade E (2013) New type of outer membrana vesicle produced by the gram-negative bacterium *Shewanella vesículosa* M7T: implications for DNA content. Appl Environ Microbiol 79:1874–1881

Pierobon P (2009) Traffic of molecular motors: from theory to experiments. In Appert-Rolland C, Chevoir F, Gondret P, Lassarres S, Lebacque J-P, Schreckenberg M (eds) Traffic and granular flow '07, Springer, Berlin-Heidelberg, pp 379–388

Pukatzki S, Ma AT, Sturtevant D, Krasins B, Sarracino D, Nelson WC, Heidelberg JF, Mekalanos JJ (2006) Identification of a conserved bacterial protein secretion system in *Vibrio cholera* using the *Dictostelium* host model system. Proc Natl Acad Sci U S A 103:1528–1533

Rabaey K, Rozendal RA (2010) Microbial electrosynthesis—revisiting the electrical route for microbial production. Nat Rev Microbiol 8:706–716

Rastogi VK, Girvin ME (1999) Structural changes linked to proton translocation by subunit c of the ATP synthase. Nature 402:263–268

Reguera G, McCarthy K, Mehta T, Nicoll JS, Tuominen MT, Lovley DR (2005) Extracellular electron transfer via microbial nanowires. Nature 435:1098–1101

Reguera G, Nevin KP, Nicoll JS, Covalla SF, Woodard TL, Lovley DR (2006) Biofilm and nanowire production leads to increased current in *Geobacter sulfurreducens* fuel cells. Appl Environ Microbiol 72:7345–7348

Reid T (2008) Optical tweezers: gold standard. Nature Nanotechnol 3:321. doi:10.1038/nnano.2008.137

Ripoll-Rozada J, Zunzunegut S, de la Cruz F, Arechaga I, Cabezón E (2013) Functional interactions of virB11 traffic ATPases with virB4 and virD4 molecular motors in type IV secretion systems. J Bacteriol 195:4195–4201

Roberts AJ, Kon T, Knight PJ, Sutoh K, Burgess SA (2013) Functions and mechanics of dynein motor proteins. Nat Rev Mol Cell Bio 14:713–726. doi:10.1038/nrm3667

Romberg L, Levin PA (2003) Assembly dynamics of the bacterial cell division protein FTSZ: poised at the edge of stability. Annu Rev Microbiol 57:125–154

Saier M (2004) Evolution of bacterial type III protein secretion systems. Trends Microbiol 12:113–115

Saier M (2013) Microcompartments and protein machines in prokaryotes. J Mol Microbiol Biotechnol 23:243–269

Scherizer JW, Whiteley M (2012) A bilayer-couple model of bacterial outer membrane vesicle biogenesis. mBio 3:e00297–11

Scherizer JW, Whiteley M (2013) Bacterial outer membrane vesicles in trafficking, communication and the host-pathogen interaction. J Mol Microbiol Biotechnol 23:118–130

Schwartz C, DeDonatis GM, Fang H, Guo P (2013) Revolution rather than rotation of AAA+ hexameric phi29 nanomotor for viral dsDNA packaging without coiling. Virology 443:28–39

Shao PP, Comolli LR, Bernier-Latmani R (2014) Membrane vesicles as a novel strategy for shedding encrusted cell surfaces. Minerals 4:74–88

Shetty A, Hickey WJ (2014) Effects of outer membrane vesicle formation, surface-layer production and nanopod development on themetabolism of phenanthrene by *Delftia acidovorand* Cs1–4. PLos ONE 9:e92143. doi:10.1471/journal.pone009214

Shetty A, Chen S, Tocheva EL, Jensen GJ, Hickey WJ (2011) Nanopods: a new bacterial structure and mechanism for development of outer membrane vesicles. PLoS ONE 6:e20725. doi:10.1371/journal.pone.0020725

Sikora AE (2013) Proteins secreted via the type II secretion system: smart strategies of *Vibrio cholera* to maintain fitness in different ecological niches. PLOS Pathog 9(2):e1003126. doi:10.1371/journal.ppat.1003126

Silverman M, Simon M (1974) Flagellar rotation and the mechanism of bacterial motility Nature 249:73–74

Silverman JM, Brunet YR, Cascales E, Mougous JD (2012) Structure and regulation of the type VI secretion system. Annu Rev Microbiol 66:453–472

Smith DE, Tans SJ, Smith SB, Grimes S, Anderson DL, Bustamante C (2001) The bacteriophage straight phi29 portal motor can package DNA against a large internal force. Nature 413:748–752

Tseng TT (2009) Protein secretion systems in bacterial-host associations. BMC Microbiol 9(Suppl):S2. doi:10.1186/1471-2180-9-S1-S2

Tsunoda SP, Aggler R, Toshida M, Capaldi RA (2001) Rotation of the c subunit oligomer in fully functional F_1F_0 ATP synthase. Proc Natl Acad Sci U S A 98:898–902

Uenoyama A, Miyata M (2006) Gliding ghosts of *Mycoplasma mobile*. Proc Natl Acad Sci U S A 102:12754–12758

Vale RD, Milligan RA (2000) The way things move: looking under the hood of molecular motor proteins. Science 288:88–95

Vargas M, Malvankar NS, Tremblay P-L, Leang C, Smith JA, Patel P, Snoeyenbos-West O, Kevin KP, Lovley DR (2013) Aromatic amino acids required for pili conductivity and long-range extracellular electron transport in *Geobacter sulfurreducens*. mBio 4(2):e00210-13

Verhey KJ, Dishinger J, Kee HL (2011) Kinesin motors and primary cilia. Biochem Soc Trans 39:1120–1125. doi:10.1042/BST0391120

Wai SN, Lindmark B, Soderblom T, Takade A, Westermark M, Jass J, Mizunoe Y, Uhlin BE (2003) Vesicle-mediated export and assembly of pore-forming oligomers of the enterobacterial ClyA cytotoxin. Cell 115:25–35

Wang MD, Schnitzer MJ, Yin H, Landick R, Gelles J, Block SM (1998) Force and velocity measured for single molecules of RNA polymerase. Science 282:902–907

Weber J, Senior AE (2003) ATP synthesis driven by proton transport in F_1F_0-ATP synthase. FEBS Lett 545:61–70

Weibel DB, Garstecki P, Ryan D, DoLuzio WR, Mayer M, Seto J, Whitesides GM (2005) Microoxen: microorganisms to move microscale loads. Proc Natl Acad Sci U S A 102:11963–11967

Willey JM, Sherwood LM, Woolverton CJ (2014) Prescott's microbiology. McGraw-Hill, New York

Yokoyama K, Hori T, Yamashino T, Hashikawa S, Barua S et al (2000) Production of shiga toxin by *Escherichia coli* measured with reference to the membrane vesicle-associated toxins. FEMS Microbiol Lett 192:139–144

Yoshida M, Muneyuki E, Hisabori T (2001) ATP synthase—a marvelous rotary engine of the cell. Nature Rev Mol Cell Biol 2:669–677

Chapter 6
The Mechanism of Bacterial Gliding Motility: Insights from Molecular and Cellular Studies in the Myxobacteria and Bacteroidetes

Morgane Wartel and Tâm Mignot

In bacteria, motility is a ubiquitous phenotypic trait allowing a variety of lifestyles and environmental adaptations. Bacterial motility is pivotal to biofilm formation and can also support virulence. For these reasons, motility and its regulation have been intensively studied in a variety of bacterial model systems. However, while these studies have shed light to fundamental aspects of bacterial motility, they have largely focused on 3D swimming in viscous media using a flagellum (Jarrell and McBride 2008). Yet, bacteria are also capable of moving over solid surfaces, which is important for a number of cooperative behaviors. One mode of surface locomotion, called twitching motility is relatively well understood and employs fibrillar appendages called *t*ype-*IV p*ili (T4P) that pull cells like retractile grappling hooks (Skerker and Berg 2001). Twitching motility is widespread in bacteria and although the molecular mechanisms underlying pilus function still need to be resolved, the propulsion mechanism is relatively unambiguous. Another form of surface motility, called gliding motility, occurs without the aid of pili, flagella, or any obvious organelles, and without observable changes in cell morphology (Jarrell and McBride 2008). Gliding motility is observed in very diverse phylogenetically unrelated bacterial groups and has been studied mechanistically in the Cyanobacteria, the Mollicutes, the Bacteroidetes, and the Myxobacteria (Mignot 2007). Studies in these organisms suggest that in each case, the gliding motility mechanism is distinct and does not result from a universal gliding machinery. Thus, gliding motility may have evolved independently on several occasions and may involve more than one motility mechanism. While mechanistic studies are available in the Cyanobacteria, the lack of molecular tools has hampered in-depth characterization of the motility mechanism and currently, the cyanobacterial motility machinery remains elusive. Molecular work in the Mollicutes has shown that *Mycoplasma* can use a variety of mechanisms involving the so-called terminal organelle of *Mycoplasma pneumoniae* and large leg proteins located at the "neck" of *Mycoplasma mobile* (Mignot 2007). Since the Mollicutes have a very particular cell architecture and their motility

T. Mignot (✉) · M. Wartel
Laboratoire de Chimie Bactérienne, CNRS UMR 7283, Aix-Marseille Université, Institut de Microbiologie de la Méditerranée, 31 chemin Joseph Aiguier, 13009 Marseille, France
e-mail: tmignot@imm.cnrs.fr

L. L. Barton et al. (eds.), *Nanomicrobiology,* DOI 10.1007/978-1-4939-1667-2_6

mechanisms are mostly likely unique and clade-specific, they are not discussed here (see Mignot 2007 for more information). In recent years, much progress has been made to understand gliding motility in the Myxobacteria and in the Bacteroidetes. While the gliding mechanisms share common features, key differences are also observed. In this book chapter, we review the latest findings on each of these systems and attempt to delineate general principles underlying this complex and widespread form of bacterial locomotion.

6.1 Gliding Motility in Myxococcus Xanthus

Myxococcus xanthus, a member of the delta-subgroup of bacteria, displays a remarkable multicellular lifestyle. When facing starvation, *Myxococcus* enters a developmental program where thousands of *Myxococcus* cells cooperate to build multicellular structures called fruiting bodies, wherein the cells differentiate into environmentally resistant spores (Kaiser 2003). To realize this life cycle*, M. xanthus* uses two distinct motility systems (Hodgkin and Kaiser 1979). One motility system, the so-called *s*ocial *motility* (S-motility), promoting the coordinated movement of large cell groups, consists of a polar T4P. S-motility is driven by the tight cooperation of T4P and a specific surface *e*xo*p*oly*s*accharide (EPS; Li et al. 2003). S-motility is therefore a cooperative form of twitching motility and has been reviewed extensively (Zhang et al. 2012). This book chapter discusses the second motility system, called the A-motility system. *Myxococcus* cells that lack T4P are still able to move as individual cells (hence the term *a*dventurous (A)-motility), smoothly along their long axis by a typical gliding motility process. Because this movement occurs in absence of visible extracellular organelles (Burchard 1981), its mechanism has been a mystery for a long time. One visible manifestation of A-motility is the deposition of a mucus (slime), readily observable by a phase contrast microscopy of A-motile *Myxococcus* cells (Beebe 1941). Since Cyanobacteria also deposit slime trails, which could be directly linked to the propulsion of cyanobacterial filaments (Dhahri et al. 2013; Hoiczyk and Baumeister 1998), it has also been proposed that *Myxococcus* A-motility is driven by slime secretion through jet-like secretory organelles located at the back of the cells. However, the recent characterization of the A-motility machinery and its localization in live moving cells argues strongly against this model. Moreover, slime secretion has been observed at high resolution which suggests a function in adhesion (see below).

6.1.1 The Myxococcus A-Motility Machinery

The A-Motility Machinery Forms at Bacterial Focal Adhesion The mechanism of A-motility was suggested in 2007 by single cell studies of a critical A-motility protein, AglZ. Using a strain expressing a functional AglZ–YFP fusion protein,

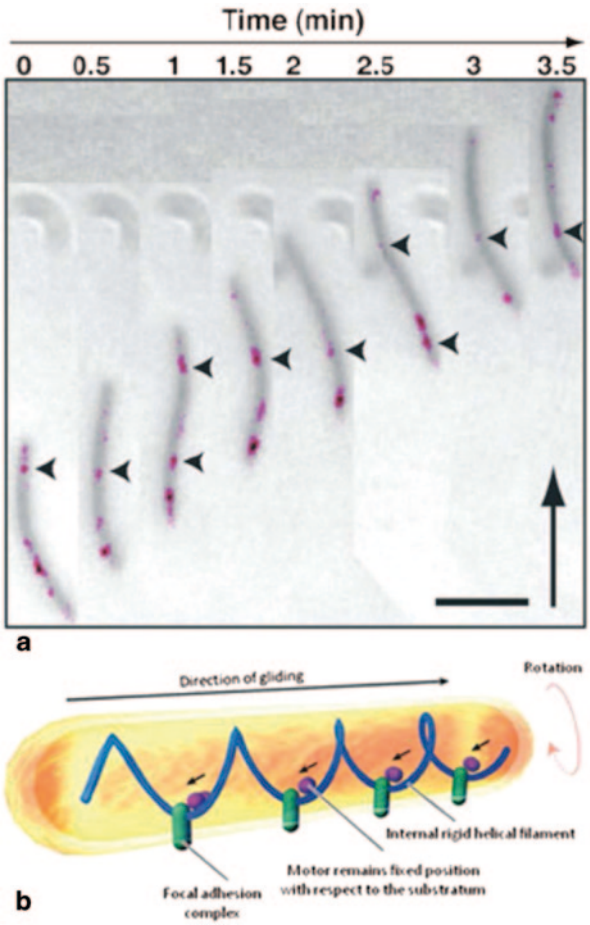

Fig. 6.1 The focal adhesion hypothesis. a AglZ–YFP localizes to periodic sites that remain fixed relative to the substratum in a moving cell. Overlay of the phase and the YFP (*magenta*, artificially colored for improved clarity) images captured every 30 s are shown. *Arrowheads* highlight selected *bright fluorescence* clusters. Scale bar = 2 μm (modified from Mignot 2007). **b** Motility mechanism suggested by Mignot et al. (2007). In this model, large focal adhesion complexes would penetrate the cell envelope, stick to the substratum at one end, and connect to cytoskeletal filaments at the other end. Cytoskeletal motor proteins would travel opposite to the direction of the cell and thus push backward (*small arrows*) against the adhesions, thus propelling the cell forward. (Modified from Nan and Zusman 2011)

Mignot et al. (2007) observed that AglZ localized in clusters, distributed at regular intervals along the cell body (Figure 6.1a). Remarkably, time-lapse experiments revealed that these clusters were initially assembled at the leading pole and retained a fixed position with respect of the substratum as the cell moved forward. Since the cell was in motion, the clusters appeared stationary relative to the substratum (hence a fixed reference), but they were in fact moving in the direction opposite to the direction of movement and at the same velocity. The clusters eventually reached the back of the cell where they became dispersed (Figure 6.1a). Based on these observations, Mignot et al. (2007) proposed that the AglZ clusters reflect the localization of the A-motility machinery. This machinery would consist of intracellular motors moving on cytoplasmic cytoskeletal filaments and transmitting force through the cell envelope, which ultimately would cause the forward translocation of the cell body (Figure 6.1b). This hypothesis predicted that the motility machinery localizes at the focal adhesion sites.

Identification of the A-Motility Machinery Although the AglZ protein might point to the localization of the motility machinery, it is not *per se* a structural component of this machinery because genetic evidence suggests that it functions to regulate its spatial positioning (Luciano et al. 2011; Mauriello et al. 2009). The structural components of the machinery itself have long remained elusive. In fact, the genetic evidence for the existence of A-motility was obtained as early as in 1979 by Hodgkin and Kaiser, who found that two distinct sets of genes promote *Myxococcus* motility independently (Hodgkin and Kaiser 1979). However, while the first set of genes was found to encode a T4P (the S-motility apparatus), the molecular identity of the A-motility system remained unknown until very recently. Over the years, several genetic screens have sought to identify the A-motility machinery; however, while approximately 50 genes were identified, their annotation did not reveal a conspicuous molecular machinery, mainly because the inactivation of many housekeeping genes is also likely to impair motility (Youderian et al. 2003; Yu and Kaiser 2007). In addition, transposons were found in many genes of unknown function, which also rendered the identification of a gliding machinery difficult (Youderian et al. 2003; Yu and Kaiser 2007).

To identify the gliding machinery proteins, 51 genes previously identified by transposon-based genetic screens (Youderian et al. 2003; Yu and Kaiser 2007) were reinvestigated under the assumption that if some of them encoded the actual machinery components, they must have coevolved. Doing so, three main genetic loci, a seven-gene operon (named *gltD-J*), a four-gene operon (*gltA-C* and *gltK*), and a three-gene operon (*aglR-S*; Figure 6.2a), for a total of 14 genes, became apparent (Luciano et al. 2011). Remarkably, the taxonomic distribution of these genes revealed that 7 of the 14 genes were clustered together in several bacterial genomes and this core set of genes contained genes of each of the three separate loci identified in *Myxococcus,* suggesting that they encode a functional machinery (Luciano et al. 2011). These findings suggested that the *Myxococcus* A-motility machinery may consist of up to 14 genes and could have emerged by the functional specialization of a broadly conserved core system of seven genes. The predicted function of the *agl* and *glt* genes also suggested that they encode a transenvelope complex (Figure 6.2b). Remarkably, the *agl* genes encode a flagellar stator homologue, a class of ion-driven motor proteins. The direct function of the *agl* and *glt* genes in A-motility was further proven experimentally (Luciano et al. 2011, see below) and thus the machinery was named Agl–Glt. An independent biochemical search of the A-motility machinery identified critical interactions between some of the Glt proteins as essential for A-motility, confirming that the A-motility machinery had been identified (Nan et al. 2010).

When possible, functional fusions were made to the components of the Agl–Glt complex. All tested proteins (GltD, GltF, AglQ, and AglR) localized to the focal adhesion sites together with AglZ, showing unambiguously that the *Myxococcus* A-motility machinery is assembled at these sites (Luciano et al. 2011; Nan et al. 2010).

The Motility Motor is a Flagellar Stator Homologue The *agl* genes encode proteins with similarities to the flagellar stator proteins (MotAB) or the TolQR/ExbBD proteins that energize colicin and iron siderophore transport, respectively

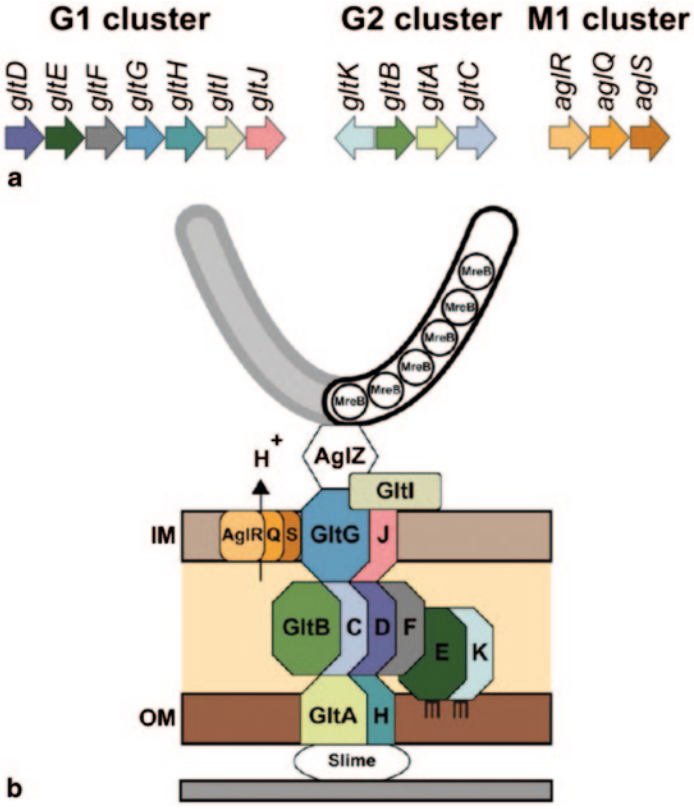

Fig. 6.2 The Agl–Glt complex. a Genetic organization of the 14 genes encoding the components of the gliding machinery in *Myxococcus xanthus*. The G1 and G2 clusters correspond to the *glt* genes, and M1 cluster corresponds to the *aglRQS* genes. **b** Predicted structures of the Agl–Glt machinery based on experimental and bioinformatics predictions. The PG is not represented because its connection to Glt proteins is unknown

(Sun et al. 2011). This class of bacterial proton-conducting channels operates by harnessing the proton gradient across the inner membrane to generate mechanical force (Cascales et al. 2000). Consistent with *p*roton *m*otive *f*orce (PMF) acting as the major energy source for A-motility, PMF uncoupling drugs (*c*arbonyl *c*yanide m-*c*hlorophenylhydrazone (CCCP)) and more specifically pH gradient-dissipating drugs (Nigericin), rapidly and reversibly inhibited A-motility (Sun et al. 2011). In frame deletions of the *algRQS* genes further led to a complete defect in gliding motility. The Agl complex is predicted to form a complex where AglR associates both with AglQ and AglS to form a transmembrane proton channel (Figure 6.2b). Consistent with this, the mutation of a conserved aspartate in AglQ (D28N) predicted to bind H^+ ions in the lumen of the channel, abolished A-motility (Sun et al. 2011). Importantly, the motility complex is still assembled at focal adhesions sites in the $AglQ_{D28N}$ mutant but it is not dynamics, further suggesting that the Agl complex

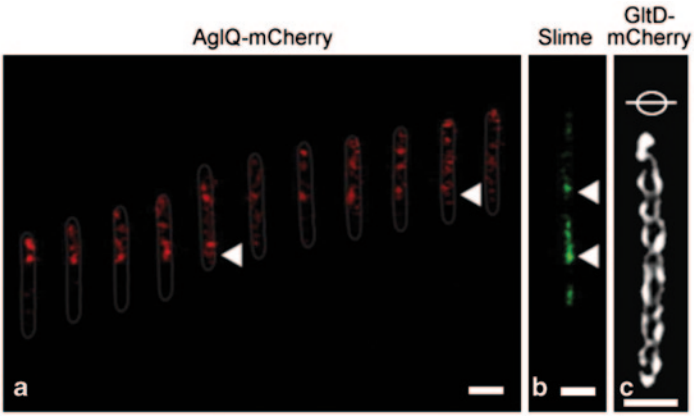

Fig. 6.3 Localization of *Myxococcus* motility proteins. a Time lapse of a cell expressing AglQ-mCherry is shown. Fixed clusters are marked by *white arrowheads*. *Fluorescent* micrographs were taken every 15 s. Scale bar = 1 μm (reprinted with permission from Ducret et al. 2012). **b** Slime patches are deposited where the Agl/Glt machinery assembles. Slime was stained with a lectin after the cell left the positions shown on *A* and *B*. *Triangular arrows* point to fixed AglQ-bright motility complexes at positions where conspicuous slime patches were deposited. Scale bar = 1 μm (reprinted with permission from Ducret et al. 2012). **c** Deconvolved images of potential *gltD-mCherry* helices. Scale bar = 1 μm. (reprinted with permission from Nan et al. 2011)

is not involved in the assembly of the complex but in its energization. Last, the localization of AglQ-mCherry overlapped with that of AglZ–YFP at the *f*ocal *a*dhesion *c*omplexes (FAC), proving that focal adhesions contain the energy-producing component of the motility machinery (Figure 6.3a; Sun et al. 2011). How exactly Agl motor activity translates into motion remains to be understood, but based on knowledge of TolQR-TolA studies, it is currently thought that a conformational change in the lumen of the Agl channel is transduced to the TolA-like GltG protein and ultimately to the bacterial outer membrane. Consistent with this, AglR has been shown to interact directly with GltG (Luciano et al. 2011). Force-generation by the Agl complex was shown directly by adding polystyrene beads to the outer surface of cells with an optical trap. When the beads collided with traveling complexes, they became bound and co-tracked with these complexes directionally towards the lagging cell pole. Experiments with *agl* mutants and PMF uncouplers proved that bead-transport was energized by the Agl complex (Sun et al. 2011).

6.1.2 The Mechanism of A-Motility

The molecular characterization and localization of major motility proteins strongly argues that A-motility is propelled by a periodically assembled transenvelope complex that links a molecular motor in the bacterial inner membrane to the outer substrate (Figure 6.2b). However, the exact mechanism by which the Agl–Glt complex powers motility remains to be determined. Ultimately, solving the mechanism

requires answers to several outstanding questions: What is the mechanism of force transduction and how does the complex transmit forces through the rigid cell wall? What is the mechanism of directionality and is there a track for the motility complex? How does the complex connect with the surface?

Evidence for the Existence of a Track The Agl–Glt machinery is thought to act as a stator that propels the cell as it threads along a rotor connected to rigid scaffolds in the cell. The bacterial MreB-actin cytoskeleton was initially proposed to constitute the rigid track because MreB depolymerization with the MreB-specific inhibitor A22 rapidly and reversibly blocks A-motility (Mauriello et al. 2010). Additionally, polystyrene beads and AglR motions are also blocked by the action of A22 (Nan et al. 2013; Sun et al. 2011). However, even though MreB may be essential for motility, it may not function as a motility rotor. First, the structure of the AglRQS motor suggests that it functions to generate a power stroke in the periplasmic space and not in the cytosolic compartment where MreB is localized. As mentioned above, AglRQS is a TolQR-like complex and this complex energizes envelope processes in the periplasmic space. Specifically, in the Tol-Pal system, the interaction between TolQR and TolA, the suspected energy transducer, likely allows dynamic contacts with the outer membrane through the Pal lipoprotein (Cascales et al. 2000). Since GltG is a TolA homologue, the power stroke of the AglRQS likely occurs in the periplasm. Second, in bacteria, MreB is centrally linked to the synthesis of new *p*eptido*g*lycan (PG; Domínguez-Escobar et al. 2011). Recently, MreB has been shown to form short patch-like bundles rather than a continuous helix as initially thought (Domínguez-Escobar et al. 2011; Garner et al. 2011; van Teeffelen et al. 2011). Therefore, it is unlikely that MreB could form a continuous track in *Myxococcus* cells. MreB may function to position the motility complex or allow its insertion in the PG or both.

Recent high-resolution tracking of single AglR particles suggested that they follow trajectories consistent with a helical path (Nan et al. 2013). Consistent with this, deconvolution microscopy suggests that GltD-mCherry forms a closed loop structure in the bacterial cell envelope (Figure 6.3c; Nan et al. 2011). However, deconvolution is prone to many artifacts and apparent helical structures may be interpreted with a grain of salt as shown by earlier interpretations of MreB helices. If the rigid track is a helix, the cell body should rotate with respect to its point of attachment to the substratum, which could be tested experimentally.

Contact with the Substrate—The Role of Slime Although slime deposition by gliding *Myxococcus* cells was observed as early as in the 1940s, its exact function has remained largely mysterious (Beebe 1941). Recently, Ducret et al. (2012) developed a new imaging method called *s*urface *e*nhanced *e*llipsometric *c*ontrast microscopy in *wet* condition (Wet-SEEC) to image slime deposition at high resolution. This analysis revealed that slime is deposited at constant rates underneath the cell body and that during motility, slime patches are specifically bound by the Agl–Glt gliding machinery (although the secretion of slime does not depend on the motility machinery, Figure 6.3b). These observations suggested that slime acts as a self-secreted substrate, favoring the connection between the outermost components

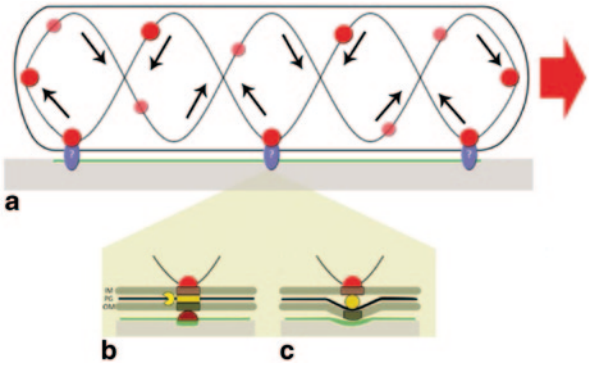

Fig. 6.4 The *Myxococcus xanthus* **gliding motility model. a** The *red arrow* represents the direction of movement. Motility motors loaded with the Glt complex (*big dark red circles*) or unloaded motors (*small transparent red circles*) translocate along an endless closed loop. Only the motors loaded with the Glt complex are proficient for movement. The machinery could afford the rigid PG by two different ways: **b** The motility complex may span the entire cell envelope and a PG-hydrolase may facilitate insertion of the complex through the PG. **c** Alternatively, the motility complex could deform the PG, creating surface depression and drag. Outer membrane proteins may, in this system, reinforce local contacts at the depressions

of the motility machinery and the underlying surface. The exact composition of slime is unknown but it appears to be composed of major carbohydrate polymer. More work is needed to determine the exact slime composition and how it becomes bound by the motility machinery.

The Current A-Motility Model During the past 5 years, the understanding of A-motility has made a tremendous leap forward and a new updated model can be proposed (Figure 6.4a). The motility machinery is composed by a stator formed by AglRQS, which is anchored in the bacterial inner membrane, and a rotor consisting of Glt proteins and/or the MreB cytoskeleton. Following their assembly at the leading cell pole, active motor AglRQS units become loaded with Glt proteins and the resulting complex then moves directionally along the helical track of the rotor toward the lagging cell pole. When the motility machinery reaches the face of the cell that is in direct contact with the substrate, it becomes immobilized locally (hence forming focal adhesions) by its interaction with slime, creating a drag force that propels the cell body forward. Persistent movements would result from an inherent cell asymmetry ensuring that the Agl motor moves along the helical track in two conformations: as an active motility machinery, when it is loaded with the Glt complex and moves from the leading cell pole to the lagging cell pole; or as an inactive machinery as it moves back in the opposite direction from the lagging pole to the leading pole. This idea is supported by the existence of pole-specific motility proteins that discriminate the leading and the lagging pole (Leonardy et al. 2010; Zhang et al. 2010). At the leading cell pole, a Ras-like small G-protein MglA is essential for the polar assembly of the motility complex, while its negative regulator, MglB is required for the inactivation of the motility complex at the opposite pole (Leonardy et al. 2010; Zhang et al. 2010).

Given that the motility motor is located in the bacterial inner membrane, it must interact with the substrate beyond the rigid bacterial cell wall. How this connection occurs is undetermined. At the point of attachment, the motility complexes could span the entire cell envelope (inner membrane, PG, and outer membrane) and engage elastic interactions with slime and the substrate with specific outer membrane proteins (Figure 6.4b). This hypothesis is supported by the presence of gliding proteins in each envelope layer (Figure 6.2b; Luciano et al. 2011), and by the observation that the slime is directly connected to the Agl–Glt machinery (Figure 6.3a, b; Ducret et al. 2012). However, such attachment implies that the Agl–Glt complex forms a continuous envelope-spanning complex that pokes through the PG layer and must traverse it at all times. This difficulty would be solved if the motility machinery is associated with a PG-degrading activity, i.e., a hydrolase, to degrade the PG locally, allowing its insertion in the PG (Figure 6.4b). Such hydrolase activity is yet to be found. Alternatively, as discussed above, the interaction with MreB could facilitate the insertion of the gliding machinery in the PG.

In an alternative mechanism, the gliding machinery would not cross the cell wall but would distort it when it is loaded with the Glt complex (Nan et al. 2011). This distortion would push against the outer membrane, literally creating bumps, and thus contact zones against the substratum (Figure 6.4c). Propulsion would then occur due to viscous coupling at the contact zones. Further experiments are needed to discriminate between these two possibilities, on one hand, *t*otal *i*nternal *r*eflection *f*luorescence (TIRF) microscopy suggests the existence of periodic undulations in the bacterial envelope in contact with the substrate, which is consistent with the viscous coupling mechanism (Nan et al. 2011); and on the other hand, the Glt proteins comprise several critical outer membrane proteins that should only be important if the coupling is elastic (Luciano et al. 2011).

6.2 Gliding Motility in the Bacteroidetes

Gliding motility is largely represented in the Bacteroidetes phylum, where it has been mostly studied in the Cytophagales and the Flavobacteriales. In this bacterial branch, gliding motility contributes to a number of cell behaviors and environmental adaptations (Jarrell and McBride 2008). Recently, gliding motility has been shown to contribute to the formation of uniquely structured biofilms with iridescent properties in *Cellulophaga* spp. (Kientz et al. 2012). At the molecular level, the mechanism of gliding motility has been mostly studied in *Flavobacterium*. Although many features of the gliding mechanism resemble gliding features in *Myxococcus xanthus,* there are also key differences. One fundamental difference is the speed of gliding in the μm/s range, which thus far exceeds the speed of *Myxococcus* gliding motility (μm/min), suggesting major differences in the motility engines. In this part of the chapter, we discuss recent progress in the study of *Flavobacterium johnsoniae* motility. Contrary to *Myxococcus xanthus*, the *Flavobacterium* motility engine has not been identified. But overall, the evidence suggests a propulsion

mechanism involving the helical trafficking of outer-membrane adhesins and the involvement of a new type of secretion system.

6.2.1 *Flavobacterium Gliding Involves a Repertoire of Outer Membrane Adhesins*

At the cell surface, *Flavobacterium* gliding motility involves two major adhesins, SprB and RemA (Figures 6.5 and 6.6a). SprB, a huge protein (669 kDa), is probably the major adhesin and is required for gliding on agar and to some extent gliding on glass (Nelson et al. 2008). The binding activity of RemA is only unmasked when *sprB* is deleted, suggesting that it plays partially redundant functions (Shrivastava et al. 2012). SprB is a large repetitive cell-surface protein with an extensive beta-sheet structure. When observed by electron microscopy on whole cells, SprB is readily visible as thin filamentous spikes that extrude outwards from the cell surface (Figure 6.5a; Nakane et al. 2013). How this conformation is linked to SprB function is unknown.

RemA is likely a polysaccharide-binding protein because it contains a lectin-type domain (Shrivastava et al. 2012). Consistent with this, liquid-grown cells clump in liquid cultures while an *remA* mutant does not. This suggests that RemA binds to a self-produced polysaccharide, a potential equivalent to the *Myxococcus* slime. Interestingly, the same genetic screen that led to the identification of RemA also identified three additional genes, *remC, wza,* and *wzc* (Shrivastava et al. 2012). *remC* gene encodes a putative glycosyltransferase and *wza and wzc* encode the octameric secretion pore and the inner membrane parts of a so-called *o*uter *m*embrane *a*uxiliary (OMA or Wza), a capsular polysaccharide secretion system. Since mutations in all three genes failed to form large cell aggregates, it is tempting to suggest that the substrate of this Wza system interacts with RemA. Additional RemA-like adhesins might participate to the motility process because many proteins of this type are encoded in the *Flavobacterium* genome.

6.2.2 *The Gliding Motility Mechanism Involves Helical Trafficking of the Surface Adhesins*

The evidence that the motility mechanism is linked to the directed motion of protein complexes at the cell surface was first provided by Lapidus and Berg, who in the early 1980s observed that particles are propelled at velocities matching the gliding speed when they are bound to the *Cytophaga* cell surface (Lapidus and Berg 1982). However, at that time, video microscopy techniques did not allow high-resolution tracking of the particles and the complex trajectories could not be computed into a coherent motility model. The recent identification of proteins such as RemA and SprB provided a new opportunity to track the surface dynamics of the motility components. Indeed, both RemA and SprB move directionally at the cell surface with

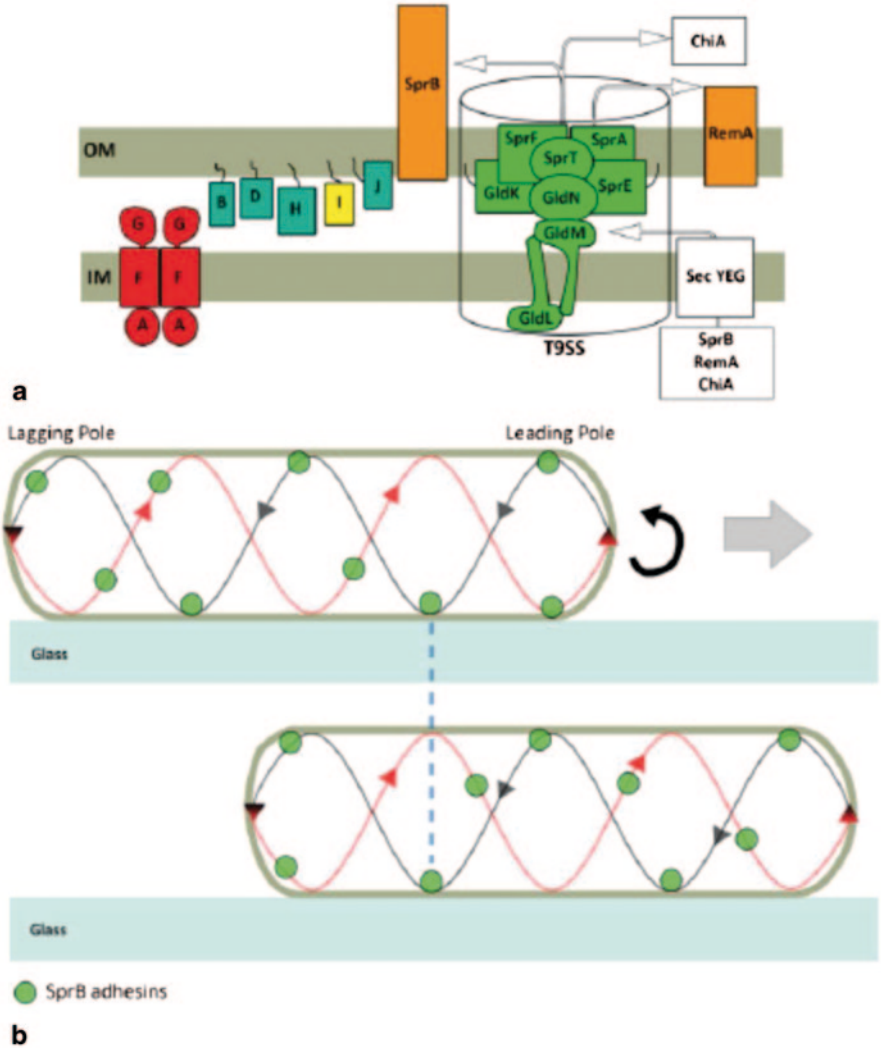

Fig. 6.5 Helical motions of the SprB adhesin. a SprB forms cell-surface filaments. Negative staining of wild-type and sprB deletion strains (reprinted with permission from Nakane et al. 2013). **b** Polystyrene spheres coated with anti-SprB move rapidly along the cell surface (reprinted with permission from Nelson et al. 2008). **c** Location of SprB observed by TIRF microscopy. A cell translocating to the right was analyzed. The SprB signals were colored from *red* to *blue* at 0.05-s intervals for 1.25 s and integrated into one image (*Lower*). (reprinted with permission from Nakane et al. 2013)

trajectories that resemble the particle movements described by Lapidus and Berg (Figure 6.5b; Nakane et al. 2013; Shrivastava et al. 2012).

Recently, the dynamics of SprB were resolved at high resolution by TIRF microscopy of moving *Flavobacterium* cells (Nakane et al. 2013). It was thus found

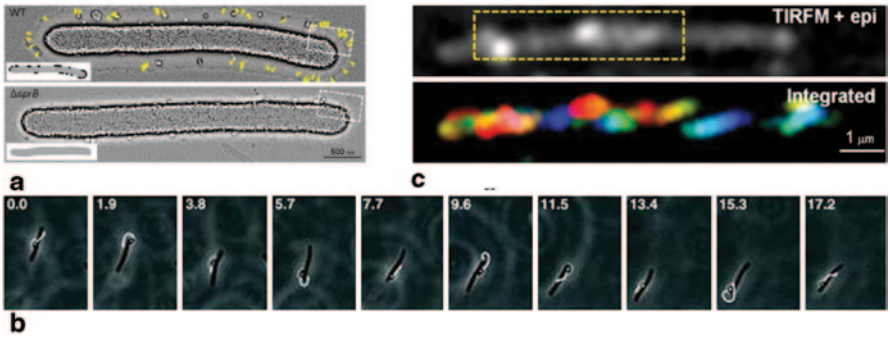

Fig. 6.6 Gliding mechanism of *F. johnsoniae*. **a** Proteins involved in *F. johnsoniae* gliding motility and protein secretion. SprB and RemA (*orange*) are thought to function as adhesins that are propelled along the cell surface by the some of the other proteins shown. GldA, GldF, and GldG (*red*) comprise an ATP-binding cassette transporter whose exact role in gliding is not known. GldI (*yellow*) is a peptidylprolyl isomerase involved in protein folding. Proteins in green (GldK, GldL, GldM, GldN, SprA, SprE, SprF, SprT) constitute the PorSS and are required for secretion of SprB and RemA and for motility. They also secrete the chitinase ChiA (*white*), which is not involved in motility. Proteins secreted by the PorSS have a predicted type-1 signal peptides and are predicted to be exported across the cytoplasmic membrane by the Sec system before being secreted across the outer membrane by the PorSS. Proteins in blue (GldB, GldD, GldH, and GldJ) are also required for gliding. Black lines indicate lipid tails on lipoproteins. **b** *Flavobacterium* gliding is thought to be powered by motors composed of Gld proteins in the cell envelope that propel adhesins, such as SprB, along the cell surface. Adhesin SprB moves along the left-handed helical loop and has two different states: SprB moving toward the front of the cell and SprB moving toward the rear of the cell. In a translocating cell, SprB moving toward the rear of the cell adheres to the surface, generating left-handed rotation and right-directed translocation of the cell

that SprB moves directionally along the length of the cell in a left-handed helical manner (Figure 6.5c). Two types of dynamic behaviors were observed: when SprB subunits moved from the leading to the lagging cell pole, they mostly formed fixed sites reminiscent of the *Myxococcus* focal adhesions. When SprB subunits reached the back of the cell, they were observed to move back to the leading cell pole along the same helical structure at a speed that matched the cell velocity. Similar to *Myxococcus xanthus,* gliding motility may be propelled by a helical machinery where active motility complexes travel directionally towards the lagging cell pole (Figure 6.6b). In the active state, corresponding to SprB moving in the anteroposterior direction, SprB presumably attaches to the substratum, immobilizing the cell body and thus propelling the cell forward. Upon reaching the rear of the cell, substrate-attached SprB adhesins are released from the substratum and recycled back to the front of the cell. How this inactivation occurs is unknown. SprB is only seen moving relative to the cell body in the posteroanterior direction. This implies that SprB adhesins have been modified at the cell rear to prevent their attachment when moving in the opposite direction (Figure 6.6b). Fundamentally, this propulsion mechanism is very similar to the propulsion mechanism of *Myxococcus*; however, the two systems are also very different, largely because the motility machineries at work are distinct.

6.2.3 The Flavobacterium Gliding Motility Genes and the Still Elusive Gliding Machinery

Over the years, the search of motility mutants has uncovered a total of 17 genes that appear to form the core of the motility complex (named *gldA, B, D, F, G, H, I, J, K, L, M, N, sprA, B, E, T,* and *remA*, Figure 6.6a; McBride and Zhu 2013). Many of these genes are only found in genomes of the Bacteroidetes phylum, suggesting that Bacteroidetes gliding employs a unique machinery (McBride and Zhu 2013). Although it appears that the structural core components of the motility machinery are likely encoded by some of the *gld* genes, the structure of the actual machinery remains unknown mostly because the motility motor cannot be predicted from annotations of the *gld* genes and a subset of the *gld* and *spr* genes encode a new secretion system, the PorSS or *t*ype-*IX s*ecretion *s*ystem (T9SS). This PorSS may have an accessory function in the secretion of key motility proteins, for example the terminal adhesins SprB and RemA (Sato et al. 2010; Shrivastava et al. 2013).

6.2.4 Gliding Motility Requires a New Secretion System and an Unknown Motor

In 2010, studies in *Porphyromonas gingivalis,* a periodontal pathogen from the Bacteroidetes subgroup, revealed that key virulence factors, such as the gingipains, are secreted by a novel secretion system (PorSS or T9SS) that is unique to the Bacteroidetes phylum (McBride and Zhu 2013; Sato et al. 2010). Remarkably, several of the newly identified *Porphyromonas* PorSS genes were paralogs to a subset of the *gld* and *spr* genes (*gldK*, *L*, *M*, *N* and *sprA*, *E*, *T*; Figure 6.6a). In *Flavobacterium,* these particular genes are required for the secretion of SprB and RemA, two essential motility outer membrane adhesins, suggesting that they also encode a PorSS-type secretion apparatus (Shrivastava et al. 2013). This finding potentially explains the long known coupling between motility and the ability of *Flavobacterium* to degrade chitin, because a critical chitinase is also secreted by the T9SS (Kharade and McBride 2014). Remarkably, the substrates of the T9SS contain a specific C-terminal domain (CTD) that seems important for their targeting to the secretion apparatus.

It is not presently clear whether the Bacteroidetes gliding machinery evolved by modular expansion of the T9SS or whether the T9SS and gliding machinery operate independently, the T9SS only being essential for gliding because it secretes the terminal motility adhesins. In bacteria, motility and secretion systems are often evolutionarily connected, conspicuously, the flagellum and *t*ype-*III s*ecretion system (T3SS; Abby and Rocha 2012) and the T4P and *t*ype-*II s*ecretion *s*ystem (T2SS; Pelicic 2008). In *Myxococcus,* the Agl–Glt system probably evolved through the specialization of a general class of surface transporters (Luciano et al. 2011), themselves evolved from a simpler core apparatus of unknown function, possibly a

protein secretion system. By analogy, the Bacteroidetes gliding machinery may well be modular and contain a T9SS for its assemblage and function.

To answer this question, it will be essential to characterize the protein system that energizes motility. As discussed above, flagellar stator homologues power *Myxococcus* gliding motility. In *Flavobacterium,* several studies also indicate that the PMF could be the energy source for gliding motility (Dzink-Fox et al. 1997; Nakane et al. 2013). Specifically, Dzink-Fox et al. showed that acetate, a protonophore known to dissipate the PMF, inhibits cell movements (Dzink-Fox et al. 1997). This effect is unlikely the indirect consequence of a block in T9SS secretion because the surface movements of SprB is blocked rapidly and reversibly by CCCP, which also dissipates the PMF across the cytoplasmic membrane (Nakane et al. 2013). Thus, similar to *Myxococcus,* proton-conducting channels of the inner membrane may energize motility. However, amongst the known Gld proteins, none have canonical features of flagellar Mot or *Myxococcus* Agl proteins. The motor genes may still need to be identified but it is also possible that the PMF acts at another level of the motility process and alternatively, ATP could fuel the motility engine. GldF and GldG were initial motor candidates because they are predicted components of an ATP-binding cassette transporter. However, although GldF and GldG are required for *F. johnsoniae* gliding, they are not present in all gliding Bacteroidetes phylum, suggesting that they are not core components of the gliding motility machinery (McBride and Zhu 2013).

In the future, it will be critical to identify the motility motor, which presumably localizes to the bacterial inner membrane (Nakane et al. 2013). Whatever the exact identity of the motor and its source of energy, it must span the bacterial inner membrane and transduce its activity beyond the periplasmic space to the outer membrane adhesins. In *Flavobacterium,* interactions with the surface are mediated by outer membrane adhesins, which clearly implies that the molecular motor must interact with the outer membrane through the PG. How this occurs is unknown. The evidence for the existence of a helical track is strong but the identity of that track is unknown.

6.3 General Conclusions

In recent years, tremendous progress has been made in the understanding of bacterial gliding motility, this long mysterious process occurring in absence of visible extracellular appendages. Studies from *Myxococcus* and *Flavobacterium* provide key and complementary pictures to understand this complex cellular behavior. Work in *Myxococcus* has tremendously improved our understanding of the intracellular protein dynamics that underlie the gliding process. Clearly, the local and transient immobilization of inner membrane motors and force transduction through the cell envelope is critical for cell motion. However, in this system, the exact propulsion mechanism remains unclear. Circumstantial evidence, such as the potential helical arrangement of GltD and possible rotational motions of motor subunits, suggest

the existence of a helical rotor. In *Flavobacterium,* the helical motion of motility adhesins is strongly supported, further suggesting that bacterial gliding motility is linked to rotational helical tracks in the cell envelope. While this exciting parallel suggests a common mechanism, it should be considered with cautious because the gliding motility machineries are not identical and there are tremendous differences in the gliding motility speeds between the two organisms. Further understanding thus awaits that the gliding machinery and motor be identified in *Flavobacterium*. Similarly, the outer membrane dynamics of the *Myxococcus* Agl–Glt machinery will have to be characterized to confirm the existence of the helical rotor.

Beyond the understanding of the exact motility mechanism, studies of bacterial gliding motility will likely deeply impact our understanding of protein movements and dynamics of the bacterial cell envelope. In this direction, studies of *Myxococcus* motility have already shown that the motility machinery is related to a new class of transport systems that contribute to the surface anchoring of capsular-type exopolysaccharides (Wartel et al. 2013).

References

Abby SS, Rocha EPC (2012) The non-flagellar type III secretion system evolved from the bacterial flagellum and diversified into host-cell adapted systems. PLoS Genet 8:e1002983

Beebe JM (1941) The morphology and cytology of *Myxococcus xanthus*. N Sp J Bacteriol 42:193–223

Burchard RP (1981) Gliding motility of prokaryotes: ultrastructure, physiology, and genetics. Annu Rev Microbiol 35:497–529

Cascales E, Gavioli M, Sturgis JN, Lloubès R (2000) Proton motive force drives the interaction of the inner membrane TolA and outer membrane pal proteins in *Escherichia coli*. Mol Microbiol 38:904–915

Dhahri S, Ramonda M, Marlière C (2013) In-situ determination of the mechanical properties of gliding or non-motile bacteria by atomic force microscopy under physiological conditions without immobilization. PLoS ONE 8:e61663

Domínguez-Escobar J, Chastanet A, Crevenna AH, Fromion V, Wedlich-Söldner R, Carballido-López R (2011) Processive movement of MreB-associated cell wall biosynthetic complexes in bacteria. Science 333:225–228

Ducret A, Valignat M-P, Mouhamar F, Mignot T, Theodoly O (2012) Wet-surface-enhanced ellipsometric contrast microscopy identifies slime as a major adhesion factor during bacterial surface motility. Proc Natl Acad Sci U S A 109:10036–10041

Dzink-Fox JL, Leadbetter ER, Godchaux W 3rd (1997) Acetate acts as a protonophore and differentially affects bead movement and cell migration of the gliding bacterium *Cytophaga johnsonae* (*Flavobacterium johnsoniae*). Microbiol Read Engl 143(Pt 12):3693–3701

Garner EC, Bernard R, Wang W, Zhuang X, Rudner DZ, Mitchison T (2011) Coupled, circumferential motions of the cell wall synthesis machinery and MreB filaments in *B. subtilis*. Science 333:222–225

Hodgkin J, Kaiser D (1979) Genetics of gliding motility in Myxococcus-Xanthus (Myxobacterales)—2 gene systems control movement. Mol Gen Genet 171:177–191

Hoiczyk E, Baumeister W (1998) The junctional pore complex, a prokaryotic secretion organelle, is the molecular motor underlying gliding motility in cyanobacteria. Curr Biol 8:1161–1168

Jarrell KF, McBride MJ (2008) The surprisingly diverse ways that prokaryotes move. Nat Rev Microbiol 6:466–476

Kaiser D (2003) Coupling cell movement to multicellular development in myxobacteria. Nat Rev Microbiol 1:45–54

Kharade SS, McBride MJ (2014) *Flavobacterium johnsoniae* chitinase ChiA is required for chitin utilization and is secreted by the type IX secretion system. J Bacteriol 196:961–970

Kientz B, Ducret A, Luke S, Vukusic P, Mignot T, Rosenfeld E (2012) Glitter-like iridescence within the bacteroidetes especially Cellulophaga spp.: optical properties and correlation with gliding motility. PLoS ONE 7:e52900

Lapidus IR, Berg HC (1982) Gliding motility of Cytophaga sp. strain U67. J Bacteriol 151:384–398

Leonardy S, Miertzschke M, Bulyha I, Sperling E, Wittinghofer A, Sogaard-Andersen L (2010) Regulation of dynamic polarity switching in bacteria by a Ras-like G-protein and its cognate GAP. Embo J 29:2276–2289

Li Y, Sun H, Ma X, Lu A, Lux R, Zusman D, Shi W (2003) Extracellular polysaccharides mediate pilus retraction during social motility of *Myxococcus xanthus*. Proc Natl Acad Sci U S A 100:5443–5448

Luciano J, Agrebi R, Le Gall AV, Wartel M, Fiegna F, Ducret A, Brochier-Armanet C, Mignot T (2011) Emergence and modular evolution of a novel motility machinery in bacteria. PLoS Genet 7:e1002268

Mauriello EM, Nan B, Zusman DR (2009) AglZ regulates adventurous (A-) motility in *Myxococcus xanthus* through its interaction with the cytoplasmic receptor, FrzCD. Mol Microbiol 72:964–977

Mauriello EMF, Mouhamar F, Nan B, Ducret A, Dai D, Zusman DR, Mignot T (2010) Bacterial motility complexes require the actin-like protein, MreB and the Ras homologue, MglA. EMBO J 29:315–326

McBride MJ, Zhu Y (2013) Gliding motility and Por secretion system genes are widespread among members of the phylum bacteroidetes. J Bacteriol 195:270–278

Mignot T (2007) The elusive engine in *Myxococcus xanthus* gliding motility. Cell Mol Life Sci 64:2733–2745

Mignot T, Shaevitz JW, Hartzell PL, Zusman DR (2007) Evidence that focal adhesion complexes power bacterial gliding motility. Science 315:853–856

Nakane D, Sato K, Wada H, McBride MJ, Nakayama K (2013) Helical flow of surface protein required for bacterial gliding motility. Proc Natl Acad Sci U S A 110:11145–11150

Nan B, Zusman DR (2011) Uncovering the mystery of gliding motility in the myxobacteria. Annu Rev Genet 45:21–39

Nan B, Mauriello EM, Sun IH, Wong A, Zusman DR (2010) A multi-protein complex from *Myxococcus xanthus* required for bacterial gliding motility. Mol Microbiol 76:1539–1554

Nan B, Chen J, Neu JC, Berry RM, Oster G, Zusman DR (2011) Myxobacteria gliding motility requires cytoskeleton rotation powered by proton motive force. Proc Natl Acad Sci U S A 108:2498–2503

Nan B, Bandaria JN, Moghtaderi A, Sun I-H, Yildiz A, Zusman DR (2013) Flagella stator homologs function as motors for myxobacterial gliding motility by moving in helical trajectories. Proc Natl Acad Sci U S A 110:E1508–E1513

Nelson SS, Bollampalli S, McBride MJ (2008) SprB is a cell surface component of the *Flavobacterium johnsoniae* gliding motility machinery. J Bacteriol 190:2851–2857

Pelicic V (2008) Type IV pili: e pluribus unum? Mol Microbiol 68:827–837

Sato K, Naito M, Yukitake H, Hirakawa H, Shoji M, McBride MJ, Rhodes RG, Nakayama K (2010) A protein secretion system linked to bacteroidete gliding motility and pathogenesis. Proc Natl Acad Sci U S A 107:276–281

Shrivastava A, Rhodes RG, Pochiraju S, Nakane D, McBride MJ (2012) *Flavobacterium johnsoniae* RemA is a mobile cell surface lectin involved in gliding. J Bacteriol 194:3678–3688

Shrivastava A, Johnston JJ, van Baaren JM, McBride MJ (2013) *Flavobacterium johnsoniae* GldK, GldL, GldM, and SprA are required for secretion of the cell surface gliding motility adhesins SprB and RemA. J Bacteriol 195:3201–3212

Skerker JM, Berg HC (2001) Direct observation of extension and retraction of type IV pili. Proc Natl Acad Sci U S A 98:6901–6904

Sun M, Wartel M, Cascales E, Shaevitz JW, Mignot T (2011) Motor-driven intracellular transport powers bacterial gliding motility. Proc Natl Acad Sci U S A 108:7559–7564

Van Teeffelen S, Wang S, Furchtgott L, Huang KC, Wingreen NS, Shaevitz JW, Gitai Z (2011) The bacterial actin MreB rotates, and rotation depends on cell-wall assembly. Proc Natl Acad Sci U S A 108:15822–15827

Wartel M, Ducret A, Thutupalli S, Czerwinski F, Le Gall A-V, Mauriello EMF, Bergam P, Brun YV, Shaevitz J, Mignot T (2013) A versatile class of cell surface directional motors gives rise to gliding motility and sporulation in *Myxococcus xanthus*. PLoS Biol 11:e1001728

Youderian P, Burke N, White DJ, Hartzell PL (2003) Identification of genes required for adventurous gliding motility in *Myxococcus xanthus* with the transposable element mariner. Mol Microbiol 49:555–570

Yu R, Kaiser D (2007) Gliding motility and polarized slime secretion. Mol Microbiol 63:454–467

Zhang Y, Franco M, Ducret A, Mignot T (2010) A bacterial Ras-like small GTP-binding protein and its cognate GAP establish a dynamic spatial polarity axis to control directed motility. PLoS Biol 8:e1000430.

Zhang Y, Ducret A, Shaevitz J, Mignot T (2012) From individual cell motility to collective behaviors: insights from a prokaryote, *Myxococcus xanthus*. FEMS Microbiol Rev 36:149–164

Chapter 7
Nanoparticles Formed by Microbial Metabolism of Metals and Minerals

Larry L. Barton, Francisco A. Tomei-Torres, Huifang Xu and Thomas Zocco

7.1 The Scope of Microbial Activities

Microorganisms have developed considerable capability of interacting with inorganic chemicals in the biosphere as a result of extensive evolutionary activities. Numerous efforts have developed our appreciation of these microbial–metal interactions. The role of bacteria, archaea, and fungi in key biogeochemical cycles of metals and metalloids, has been the subject of several recent reviews (Barton and Northup 2011; Barton et al. 2010; Gadd 2010; Konhauser 2007) where the emphasis was on mineral transformations.

As the focus was directed to environmental pollution, the interactions between microbes and trace metal(loid)s (e.g., Ag, As, Be, Cd, Cr, Cu, Hg, Ni, Pb, Sb, Se, Tl, and Zn) in the terrestrial and aquatic ecosystem have received considerable attention (Sparks 2005). Following numerous laboratory studies and field applications, it became apparent that an effective strategy for detoxification of metal(loid)-containing environments is to employ microorganisms (Banfield and Nealson 1997; Lovley 2000).

In optimizing the efforts for bioremediation of metals, numerous studies were conducted on the bacterial cell–metal interface, and new systems of metal bioprocessing were developed for treatment of metal-contaminated water and

L. L. Barton (✉)
Department of Biology, University of New Mexico, MSCO3 2020, Albuquerque, NM 87131-0001, USA
e-mail: lbarton@unm.edu

F. A. Tomei-Torres
Division of Toxicology and Human Health Sciences, Agency for Toxic Substances and Disease Registry, Atlanta, GA, USA

H. Xu
Department of Geoscience, University of Wisconsin, Madison, WI, USA

T. Zocco
Materials Science Division, Los Alamos National Laboratory, Los Alamos, NM, USA

L. L. Barton et al. (eds.), *Nanomicrobiology,* DOI 10.1007/978-1-4939-1667-2_7

radionuclide-containing streams (Lloyd et al. 2003; Gadd 2010; http://www.paques.nl) as well as for production of high-value commercial materials (Sharma et al. 2012; Suresh 2012). A feature associated with many of these microbe–metal(loid) interactions is the formation or utilization of finely divided particles of the uncharged metal or metalloid that are colloidal in nature. This chapter focuses on the mechanisms that transform metals or metalloids to nanoparticles.

7.2 Metallic and Metalloid Nanoparticles

The formation of nanoparticles by bacteria is the result of several different processes. These include specific enzymes, precipitation reactions with metabolic end products, reduction or immobilization by thiol groups, and oxidation–reduction reactions with cytochromes and other electron transport proteins. Most of the metals associated with nanoparticle utilization or production involve redox-active elements. In certain instances, the flow of electrons from metal(loid) metabolism is coupled to cellular energy production. Many metal(loid) elements are redox active, where the oxidized form is soluble and shows significant toxicity, while the reduced form is less soluble and less toxic. Some of the notable examples of these mechanisms for nanoparticle production have been recently reviewed (Thakkar et al. 2010; Popescu et al. 2010; Li et al. 2011).

7.2.1 Au^0

Complexes of cationic Au(III) and Au(I) are highly toxic to organisms with detrimental effects noted with concentrations of 0.4 ppb Au(III; Nies 1999). As a defense to Au toxicity, bacteria have developed highly regulated genetic systems. In *Salmonella enterica,* which does not produce nanoparticles of Au^0, the internal concentration of cationic gold is regulated by a transcriptional activator (GolS), a P-type ATPase exporter (GolT), and a metallochaperone (GolB; Checa et al. 2007).

As reviewed by Lengke et al. (2006a), the precipitation of gold has been reported for several heterotrophic bacteria and cyanobacteria, including the formation of insoluble gold complexes with sulfur and phosphate. The cyanobacterium, *Plectonema boryanum,* produces elemental gold from Au(III) salts by a multistep process. Following the exposure of *P. boryanum* to Au(III) chloride, there is the formation of amorphous Au(I) sulfide on the cell walls with the ultimate production of octahedral platelets of Au^0 (Lengke et al. 2006a).

Chemolithotrophic bacteria and archaea employ unique electron transport proteins to reduce inorganic compounds for energy. Many of these have been found to reduce Au(III) to Au^0. Hydrogenase was associated with the reduction of Au(III) to Au^0 by several strains of Fe(III)-reducing bacteria (*Geobacter ferrireducens* and *Shewanella algae*) and archaea (*Pyrobaculum islandicum* and *Thermotoga maritima*; Kashefi et al. 2001).

Gold nanoparticles were produced from the Au(I)–thiosulfate complex by sulfate-reducing *Desulfovibrio* sp. (Lengke and Southam 2006a). Initially, spherical gold nanoparticles were produced inside the sulfate-reducing bacterial cell, and the living cells released octahedral gold crystals or framboid-like Au^0 structures from the cell. These nanoparticles were about 1.5 μm in diameter. With continued incubation, gold foils were found surrounding silicate grains that had been added to the culture of *Desulfovibrio* sp.

Considerable attention has been given to study the systems for deposition of elemental gold by *Cupriavidus metallidurans* (Reith et al. 2009). When Au(III)–hydroxychloride complexes were added to *C. metallidurans,* the cells rapidly accumulated Au(III) inside the cells and reduced it to Au(I). Molecular species of both Au(I)-S and Au(I)-C were detected in the cells, and Au^0 collected in the periplasm. Reith et al. (2009) suggest that the Au(I)-S species is reduced to Au^0 and that the Au(I)-C species may reflect the methylation of gold. Multiple regions of reduction of Au(I) to Au^0 may occur in the cell with nanoparticles of Au^0 in the cytoplasm and periplasm.

Production of gold nanoparticles by the bacterium *Delftia acidovorans* is mediated by an extracellular compound (Johnson et al. 2013). A secondary metabolite resembling a bacterial siderophore is produced and secreted from the cell. This metabolite, delftibactin, is considered to convert gold ions to gold particles and has attracted the attention of commercial groups. This use of bacteria to extract gold would be less destructive on the environment than the current chemical extraction processes.

7.2.2 Ag^0

With over 300 tons of silver nanoparticles produced annually, there is considerable interest to find appropriate methods for synthesis that are cost effective and eco-friendly (Lengke and Southam 2007; Sintubin et al. 2011). There are two major processes reported for microbial production of silver nanoparticles: extracellular production and enzyme-mediated synthesis. In the nonenzymatic production of silver nanoparticles, deposition of silver particles occurs on the surface of the bacterial cell or in the extracellular growth media.

While not all bacteria have the potential for reduction of silver, extracellular Ag^0 has been reported with *Streptomyces glaucus, Spirulina platensis, Pseudomonas aeruginosa, Escherichia coli, Bacillus subtilis, Bacillus megaterium, Lactobacillus* spp., *Pediococcus pentosaceus, Enterococcus facium, Lactococcus garvieae,* and *Streptococcus thermophilus* (El-Raheem et al. 2011; Natarajan et al. 2010; Oza et al. 2012; Prakash et al. 2010; Tsibakhashvili et al. 2011). The chemical mechanism accounting for this extracellular reduction has not been established.

The fabrication of silver nanoparticles by bacteria has been reviewed by Suresh (2012). *S. oneidensis* converts the colorless solution containing Ag(I) to grey–black Ag^0. The silver nanoparticles absorb light at 410 nm, are 4 nm in diameter, and are red in color. However, these nanoparticles readily aggregate to produce larger

blackish particles. The small Ag^0 nanoparticles can be stabilized with capping agents or appropriate solvents. There is considerable interest in these silver nanoparticles because of their bactericidal properties and numerous commercial applications.

The enzymatic biosynthesis of silver nanoparticles has been demonstrated using cultures of *P. boryanum* (a cyanobacterium; Lengke et al. 2007a) and *E. coli* (Gurunathan et al. 2009). From research by Vaidyanathan et al. (2010) with *Bacillus licheniformis,* the reduction of silver ions may be attributed to nitrate reductase. In *Geobacter sulfurreducens*, the enzymatic reduction of silver appears to be associated with *c*-type cytochromes (Law et al. 2008). With *Lactobacillus fermentum,* silver nanoparticles with an average diameter of 11.2 nm are localized inside the cell, and the enzymes responsible for this reduction are not established (Sintubin et al. 2009).

7.2.3 Pd^0

Several strains of anaerobic bacteria are capable of reducing $Pd(NH_3)_4Cl$ to the elemental form (Pd^0). The reduction of Pd(II) by *Desulfovibrio desulfuricans* (Lloyd et al. 1998) and *D. fructosivorans* (Mikheenko et al. 2008) is attributed to hydrogenase activity. In *Cupriavidus necator, Pseudomonas putida* and *Paracoccus denitrificans* with formate as the electron donor, Pd^0 nanoparticles were produced in the periplasmic space (Bunge et al. 2010). Spherical and elongate nanoparticles of Pd^0 were produced on the cell surface of a cyanobacterium (Lengke et al. 2007c), although the mechanism of palladium reduction by this phototroph is unresolved.

7.2.4 Pt^0

The microbial reduction of $PtCl_6^{2-}$ to Pt^0 is a multistep process where Pt(IV) is first transported into the cell, Pt(IV) is reduced to Pt(II) which is ultimately reduced to metallic platinum. Resting cells of *S. algae* (Konishi et al. 2007) deposit Pt^0 nanoparticles of 5 nm in the periplasm. Sulfate reducers were reported by Rashamuse and Whiteley (2007) to reduce soluble Pt(IV).

Nanoparticles of Pt are found in the periplasm of resting cells of sulfate reducers. The reduction of Pt(IV) is attributed to hydrogenase activity (Rashamuse and Whiteley 2007). In sulfate reducers where multiple hydrogenase enzymes occur, it has been reported that Pt(VI) is reduced by a hydrogenase in the cytoplasm, and after platinum is converted to Pt(II), the periplasmic hydrogenase reduces Pt(II) to Pt^0 in the periplasm (Riddin et al. 2009).

Spherical nanoparticles of 30–300 nm are produced by *P. boryanum,* a cyanobacterium, interacting with platinum (VI) chloride (Lengke et al. 2006b, c). In *P. boryanum*, the initial complexation of Pt(IV) onto the cell surface is proposed to involve organic sulfur and phosphorus. The specificity for binding of Pt(IV) on the cell surface is further supported by the report that C=O bonds are required to absorb Pt^{4+} into the cell wall of *B. megaterium* prior to Pt^0 formation (Liu et al. 2000).

Table 7.1 Characteristics of a selection of nanoparticles of metal(loids) produced by bacteria

Example	Color	Average size (nm)	Charge (mV)	Maximum absorption (nm)	Reference
Au^0	Ruby red	12±5	−16.6±2	528	Suresh 2012
Ag^0		4±1.5	−12±2	410	Suresh et al. 2010
	Violet	30±10			Xu et al. 2004
	Blue	50±10			
	Green	70±10			
	Red	90±10			
Se^0	Red	250-350	−5.78		Barton et al. 1992
		~300		~575	Oremland et al. 2004
		150–200	−47.86		Dhanjai and Cameotra 2010
CdS	Yellow	4		424	Holmes et al. 1997b
		10–20		410	Prakash et al. 2010
PbS	Black	10–20		330	Prakash et al. 2010
		170–180	−35.28		Barton et al. 1992
ZnS		2–5		396	Labrenz et al. 2000; Duran and Seabra 2012
UO_2	Black	1–5			Marshall et al. 2006
CuO	Brown	80–128		265	Honary et al. 2012

7.2.5 UO_2

The interest in bioremediation of uranium mill tailing sites in the USA (Landa 2005; Barton and Fauque 2009) resulted in the examination of bacterial immobilization of uranium. Uranyl, UO_4^{2-}, ion is toxic and soluble but reduction of uranium to uraninite, UO_2, an insoluble nanoparticle is produced with reduced toxicity. The uraninite nanoparticle produced by *Shewanella oneidensis* is reported to be 1–5 nm in diameter (Marshall et al. 2006). As listed in Table 7.1, the anaerobic reduction of uranyl ion can be accomplished by several different species of bacteria. With intact cells of several bacteria, *c*-type cytochromes are important for uranyl reduction. Reduction of uranyl ion by *G. sulfurreducens* was markedly depressed when mutants lacking *c*-type cytochromes in the outer membrane were compared to wild-type cultures (Shelobolina et al. 2007). The formation of uraninite nanoparticles by *S. oneidensis* was dependent on *c*-type cytochromes (Marshall et al. 2006). Uranium reduction by *D. desulfuricans* G20 (currently *Desulfovibrio alaskensis*) was reduced but not eliminated in mutants lacking periplasmic *c*-type cytochrome. (Payne et al. 2002).

Cell-free extracts or stationary phase cells have been used to reduce uranyl ion to uraninite nanoparticles. Cytochrome c_3 from *Desulfovibrio vulgaris* (Lovley et al. 1993c) and *c*-type cytochromes in the outer membrane of *S. oneidensis* MR-1 (Marshall et al. 2006) are important for uranium nanoparticle formation. Reduction of uranyl ion to uraninite has been reported for *Deinococcus radiodurans* R1 (Fredrickson et al. 2000), *D. desulfuricans* (Tucker et al. 1998,2000), *Desulfovibrio aculatus, Desulfovibrio baarsii, Desulfovibrio sulfodismutans, Geobacter*

(Lovley et al. 1993b), *Clostridium* sp. (Francis et al. 1994), and *Veillonella atypical* (Wolfolk and Whiteley 1962).

Several strains of bacteria have been found to couple growth to the reduction of U(VI) to U(IV). The mesophilic *Geobacter, Shewanella*, and *Desulfotomaculum* (Pietzsch and Babael 2003; Tebo and Obraztsova 1998; Wade and DiChristina 2000) obtain energy from the formation of nanoparticles of U(IV), while examples of thermophiles with this capability include *Thermophus scotoductus, P. islandicum, Thermoferrabacterium ferrireducens,* and *Thermoanaerobacter* sp. (Khijniak et al. 2005; Kashefi and Lovley 2000; Kieft et al. 1999; Roh et al. 2002). However, the specific enzymes involved in these energy-coupling activities have yet to be determined. The end product formed by *T. ferrireducens* is noteworthy because it is not uraninite but ningyoite [$(CaU(PO_4) \cdot H_2O$] (Khijniak et al. 2005).

Dried samples of UO_2 nanoparticles are relatively stable; however, exposure of moist samples of UO_2 to the air results in rapid oxidation to UO_4^{2-}. The UO_2 nanoparticles produced by the anaerobic bacteria are most commonly found in the periplasm of bacteria, at the external surface of the bacterial cell or in the extracellular matrix.

7.3 Production of Metalloid Particles

7.3.1 Se^0

One system for elemental selenium formation in bacteria involves dissimilatory reduction processes where the growth of the organism is coupled to the reduction of selenate with the concomitant production of Se^0. There are about 16 different species of bacteria and archaea that have the capability of selenate and selenite respiration (Oremland et al. 2004; Blumb et al. 1999) and of these, *Sulfurospirillum barnesii, Bacillus selenitireducens*, and *Thauera selenatis* have received the most attention. The selenate reductase in *T. selenatis* is a trimeric molybdenum enzyme located in the periplasm that produces selenite (Schröder et al. 1997). The selenate reductases in *S. barnesii*, *Bacillus arseniciselenatis,* and *Bacillus macyae* are membrane bound and interface with the electron transport system (Lenz et al. 2011; Afkar et al. 2003; Santini et al. 2004). The mechanism of selenite reduction in the cytoplasm is not entirely clear; however, nitrate reductase in *Thauer selenatis* will reduce selenite to elemental Se (DeMoll-Decker and Macy 1993). A selenite reductase has been isolated from *Candida albica* (Falcone and Nickerson 1963). To reduce selenite to Se^0, this fungal enzyme requires glutathione (GSH), nicotinamide adenine dinucleotide phosphate (NADP) plus electron donor, and may be part of the assimilatory selenium reduction system.

Selenium resistance is broadly distributed in microorganisms which reduce selenate or selenite to Se by mechanisms that are not linked to respiration and do not contribute to bacterial energetics (Oremland et al. 2004). While reduction of

selenite is widely spread throughout bacteria, archaea, and fungi, relatively fewer organisms have been reported to reduce selenate to Se^0. A partial listing of the microorganisms that form Se^0 from selenite reduction include *Chrysiogenes arsenatis* (Kraft and Macy 1998), *Duganella* sp. and *Agrobacterium* sp. (Bajai et al. 2012), *Bacillus cerus* (Dhanjai and Cameotra 2010), *Chlorobium* sp. (Xu and Barton 2013), *Shewanella putrefaciens* 200 (Jiang et al., 2012), *B. megaterium* (Mishra et al. 2011), *G. sulfurreducens, S. oneidensis, Veillonella atypical* (Pearce et al. 2009), *Shewanella* sp. HN −41 (Tam et al. 2010), *Saccharomyces cerevisiae* (Zhang et al. 2012), *Wolinella succinogenes* (Tomei et al. 1992), *D. desulfuricans* (Tomei et al. 1995), and *Pseudomonas* sp. (Blake et al. 1993). In a cell-free system, nanotubes of Se have been produced using cytochrome c_3 from sulfate-reducing bacteria (Abdelous et al. 2000).

Elemental selenium particles from *W. succinogenes* and *D. desulfuricans* are representative of those produced by bacteria. Using thin sections of unstained cells, the presence of intracellular granules of elemental selenium produced by *D. desulfuricans* growing in selenite or selanate are shown in Figure 7.1 (Tomei et al. 1995). The verification of selenium as the element in the granule is presented by energy-dispersive X-ray (EDX) spectroscopy in Figure 7.2. Large extracellular selenium particles and small intracellular selenium particles are observed with *W. succinogenes* exposed to selenite (Figure 7.3; Tomei et al. 1992)**.** In Figure 7.4, EDX spectroscopy of the large extracellular granules in Figure 7.3 establishes the presence of selenium.

The environment contains many unique selenium metabolizing bacteria and culture conditions are important for metabolic events. When the newly isolated *Pseudomonas* strain 4C-C was grown anaerobically on ethanol, selenate was reduced to selenite but selenite was not reduced to Se^0 (Morita et al. 2007). Under anaerobic growth with ethanol, *P. denitrificans* JCM-6892 was capable of reducing selenite to Se^0, but this bacterium could not reduce selenate to selenite. However, when these two organisms were grown as co-culture in the presence of selenate, Se^0 was produced (Morita et al. 2007).

7.3.2 Te^0

The first report of tellurite reduction by bacteria occurred as a result of using cytochemical staining to assess mitochondrial equivalents in Gram-positive and Gram-negative cells. Rod-shaped structures of tellurium in the cytoplasm resulting from the reduction of tellurite were associated with the respiratory organelles and the periphery of the plasma membrane of *B. subtilis* (Iterson and Leene 1964a). In subsequent studies, Iterson and Leene (1964b), the reduction of tellurite by *Proteus vulgaris* and crystals of tellurium were deposited on the cytoplasmic side of the plasma membrane. This observation supported an earlier publication by Nermut (1960).

The terminal oxidases of several Gram-negative bacteria contribute to the reduction of tellurite with the formation of Te^0 (Trutko et al. 2000). In *P. aeruginosa*, the

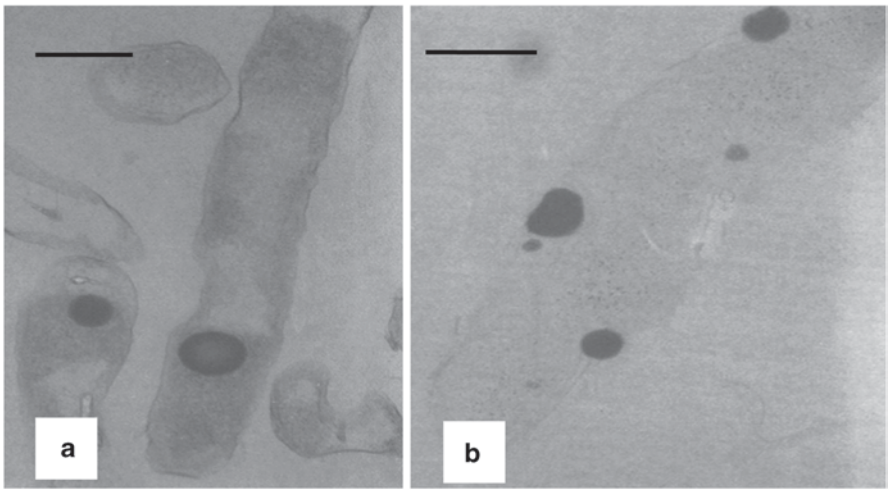

Fig. 7.1 Production of elemental selenium by *Desulfovibrio desulfuricans*. Thin section of *D. desulfricans* grown in formate/fumarate medium containing **a** 100 μM selenite and **b** 100 μM selenate

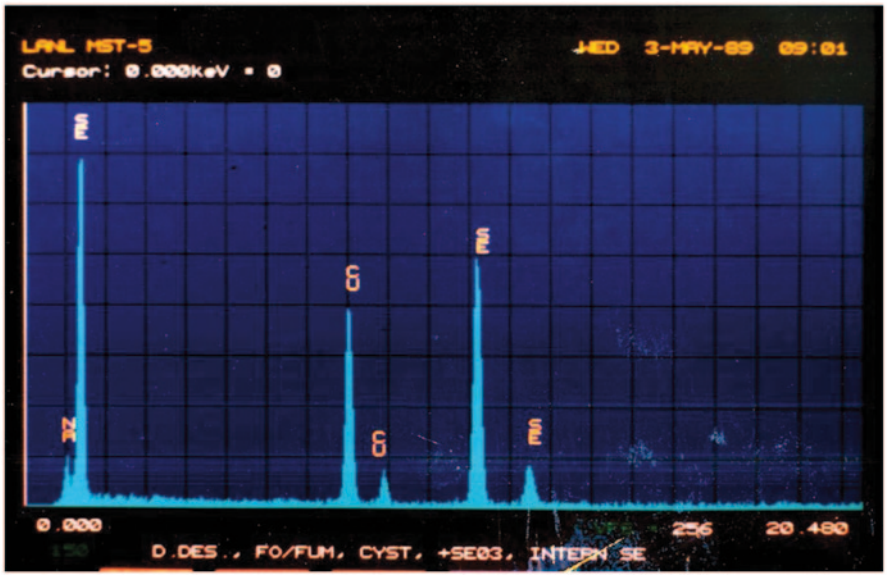

Fig. 7.2 Energy-dispersive X-ray spectrometry of internal Se granule. *D. desulfuricans* was grown in 100 μM selenite. (Used with permission from *Journal of Industrial Microbiology*)

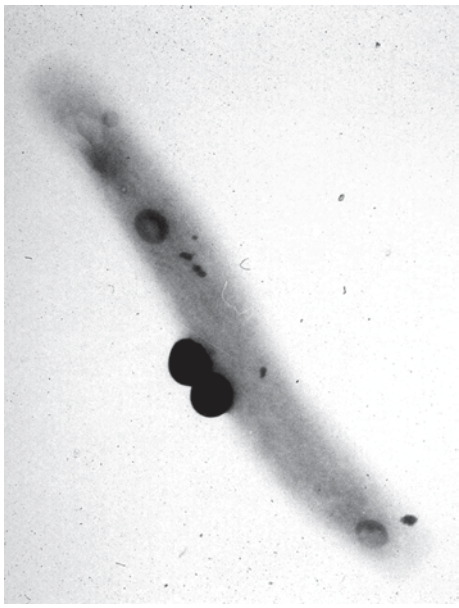

Fig. 7.3 Image of *Wolinella succinogenes* as observed by transmission electron microscopy. *W. succinogenes* was grown in formate/fumerate medium containing 1 mM selenite. The two large Se granules are outside of the cell and several smaller Se granules are inside the cell. (Used with the permission of *Canadian Journal of Microbiology*)

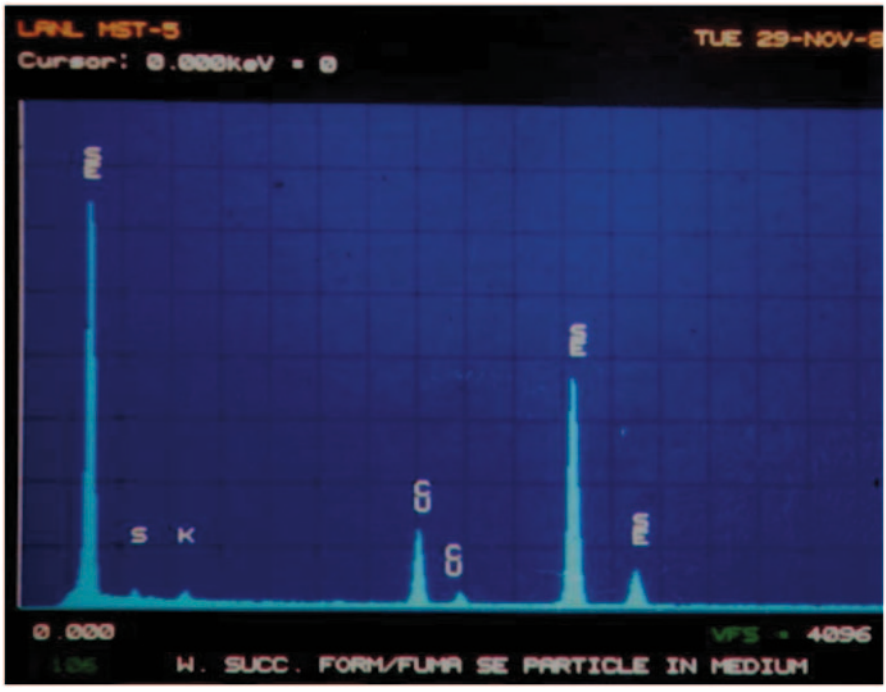

Fig. 7.4 Energy-dispersive X-ray spectrometry of Se granules on the surface of the cell in Figure 7.3

CO-binding cytochrome *c* was implicated in tellurite reduction while in strains of *Agrobacterium tumefaciens, E. coli, P. aeruginosa,* and *Erwinia carotovora*, the terminal oxidases and especially aa_3, *bb,* and *bd*-type cytochromes are involved. Tellurite reductase has been reported to be attributed to the nitrate reductase in *E. coli* (Avazéri et al. 1997). The nanocrystals resulting from the reduction of tellurite by these Gram-negative bacteria are present in the periplasm or associated with the plasma membrane. The dissimilatory metal reducer, *S. oneidensis* MR-1, reduces tellurite under anaerobic condition with the formation of intracellular crystalline Te^0 rods (Kim et al. 2012). Calderón et al. (2006) suggest that catalases in bacteria may function as tellurite reductases.

The production of Te^0 deposits from tellurite is widely distributed in nature and found in about ~10% of bacteria cultured from different environments (Ollivier et al. 2008). This includes numerous strains in the *Bacillaceae* (Ollivier et al. 2008), and bacteria that form a branch closely related to members of the genus *Pseudoalteromonas*, within the gamma-3 subclass of the Proteobacteria (Rathgeber et al. 2002). It should be pointed out that resistance and reduction of tellurite is not restricted to bacteria as it has also been demonstrated in the eukaryote *Rhodotorula* sp. (Ollivier et al. 2008).

Some anaerobic chemolithotrophic bacteria use tellurate or tellurite as the final electron acceptors in support of growth (Baesman et al. 2007). *B. selenitireducens* forms an internal Te^0 crystal that has a rod shape that is 10 nm in diameter and 200 nm long. *S. barnesii* grows with the reduction of tellurium oxyanions with the formation of crystalline nanospheres of 50 nm which can aggregate to form large aggregates. Both of these bacteria respire with the reduction of selenium oxyanions thereby indicating the chemical similarity between inorganic selenium oxides and tellurium oxides.

Bacillus beveridgei, a haloalkaliphile, produces nanocrystals of Te^0 when using tellurate or tellurite as the electron acceptor (Baesman et al. 2009). The forms of Te^0 particles produced by *B. beveridgei* were similar in structure to that seen with *S. barnesii*, in that there were principally two types: rod-like crystals forming a rosette and irregular globular precipitates. While several bacteria have the capability of reducing tellurite, the reduction of tellurate to Te^0 may be restricted to dissimilatory metal-reducing bacteria.

7.4 Production of Metal Sulfide Nanoparticles

7.4.1 CdS

Cadmium is highly toxic to biological systems. Microbes have developed a system to tolerate soluble cadmium salts by producing insoluble CdS. The production of CdS is of interest due to its use in the semiconductor industry where it constitutes one of the important types of quantum dots. *Klebsiella pneumoniae* produces CdS

that are ~4 nm in diameter. These aggregate to produce particles of about 200 nm (Holmes et al. 1997b). The photoactivity of these CdS bioparticles has been examined and determined to function in a similar manner to inorganic CdS particles of chemical origin (Holmes et al. 1997a).

In the presence of cadmium and zinc in the environment, *K. pneumoniae* produces an extracellular ternary alloy consisting of Cd (48.6%), Zn (0.04%) with the remaining quantity being sulfide. The precipitation of CdS nanoparticles on the surface of *K. pneumoniae* appears to be attributed to sulfide release from cysteine by cysteine desulfhydrase in a manner similar to that occurring in *Moorella* (formerly *Clostridium*) *thermoaceticum* (Cunningham and Lundie1993). With *Rhodopseudomonas palustris,* CdS nanoparticles of 8 nm are produced by sulfide released by action of cysteine desulfhydrase, and stabilized by a protein as it is exported from the cell (Bai et al. 2009).

7.4.2 ZnS

Nanocrystals of ZnS (sphalerite) were produced in a natural biofilm associated with zinc-containing groundwater (Labrenz et al. 2000). The sulfate-reducing bacteria in the biofilm produced H_2S which resulted in precipitating Zn(II) in nanoparticles of 2–5 nm in diameter. In a subsequent report from the Banfield group where they examined a biofilm associated with submerged wood (Moreau et al. 2004), nanocrystals of Zn/FeS (wurtzite) were dispersed among the more abundant ZnS nanoparticles. These ZnS nanocrystals are aggregated by protein of bacterial origin to produce sphaeroids reflecting alternating layers of mineral precipitation and flocculation attributed to proteins (Moreau et al. 2007). Cysteine is proposed to be an important amino acid in the extracellular protein matrix that is proposed to be critical for promoting aggregation of ZnS nanocrystals.

7.4.3 Arsenic Sulfide

Shewanella sp. HN-41 growing anaerobically in the presence of arsenate and thiosulfate produces arsenic-sulfide nanotubes that are 20–100 nm in diameter and 30 μm in length (Lee et al. 2007). The initial content of the nanotubes was As_2S_3 (orpiment) but as the nanotubes matured with time, AsS (realgar) and As_4S (duranusite) were the dominant crystals. This formation of As-S nanotubes is not restricted to *Shewanella* sp. HN-41, but has been observed also in *S. putrefaciens* CN-32, *S. alga* BrY, and *S. oneidensis* MR-1 (Jiang et al. 2009). In anaerobic environments with sulfate and arsenate, yellow As_2S_3 is produced inside and outside of cells of *Desulfosporosinus auripigmenti*, formerly *Desulfotomaculum auripigmentum* (Newman et al. 1997). As-S nanotubes were not produced by *D. auripigmenti*.

7.4.4 FeS

Sulfidogenic bacteria produce high levels of sulfide from sulfate or thiosulfate; and as a result, considerable levels of heavy metal sulfides are produced, including FeS. Copious levels of amorphous FeS precipitates result from growth of sulfate-reducing bacteria; however, in one report a nanoparticle, 45–80 nm, consisting of FeS and a minor quantity of mackinawite (an iron, nickel, sulfide crystal) has been reported (Xie et al. 2009). Under a controlled growth environment, sulfate-reducing bacteria were reported to produce a magnetic 2-nm particle consisting of FeS (troilite; Watson et al. 1999).

7.5 Production of Oxides and Phosphates

7.5.1 MnO_2

As has been recently reviewed (Tebo et al. 2010), several species of bacteria are capable of oxidizing Mn(II) with the formation of insoluble MnO_2 which exist as stacked hexagonal sheets with poor crystallinity (Spiro et al. 2010). *Leptothrix discophora* produces extracellular nanoparticles that are 4–100 nm (Nelson et al. 1999). Spores of *Bacillus* sp. strain SG-1 use two multicopper oxidases to oxidize Mn^{2+} to MnO_2. This oxidation is a sequential one-electron transition with Mn(III) being the intermediate as Mn(II) is oxidized to Mn(IV; Webb et al. 2005). Biogenic manganese oxides produced by *P. putida* were extensively analyzed and had stacking faults in the stacks of the crystal (Villalobos et al. 2006). Recently, there is a report that the nanoparticles of orthorhombic manganese oxide formed by *Bacillus* sp. strain MTCC 10650 were monodisperse spheres with an average size of 4.6 nm, displaying an absorption maximum of 329 nm (Sinha et al. 2011).

7.5.2 CuO

The extracellular synthesis of copper oxide nanoparticles has been reported for *E. coli* (Singh et al. 2010). The aerobic activity of *E. coli* involves the use of low-molecular-weight proteins (22–52 kDa) to produce and stabilize the copper oxide nanoparticles. The extracellular production of copper oxide has been reported for *Penicillium aurantiogriseum, Penicillium citrinum*, and *Penicillium waksmanii* (Honary et al. 2012). The size of the nanoparticles of CuO varied with the fungal species and pH. Generally, the copper oxide particles from *Penicillium* ranged from 80 to 200 nm, and there was evidence of protein associated with these metallic nanoparticles.

7.5.3 V(IV)

In an anaerobic environment, *S. oneidensis* reduces V(V), vanadate ion, to V(IV), vanadyl ion. The vanadyl species are insoluble and collect extracellularly (Carpentier et al. 2003). Small granules of vanadium pentoxide were found inside cells of *S. oneidensis*. As determined by electron microscopy, *Pseudomonas isachenkovii* reduces V(V) by a process where the cells take up vanadate, which is reduced at the surface of the cell membrane (Antipov et al. 2000a), using a molybdenum-free dissimilatory nitrate reductase (Antipov et al. 2000b).

7.5.4 Iron Oxide

Evaluation of the mineral crusts in the gill chambers of *Rimicaris exoculata* (shrimp) from the Mid-Atlantic Ridge reveals the presence of aggregated nanoparticles consisting of ferrihydrite (Corbari et al. 2008). The iron oxide is proposed to be produced by ectosymbiotic bacteria and associated with the layered deposits of iron oxide are trace levels of Si, Ca, Mg, and P, which may be deposited by abiotic processes.

Magnetosomes containing Fe_3O_4 are found in magnetotactic bacteria. These structures are discussed in the chapter by Bazyliniski in this book.

7.5.5 Silicon Dioxide

A*ctinobacter* sp. has been reported to produce Si/SiO_2 composite from K_2SiF_6 under ambient conditions (Singh et al. 2008). At this time, the mechanism for extracellular deposition of silicon/silica composite nanoparticles by *Actinobacter* is unresolved but may be similar to the formation of iron oxides by the same organism. A silicon-germanium oxide nanocomposite has been produced by *Stauroneis* sp., a fresh water diatom (Ali et al. 2011). The diatom was cultivated in a limited quantity of silicon and when silicon was depleted from the medium, salts of silicon and germanium were added at a ratio where the diatom structure was not affected. After several days of growth, germanium in the cell surface of the diatom was demonstrated by energy-dispersive X-ray spectrometry.

7.5.6 Phosphates

Phosphate released from organic phosphates by periplasmic phosphatases provides a suitable anion for the precipitation of metal cations. Nanocrystallites of lead phosphate precipitate on the surface of *Citrobacter* sp. as a mechanism of detoxification (Aicken et al. 1979). Macaskie and Dean (1987) report that *Citrobacter* sp. precipitates uranium, lead, and cadmium on the cell surface as metal-phosphate particles.

7.6 Physiological Features of Bioproduced Nanoparticles

The general size for nanoparticles produced by microorganisms is considered to be 20–200 nm in diameter. The factors limiting the size of these nanoparticles are unresolved. It is known that a few metal nanoparticles are only a few nm in diameter as well as occurring in particles of the 200 nm range (Table 7.1). The charge on the nanoparticle is one of the factors contributing to the size of the particle. In the case of elemental selenium particles, the nanoparticles can be produced from large particles by the dispersive effect of Na_2S (Biswas et al. 2011). The greater the charge on the nanoparticle (see Table 7.1), there is a repulsion of elements added to the particle. In some cases, it may be the surface metals on the nanoparticle contributing to the charge and in other cases it may be the proteins adhering to the metal atoms that are being added to the nanoparticle. It appears that for many of the nanoparticles formed, there are several different stages of activity: (1) nucleation—the point where nanoparticle formation is initiated, (2) addition to the growing nanoparticle which results in a specific form that is spherical or rod shaped, and (3) termination with no additions to the nanoparticle.

Biologically produced nanoparticles have specific wavelengths at which light is absorbed. Some of the absorption of light by nanoparticles is given in Table 7.1. Characteristic of metallic nanoparticles is the absorption and scattering of light by bands of atoms in the solid state which results in a specific wavelength of absorption in the visible spectra (Suresh 2010). This interaction between the valence-band electrons of atoms in the nanoparticle and the electromagnetic field is characteristic of nanoparticles and not larger aggregates.

The study of nanoparticle production by microorganisms has not been systematic. As indicated in Table 7.2, there are numerous instances where only a specific nanoparticle is formed by an organism. With a continued evaluation of newly isolated microorganisms and the application of green technology for the production of nanoparticles, the list of bacteria- and fungi-producing metal(loid) nanoparticles will certainly increase.

Nanoparticle formation may be specific for a given microbial species if the formation of particles contains two or more elements. Some examples of nanoparticles containing more than one element are listed in Table 7.3. In the detoxification by culture with tellurite present, there may not only be the release of volatile dimethyltelluride (DMT) but also dimethyltelluridesulfide (DMTS). The mechanisms for the formation of mixed-element nanoparticles or volatile telluride compounds are not understood at this time.Crystalline array is seen when nanocrystals are observed by high-resolution transmission electron microscopy. Examination of Se-rich particles produced by *Deslfovibrio desulfuricans* reveals the crystalline character (Figure 7.5) with lattice fringe. Observation of uranium (IV) nanoparticles produced by *D. desulfuricans* are shown in Figure 7.6.

Table 7.2 A selection of nanoparticles indicating the diversity of microbial metabolism

Nanoparticle	Characteristic	Reference
CuS	A spherical particle of 2–5 nm diameter produced *Fusarium oxysporum*	Hosseini et al. 2012
$PbCO_3$	An extracellular spherical particle, 20 nm diameter, produced by *Fusarium oxysporum*	Sanyal et al. 2005
$CdCO_3$	A linear nanoparticle 5–10 nm in length produced by *Fusarium oxysporum*	Sanyal et al. 2005
$SrCO_3$	A linear crystal 10 x 50 nm produced extracellularly by *Fusarium oxysporum*	Rautaray et al. 2004
Sb_2O_3	A spherical particle of 2–10 nm produced intracellularly by *Saccharomyces cerevisiae*	Jha et al. 2009
TiO_2	A spherical particle with a diameter of 8–35 nm produced extracellularly by *Lactobacillus* sp. and *Saccharomyces cerevisiae*	Jha et al. 2010
ZrO_2	A spherical particle of 3–11 nm produced extracellularly by *Fusarium oxysporium*	Bansal et al. 2004
CdSe	A spherical particle of 9–15 nm diameter produced extracellularly by *Fusarium oxysporum*	Kumar et al. 2007
Te^0	*Bacillus beveridgei* produces nanocrystals of 10 x 200 (rods) when tellurite or tellurate is the final electron acceptor	Baesman et al. 2007
Ni^0	*Pseudomonas* sp. MBR is reported to reduce Ni(II) to elemental Ni by co-metabolism	Zhan et al. 2012
Hg^0	A strain of *Enterobacter* produces elemental mercury as 2–5 nm spheres inside the cells	Sinha and Khare 2011

7.6.1 Thiol-Mediated Reactions Leading to Reduction of Selenite

Microorganisms have developed a glutathione–glutathione disulfide (GSH:GSSG) redox system in response to osmotic shock, acidity, halogenated compounds, and oxidative stress (Masip et al. 2006). Bacteria maintain a stable ratio of GSH to GSSG in the cytoplasm, and the redox couple for these two peptides is −240 mV. Bacteria have a glutaredoxin system in which GSH is required for the reduction of ribonucleotides for DNA synthesis and for reduction of arsenate to arsenite by interacting with the arsenate reductase (Ritz and Beckwith 2001). Additionally, GSH may participate in the intracellular reduction of selenite with the production of Se^0 (Blake et al. 1993). GSH is exported by bacteria (Owens and Hartman 1986), and it is unknown if this could contribute to extracellular reduction of selenite with production of Se^0.

Selenite (SeO^{2-}_3) chemically reacts with GSH to produce selenodiglutathione (GS–Se–SG; Ganther 1971), see Reaction 1. The reaction involving reduction of selenite by GSH is given in Reactions 1–4. Reaction 5 indicates the regeneration of GSH by GSH reductase:

Table 7.3 Microbial production of mixed nanoparticles

Particle	Characteristic
$BaTiO_3$	Nanoparticles of 20–80 nm were formed by *Lactobacillus* sp. (Jha and Prasad 2010)
Au/Ag	*Fusarium oxysporum* produces 8–14 nm nanoparticles of an alloy of Au/Ag (Senapati et al. 2005). A gold/silver alloy is produced by *Neurospora crassa* (Castro-Longoria et al. 2011)
Fe/Ni/S	A sulfate-reducing bacteria produces this nanoalloy of iron, nickel, and sulfide along with NiS crystals (Xie et al. 2009)
Si/Ge/O	*Stauroneis* sp. produces a mixed-element nanocomposite (Ali et al. 2011)
Se/S	An anaerobic biofilm containing *Chromatium* growing in an environment containing reduced selenium and sulfur (Xu and Barton 2013)
As/S	Formation of AsS_3 by a sulfate reducer (Newman et al. 1997) and As–S nanotubes with arsenic-rich phases containing As_4S_4, AsS, and As_4S_3(Jiang et al. 2009)

$$\textit{Reaction}\,1: \quad \mathbf{Se}O_3^{2-} + 4GSH + 2H^+ \rightarrow GS - \mathbf{Se} - SG + GSSG + 3H_2O$$

$$\textit{Reaction}\,2: \quad GS - \mathbf{Se} - SG + GSH \rightarrow GS - \mathbf{Se}H + GSSG$$

$$\textit{Reaction}\,3: \quad GS - \mathbf{Se}H \rightarrow \mathbf{Se}^0 + GSH$$

$$\textit{Reaction}\,4: \quad GS - \mathbf{Se}H + GSH \rightarrow H_2\mathbf{Se} + GSSG$$

$$\textit{Reaction}\,5: \quad NADPH + H^+ + GSSG \rightarrow NADP^+ + 2GSH$$

GSH is present in cyanobacteria and proteobacteria in concentrations of 0.1–10 mM (Fahey et al. 1978). These organisms could potentially use GSH for selenite reduction. However, some microorganisms lack GSH but use other types of thiols (Fahey 2001; Pieulle et al. 2011). Reduction of selenite by these novel thiols has not been reported.

One of the ways for demonstrating the involvement of GSH in the reduction of selenite is to use buthionine sulfoximine (BSO, *s-n*-butyl homocysteine sulfoximide) to inhibit the synthesis of GSH synthesis. When BSO was added to the growing culture of *Pseudomonas* sp. (Blake et al. 1993) or to stationary phase cells of *Rhodospirillum rubrum* and *Rhodobacter capsulatus* (Kessi 2006) the amount of Se^0 produced was less than when no BSO was added.

7.6.2 Enzymes Associated with Metal and Metalloid Reduction

Except for a few cases, the reduction of metal(loid)s is nonspecific and involves enzymes or cytochromes that are not saturated with their appropriate substrates.

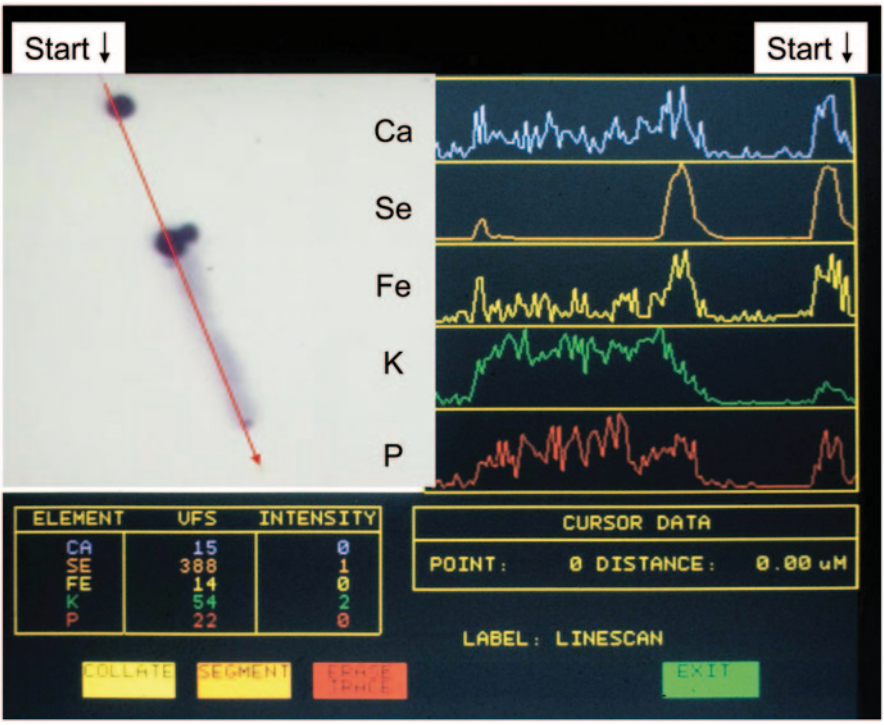

Fig. 7.5 Line scan of *Wolinella succinogenes* indicating the abundance of five elements in *Wolinella succinogenes*. Cells were grown in formate/fumerate medium containing 100 μM selenite and examined by energy-dispersive X-ray spectrometry

There are specific enzymes for the reduction of arsenate, arsenite, selenate, and selenite in the dissimilatory metalloid reducers (Oremland et al. 2004); however, only selenite reductase results in the formation of elemental form of Se. The formation of diverse examples of nanoparticles involves the reduction of metals and metalloids by redox-active centers of enzymes and cytochromes. The reduced Fe–S clusters or metal-active centers found in many of the enzyme interface with appropriate metal(loid) ions and chemical reduction occurs (see examples in Table 7.4).

Many of the cytochromes in anaerobic bacteria have a reduction potential of −200 to −300 mV with multiple hemes per molecule and become effective electron sources for metal(loid) ions. Thus, through manipulation of the nutrients available to the bacterial cells, bioreduction of metal(loid)s can be achieved. In *S. oneidensis,* the formation of extracellular UO_2 nanoparticles is attributed to the reduction of uranyl ion by MtrC, a decaheme *c*-type cytochrome (Marshall et al. 2006).

A process frequently used to generate nanoparticles is to introduce a metal(loid) solution to a bacterial suspension with an active electron transport system. Many species of bacteria have hydrogenase systems and hydrogen is an effective electron donor due to the reaction potential of −440 mV. Perhaps the best example of

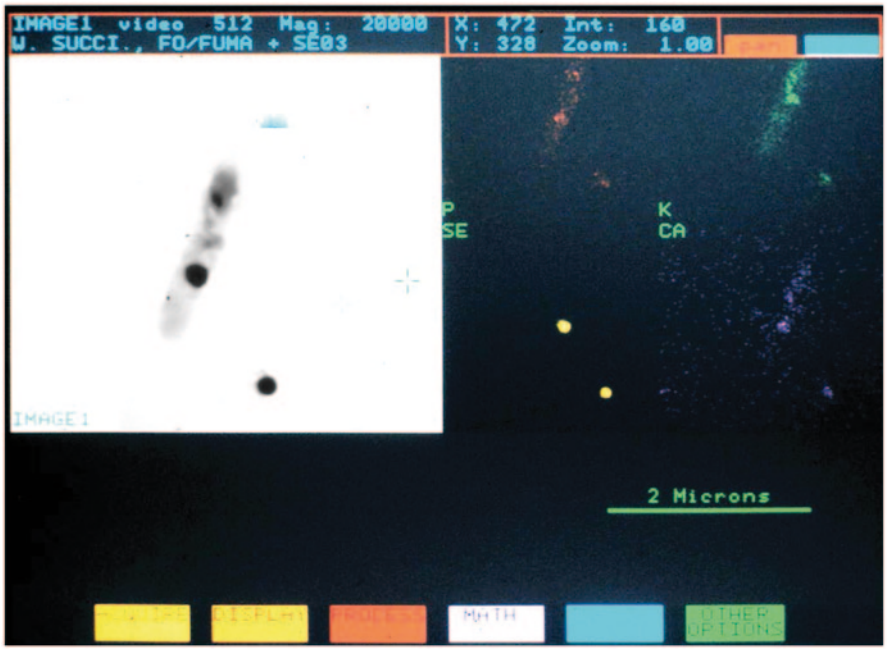

Fig. 7.6 Mapping of *Wolinella succinogenes* cell using energy-dispersive X-ray spectrometry, X-ray emission, and absorption spectroscopy

hydrogenase-mediated reduction of metal(loid)s is reported for *Micrococcus lactilyticus* (Woolfolk and Whiteley 1962). As reported in Table 7.5, a single speces of bacteria has considerable potential in reduction of chemically distinct compounds.

Given the lack of specificity for reduction of most of the metal(loid) compounds, it is not surprising that a single organism may account for numerous nanoparticles formed, and for many different microbial species to be involved in this process. As indicated in Table 7.6, a large number of different microbial species that have been documented to form nanoparticles of Ag^0 and Au^0. Using cell extracts of *Geobacter metallireducens,* the reduction of silver and gold was coupled to the oxidation of cytochrome reduction (Lovley et al. 1993a). From reports in the literature and this chapter, it is apparent that a large percentage of bacteria and fungi in the environment can reduce selenite to Se^0.

7.6.3 Membrane Permeability of Ag^0 Nanoparticles

Using chemically produced Ag^0 nanoparticles, Xu et al. (2004) studied the uptake of Ag^0 nanoparticles by *P. aeruginosa*. The uptake of Ag^0 nanoparticles less than 80 nm was attributed to the MexAB–OprM system which is an efflux pump associated with multidrug resistance. This pump consists of two proteins associated

Table 7.4 Production of nanoparticles with enzymes and cytochtomes from bacteria

Enzyme/ Cytochrome	Nanoparticle	Organism	Reference
Catalase	Te^0	*Staphylococcus epidermidis*	Calderón et al. 2006
Hydrogenase[a]	Au^0	*Geobacter ferrireducens*, *Shewanella algae, Pyrobaculum islandicum, Thermotoga maritime*	Kashefi et al. 2001
	Pt^0	Sulfate reducers	Rashamuse and Whiteley 2007
	Pd^0	*Desulfovibrio desulfuricans*	Lloyd et al. 1998
		D. fructosivorans	Mikheenko et al. 2008
	Se^0	*Clostridium pasteurianum*	Yanke et al. 1995
Nitrate reductase	Ag^0	*Bacillus licheniformis*	Vaidyanathan et al. 2010
Nitrite reductase	Se^0	*Thauera selenatis*	DeMoll-Decker and Macy 1993
	Te^0	*Escherichia coli*	Avazéri et al. 1997
Selenite reductase	Se^0	*Bacillus arsenicoselenatis*	Blum et al. 1999
Cytochrome[b]	UO_2	*Desulfovibrio vulgaris*	Lovley et al. 1993b
		Shewanella oneidensis	Marshall et al. 2006
	Ag^0	*Geobacter sulfurreducens*	Law et al. 2008
	Te^0	*Pseudomonas aeruginosa, Agrobacterium tumefaciens, Escherichia coli, Erwinia carotovora*	Trutko et al. 2000
	Se^0	*Desulfovibrio vulgaris*	Abdelous et al. 2000

[a] Hydrogenases produced by different organisms or multiple hydrogenases from the same organism have this single entry
[b] Cytochromes of the *c*-type and these are collectively presented by a single entry

with the plasma membrane (Mex A and Mex B) and a protein associated with the outer membrane (OprM). Wild-type *P. aeruginosa* would take up Ag^0 nanoparticles. However, mutants lacking the MexAB–OprM system were unable to accumulate silver particles. If mutants lacked the Mex AB proteins, but produced the OprM protein, Ag^0 nanoparticles accumulated in the periplasm. At 1.3 pM inside *P. aeruginosa* cells, no toxicity was observed. If one extrapolates from this observation that Ag^0 uptake involves the MexAB–OprM system, it would seem reasonable to propose that the export of Ag^0 may also involve these or similar transport systems.

7.6.4 Protein Capping of Se^0 Nanoparticles

Examination of many of the Se^0 nanoparticles produced by microorganisms reveals the presence of proteins. A 95 kDa protein is associated with the formation of Se nanoparticles with selenate respiration by *Thauera selenates*. It is proposed that this protein stabilizes the nanoparticle (Devieux et al. 2011). A protein coat is described around the selenium nanoparticle produced by *Alternaria alternata,* and it

Table 7.5 Metal nanoparticles reduced by hydrogenase in cell extracts of *Veillonella alcalescens* (formerly *Micrococcus lactilyticus*; Woolfolk and Whiteley 1962)

Chemical	Reactions
Bismuth hydroxide	$Bi(OH)_3 + 7H \rightarrow Bi^0 \downarrow + 3H_2O$
Bismuthate	$BiO_3^- + 5H \rightarrow Bi^0 \downarrow + 2H_2O + OH^-$
Osmium dioxide	$OsO_2 + 4H \rightarrow Os^0 \downarrow + 2H_2O$
Selenite	$HSeO_3^- + 4H \rightarrow Se^0 \downarrow + 2H_2O + OH^-$
Tellurite	$HTeO_3^- + 4H \rightarrow Te^0 \downarrow + 2H_2O + OH^-$
Tellurate	$HTeO_4^- + 6H \rightarrow Te^0 \downarrow + 3H_2O + OH^-$
Uranyl	$UO_2^{+2} + 2H \rightarrow UO_2 \downarrow + 2H^+$
Vanadate	$H_2VO_4 + 2H \rightarrow VO(OH)_2 \downarrow + OH^-$

is proposed that this protein stabilizes this fungal nanoparticle (Sarkar et al. 2011). A 15 kD *c*-type cytochrome is associated with Se^0 nanoparticles produced by *G. sulfurreducens*. It is proposed that this protein is involved in the formation of the nanoparticle (Pearce et al. 2009).

7.7 Cell Mapping for Localization of Metals

The localization of nanoparticles of metals in bacterial cells has been examined by various spectroscopic methods. When used in conjunction with other bioinorganic analytical methods, these techniques can provide information on the species of the metals involved and mechanisms of cellular compartmentalization. These mapping studies involve examination of individual cells for activity, and these observations provide a perspective not revealed in bulk analysis of a bacterial culture.

7.7.1 Se^0 Nanoparticles Produced by W. succinogenes

A rapid process to evaluate the production of extracellular nanoparticles and the relationship of these nanoparticles to cellular constituents can be accomplished by using transmission electron microscopy with EDX. As reported earlier, *W. succinogenes* readily reduces selenite to Se^0 when grown in a defined medium with formate as the electron donor and fumarate as the electron acceptor (Tomei et al. 1992). Based on the evaluation of several elements, the extracellular Se^0 nanoparticles have a composition similar to the Se^0 inside the cell (Figure 7.7). The presence of Ca, Fe, and P with the extracellular Se^0 nanoparticle is similar to the abundance of these elements with intracellular Se^0 nanoparticles. When cells of *W. succinogenes* are mapped by EDX, the location of Se with respect to Ca, P, and K can be readily

Table 7.6 Microorganisms reported to produce nanoparticles of selected metals

Metals produced	Organisms
Ag^0	*Aspergillus flavus, Aspergillus fumigatus, Bacillus cerus, Bacillus licheniformis,*
	Bacillus megaterium, Bacillus subtilis, Brevibacterium casei,
	Corynebacterium glutamicum, Enterococcus facium, Escherichia coli,
	Fusarium, oxysporum Geobacter sulfurreducens, Lactobacillus fermentum, Lactococcus arvieae
	Lactococcus arvieae Pediococcus pentosaceus, Phaenerochaete chrysosporium,
	Plectonema boryanum, Pseudomonas aeruginosa, Spirunlina platensis, Streptococcus thermophilus,
	Streptomyces glaucus, Trichoderma viridae, Trichoderma viride, Verticillium sp.[a]
Au^0	*Brevibacterium casei, Candida utilis, Cupriavidus metallidurans, Escherichia coli,*
	Geobacter ferrireducens, Neurospora crassa, Plectonema boryanum, Pseudomonas aeruginosa,
	Pyrobaculum islandicum, Rhodococcus sp., Rhodopseudomonas capsulate, Shewanella algae, Shewanella oneidensis, Thermotoga maritime, Yarrowia lipolytica[a]
Se^0	*Agrobacterium sp.,Aquificales sp., Bacillus cereus, Bacillus megaterium, Bacillus*
	selenitireducens, Bacillus subtilis, Clostridium pasteurianum, Desulfovibrio desulfuricans,
	Duganella sp., Escherichia coli, Geobacter sulfurreducens, Moraxella bovis,
	Pseudomonas aeruginosa, Pseudomonas alcaliphila, Pseudomonas denitrificans, Pseudomonas fluorescens, Rhodospirillum rubrum, Rhodobacter capsulatus, Shewanella oneidensis,
	Selenihalanaerobacter shriftii, Sulfurospirillum barnesii, Tauera selenatis, Veillonella atypical, Wolinella succinogenes
UO_2	*Anaeromyxobacter dehalogenans, Cellulomonas flaigena, Cellulomonas sp.*
	WS01, Cellulomonas sp. WS18, Cellulomonas sp. ES5, Clostridium sphenoides,
	Clostridium acetobutylicum, Clostridium pasteurianum, Deinococcus radiodurans,
	Desulfomicrobium norvegicum, Desulfotomaculum reducens, Desulfosporosinus orientis, Desulfosporosinus sp. P3,
	Desulfovibrio baarsii, Desulfovibrio desulfuricans,
	Desulfovibrio alaskensis (formerly Desulfovibrio desulfuricans strain G20, Desulfovibrio sp. UFZB490*,*
	Desulfovibrio sulfodismutans, Desulfovibrio vulgaris, Geobacter
	metallireducens, Geobacter sulfurreducens, Pseudomonas putida, Pyrobaculum
	islandicum, Salmonella subterranean, Shewanella alga, Shewanella oneidensis,
	Shewanella putrefaciens, Veillonella alcalescens, Thermoanaerobacter sp., Thermus scotoductus, Thermoterrabacterium ferrireducens[b]

[a] References: Li et al. 2011, text and tables)
[b] Reference: Wall and Krumholz 2006; Gao and Francis, 2013

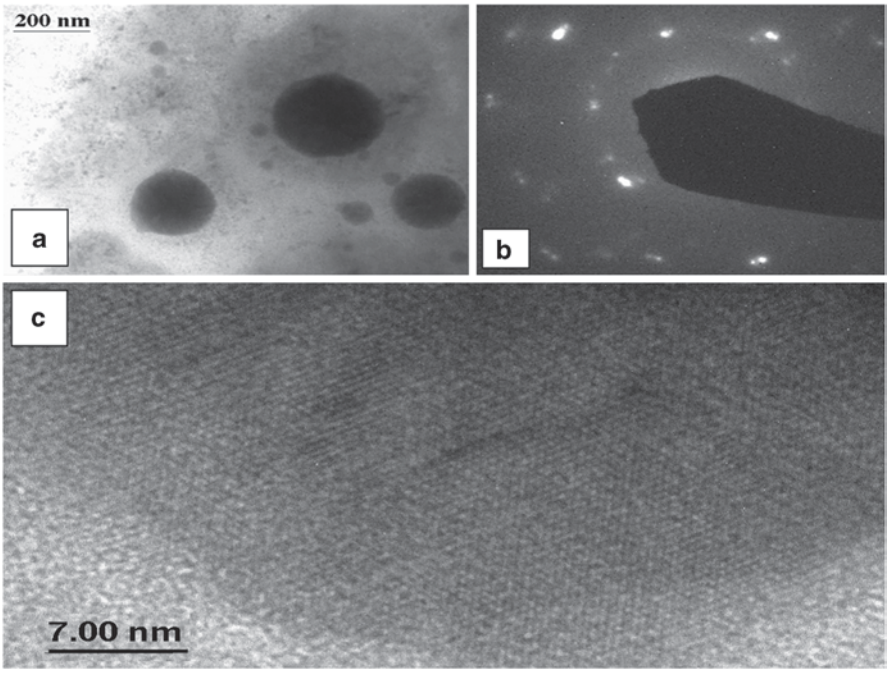

Fig. 7.7 Selenium-rich nanoparticles produced by *Desulfobvibrio desulfuricans* in a lactate/sulfate medium containing 100-mM selenite. **a** Presence of crystalline nanoparticles observed inside the cells. **b** SAED patterns show crystalline character of the Se,S particles shown in **a**. **c** Highresolution TEM image of a crystalline particle showing lattice fringes. (Used with permission from *Advances in Microbiology*)

assessed (Figure 7.8). The release of elemental selenium from *W. succinogenes* has not been established. It is known that some intracellular Se^0 granules approach the diameter of the cell, and release of these particles could not occur by export processes.

X-ray emission and absorption spectroscopy techniques can be used to determine elemental composition and valence state of metals accumulated in the cytoplasm, cell membrane, periplasm, or on the cell wall of microorganisms. X-ray emission/fluorescence is particularly suited for identifying elemental composition/distribution. Absorption spectra, e.g., X-ray absorption near edge structure (XANES), are used to determine the valence state of the element. In conjunction with an electron microscope, these techniques are used to map the distribution of metals in cells.

Chen et al. (2011) grew a *P. putida* strain resistant to copper on an unsaturated biofilm. The growth substrate was citrate, which chelates copper, thus facilitating the transport of the later into the biofilm. The authors used synchrotron-based X-ray fluorescence microscopy (XRF) to map the movement and distribution of copper in the biofilm. They also used CuK-edge X-ray absorption near edge structure (XANES) to determine the chemical nature of the copper in the biofilm. Copper

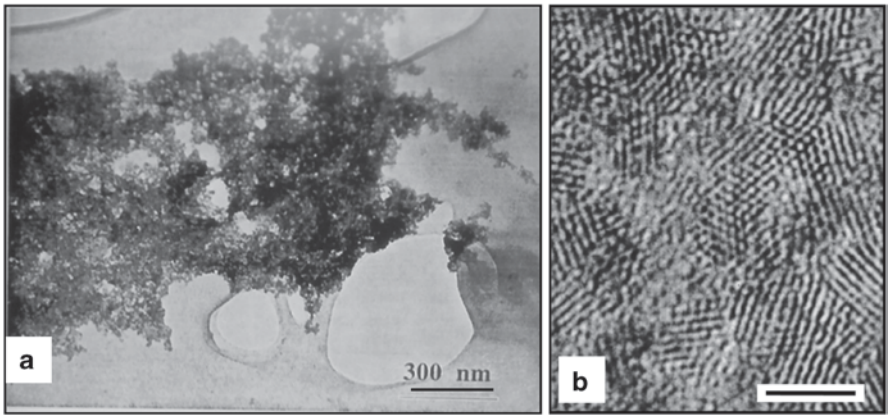

Fig. 7.8 Crystalline particles produced by *Desulfovibrio desulfuricans*. The culture was grown in a lactate/sulfate medium containing 1 mM uranyl acetate. **a** Image of extracellular uraninite particles. **b** High-resolution TEM image of crystalline uranium nanoparticle showing lattice arrangement (bar = 5 μM)

migrated readily into the biofilm as a citrate complex. The evidence suggests that as the citrate was consumed within the biofilm, the liberated copper precipitated as cupric phosphate near the biofilm–air interface.

Kemner et al. (2004) used the same two techniques used by Chen et al. (2011) to map single cells of *Pseudomonas fluorescens*. They mapped the intracellular distribution of metals in cells grown in suspension or on a biofilm by XRF and determined the redox state of chromium using XANES. Changes in distribution were noted when the cells were exposed to a potassium dichromate [Cr(VI)] solution (1000 ppm) for 6 h. They found that the cells in suspensions died after being exposed to the chromium preparation, while the cells in the biofilm showed enhanced resistance to chromium and death. Attached cells showed changes in the concentrations of transition metals and reduction of Cr(VI) to Cr(III).

Glasauer et al. (2007) also used XRF and XANES to study the deposition of internal iron granules in *S. putrefaciens* CN32, a dissimilatory ferric ion reducer. This strain, contrary to other strains and species in the genus *Shewanella*, deposits cytoplasmic iron granules of mixed valence. The authors proposed that the average valence of the iron deposits was close to that of magnetite. In their proposed model, Fe^{2+} is transported into the cells as the external dissimilatory reduction of Fe^{3+} proceeds, and it is partly reoxidized.

Dunham-Cheatham et al. (2011) used similar X-ray emission and absorption measurements to study passive cell wall biomineralization of uranyl, lead, and calcium phosphates by nonmetabolizing bacteria exposed to a range of oversaturated conditions.

Experiments with Gram-positve *B. subtilis* and Gram-negative *S. oneidensis* provided evidence of cell wall nucleation sites for mineral precipitation reactions in

saturated systems. While the bacteria did not change the mineral that precipitated, they played a role on the size or the precipitate that formed during the experiments.

C. metallidurans, a Gram-negative bacterium, is highly resistant to numerous metal ions including gold. When Au(III)–hydroxychloride complexes were added to *C. metallidurans,* and individual cells were examined by synchrotron μ-X-ray fluorescence (μXRF), it was observed that this metallophilic bacterium rapidly accumulates gold in discrete regions within the cytoplasm (Reith et al. 2009). In a few hours, the amount of intercellular gold decreased and Au^0 accumulated in the periplasm. Through the use of X-ray absorption near edge structure (XANES), speciation of the gold was achieved, and it was determined that Au(III) was reduced to Au(I).

7.8 Summary and Perspective

The feature of nanoparticle formation of metallic materials by biological systems is widely distributed in the various species of microorganisms. Currently, the literature concerning formation of elemental nanoparticles is dominated by the bacteria; however, the understanding of nanoparticle formation in archaea will increase as the study of archaea and fungi continues. There are a few different strategies employed by bacteria and archaea to produce metallic nanoparticles. Soluble minerals are the source of metals for nanoparticle formation. For the most part, nanoparticle production is a process that involves the reduction of soluble oxidized metals to the elemental state and this diminishes the toxicity on microorganisms.

One of the strategies employed by the prokaryotes is the nonspecific reduction of highly oxidized metal ions by enzymes that have (Fe–S) clusters or heme centers with half reactions more electronegative than the half reaction associated with reduction of the metal. The heme or (Fe–S) center must be appropriately exposed in soluble proteins and properly orientation if it is bound on the plasma membrane. In the case of *Shewanella* and *Geobacter,* appropriate orientation of cytochromes on the outer membrane is required.

Another approach used by bacteria in production of metallic or metalloid nanoparticles is the coupling of metal reduction to energy production with cell growth as a result. Chemolithotrophic bacteria (*S. barnesii, B. selenitireducens,* and *T. selenatis*) have specific enzymes for reduction of selenate and selenite to elemental selenium. The enzymology of reduction of uranyl (UVI) ion to uraninite (UIV) by those bacteria that couple uranium reduction to uranium nanoparticles remains to be established.

A third approach accounting for nanoparticle formation is the reduction of oxyanions by GSH. The formation of nanoparticles of elemental selenium appears to be attributed to the reduction of selenite by reduced GSH in the cytoplasm of the cells. Most aerobes have the enzymology to produce GSH and reduction occurs with an NADH-coupled GSH reductase. The reaction between reduced GSH and selenite does not require enzymes but is the result of a chemical reaction. The extent

to which oxyanions other than selenite or selenite can be reduced to nanoparticles remains to be explored. Since anaerobes have low concentrations of GSH, the formation of nanoparticles of selenium from selenite may be attributed to reactions driven by glutaredoxin or other sulfhydryl compounds dealing with oxygen stress reactions in anaerobes.

With reduction of metals by cellular systems, proteins are reportedly associated with several metallic nanoparticles. There is some suggestion that these proteins may contribute to the formation and stability of the nanoparticle or are associated with export of the nanoparticles from the cell. However, in the case of metal nanoparticle formation by cytochrome or nonheme iron systems, the only protein in the system is the one that carries electrons to the oxidized metal ion. Proteins present in the nanoparticle are important for commercialization of nanoparticle production by bacteria.

Disclaimer *The findings and conclusions in this report are those of the author(s) and do not necessarily represent the official position of the Agency for Toxic Substances and Disease Registry.*

References

Abdelous A, Gong WL, Lutze W, Shelnutt JA, Franco R, Moura (2000) Using cytochrome c3 to make selenium wires. Chem Mat 12:1510–1512

Afkar E, Lisak J, Saltikov C, Basu P, Oremland RS, Stolz JF (2003) The respiratory arsenate reductase from Bacillus selenitireducens strain MLS10. FEMS Microbiol Lett 226:107–112

Aickin RM, Dean, ACR, Cheetham, AK, Skarnulis. AJ (1979) Electron microscope studies on the uptake of lead by a *Citrobacter* species. Microbios Lett 9:7–15

Ali DM, Divya C, Gunasekaran M, Thajuddin N (2011) Biosynthesis and characterization of silicon-germanium oxide nanocomposite by diatom. Digest J Nanomater Biostruct 6:117–120

Antipov AN, Lyalikova NN, Khijniak TV, L'vov NP (2000a) Vanadate reduction by molybdate-free dissimilatory nitrate reductases from vanadate-reducing bacteria. IUBMB Life 50:39–42

Antipov AN, Lyalikova NN, L'vov NP (2000b) Vanadium-binding protein excreted by vanadate-reducing bacteria. IUBMB Life 49:137–141

Avazéri C, Turner RJ, Pommier J, Weiner JH, Giordano G, Verméglio A (1997) Tellurite reductase activity of nitrate reductase is responsible for the basal resistance of *Escherichia coli* to tellurite. Microbiology 143:1181–1189

Baesman SM, Bullen TD, Dewald J, Zhang D, Curran S, Islam FS, Beveridge TJ, Oremland RS (2007) Formation of tellurium nanocrystals during anaerobic growth of bacteria that use Te oxyanions as respiratory electron acceptors. Appl Environ Microbiol 73:2135–2143

Baesman SM, Stolz JF, Kulp TR, Oremland RS (2009) Enrichment and isolation of *Bacillus beveridgei* sp. nov., a facultative anaerobic haloalkaliphile from Mono Lake, California, that respires oxyanions of tellurium, selenium, and arsenic. Extremophiles 13:695–705

Bai HJ, Zhang ZM, Guo Y, Yang GE (2009) Biosynthesis of cadmium sulfide nanoparticles by photosynthetic bacteria *Rhodopseudomonas palustris*. Colloids Surf B Biointerfaces 70:142–146. doi:10.1016/j.colsurfb.2008.12.025

Bajaj M, Schmidt S, Winter J (2012) Formation of Se(0) nanoparticles by *Duganella* sp. and *Agrobacterium* sp. isolated from Se-laden soil of North-East Punjab, India. Microbial Cell Factories 11:64. http://www.microbialcellfactories.com/content/11/1/64

Banfield JF, Nealson KH (eds) (1997) Geomicrobiology: Interactions between microbes and minerals. Rev Microbiol Geochem, vol 35. Washington DC, Mineralogical Society of America

Bansal V, Rautaray D, Ahmad A, Sastry M (2004) Biosynthesis of zirconia nanoparticles using the fungus *Fusarium oxysporum*. J Mater Chem 14:3303–3305

Barton LL, Fauque G (2009) Biochemistry physiology and biotechnology of sulfate-reducing bacteria. Adv Appl Microbiol 68:41–98

Barton LL, Northup DE (2011) Microbial ecology. Wiley-Blackwell, Hooboken

Barton LL, Fekete FA, Marietta EV, Nuttall HE Jr, Jain R (1992) Potential for bacterial remediation of waste sites containing selenium or lead. In: Sabatini DA, Knox RC (eds) Transport and remediation of subsurface contaminants: Colloidal, interfacial and subsurface phenomena, pp 99–107. Washington DC, American Chemical Society

Barton LL, Mandl M, Loy A (eds) (2010) Geomicrobiology: Molecular and environmental perspective. Springer Science + Business Media B.V., Dordrecht, The Netherlands

Biswas KC, Barton LL, Tsui WL, Shuman K, Gillespie J, Eze CS (2011) A novel method for the measurement of elemental selenium produced by bacterial reduction of selenite. J Microbiol Methods 86:140–144

Blake RC, II, Choate D, Bardhan S, Revis N, Barton LL, Zocco T (1993) Chemical transformations of toxic metals by a *Pseudomonas* strain from a toxic waste site. Environ Toxicol Chem 12:1365–1376

Blumb JS, Bindi AB, Buzzelli J, Stolz JF, Oremland RS (1999) *Bacillus arsenoselenatis*, sp. nov., and *Bacillus selenitireducens*, sp. nov.: Two halophiles from Mono Lake, California that respire oxyanions of selenium and arsenic. Arch Microbiol 171:19–30

Bunge M, Søbjerg LS, Rotaru A-E, Gauthier D, Lindhardt AT, Hause G, Finster K, Kingshott P, Skrydstrup T, Meyer RI (2010) Formation of palladium(0) nanoparticles at microbial surfaces. Biotechnol Bioeng 107:206–215

Calderón IL, Arenas FA, Pérez JM, Fuentes DE, Araya MA, Saavedra CP, Tantaleán JC, Pichuantes SE, Youderian PA, Vásquez CC (2006) Catalases are NAD(P)H—dependent tellurite reductases. PLoS ONE. 1:e70. doi:10.1371/journal.pone.0000070

Carpentier W, Sandra K, De Smet I, Brige A, DeSmit L, Van Beeumen J (2003) Microbial reduction and precitiatation of vanadium by *Shewanella oneidensis*. Appl Environ Microbiol 69:3636–3639

Castro-Longoria E, Vilchis-Nestor AR, Avalos-Borja M (2011) Biosynthesis of silver, gold and bimetallic nanoparticles using the fungus *Neurospora crassa*. Colloids Surface B 83:42–48

Checa SK, Espariz M, Audero ME, Botta PE, Spinelli SV, Soncini FC (2007) Bacterial sensensing of and resistance to gold salts. Mol Microbiol 63:1307–1318

Chen G, Chen X, Yang Y et al. (2011) Sorption and distribution of copper in unsaturated Pseudomonas putida CZ1 biofilms as determined by X-ray fluorescence microscopy. Appl Environ Microbiol 77:4719–4727

Corbari L, Cambon-Bonavita M-A, Long GJ, Grandjean F, Zbinden M, Gaill F, Compère P (2008) Iron oxide deposits associated with the ectoendosymbiotic bacteria in the hydrothermal vent shrimp *Rimicaris exoculata*. Biogeosciences 5:1295–1310

Cunningham DP, Lundie LL (1993) Precepitation of cadmium by *Clostridium thermoaceticum*. Appl Environ Microbiol 59:7–14

DeMoll-Decker H, Macy JM (1993) The periplasmic nitrite reductase of *Thauera selenatis* may catalyze the reduction of selenite to elemental selenium. Arch Microbiol 160:241–247

Devieux CM, Dridge EJ, Mueller CM, Splatt P, Paszkiewicz K, Knight I, Florance H, Lore J, Titball RW, Lewis RJ, Richardson DJ, Butler CD (2011) A bacterial process for selenium nanosphere assembly. Proc Natl Acad Sci 108:13480–13485

Dhanjai S, Cameotra SS (2010) Aerobic biogenesis of selenium nanospheres by *Bacillus cerus* isolated from coalmine soil. Microbial Cell Factories 9:52–58

Dunham-Cheatham S, Rui X, Bunker B, Munguy N, Hellmann R, Fein J (2011) The effects of non-metabolizing bacterial cells on the precipitation of U, Pb and Ca phosphates. Geochim Cosmochim Acta 75:2828–2847

Duran N, Seabra AB (2012) Microbial synthesis of metallic sulfide nanoparticles: An overview. Curr Biotechnol 1:287–296

El-Raheem A, El-Shanshoury R, Elsik SL, Ebeid ME (2011) Extracellular biosynthesis of silver naoparticles using *Escherichia coli* 8739, *Bacillus subtilis* ATCC 6633, and *Streptococcus thermophilus* ESh1 their antimicrobial activities. ISRN Nanotechnol. Article ID 385480 (7 pages). doi:5402/2011/385480

Fahey RC (2001) Novel thiols of prokaryotes. Ann Rev Microbiol 55:333–356

Fahey RC, Brown WC, Adams WB, Worsham MB (1978) Occurence of glutathione in bacteria. J Bacteriol 133:1126–1129

Falcone G, Nickerson WJ (1963) Reduction of selenite by intact yeast cells and cell-free preparations. J Bacteriol **85**:754–762

Francis AJ, Dodge CJ, Lu F, Halada GP, Clayton CR (1994) XPS and XANES studies of uranium reduction by *Clostridium* sp. Environ Sci Tech 28:636–639

Fredrickson JK, Kostandarithes HM, Li SW, Plymale AE, Daly MJ (2000) Reduction of Fe(III), Cr(VI), U(VI), and Tc(VII) by *Deinococcus radiodurans* R1. Appl Environ Microbiol 66:2006–2011

Gadd GM (2010) Metals, minerals and microbes: Geomicrobiology and bioremediation. Microbiology 156:609–643

Ganther HE (1971) Reduction of selenotrisulfite deravites of glutathione to a persulfite analog by glutathione reductase. Biochemistry 16:4089–4098

Gao W, Francis AJ (2013) Fermentation and hydrogen metabolism affect uranium reduction by clostridia. ISRN Biotechnol. http://dx.doi.org/10.5402/2013657160

Glasauer S, Langley S, Boyanov M, Lai B, Kemner K, Beveridge TJ (2007) Mixed-valence cytoplasmic iron granules are linked to anaerobic respiration. Appl Environ Microbiol 73:993–996

Gurunathan S, Kalishwaralal K, Vaidyanathan R, Venkataraman D, Pandian SR, Muniyandi J, Hariharan N, Eom SH (2009) Biosynthesis, purification and characterization of silver nanoparticles using *Escherichia coli*. Colloids Surf B Biointerfaces 74:328–335

Holmes JD, Farrer JA, Richardson DJ, Russell DA, Sodeau JR (1997a) Bacterial cadmium sulfide semiconductor particles: an assessment of their photoactivity by EPR spectroscopy. Photochem Photobiol 65:811–817

Holmes JD, Richardson DJ, Saed S, Evans-Growing R, Russell DA, Sodeau JR (1997b) Cadmium-specific formation of metal sulfide 'Q-particles' by *Klebsiella pneumoniae*. Microbiology 143:2521–2530

Honary S, Barabadi H, Gharael-Fathabad E, Naghibi F (2012) Green synthesis of copper oxide nanoparticles using *Penicillium aurantigriseum, Penicillium citrinum* and *Penicillium wakshami*. Digest J Nanomater Biostruct 7:999–1055

Hosseini MR, Schaffie M, Pazouki M, Darezereshki E, Ranjbar M (2012) Biologically synthesized copper sulfide nanoparticles: production and characterization. Mat Sci Semicon Proc 15:222–225

Iterson Wv, Leene W (1964a) A cytochemical localization of reductive sites in a Gram-positive bacterium. Tellurite reduction in *Bacillus subtilis*. J Cell Biol 20:361–375

Iterson Wv, Leene W (1964b) A cytochemical localization of reductive sites in a Gram-negative bacterium. J Cell Biol 20:377–387

Jha AK, Prasad K (2010) Ferroelectric $BaTiO_3$ nanoparticles: Biosynthesis and characterization. Colloids Surfaces B Biointerfaces 1:330–334

Jha AK, Prasad K, Prasad K (2009) A green low-cost biosynthesis of Sb_2O_3 nanoparticles. Biochem Eng. J 43:303–306

Jiang S, Lee J-H, Kim M-G, Myung NV, Fredrickson JK, Sadowsky MJ, Hur H-G (2009) Biogenic formation of As–S nanotubes by diverse *Shewanella* strains. App Environ Microbiol 75:6896–6899

Jiang S, Ho CT, Lee J-H, Duong HV, Han S, Hur H-G (2012) Mercury capture into biogenic amorphous selenium nanospheres produced by mercury resistant *Shewanella putrefaciens* 200. Chemosphere 87:621–624

Johnson CW, Wyall MA, Li X, Ibrahim A, Schuster J, Southam G, Magarvey NA (2013) Gold biomineralization by a metallophore from a gold-associated microbe. Nat Chem Biol 9:241–243

Kashefi K, Lovley DR (2000) Reduction of Fe(III), Mn(IV) and toxic metals at 100°C by *Pyrobaculum islandicum*. Appl Environ Microbiol 66:1050–1056

Kashefi K, Tor JM, Nevin KP, Lovley DR (2001) Reductive precipitation of gold by dissimilatory Fe(III)-Reducing *Bacteria* and *A*Appl Environ Microbiol 67:3275–3279. Applied and Environmental Microbiologyaem.asm.org

Kemner K, Kelly S, Lai B et al. (2004) Elemental and redox analysis of single bacterial cells by X-ray microbeam analysis. Science 306:686–687

Kessi J (2006) Enzymatic systems proposed to be involved in the dissimilatory reduction of selenite in the purple non-sulfur bacteria *Rhosospirillus rubrum* and *Rhodobacter capsulatus*. Microbiology 152:731–743

Khijniak TV, Slobodkin AI, Coker V, Renshaw JC, Livens FR, Bonch-Osmolovskaya N-K, Medvedeva-Lyalikova, NN, Lyoyd JR (2005) Reduction of uranium phosphate during growth of the thermophyllic bacterium *Thermoterrabacterium ferrireducens*. Appl Environ Microbiol 71:6423–6426

Kieft TL, Fredrickson JK, Onstott TC, Gorby YA, Kostandarithes HM, Bailey TJ, Kennedy DW, Li SW, Plymale AE, Spadoni CM, Gray MS (1999) Dissimilatory reduction of Fe(III) and other electron acceptors by a *Thermus* isolate. Appl Environ Microbiol 65:1214–1221

Kim D-H, Kanaly RA, Hur H-G (2012) Biological accumulation of tellurium nanorod structures via reduction of tellurite by *Shewanella oneidensis* MR –1. Bioresource Technol 125C:127–131

Konhauser K (2007) Introduction to geomicrobiology. Blackwell Publishing, Oxford, UK. Applied and Environmental Microbiologyaem.asm.org

Konishi Y, Ohno K, Saitoh N, Nomura T, Nagamine S, Hishida H, Takahashi Y, Uruga T (2007) Bioreductive deposition of platinum nanoparticles on the bacterium *Shewanella algae*. J Biotechnol 128:648–653

Kraft T, Macy JM (1998) Purification and characterization of the respiratory arsenate reductase of *Chrysiogenes arsenatis*. Eur J Biochem 255:647–653

Kumar SA, Ansary AA, Abroad A, Khan MI (2007) Extracellular biosynthesis of CdSe quantum dots by the fungus *Fusarium oxysoprum*. J Biomedical Nanotechnol 3:190–194

Labrenz M, Druschel GK, Thomsen-Ebert T, Gilbert B, Welch SA, Kemner KM, Logan GA, Summons RE, De Stasio G, Bond PL, Lai B, Kelly SD, Banfield JF (2000) Formation of sphalerite (ZnS) deposits in natural biofilms of sulfate-reducing bacteria. Science 290:1744–1747

Landa ER (2005) Microbial geochemistry of uranium mill tailings. Adv Appl Microbiol 27:113–130

Law N, Ansari S, Livens FR, Renshaw JC, Lloyd JR (2008) Formation of nanoscale elemental silver particles via enzymatic reduction by *Geobacter sulfurreducens*. Appl Environ Microbiol 74:7090–7093

Lee J-H, Kim M-G, Yoo B, Myung NV, Maeng J, Lee T, Dohnalkova AC, Fredrickson JK, Sadowsky MJ, Hur H-G (2007) Biogenic formation of photoactive arsenic-sulfide nanotubes by *Shewanella* sp. strain HN –41. Proc Natl Acad Sci 104:20410–20415

Lengke MF, Southam G (2007) The deposition of elemental gold from gold(I)-thiosulfate complexes mediated by sulfate-reducing bacterial conditions. Econ Geol 102:109–126

Lengke MF, Ravel B, Fleet ME, Wanger G, Gordon RA, Southam G (2006a) Mechanisms of gold bioaccumulation by filamentous cyanobacteria from gold(III)-chloride comolex. Environ Sci Technol 40:6304–6309

Lengke MF, Fleet ME, Southam G (2006b) Synthesis of platinum nanoparticles by reaction of filamentous cyanobacteria with platinum(IV) chloride complexes. Langmuir 22:7318–7323

Lengke MF, Fleet ME, Southam G (2007a) Biosynthesis of silver nanoparticles by filamentous cyanobacteria from a silver(I) nitrate complex. Langmuir 23:2694–2699

Lengke ML, Fleet ME, Southam F (2007c) Synthesis of palladium nanoparticles by reaction of filamentous cyanobacterial biomass with a palladium(II) chloride complex. Langmuir 23:8982–8987

Lenz M, Kolvenbach B, Gygox B, Moes S, Corvini PFX (2011) Shedding light on selenium biomineralization: proteins associated with bionanominerals. Appl Environ Microbiol 77:4676–4680
Li X, Xu H, Chen Z-S, Chen G (2011) Biosynthesis of nanoparticles by microorganisms and their application. J Anomaterials 16 pages. doi:10.1155/2011/270974
Liu Y-Y, Fu J-K, Zhou Z-H, Yu X-S, Yao B-X (2000) A study of Pt^{4+} absorption and its reduction by Bacillu*s megaterium* D01. Chem Res Chinese Univ 16:246–249
Lloyd JR, Yong P, Macaskie LE (1998) Enzymatic recovery of elemental palladium by using sulfate-reducing bacteria. Appl Environ Microbiol 64:4607–4609
Lloyd JR, Lovley DR, Macaskie LE (2003) Biotechnological applications of metal-reducing microorganisms. Adv Appl Microbiol 53:85–128
Lovley DR (ed) (2000) Environmental microbe-metal interactions. ASM Press, Washington DC
Lovley DR, Giovannoni SJ, White DC, Champine JE, Phillips EJ, Gorby YA, Goodwin S (1993a) *Geobacter metallireducens* gen. nov. sp. nov., a microorganism capable of coupling the complete oxidation of organic compounds to the reduction of iron and other metals. Arch Microbiol 159:336–344
Lovley DR, Roden EE, Phillips EJP, Woodward JC (1993b) Enzymatic iron and uranium reduction by sulfate-reducing bacteria. Marine Geol 113:41–53
Lovley DR, Wildman PK, Woodward JC, Phillips EJP (1993c) Reduction of uranium by cytochrome c_3 of *Desulfovibrio vulgaris*. Appl Environ Microbiol 59:33572–3576
Macaskie LE, Dean ACR (1987) Use of immobilized biofilm of *Citrobacter sp*. for the removal of uranium and lead from aqueous flows. Enzyme Microbial Technol 9:2–4
Marshall MJ, Alexander S, Beliaev AS, Dohnalkova AC, Kennedy DW, Shi L, Wang Z, Boyanov MI, Lai B, Barry K, Kemmer MK, McLean JS, Reed SB, Culley DE, Bailey VL, Simonson CJ, Saffarini DA, Romine MF, Zachara JM, Fredrickson JK (2006) c-type cytochrome-dependent formation of U(IV) nanoparticles by *Shewanella oneidensis*. PLOS Biol 4:1324–1333
Masip L, Veeravalli K, Georgiou G (2006) The many faces of glutathione in bacteria. Antioxid Redox Signal 8:753–762
Mikheenko IP, Rousset M, Dementin S, Macaskie LE (2008) Bioaccumulation of palladium by *Desulfovibrio fructoslvorans* wild-type and hydrogenase-deficient strains. Appl Environ Microbiol 74:6144–6146
Mishra RR, Prajapati S, Das J, Dangar TK, Das N, Thatoi H (2011) Reduction of selenite to red elemental selenium by moderately halotolerant *Bacillus megaterium* strains isolated from Bhitarkanika mangrove soil and characterization of reduced product. Chemosphere 84:1231–1237
Moreau JW, Webb RI, Banfield JF (2004) Ultrastructure, aggregation-state, and crystal growth of biogenic nanocrystalline sphalerite and wurtzite. Amer Minerologist 89:950–960
Moreau JW, Weber PK, Martin MC, Gilbert B, Hutcheon ID, Banfield JF (2007) Extracellular proteins limit the disopersal of biogenic nanoparticles. Science 316:1600–1603
Morita M, Uemoto H, Watanabe A (2007) Reduction of selenium oxyanions in wastewater using two bacterial strains. Eng Life Sci 7:235–240
Natarajan K, Selvaraj S, Murty VR (2010) Microbial production of silver nanoparticles. Digest J Nanopart Biostruct 5:135–140
Nelson YM, Lion LW, Ghiorse WC, Schuler ML (1999) Production of biogenic Mn oxides by *Leptothrix discoophora* SS –1 in a chemically defined growth medium and evaluation of their Pb adsorption characteristics. Appl Environ Microbiol 65:175–180
Nermut MV (1960) Über die Lage der Tellurit-Reduktionsorte in Zellen von *Proteus vulgaris*. Zentr. Bakt 1. Orig 178:348–358
Newman DK, Beveridge TJ, Morel FMM (1997) Precepitation of arsenic trisulfide by *Desulfotomaculum auripigmentum*. Appl Environ Microbiol 63:2022–2028
Nies DH (1999) Microbial heavy metal resistance. Appl Microbiol Biotechnol 51:730–750
Ollivier PRL, Bahrou AS, Marcus S, Cox T, Church TM, Hanson TE (2008) Volatilization and precipitation of tellurium by aerobic, tellurite-resistant marine microbes. Appl Environ Microbiol 74:7163–7173

Oremland RS, Herbel MJ, Blum JS, Langley S, Beveridge TJ, Alayan PM, Sutto T, Ellis AV, Curran S (2004) Structural and special features of selenium mamospheres by Se-respiring bacteria. Appl Environ Microbiol 70:52–60

Owens RA, Hartman PE (1986) Export of glutathione by some widely used *Salmonella typhimurium* and *Escherichia coli* strains. J Bacterial 168:109–114

Oza G, Pandey A, Shah R, Sharon M (2012) Extracellular fabrication of silver nanoparticles using *Pseudomonas aeruginosa* and its antimicrobialassay. Adv Appl Sci Res 3:1776–1783

Payne RB, Gentry DM, Rapp-Giles BJ, Casalot L, Wall JD (2002) Uranium reduction by *Desulfovibrio desulfuricans* G20 strain G20 and a cytochrome c_3 mutant. Appl Environ Microbiol 68:3129–3132

Pearce C, Pattrick R, Law N, Charnock JM, Coker VS, Fellowes JW, Oremland RS, Lloyd JR (2009) Investigating different mechanisms for biogenic selenite transformations: *Geobacter sulfurreducens, Shewanella oneidensis* and *Veillonella atypical*. Environ Technol 30:1313–1326

Pietzsch K, Babael W (2003) A sulphate-reducing bacterium that can detoxify U(VI) and obtain energy via nitrate reduction. J Basic Microbiol 4:348–361

Pieulle L, Stocker P, Vinay M, Nouailler M, Vita N, Brasseur G, Garcin E, Sebban-Kreuzer C, Dolla A (2011) Study of the thiol/disulfide redox systems of the anaerobe *Desulfovibrio vulgaris* points out pyruvate:ferredoxin oxidoreductase as a new target for thioredoxin 1. J. Biol. Chem. 286:7812–7821

Popescu M, Velea A, LÓ§rinczi A (2010) Biogenic production of nanoparticles. Digest J Nanomater Biostruct 5:1035–1040

Prakash A, Sharma S, Ahmad N, Ghosh A, Sinha P (2010) Bacteria mediated extracellular synthesis of metallic nanoparticles. Int Res J Biotechnol 1:71–79

Rashamuse KT, Whiteley CG (2007) Bioreduction of Pt(IV) from aqueous solution using sulphate-reducing bacteria. Appl Microbiol Biotechnol 75:1429–1435

Rathgeber C, Yurkova N, Stackebrandt E, Beatty JT, Yurkov V (2002) Isolation of tellurite- and selenite-resistant bacteria from hydrothermal vents of the Juan de Fuca Ridge in the Pacific Ocean. Appl Environ Microbiol 68:4613–4622

Rautaray D, Sanyal A, Adyanthaya SD, Ahmad A, Sastry M. 2004. Biological synthesis of strontium carbonate crystals using the fungus *Fusarium oxysporum*. Langmuir 20:6827–6833

Reith F, Etschmann B, Grosse C, Moors H, Benotmane MA, Monsieurs P, Grass G, Doonan C, Vogt S, Lai B, Martinez-Criado G, George GH, Nies DH, Mergay M, Pring A, Southam G, Brugger J (2009) Mechanisms of gold biomineralization in the bacterium *Cupriavidus metallidurans*. Proc Natl Acad Sci 106:17757–17762

Riddin TL, Govender Y, Gericke M, Whiteley CG (2009) Two different hydrogenase enzymes from sulphate-reducing bacteria are responsible for the bioreductive mechanism of platinum into nanoparticles. Enzyme Microbial Technol 45:267–273

Ritz D, Beckwith J (2001) Roles of thiol-redox pathways in bacteria. Ann Rev Microbiol 55:21–48

Roh Y, Liu SV, Li G, Huang H, Phelps TJ, Zhou J (2002) Isolation and characterization of metal-reducing *Thermoanaerobacter* strains from deep subsurface environments of the Piceance Basion, Colorado. Appl Environ Microbiol 68:6013–6020

Santini JM, Streimann ICA, vander Hoven RN (2004) *Bacillus macyae* sp. nov., an arsenate-respiring bacterium isolated from an Australian gold mine. IJSEM 54:2241–2244

Sanyal A, Rautaray D, Bansal V, Ahmad A, Sastry M (2005) Heavy-metal remediation by a fungus as a means of production of lead and cadmium carbonate crystals. Langmuir 21:7222–7224

Sarkar J, Dey P, Saha S, Acharya K (2011) Mycosynthesis of selenium nanoparticles. Micro Nano Lett 6:599–602

Schröder I, Rech S, Krafft T, Macy JM (1997) Purification and characterization of the selenate reductase from *Thauera selenatis*. J Biol Chem 272:23765–23768

Senapati S, Ahmad A, Khan MI, Sastry M, Kumar R (2005) Extracellular biosynthesis of biometallic Au–Ag alloy nanoparticles. Small 1:517–520

Sharma N, Pinnaka AK, Raje M, Fnu A, Bhattacharyya MS, Choudhury AR (2012) Exploitation of marine bacteria for production of gold nanoparticles. Microbial Cell Factories 11:86–87

Shelobolina ES, Coppi MV, Korenivsky AA, DiDonato LN, Sullivan SA, Konishi H, Xu H, Leang C, Butler JE, Kim S-C, Lovley DR (2007) Importance of c-type cytochromes for U(VI) reduction by *Geobacter sulfurreducens*. BMC Microbiol 7:16

Singh S, Bhatta UM, Satyam PV, Dhawan A, Sastry M, Prasad BLV (2008) Bacterial synthesis of silicon/silica nanocomposites. J Mater Chem 18:2601–2606

Singh V, Patil R, Anand A, Milani P, Gade WN (2010) Biological synthesis of copper oxide nano particles using *Escherichia coli*. Curr Nanosci 6:365–369

Sinha A, Khare S (2011) Mercury bioaccumulation and simultaneous nanoparticle synthesis by *Enterobacter* sp. cells. Bioresour Technol 102:4281–4284

Sinha A, Singh VN, Mehta BR, Khare SK (2011) Synthesis and characterization of monodispersed orthorhombic manganese oxide nanoparticles produced by *Bacillus* sp. cells simultaneous to its bioremediation. J Hazard Mater 192:620–627

Sintubin L, De Windt W, Dick J, Mast J, van der Ha D, Verstraete W, Boon N (2009) Lactic acid bacteria as reducing and capping agents for the fast and efficient production of silver nanoparticles. Appl Microbiol Bacteriol 84:741–749

Sintubin L, Verstraete W, Boon N (2011) Biologically produced nanosilver: Current state and future perspectives. Biotechnol Bioeng 109:2422–2436

Sparks DL (2005) Toxic metals in the environment: the role of surfaces. Elements 1:193–196

Spiro TG, Bargar JR, Sposito G, Tebo BM (2010) Bacteriogenic manganese oxides. Acc Chem Res 43:2–9

Suresh AK (2012) Metallic nanocrystallites and their interaction with microbial systems. Springer, London, UK

Suresh AK, Pelletier DA, Wang W, Moon J-W, Gu B, Mortensen NP, Allison DP, Joy DC, Phelps TJ, Doktyez MJ (2010) Silver nanocrystallites: Biofabrication using *Shewanella oneidensis* and an evaluation of their comparative toxicity on Gram-negative and Gram-positive bacteria. Environ Sci Technol 44:5210–5215

Tam K, Ho CT, Lee J-H, Lai M, Chang CH, Rheem Y, Chen W, Hur HG, Myung NV (2010) Growth mechanisms of amorphous selenium nanoparticles synthesized by *Shewanella* sp. HN –41. Biosci Biotechnol Biochem 74:696–700

Tebo BM, Obraztsova AY (1998) U(VI) sulphate-reducing bacterium grows with Cr(VI), Mn(IV), and Fe(III) as electron acceptors. FEBS Microbiol Lett 162:193–198

Tebo BM, Geszvain K, Lee S-W (2010) The molecular geomicrobiology of bacterial manganese(II) oxidation. In: Barton LL, Mandl M, Loy A (eds) Geomicrobiology: Molecular and environmental perspective. Springer, Dordrecht, pp 285–308

Thakkar KN, Mhatre SS, Parikh RY (2010) Biological synthesis of metallic nanoparticles. Nanomedicine 6:257–262

Tomei FA, Barton LL, Lemanski CL, Zocco TG (1992) Reduction of selenate and selenite to elemental selenium by *Wolinella succinogenes*. Can J Microbiol 38:1328–1333

Tomei FA, Barton LL, Lemanski CL, Zocco TG, Fink NH, Sillerud LO (1995) Transformation of selenate and selenite to elemental selenium by *Desulfovibrio desulfuricans*. J Ind Microbiol 14:329–336

Trutko SM, Akimenko VK, Suzina NE, Anisimova LA, Shlyapnikov MG, Baskunov BP, Duda VI, Boronin AM (2000) Involvement of the respiratory chain of Gram-negative bacteria in the reduction of tellurite. Arch Microbiol 173:178–186

Tsibakhashvili NY, Kirkesali EI, Pataraya DT, Gurielidze MA, Kalabegishvili TL, Gvarjaladze DN, Tsertsvadze GI, Frontasyeva MV, Zinicovscais II, Wakstein MS, Khakhanov SN, Shvindina NV, Shklover VY (2011) Microbial synthesis of silver nanoparticles by *Streptomyces glaucus* and *Spirulina platensis*. Nanomater Appl Prop 2:306–310

Tucker MD, Barton LL, Thomson BM (1998) Reduction of Cr, Mo, Se and U by *Desulfovibrio desulfuricans* immobilized in polyacrylamide gels. J Ind Microbiol Biotechnol 20:13–19

Tucker MD, Barton LL, Thomson BM (2000) Removal of U and Mo from water by immobilized *Desulfovibrio desulfuricans* in column reactors. Biotechnol Bioeng 60:88–96

Vaidyanathan R, Gopalram S, Kalishwaralal K, Deepak V, Pandian SRK, Gurunathan S. 2010. Enhanced silver nanoparticle synthesis by optimization of nitrate reductase activity. Colloids Surf B Biointerfaces 75:7

Villalobos M, Lanson B, Manceau A, Toner B, Sposito G. 2006. Structural model for the biogenic Mn oxide produced by *Pseudomonas putida*. Amer Mineralogist 91:489–502

Wade R, DiChristiana TJ (2000) Isolation of U(VI) reduction-deficient mutants of *Shewanella putrefaciens*. FEBS Microbiol Lett 184:143–148

Wall JD, Krumholz LR (2006) Uranium reduction. Ann Rev Microbiol 60:149–166

Watson JHP, Ellwood DC, Soper AK, Chamock SJ (1999) Nanosized strongly-magnetic bacterially-produced iron sulphide materials. J Magn Magn Mater 203:69–72

Webb SM, Dick GJ, Bargat JR, Tebo BM (2005) Evidence for the presence of Mn(III) intermediates in the bacterial oxidation of Mn(II). Proc Natl Acad Sci U S A 102:5558–5563

Woolfolk CA, Whiteley HR (1962) Reduction of inorganic compounds with molecular hydrogen by *Micrococcus lactilyticus*. 1. Stoichiometry with compounds of arsenic, selenium, tellurium, transition and other metals. J Bacteriol 84:647–658

Xie YF, Li XD, Li FD (2009) Property analysis of nanosized iron sulfide producing sulfate-reducing bacterium and its application in the treatment of wastewater containing high concentration of Cr(VI). Huan Jing KeXue 30:1060–1065

Xu H, Barton LL (2013) Se-bearing colloidal particles produced by sulfate-reducing bacteria and sulfide-oxidizing bacteria: TEM study. Adv Microbiol 3:205–211

Xu X-H N, Brownlow W, Kyriacou S, Wan Q, Viola JJ (2004) Real-time probing of membrane transport in living microbial cells using single nanoparticle optics and living cell imaging. Biochemistry 43:10400–10413

Yanke LJ, Bryant RD, Laishley EJ (1995) Hydrogenase of *Clostridium pasteurianum* functions as a novel selenite reductase. Anaerobe 1:61–67

Zhan G, Li D, Zhang L (2012) Aerobic bioreduction of nickel(II) to elemental nickel with concomitant biomineralization. Appl Microbiol Biotechnol 96:273–281

Zhang L, Li D, Gao P (2012) Expulsion of selenium/protein nanoparticles through vesicle-like structures by *Saccharomyces cerevisiae* under microaerophilic environment. World J Microbiol Biotechnol, pp 1–6. doi:10.1007/s11274–01201150-y

Index

L. L. Barton et al. (eds.), *Nanomicrobiology,* DOI 10.1007/978-1-4939-1667-2